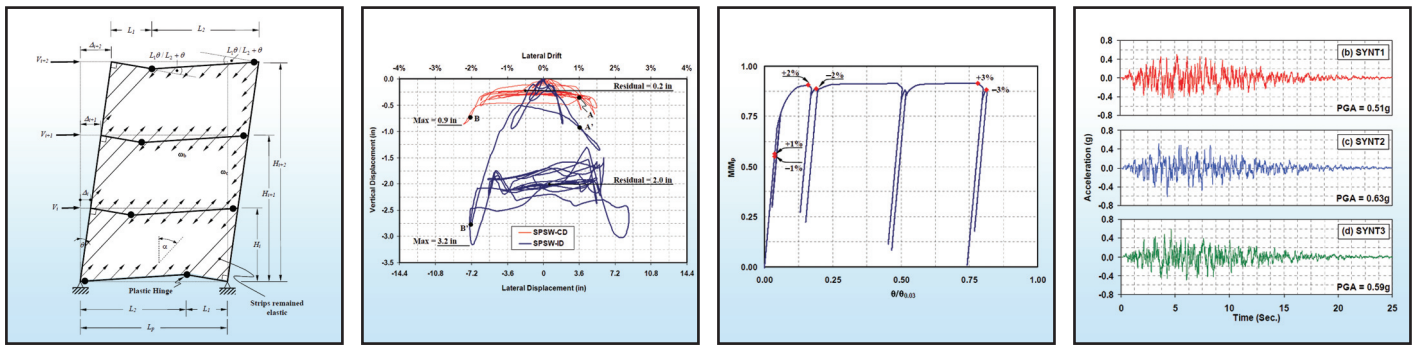


Impact of Horizontal Boundary Elements Design on Seismic Behavior of Steel Plate Shear Walls

by
Ronny Purba and Michel Bruneau



Technical Report MCEER-10-0007

November 14, 2010

NOTICE

This report was prepared by the University at Buffalo, State University of New York, as a result of research sponsored by MCEER and the George E. Brown, Jr. Network for Earthquake Engineering Simulation (NEES) program of the National Science Foundation, NEESR award number CMMI-0830294. Neither MCEER, associates of MCEER, its sponsors, the University at Buffalo, State University of New York, nor any person acting on their behalf:

- a. makes any warranty, express or implied, with respect to the use of any information, apparatus, method, or process disclosed in this report or that such use may not infringe upon privately owned rights; or
- b. assumes any liabilities of whatsoever kind with respect to the use of, or the damage resulting from the use of, any information, apparatus, method, or process disclosed in this report.

Any opinions, findings, and conclusions or recommendations expressed in this publication are those of the author(s) and do not necessarily reflect the views of MCEER, the National Science Foundation, or other sponsors.

Impact of Horizontal Boundary Elements Design on Seismic Behavior of Steel Plate Shear Walls

by

Ronny Purba¹ and Michel Bruneau²

Publication Date: November 14, 2010

Submittal Date: June 11, 2010

Technical Report MCEER-10-0007

George E. Brown, Jr. Network for Earthquake Engineering Simulation (NEES)
Program of the National Science Foundation
NEESR Award Number CMMI-0830294

- 1 Ph.D. Candidate, Department of Civil, Structural, and Environmental Engineering, University at Buffalo, State University of New York
- 2 Professor, Department of Civil, Structural, and Environmental Engineering, University at Buffalo, State University of New York

MCEER

University at Buffalo, State University of New York

Red Jacket Quadrangle, Buffalo, NY 14261

Phone: (716) 645-3391; Fax (716) 645-3399

E-mail: mceer@buffalo.edu; WWW Site: <http://mceer.buffalo.edu>

Preface

MCEER is a national center of excellence dedicated to the discovery and development of new knowledge, tools and technologies that equip communities to become more disaster resilient in the face of earthquakes and other extreme events. MCEER accomplishes this through a system of multidisciplinary, multi-hazard research, in tandem with complimentary education and outreach initiatives.

Headquartered at the University at Buffalo, The State University of New York, MCEER was originally established by the National Science Foundation in 1986, as the first National Center for Earthquake Engineering Research (NCEER). In 1998, it became known as the Multidisciplinary Center for Earthquake Engineering Research (MCEER), from which the current name, MCEER, evolved.

Comprising a consortium of researchers and industry partners from numerous disciplines and institutions throughout the United States, MCEER's mission has expanded from its original focus on earthquake engineering to one which addresses the technical and socio-economic impacts of a variety of hazards, both natural and man-made, on critical infrastructure, facilities, and society.

The Center derives support from several Federal agencies, including the National Science Foundation, Federal Highway Administration, National Institute of Standards and Technology, Department of Homeland Security / Federal Emergency Management Agency, and the State of New York, other state governments, academic institutions, foreign governments and private industry.

The seismic behavior of Steel Plate Shear Walls (SPSWs) with boundary elements that have been designed using two different philosophies is investigated in this study. The first design approach does not guarantee that it can prevent the formation of in-span plastic hinges on horizontal boundary elements; while the second approach guarantees that plastic hinges will only occur at the ends of the horizontal boundary elements. The results from pushover and nonlinear time history analyses showed that the development of in-span plastic hinges has significant consequences on the behavior of the structure. Nonlinear time history analyses further demonstrates that increasing the severity of the ground excitations accentuates the accumulation of plastic incremental deformations on the horizontal boundary elements. This study also investigates the plastic strength of SPSWs with in-span plastic hinges and develops an alternative plastic mechanism to match the results from pushover analysis. A cycle by cycle investigation on horizontal boundary element deformation history under cyclic loading is presented and several key behaviors observed during the cyclic loading history are identified.

ABSTRACT

A case study was conducted to investigate the seismic behavior of steel plate shear walls having boundary elements designed by two different philosophies. The first design approach does not guarantee that formation of in-span plastic hinges on horizontal boundary elements (HBEs) will be prevented; while the second approach guarantees that plastic hinges can only occur at the ends of HBEs. Pushover and nonlinear time history analyses were conducted to investigate behavior. Results show that the development of in-span plastic hinges has significant consequences on the behavior of the structure through inducing: (1) significant accumulation of plastic incremental deformations on the HBEs; (2) partial yielding of the infill plates; (3) lower global plastic strength compared to the values predicted by code equations; and (4) total (elastic and plastic) HBE rotations greater than 0.03 radians after the structure was pushed cyclically up to a maximum lateral drift of 3%. Nonlinear time history analyses also demonstrated that increasing the severity of the ground excitations (i.e., from DBE to MCE) acting on the structure with in-span plastic hinge accentuated the accumulation of plastic incremental deformations on the HBEs. In addition, this study investigates plastic strength of SPSW having in-span plastic hinges and develops an alternative plastic mechanism needed to match results from pushover analysis. A cycle by cycle investigation on HBE deformation history under cyclic loading was presented and several key behaviors observed during the cyclic loading history were identified.

ACKNOWLEDGEMENTS

This work was supported primarily by the George E. Brown, Jr. Network for Earthquake Engineering Simulation (NEES) Program of the National Science Foundation under NSF NEESR Award Number CMMI-0830294. The financial support of the Fulbright Indonesia Presidential Scholarship to the first author is gratefully appreciated.

TABLE OF CONTENTS

SECTION	TITLE	PAGE
1	INTRODUCTION	1
1.1	General	1
1.2	Scope and Objectives	2
1.3	Outline of Report	3
2	DESIGN OF THREE-STORY STEEL PLATE SHEAR WALLS AND ANALYTICAL MODEL DEVELOPMENT	5
2.1	General	5
2.2	Structure Description and Design of 3-Story SPSW	5
2.2.1	Indirect Capacity Design Approach (ICD)	8
2.2.2	Combined Plastic and Linear Analysis (Capacity Design)	11
2.3	Analytical Model Development	13
2.4	Summary	22
3	NONLINEAR STATIC ANALYSIS	23
3.1	General	23
3.2	Monotonic Pushover Analysis	23
3.3	Plastic Analysis of SPSW having In-Span HBE Plastic Hinge	28
3.4	Cyclic Pushover Analysis	36
3.4.1	Plastic Hinge and Strip Yielding Distributions	40
3.4.2	HBE Vertical Deformation	47
3.4.3	Cycle by Cycle Investigation on HBE Deformation History of SPSW-CD	53
3.4.4	Moment-Rotation Comparison	62
3.5	Summary	67
4	NONLINEAR TIME HISTORY ANALYSIS	69
4.1	General	69
4.2	Synthetic Ground Motions	70

TABLE OF CONTENTS (cont'd)

SECTION	TITLE	PAGE
4.3	Analysis Results	70
4.4	Summary	79
5	SUMMARY, CONCLUSIONS, AND RECCOMENDATIONS	81
5.1	Summary	81
5.2	Conclusions	82
5.3	Recommendations for Future Research	83
6	REFERENCES	85
APPENDIX		
A	DESIGN CALCULATION OF THREE-STORY STEEL PLATE SHEAR WALLS USING INDIRECT CAPACITY DESIGN APPROACH	89
B	DESIGN CALCULATION OF THREE-STORY STEEL PLATE SHEAR WALLS USING CAPACITY DESIGN APPROACH	95
C	FIBER HINGE STUDY	103
C.1	General	103
C.2	Case Study Set-up: Cantilever Column W14x48	103
C.3	Analysis Results	105
D	HOOK ELEMENT STUDY	107
D.1	General	107
D.2	Application of Hook Element on Strip Model	107
E	COMPARISON OF NORMALIZED MOMENT ROTATION HYSTERESIS CURVE BETWEEN STEEL PLATE SHEAR WALLS AND SPECIAL MOMENT RESISTING FRAMES	111

LIST OF ILLUSTRATIONS

FIGURE	TITLE	PAGE
2-1	Design Response Spectra for San Francisco, California ($\xi = 5\%$)	6
2-2	VBE and HBE Sizes with Demand to Capacity Ratio Results	10
2-3	Free Body Diagrams (Berman & Bruneau 2008)	12
2-4	Schematic Moment Diagram along HBES Obtained from Nonlinear Static Analysis at 4% Drifts	15
2-5	Strip Model for Monotonic Pushover Analysis	16
2-6	Dual Strip Model for Cyclic Pushover and Time History Analyses	20
3-1	SAP2000 Monotonic Pushover Analysis versus Plastic Analysis Calculations	25
3-2	Plastic Hinge and Strip Yielding Distributions at 4% Lateral Drift	27
3-3	Schematic Deformed Shapes of Monotonic Pushover Analysis	29
3-4	Sway and Beam Combined Plastic Mechanism for Single Story SPSW	30
3-5	Sway and Beam Combined Plastic Mechanism for Multistory SPSW	33
3-6	Displacement History for Cyclic Pushover Analysis	37
3-7	Typical Force-Displacement Hysteresis of Slender Strip	38
3-8	Cyclic Pushover Analysis Results	39
3-9	Plastic Hinge and Strip Yielding Distributions on SPSW-ID	42
3-10	Plastic Hinge and Strip Yielding Distributions on SPSW-CD	43
3-11	HBE3 Free-Body Diagram and Moment Diagram for SPSW-ID at Various Lateral Drifts during 3% Drift Cycle	46
3-12	Schematic Deformed Shapes of Cyclic Pushover Analysis	48
3-13	HBE3 Vertical Displacement versus Top Floor Lateral Displacement Obtained from Cyclic Pushover Analysis	50
3-14	Structure Lateral Displacement versus HBE Vertical Displacement	52

LIST OF ILLUSTRATIONS (cont'd)

FIGURE	TITLE	PAGE
3-15	HBE3 Vertical Displacement and Structural Base Shear versus Top Floor Lateral Displacement for SPSW-CD	54
3-16	HBE3 Deformed Shapes at Various Lateral Drifts (“Bump” Behavior Observed in SPSW-CD)	61
3-17	Normalized Moment Rotation Hysteresis at HBE Left End	63
3-18	Normalized Moment Rotation Hysteresis at Mid-Span of HBE2 (SPSW-ID)	66
4-1	Spectral Acceleration and Synthetic Ground Motions	71
4-2	HBE3 Vertical Displacement versus Top Floor Lateral Displacement Obtained from Time History Analysis (SYNT2)	74
4-3	Nonlinear Time History Analysis Results (SYNT2): Structure Lateral Displacement versus HBE Vertical Displacement	75
4-4	Plastic Hinge and Strip Yielding Distributions at the end of Nonlinear Time History Analysis (SYNT2)	79
C-1	Case Study Set-up for Fiber Hinge Study	104
C-2	Normalized Plastic P-M Interaction Diagram of W14x48	106
D-1	Hook Property in SAP2000 (CSI 2007)	107
D-2	Application of Hook Element on Strip Model	108
D-3	Result Comparison between SPSW-ID with Modified Axial P-Hinge and SPSW-ID with Hook Element	109
D-4	Deformation of SPSW-ID with Hook Element at +3% Drift	110
E-1	Comparison of Normalized Moment Rotation Hysteresis of SPSW-ID	112
E-2	Comparison of Normalized Moment Rotation Hysteresis of SPSW-CD	113

LIST OF TABLES

TABLE	TITLE	PAGE
2-1	Lateral Forces on Each Floor and Story Shear Forces	7
2-2	Vertical and Horizontal Boundary Element Sizes	9
2-3	Fiber Hinge Tributary Area and Ordinate along Y-Axis (SPSW-ID)	18
4-1	HBE Maximum and Residual Vertical Deformations (DBE Case)	72
4-2	Comparison of HBE Maximum Vertical Deformation Obtained from Cyclic Pushover Analysis and Nonlinear Time History Analysis (SYNT2)	76
4-3	HBE Maximum and Residual Vertical Deformations (MCE Case)	77
4-4	Comparison of HBE Maximum Vertical Deformation Obtained from Nonlinear Time History Analysis of DBE and MCE Case	78

NOTATIONS

A_i	fiber cross section area
B	amplification factor
C_{vi}	vertical distribution factor for the i -th story
F_i	lateral force at i -th story
F_y	yield stress of steel
F_{yb}	HBE yield stress
F_{yp}	infill plate yield stress
h_i	height from the base to the i -th story (Section 2)
H_i	height from the base to the i -th story (Section 3)
H_s	story height
I	importance factor
k	natural period coefficient
L_1, L_2	location of plastic hinge from the left and right joints (Section 3)
L_b	HBE span
L_p	clear length of the infill plate
M_{max}	maximum moment along the HBE span
M_p	theoretical flexural plastic moment capacity
M_{pbi}	plastic moment of HBE at the i -th story
M_{pr}	reduced flexural plastic moment capacity on HBE
M_w	moment magnitude of seismic source
M_y	theoretical flexural yield moment
P	axial force of a strip
P_b	axial force on HBE
P_y	yield force of a strip
R	response modification factor (Section 2); site-to-source distance (Section 4)
R_{yp}	ratio of the expected to the specified steel plate yield stress
S	strip width (Section 2.3)
S_{DI}	one-second spectral ordinates
S_{DS}	design short spectral ordinates

T	fundamental period of a structure
t_{pi}	infill thickness provided at the i -th story
t_{wi}	required infill plate thickness to resist story shear forces at the i -th story
V	total base shear
V_b	shear force on HBE
V_{ei}	expected shear strength at the i -th story
V_i	story shear force or applied lateral load at the i -th story
V_{ui}	lateral seismic force at the i -th story
$W_{external}$	external work component in kinematic method of plastic analysis
W_i	i -th story weight
$W_{internal}$	internal work component in kinematic method of plastic analysis
W_t	total weight of the structure
Z	plastic modulus
α	tension field inclination angle
δ	HBE vertical deformations
Δ	top story lateral displacement
$\delta_{max}; \delta_{res}$	HBE maximum vertical deformations; HBE residual vertical deformations
δ_y	strip yield displacement
ε_y	yield strain of steel
ϕ	strength resistance factor for the SPSW web
θ	angle between the deformed structure and the vertical in kinematic method; angle of flexural rotation
$\theta_{0.03}$	required plastic rotation capacity of a special moment resisting frame (0.03 radians)
σ_y	yield stress of steel
Ω_s	system overstrength as defined in FEMA 369
ω_{xb}	horizontal component of infill plate stress on HBE
ω_{xc}	horizontal component of infill plate stress on VBE
ω_{yb}	vertical component of infill plate stress on HBE
ω_{yc}	vertical component of infill plate stress on VBE
ξ	viscous damping ratio

ABBREVIATIONS

AISC	American Institute of Steel Construction
ASTM	American Society for Testing and Materials Standard
CD	Capacity Design
DBE	Design Basis Earthquake
FEMA	Federal Emergency Management Agency
HBE	Horizontal Boundary Elements
ICD	Indirect Capacity Design
ID	Indirect Design
MCE	Maximum Considered Earthquake
PGA	Peak Ground Accelerations
SAP2000	Structural Analysis Program 2000
SMRF	Special Moment Resisting Frame
SPSW	Steel Plate Shear Walls
TARSCTHS	Target Acceleration Spectra Compatible Time Histories
VBE	Vertical Boundary Elements

SECTION 1

INTRODUCTION

1.1 General

There have been numerous experimental and analytical studies investigating the behavior of unstiffened Steel Plate Shear Walls (SPSW) in the past thirty years. An AISC Design Guide summarizes that research (Sabelli and Bruneau 2007) which has addressed the designing and modeling of SPSW web plates, general SPSW analysis methods, validation of satisfactory cyclic inelastic and seismic performances, and analytical procedures to calculate demands in the horizontal and vertical boundary elements (HBEs and VBEs) of the SPSW (e.g., Thorburn *et al.* 1983; Timler and Kulak 1983; Caccese *et al.* 1993; Driver *et al.* 1997, Berman and Bruneau 2003, 2008; Qu *et al.* 2008; to name a few). As a result of this research, provisions for SPSW design have been adopted (e.g. AISC 2005) and they have been increasingly implemented in seismic regions.

The seismic behavior of SPSW has traditionally benefited from the overstrength introduced in the HBEs and VBEs of the boundary frame by capacity design principle requirements followed in past research, but as practicing engineers are becoming more familiar with this structural system, they are finding ways to optimize the system and eliminate much of that overstrength, to achieve smaller boundary element member sizes (Qu and Bruneau 2009). This can become problematic in light of the challenges that sometimes exist in determining satisfactory demands in designing the HBEs (e.g. Lopez-Garcia and Bruneau 2006, Qu *et al.* 2008, Vian and Bruneau 2005).

The 2005 AISC Seismic Provisions for Structural Steel Buildings (AISC 2005b) requires that HBEs and VBEs shall be designed to remain essentially elastic under the maximum tension forces from the yielded infill plates, with the exception of plastic hinging at the ends of HBEs. However, it does not specify an analysis procedure to guarantee that this intent is met (although the commentary provides some guidance that could be used for this purpose). As a result, there are at least two different common design approaches that have been encountered in practice for

which SPSWs are likely to develop in-span hinges. In a first approach, structural engineers typically use the results of elastic analysis program and verify that the moments do not exceed plastic moment capacity of the HBE. That by itself does not protect against in-span hinges. In the second approach, compounding on the first one, structural engineers seek to optimize the distribution of resistance to the lateral load between the boundary elements and infill plate, such as to obtain a boundary frame having a strength to resist its share of the lateral loads equal to that required to resist the demands from capacity design principles (i.e. due to the yielding plates), effectively eliminating the overstrength of the boundary frame (even though it is not strictly compliance with the AISC requirement which states that the entire lateral loads be resisted by the infill plate). In both cases, structural engineers might not anticipate that their design may lead to in-span HBE plastic hinges (unless these analyses are complemented by the use of nonlinear analysis programs to predict the plastic mechanism of structures). In parallel, some structural engineers fully recognize the potential for in-span hinging to develop, but question the merit of limiting the location of plastic hinges to only occur at the ends of HBEs because, in general, this design requirement results in a relatively substantial size of boundary elements. Thus, to achieve more economical designs, structural engineers are trying to minimize overstrength by allowing plastic hinges to occur along HBE span as this leads to relatively smaller boundary elements. Whether or not this is acceptable has been a contentious issue, particularly in the absence of factual data.

1.2 Scope and Objectives

To investigate the aforementioned concern, one must first determine whether in-span HBE hinging, when it happens, can impact in any way to the seismic performance of SPSWs – irrespectively of whether it develops in a SPSW intentionally or as a result of unintended design consequences. This report presents results from an investigation of that question using a “case-study” for this purpose. Undoubtedly, subsequent research and parametric studies would be useful to identify the specific conditions and wall geometries (e.g. aspect ratios, number of stories, etc.) for which specific behaviors would be obtained, to quantify their likelihood of occurrence, and to determine if other attenuating factors can be relied upon to counter potential undesirable behaviors. However, an understanding of the possible consequences of in-span HBE

plastic hinging is pre-requisite to any such further questioning. In that perspective, while it is recognized that overstrength in SPSWs may arise from a number of sources during design, the case study presented here has been careful to ensure that its conclusions would not be biased by accidental sources of overstrength that may or may not be present from case to case – future analysis would allow to quantify and assess the reliability of various sources of uncontrolled overstrength.

Hence, to answer the fundamental question in this debate, this report presents the results of a case study, analytically investigating the seismic behavior of two steel plate shear walls having HBEs designed to have different plastic mechanisms. In the first SPSW, one of the above design approaches is used and formation of in-span plastic hinges on horizontal boundary elements is possible, whereas in the second SPSW, plastic hinges can only occur at the ends of HBEs. Results and observations from monotonic and cyclic pushover analyses as well as time-history analyses are used to assess the relative performance of the two SPSWs.

1.3 Outline of Report

Section 2 describes the design process of a three-story steel plate shear walls used as a case study for the above objectives. Several key techniques on how to model the two design outcomes using strip model and dual strip model in SAP2000 are discussed, which includes modeling *Tension only Bracing Element*, defining *Axial-Hinge* that can capture the actual behavior of slender strips, and defining *Fiber-Hinge* that can capture the interaction between the axial loads and moments that occur in the boundary elements.

Using the resulting numerical models, nonlinear static analysis is conducted in Section 3 to investigate the possible significance of in-span plastic hinge developed on horizontal boundary elements (HBE). Here, behavior of two shear walls designed to have different plastic mechanisms is examined under monotonic and incrementally cyclic pushover loadings, which includes comparing global plastic strength, plastic hinge and strip yielding distributions, vertical and residual deformations on HBE, and HBE plastic rotation demands. In addition, a general equation to calculate the ultimate strength of both single and multistory SPSW with in-span plastic hinge

(i.e., sway and beam combined mechanism) is developed using the kinematic method of plastic analysis. Several key behaviors observed during a cycle by cycle investigation on HBE deformation history under the cyclic pushover loading are identified.

Section 4 describes time history analyses conducted on the two shear walls to investigate whether the cyclic pushover analysis results would be replicated during earthquakes excitations and whether additional seismic behaviors for the aforementioned SPSW systems would emerge as a consequence of the random nature of earthquake records. Synthetic ground motions are used in this investigation. Their response spectra are scaled to match both the design basis earthquake (DBE) and the maximum considered earthquake (MCE) target spectra. Finally, summary, conclusions, and recommendations for future research are presented in Section 5.

SECTION 2

DESIGN OF THREE-STORY STEEL PLATE SHEAR WALLS AND ANALYTICAL MODEL DEVELOPMENT

2.1 General

This section describes the design process of a three-story steel plate shear walls. Two different design philosophies are used: (1) Indirect Capacity Design Approach, a common design approach encountered in practice, and (2) Capacity Design Approach, as described in the commentary to the new 2010 AISC Seismic Provisions (AISC 2010). Several key techniques on how to model the two design outcomes using strip model and dual strip model in SAP2000 are discussed, which includes modeling *Tension only Bracing Element*, defining *Axial-Hinge* that can capture the actual behavior of slender strips, and defining *Fiber-Hinge* that can capture the interaction between the axial loads and moments that occur in the boundary elements. Numerical models developed in this section will be used in the next two sections to investigate the possible significance of in-span plastic hinge developed on horizontal boundary elements (HBE).

2.2 Structure Description and Design of 3-Story SPSW

As a case study to investigate the possible significance of in-span HBE plastic hinges, a three-story single-bay SPSW was selected. Bay width and typical story height were arbitrarily chosen equal to 20 and 10 ft., respectively, resulting in an infill plate aspect ratio of 2.0. Note that SPSWs having such an aspect ratio are common nowadays (e.g. AISC 2007, 2008), and that larger values are anticipated as the 2010 edition of the AISC Seismic provisions (AISC 2010) has eliminated the previously prescribed upper limit for that ratio. It was also assumed that the structure is located on Class D soil in downtown San Francisco, California and designed for an office building. This SPSW was assumed to carry a tributary weight W_t of 1085 kips, which corresponds to one sixth of the total weight of the structure; distributed as 352 kips on the first two stories and 381 kips on the roof. Different approaches were possible to ensure that the strength of the chosen web plates closely matched the design demands (to avoid having infill plate overstrength bias the findings of this study). For example, (i) the SPSW's tributary mass

could have been modified to match the strength of available hot rolled plates, (ii) regular perforation layouts in compliance with the AISC 341-10 requirements for “Special Perforated Steel Plate Walls” (AISC 2010) could have been detailed, or (iii) cold rolled steel plates could have been used. Given that all these approaches would lead to the same end-results, for expediency, the later approach was taken, knowing that satisfactory ductile behavior of SPSWs having such infill plates can be obtained (Berman and Bruneau 2005). Thus, light gauge steel ($F_y = 30$ ksi) was used for the infill plates. ASTM A572 Gr. 50 ($F_y = 50$ ksi) steel was selected for the VBEs and HBEs.

Based on the spectral acceleration maps in FEMA 450 provisions, the design short and one-second spectral ordinates, S_{DS} and S_{D1} , for the aforementioned site are 1.14g and 0.85g, respectively. The complete design spectrum for this structure is shown in figure 2-1 for an assumed 5% viscous damping ratio.

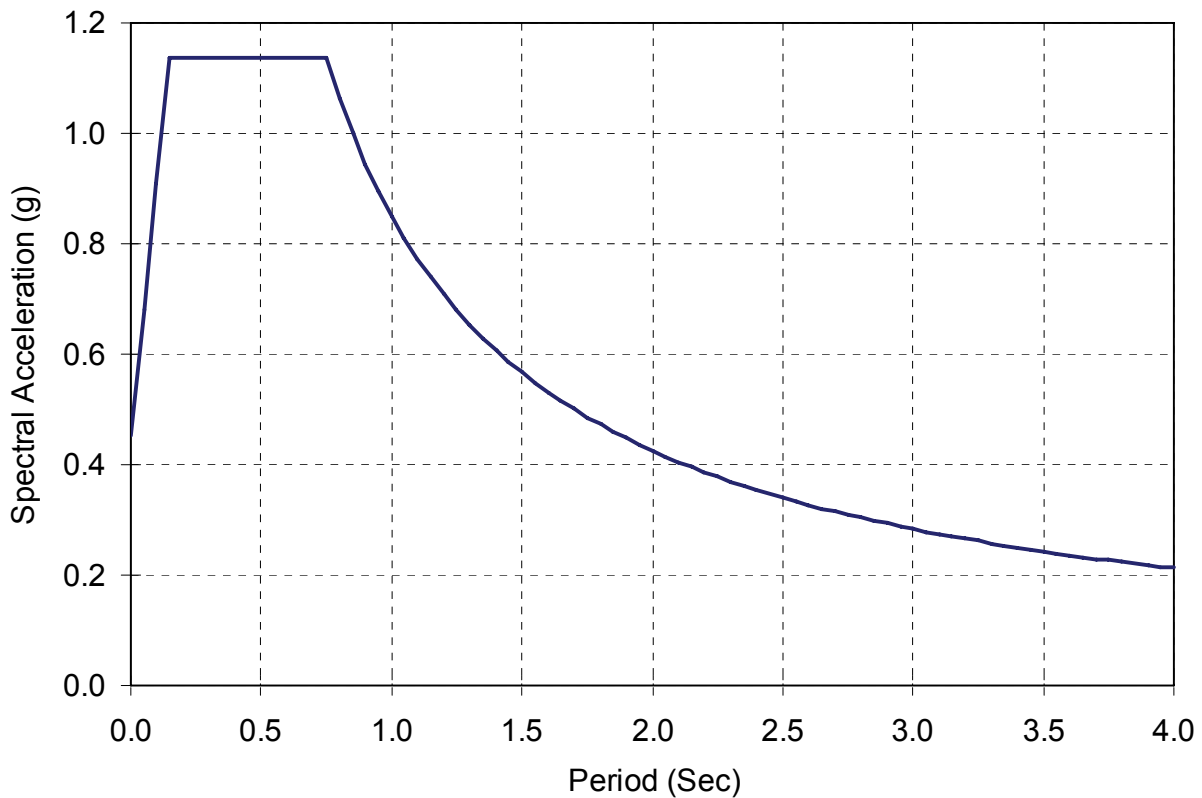


FIGURE 2-1 Design Response Spectra for San Francisco, California ($\xi = 5\%$)

The fundamental period of the structure T was estimated using the FEMA 450 procedures as 0.26 sec.; and using a response modification factor R of 7 and an importance factor I of 1, the total base shear V resisted by the structure is 176 kips. This base shear was distributed vertically using the following equation:

$$F_i = C_{vi} V = \frac{W_i h_i^k}{\sum_{i=1}^n W_i h_i^k} V \quad (2-1)$$

where C_{vi} is the vertical distribution factor for the i -th story; W_i is the i -th story weight; h_i is the height from the base to the i -th story; k is the natural period coefficient which equal to 1.0 for $T \leq 0.5$ sec., 2.0 for $T \geq 2.5$ sec, and linear interpolation value for intermediate values of T . The resulting values of lateral loads applied on each floor and story shear forces are summarized in table 2-1.

TABLE 2-1 Lateral Forces on Each Floor and Story Shear Forces

Level	Story Weight, W_i (kips)	Height from Base, h_i (ft)	Lateral Force, F_i (kips)	Story Shear Force, V_i (kips)
3 rd Floor (Roof)	351.60	30	91.44	91.44
2 nd Floor	351.60	20	56.28	147.73
1 st Floor	380.83	10	28.14	175.87
	1084.03		175.87	

In the current design procedures for SPSW, it is specified that infill plates must be designed to resist those shear forces, without considering the possible contribution to lateral strength that is provided by the infill plates' surrounding boundary frames. The required infill plate thickness to resist story shear forces can be obtained using the following equation:

$$t_{wi} = \frac{V_i \Omega_s}{\phi 0.5 R_{yp} F_{yp} L_p \sin(2\alpha)} \quad (2-2)$$

where V_i is the i -th story shear force; Ω_s is the system overstrength as defined in FEMA 369, and taken as 1.2 for SPSW (Berman and Bruneau 2003); ϕ is the strength resistance factor for the SPSW web and equal to 0.9; R_{yp} is the ratio of the expected to the specified steel plate yield stress, which in this case is assumed to be equal to 1.0; F_{yp} is the infill plate yield stress; L_p is the

clear length of the infill plate; α is the tension field inclination angle. Although the value of α is dependent on the geometric proportions of the boundary frames, for preliminary design it can be assumed as 42° from the vertical (Driver *et al.* 1997). Hence for this case study, the resulting infill plate thicknesses are 0.072, 0.059, and 0.036 in. for the first, second, and third floor, respectively. Note that the minimum plate thickness available in practice might be thicker than those. However, again, to avoid unnecessary overstrength design, those required thicknesses were assumed to be available (slightly thicker plates would have imparted greater demands on the HBEs, but not significantly changed the observed behavior described in later sections).

Two design procedures were then applied to design the boundary elements. They are: (1) the Indirect Capacity Design approach as described in the commentary to the 2005 AISC Seismic Provisions for Structural Steel Building (AISC 2005b) and (2) the design procedure proposed by Vian and Bruneau (2005) for HBE, combined with capacity design procedure of VBE proposed by Berman and Bruneau (2008) and referred to as the “Combined Plastic and Linear Analysis” in the commentary to the 2010 AISC Seismic Provisions (AISC 2010). Each design procedure is presented in the following sub-sections.

2.2.1 Indirect Capacity Design Approach (ICD)

According to the Indirect Capacity Design Approach, loads in the boundary elements can be determined from the gravity loads combined with equivalent seismic loads increased by the amplification factor

$$B_i = \frac{V_{ei}}{V_{ui}} \quad (2-3)$$

where V_{ei} and V_{ui} are the expected shear strength and lateral seismic force at floor i , respectively. The expected shear strength is calculated for the infill plate thickness provided, namely

$$V_{ei} = 0.5 R_{yp} F_{yp} t_{pi} L_p \sin(2\alpha) \quad (2-4)$$

where t_{pi} is the infill thickness provided and the other parameters have been defined previously. As mentioned previously, here the infill plate thickness provided is similar to that required (i.e., $t_{pi} = t_{wi}$). As a result, comparing (2-4) to (2-2), one can calculate that the amplification factor B_i is equal to 1.33, which basically is the ratio of the overstrength factor divided by the resistance factor (Ω_s/ϕ).

Following this procedure, a linear analysis program is typically used to analyze the SPSW and size the boundary elements. Here, the commercially available software SAP2000 v. 11.0.8 (CSI 2007) was used to size the optimum section for the VBEs and HBEs with the objective of obtaining demand-to-capacity ratio close to 1.0 (without exceeding it) when resisting the combination of gravity loads and earthquake loads increased by the amplification factor B_i . To expedite the design process, the *Auto Selection Sections* feature in SAP2000 was used such that the program automatically selects a W-section from the available AISC section list for each HBE and VBE which has sufficient strength to resist the applied load combination. In general, the SAP2000 auto-selection was based on the minimum weight criteria and in some cases it did not necessary satisfied the above optimum strength-based design criterion (i.e., the present objective to have demand-to-capacity ratio approaching 1.0). Hence, again, to avoid introducing overstrengths that could bias the subsequent findings, several manual modifications to the given sections were also conducted to achieve the optimum section. The resulting sizes of VBEs and HBEs are summarized in table 2-2 and the demand-to-capacity ratio for each element is displayed in parenthesis under the resulting section shape in figure 2-2(a). Note that the selected sections might not be the lightest W-section available and that the VBE section is varied from floor to floor, again, to insure that the following observations are not tainted by accidental overstrengths.

TABLE 2-2 Vertical and Horizontal Boundary Element Sizes

Boundary Frame Member ID⁽¹⁾	SPSW-ID	SPSW-CD
HBE-3	W16x36	W18x76
HBE-2	W12x22	W14x61
HBE-1	W12x19	W12x45
HBE-0	W24x62	W24x117
VBE-3	W16x40	W16x89
VBE-2	W18x50	W18x76
VBE-1	W24x62	W24x146

Note: ¹⁾ HBE and VBE at the i^{th} story are represented by HBE- i and VBE- i , respectively.

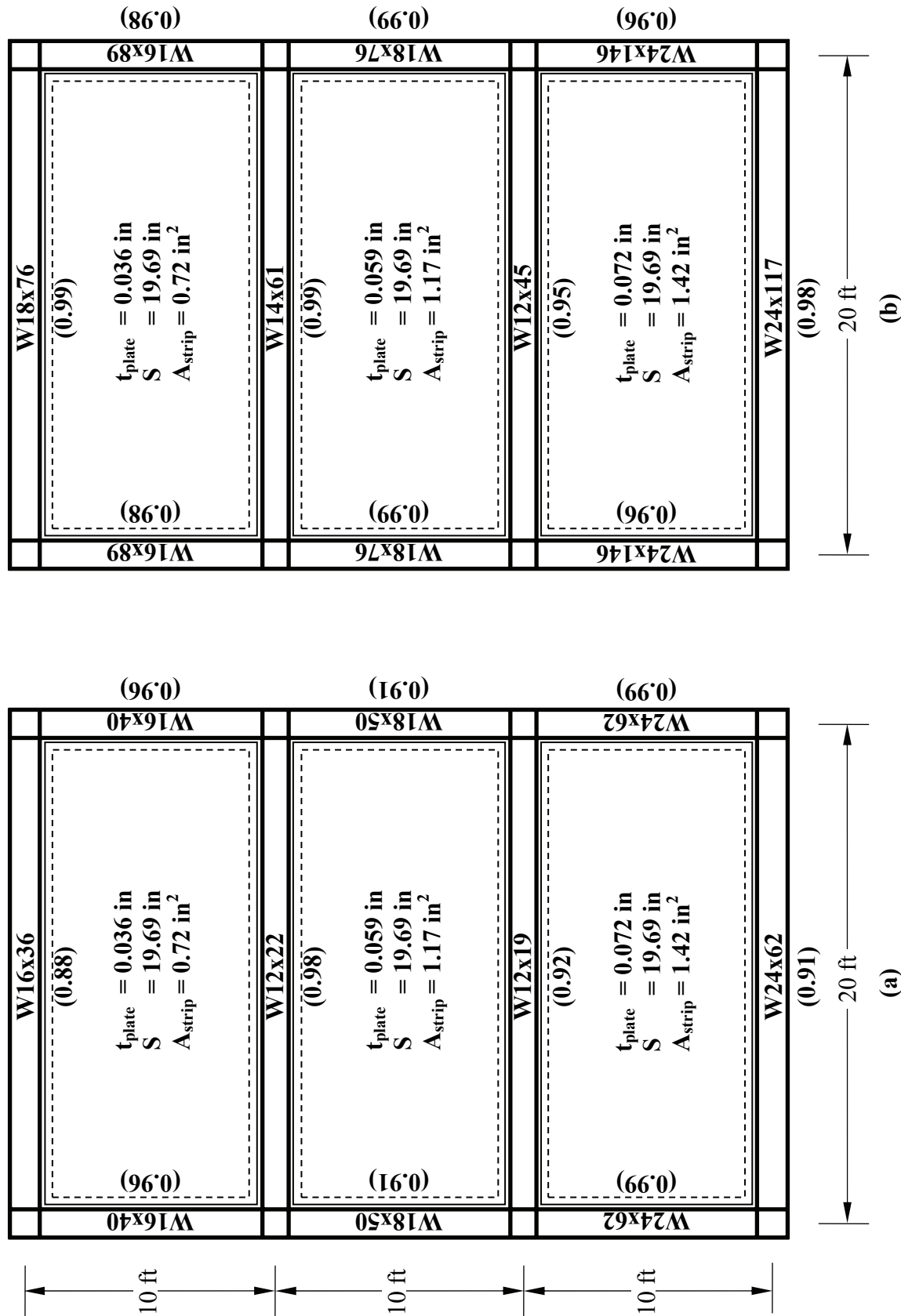


FIGURE 2-2 VBE and HBE Sizes with Demand to Capacity Ratio Results (a) SPSW-ID; (b) SPSW-CD

In addition, compactness of the selected VBE and HBE sizes, inter-story drift limits ($\leq 2\%$), and strong-column weak-beam requirements were also checked during the design process. Detail explanations of these design checks and the aforementioned design calculations are presented in Appendix A.

2.2.2 Combined Plastic and Linear Analysis (Capacity Design)

Vian and Bruneau (2005) proposed an equation to size anchor beams such that they can resist forces generated by fully yielding infill plates without developing in-span HBE plastic hinges. It estimates the minimum required HBE plastic modulus as follows:

$$Z_i = \frac{\omega_{ybi} L_b^2}{4 F_{yb}} \quad (2-5)$$

where L_b and F_{yb} are HBE span and yield stress, respectively; and ω_{ybi} is the vertical component of infill plate stress, calculated based on the infill plate properties and defined as:

$$\omega_{ybi} = F_{yp} t_{wi} \cos^2 \alpha \quad (2-6)$$

Though (2-5) was developed for anchor beams (bottom and top HBE), it can also be applied to the design of intermediate HBEs, by considering the net stress resulting from the adjacent top and bottom infill plates of different thicknesses.

Furthermore, VBEs were designed based on the procedure proposed by Berman and Bruneau (2008). It estimates the design loads for VBEs derived from the free body diagrams of the SPSW having a uniform plastic sway mechanism (i.e., full web yielding and plastic hinge at HBE ends) as shown in figure 2-3 for a generic four-story SPSW. The design loads for VBEs include distributed loads from infill plate yielding (ω_{xci} and ω_{yeci}); axial, shear and reduced plastic moment from HBEs (P_{bi} , V_{bi} , and M_{pri}); and applied lateral seismic loads that caused the uniform plastic sway mechanism. Detail explanation of how those components are determined can be found in the aforementioned reference. Having all those force components calculated and assuming lateral bracing at every floor, the VBEs were sized using the moment-axial interaction equation given by equation H1-1 of the AISC Specification for Structural Steel Buildings (AISC 2005a). Detail calculations for this approach are presented in Appendix B.

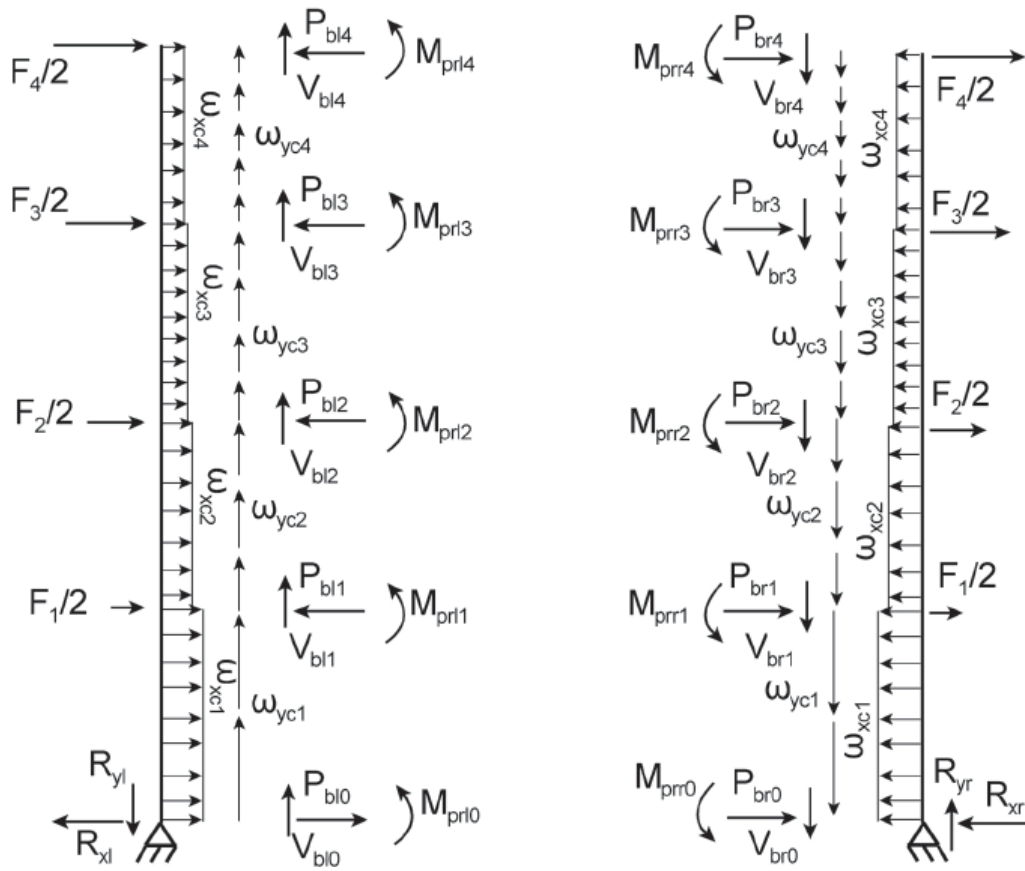


FIGURE 2-3 Free Body Diagrams (a) Left VBE; (b) Right VBE (Berman & Bruneau 2008)

In selecting the VBE and HBE sections, the same previously used optimum design objective (i.e., achieving a demand-to-capacity ratio close to 1.0, without exceeding it) was again followed. To compare with the previous design results, the sizes of VBEs and HBEs obtained by the two different design procedures are summarized in table 2-2 and demand-to-capacity ratio for each element is compared in figure 2-2. For SPSW designed by the capacity approach (the second approach), all the HBE demand-capacity ratios exceed 0.98, except one at 0.95. For SPSW designed by the indirect capacity approach (the first approach), the HBE ratios varied from 0.88 to 0.99; but this slight difference from the second SPSW case will not violate the conclusions reached by this study as will be shown later.

As presented in table 2-2 and figure 2-2, the two design approaches result in somewhat different boundary member sizes. For the same respective floor, the first design approach gives smaller VBE and HBE sizes compared to the second one. Subsequently, the SPSW resulting from the

first design approach that gives smaller size boundary elements will be denoted as SPSW-ID while the SPSW resulting from the second design approach that gives bigger size boundary elements as SPSW-CD, where the ID and CD labels stand for “Indirect Design” and “Capacity Design”, respectively.

2.3 Analytical Model Development

To investigate the behavior of both SPSW-ID and SPSW-CD, nonlinear static analysis (pushover analysis) and time history analysis were conducted. Two analytical models were developed for this purpose: (1) a strip model for monotonic pushover analysis and (2) a dual strip model for cyclic pushover analysis and time history analyses.

Originally proposed by Thorburn *et al.* (1983), the *Strip Model* consists of series of tension strips (of equal width), pin-ended and inclined in the direction of the tension field. Previous researchers have reported that this model can adequately capture the behavior of single-story as well as multistory SPSW with unstiffened infill plates (e.g., Timler and Kulak 1983; Tromposch and Kulak 1987; Driver *et al.*, 1998; Elgaaly 1998; Berman and Bruneau 2003, 2005; Qu and Bruneau 2008; etc.). In this study, twelve strips having an equal width S of 19.7 in. were provided at every floor to model the infill plates of the two 3-story SPSWs discussed in the previous section. Moreover, multiplying the strip width by the plate thickness of each floor, one obtains the strip gross area of 1.42, 1.17, and 0.72 in² for the first, second, and third floor, respectively (figure 2-2). In the SAP2000 v. 11.0.8 (CSI 2007) used to analyze those SPSWs, those strips were modeled as series of *Tension only Bracing Element*, which has strength only in tension but no strength in compression (as commonly done in such SPSW inelastic analyses). As for the VBEs and HBEs, they were modeled as regular *Frame Element*. Both steels used in these elements were represented by an idealized elasto-perfectly plastic stress-strain material (i.e., no strain hardening included, as conventionally done using simple plastic theory).

To capture nonlinear behavior of the structure, nonlinear hinges (plastic hinges) were also defined in the analytical models. Assuming development of the uniform plastic sway mechanism for multistory SPSW presented in Berman and Bruneau (2003), plastic hinges were located at

both ends of the HBEs and at the base of the VBEs. In addition, to capture yielding of strips, axial ‘hinge’ were located at every tension strip over the entire stories. Although the term ‘hinge’ is normally used for a flexural element (e.g., frame element), in the context of an axially loaded tension strip, the term ‘axial hinge’ used here for the numerical model of the strips should be understood as member-yielding under tension forces.

Furthermore, after running a nonlinear static analysis and observing the resulting moment distribution along the HBEs (as shown in figure 2-4 at 4% drifts), it was determined that structural elements capable of developing plastic hinges should be inserted at several other possible locations on the HBEs (in addition to those previously located on the span’s ends). As shown in figure 2-4(a) for SPSW-ID, the points of maximum positive and negative moments (where plastic hinges will likely develop) were located both at the ends of the HBEs and somewhere along their span; whereas they only occurred at the HBE ends for SPSW-CD as shown in figure 2-4(b). Hence, to develop a more general model and expedite the modeling process for both the monotonic and cyclic pushover analyses, plastic hinges were also defined at the quarter-, mid-, and third-quarter-span of each HBE. One might argue that introducing more plastic hinge elements along the HBE span (e.g., every one tenth of the HBE length) would have allowed to more closely approximate the exact location of the plastic hinges and thus give a more precise estimate of the SPSW ultimate strength. However, this additional computational expense would only lead to marginal benefits, as known from the study of plastic mechanism under uniformly distributed loads (e.g. Bruneau et al. 1998) – recognizing that the distributed tension loads from the infill plates act as a distributed load on the HBEs. The resulting strip model for monotonic pushover analysis showing all considered possible plastic hinges locations is shown in figure 2-5(a).

The *Axial-P Hinge* (one of several hinge models that SAP2000 offers) was chosen to define the inelastic behavior of the strips. This ‘hinge’ only accounts for yielding caused by axial loads, as is the case for the strips. Note that the default definition of this hinge considers yielding both in tension and compression. This model is satisfactory for monotonic pushover analysis, because in this analysis, the structure is only displaced in one direction [e.g. to the right in figure 2-5(a)], such that the strips will only experience tension forces. However, to develop the model from the

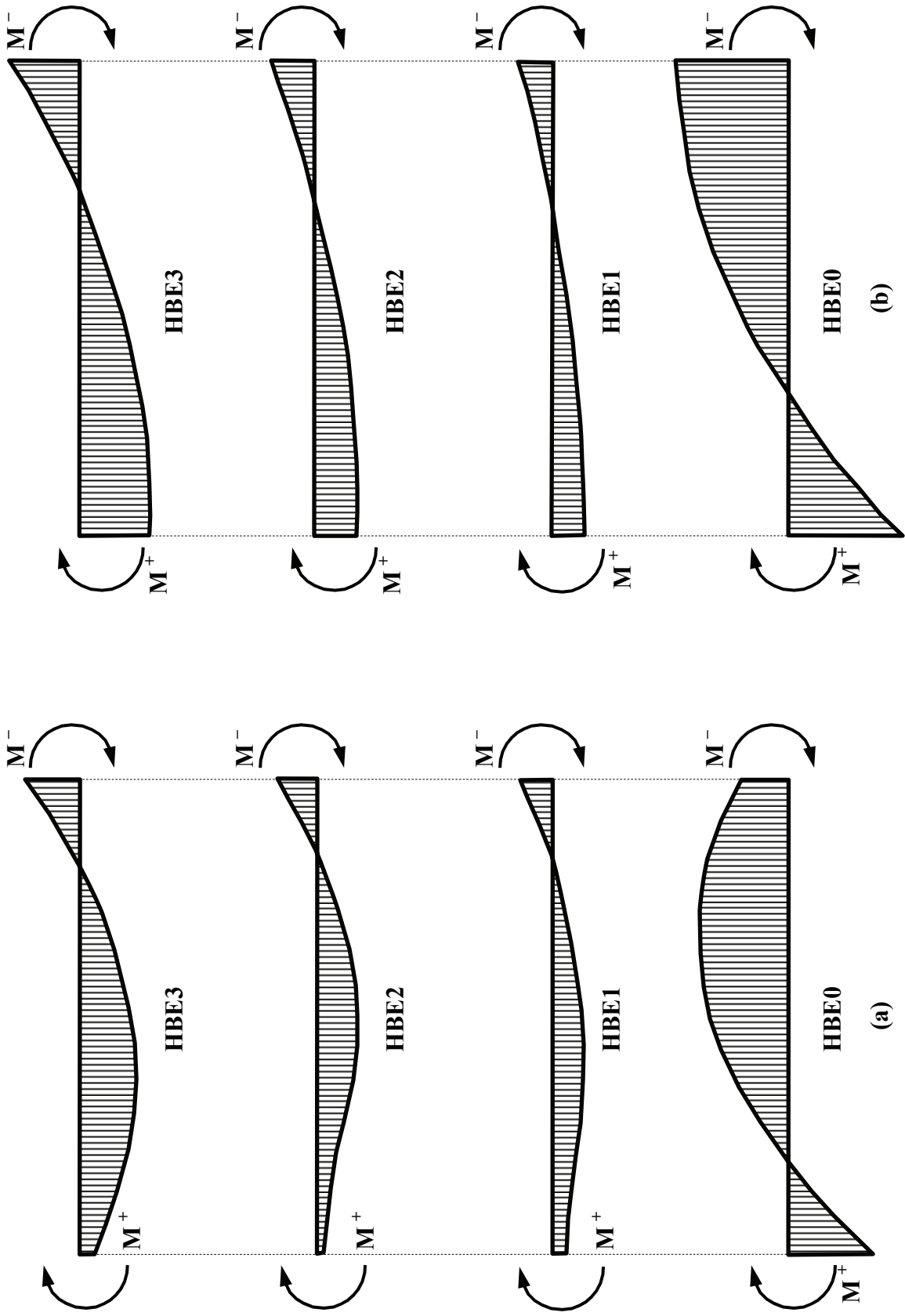


FIGURE 2-4 Schematic Moment Diagram along HBEs Obtained from Nonlinear Static Analysis at 4% Drifts
 (a) SPSW-ID; (b) SPSW-CD

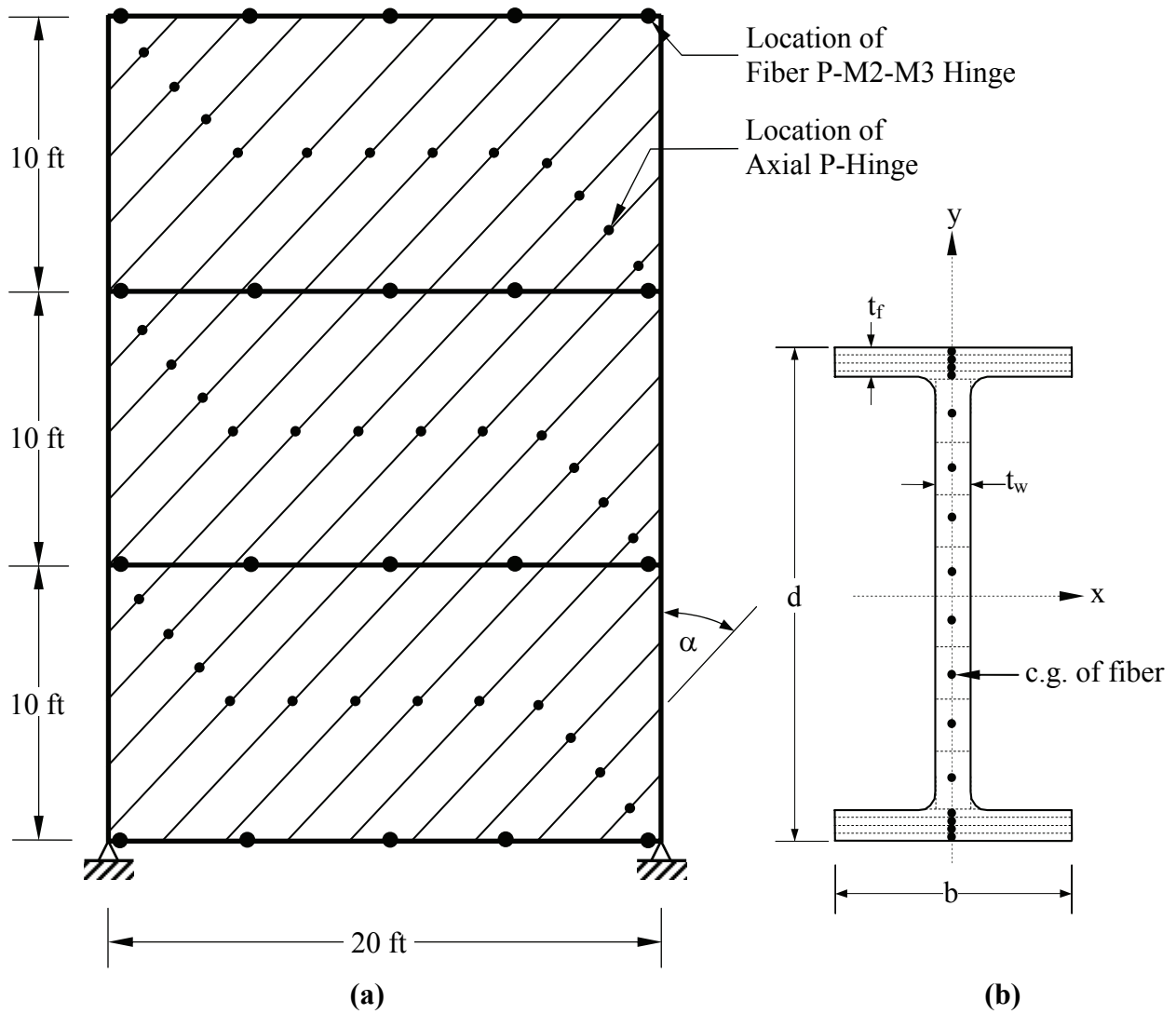


FIGURE 2-5 Strip Model for Monotonic Pushover Analysis (a) Location of Hinges; (b) Generic Fiber Hinge of W-cross Section; (c) Stress-Strain Curve for Axial-Hinge; (d) Stress-Strain Curve for Fiber-Hinge

onset to also accommodate the case of cyclic pushover analysis using the dual strip model, the ‘compression’ part in the hinge needs to be eliminated to match the actual behavior of the slender strips (i.e., resulting in a strip that can only yield in tension and without any compression strength or buckling elastically as soon as in compression). The process of how to define this behavior in SAP2000 will be presented in the discussion of the dual strip model as it becomes more relevant there. Here, the elasto-perfectly plastic stress-strain behavior assigned to this hinge is shown in figure 2-5(c). The reference point A to E plotted in the stress-strain curve follow their definition described in FEMA 356.

The *Fiber P-M2-M3 Hinge* was chosen to define plastic hinges in the VBEs and HBEs. This type of hinge automatically accounts for the interaction between the axial loads and moments that can occur in the HBEs and VBEs. Using this hinge model, a cross section is modeled as having several fibers with a certain tributary area and placed at specified locations along the cross section. In addition, each fiber can have its own stress-strain relationship (CSI 2007). Prior to selecting number of fibers, a limited case study was conducted to investigate the accuracy of numerical results by changing the number of fibers and verifying whether the *Fiber Hinge* matched the theoretical P-M interaction behavior. Figure 2-5(b) illustrates the application of fiber hinge on a generic W-cross section. In this example, the cross section was vertically sliced into 16 fibers, for which the center of gravity of each fiber is located along the Y-axis. Detail information about the tributary area of each fiber and its ordinate along the Y-axis for HBE sections of SPSW-ID are summarized in table 2-3. Each fiber was assigned the same stress-strain behavior, which is idealized as elasto-perfectly plastic material as shown in figure 2-5(d).

In addition, plastic hinge length was set equal to 90% of the associated member depth, which for the HBEs considered corresponds to lengths of 11 to 22 inches (or approximately 5% to 10% of the HBE length). Note that in the theoretical simple plastic analysis, it is generally assumed that plastic hinges are of zero-length. In reality, however, plastification develops over a certain length. That length depends on the applied loading, boundary conditions, and cross-section of a structural member (Liew and Shanmugam 2003). Moreover, in the implementation of the concept of plastic analysis for some computer programs (such as for SAP2000 used here), for some types of structural elements, a plastic hinge length must be defined for the element model to perform

TABLE 2-3 Fiber Hinge Tributary Area and Ordinate along Y-Axis (SPSW-ID)

Fiber ID	W16x36 (HBE-3)		W12x22 (HBE-2)		W12x19 (HBE-1)		W24x62 (VBE-0)	
	A _i (in ²)	Y (in)	A _i (in ²)	Y (in)	A _i (in ²)	Y (in)	A _i (in ²)	Y (in)
1	0.751	7.896	0.428	6.097	0.351	6.056	1.038	11.776
2	0.751	7.789	0.428	5.991	0.351	5.969	1.038	11.629
3	0.751	7.681	0.428	5.884	0.351	5.881	1.038	11.481
4	0.751	7.574	0.428	5.778	0.351	5.794	1.038	11.334
5	0.555	6.580	0.372	5.009	0.338	5.031	1.210	9.853
6	0.555	4.700	0.372	3.578	0.338	3.594	1.210	7.038
7	0.555	2.820	0.372	2.147	0.338	2.156	1.210	4.223
8	0.555	0.940	0.372	0.716	0.338	0.719	1.210	1.408
9	0.555	-0.940	0.372	-0.716	0.338	-0.719	1.210	-1.408
10	0.555	-2.820	0.372	-2.147	0.338	-2.156	1.210	-4.223
11	0.555	-4.700	0.372	-3.578	0.338	-3.594	1.210	-7.038
12	0.555	-6.580	0.372	-5.009	0.338	-5.031	1.210	-9.853
13	0.751	-7.574	0.428	-5.778	0.351	-5.794	1.038	-11.334
14	0.751	-7.681	0.428	-5.884	0.351	-5.881	1.038	-11.481
15	0.751	-7.789	0.428	-5.991	0.351	-5.969	1.038	-11.629
16	0.751	-7.896	0.428	-6.097	0.351	-6.056	1.038	-11.776
A _g ⁽¹⁾	10.448		6.403		5.510		17.991	

Note: ¹⁾ Total area of fibers is somewhat different from gross area listed in AISC section list because rounded shape areas, in the inner corner of W-section, were not counted.

correctly and for the program execute properly (CSI 2007). For reference, a cantilever beam of W-section (having a shape factor approximately equal to 1.12) with a concentrated lateral loads applied at its tip develops a plastic hinge length of about 10% of the beam length (Bruneau *et al.* 1998). Therefore, for the steel structure analyzed in this study, the above selected plastic hinge length is considered reasonable.

As expected from the case study investigating variation in the number of fibers, the larger number of fibers, the better the match to the theoretical results though the more computationally expensive the analysis is. Detail results of this case study are presented in Appendix C. Based on the results of this study, the cross sections of the W-sections used for the VBEs and HBEs were vertically sliced into 65 fibers (16 fibers on each top and bottom flanges, and 33 fibers on the web), with the fibers on the flanges and the web chosen to have somewhat similar tributary areas.

Moreover, the strip model shown in figure 2-5(a) can only capture the tension field in one direction. When the structure experiences reversed loading, as in the case of a cyclic pushover analysis or earthquake excitation, the model with unidirectional strips would be unable to capture the nonlinear behavior when displacing in the other direction. For this purpose, a dual strip model was developed to represent the infill plates accounting for reorientation of the tension field direction as loading direction changes.

Figure 2-6 displays the dual strip model. This model is similar to the previous model shown in figure 2-5, except that strips were added in the opposite direction at the same inclination angle. Plastic hinge definitions in the VBEs, HBEs, and tension strips are similar to the ones described previously; however for clarity they are not shown in the figure. Qu and Bruneau (2008) reported that the dual strip model (with 15 strips in each direction to analytically model a two-story SPSW) adequately replicated the global behavior of the structure subjected to pseudo-dynamic loading. In the SAP2000, these new strips were developed using the *Mirror Replicate* procedure by rotating (flipping) the existing strips along a vertical axis (the Z-axis) at the geometric center of the frame.

As mentioned previously, to capture the actual behavior of the slender strips that can yield in tension but have no compression strength (i.e. that buckle elastically in compression), the ‘compression’ part in the definition of the *Axial-P Hinge* model must be eliminated. Before presenting the customized *Axial-P Hinge* used here, it is important to elaborate here how inelastic axial hinge properties are defined by SAP2000. In general, the program automatically generates inelastic hinge properties of an axial member based on the provided cross-section and its material properties. Therefore, for any of the strips used here, the program automatically calculated the

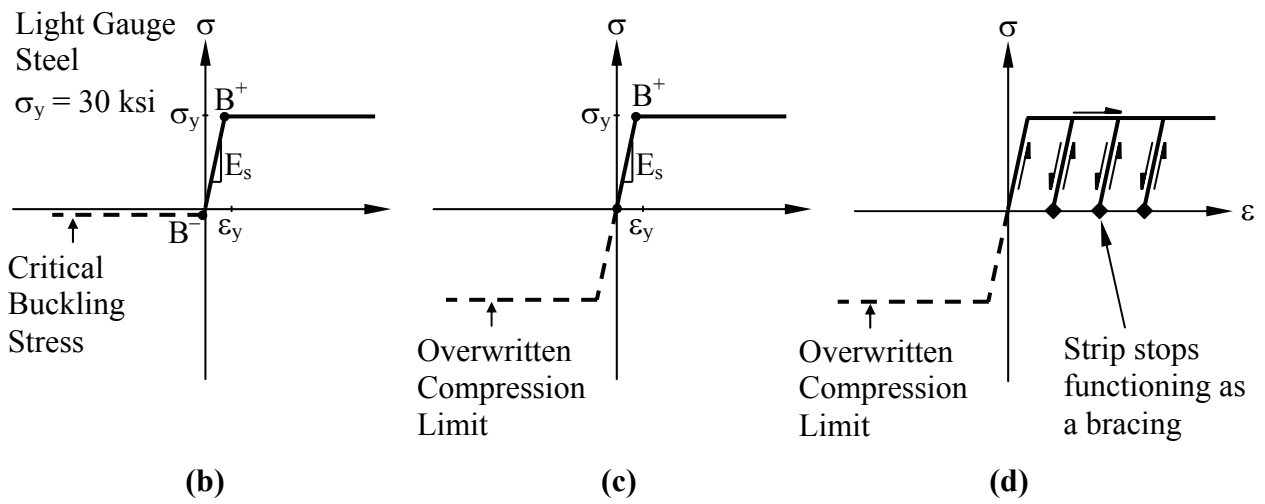
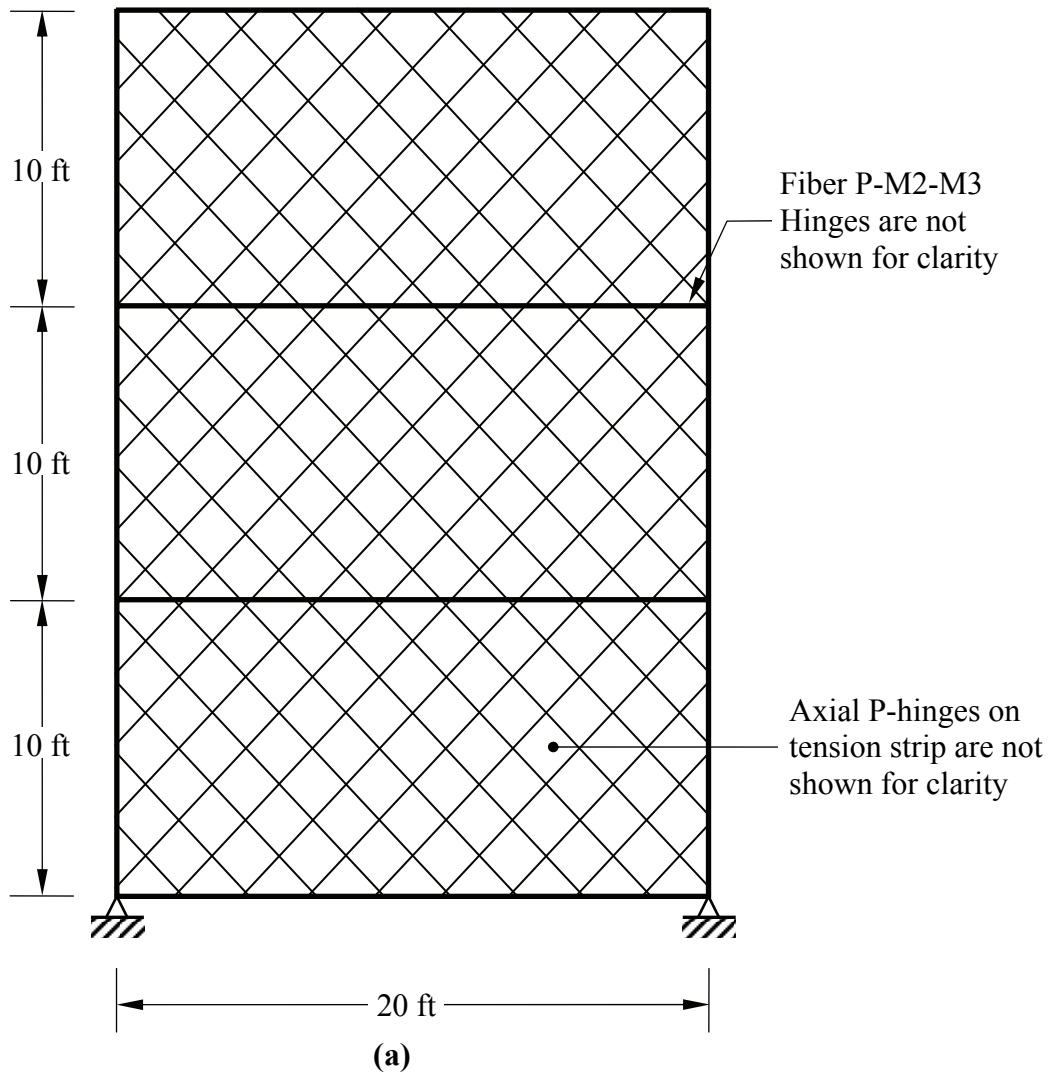


FIGURE 2-6 Dual Strip Model for Cyclic Pushover and Time History Analyses
(a) Schematic of Dual Strips; (b) Behavior of Slender Strip; (c) Modified Hinge Definition;
(d) Generic Strip Hysteretic Behavior

elastic limits both for tension and compression conditions. Those limits were associated with the yield stress and critical buckling stress of the strip, respectively. Since the strips used in the model were extremely slender (i.e., having a high slenderness ratio), the resulting compression limit of a typical pin-ended strip was significantly low as illustrated in figure 2-6(b). Note that points B^+ and B^- on the positive and negative regions correspond to the yield stress in tension and the critical buckling stress in compression, respectively. When these default SAP2000 axial hinge properties were used, the program flagged the strip that was in compression at the beginning of pushover displacement as being a “failed member”; and during cyclic inelastic push-over analysis, when lateral displacement of the SPSW reversed direction, the program also flagged the strip that was previously in tension and subsequently underwent compression as being a “failed member”; and this happened at a considerably low drift. As a consequence, the failed strips stopped contributing to hysteretic energy dissipation even when in subsequent cycles the strips were in tension, which is not the intended behavior.

Theoretically, a *No Compression Strength* feature exists in SAP2000 that can be activated to prevent the failure of the strip in compression as described above and achieve the intended behavior. In other words, activating this feature enables the program to keep the strip functioning (without becoming “failed”) as a bracing element during the cycles which the strip experiences compression forces. Physically, it means that the strip buckles elastically. The program in this case remembers the last deformation of the strip corresponding to the occurrence of buckling and the strip must recover all of its elastic buckling deformation before it can dissipate energy once more. However, this scheme did not work properly, and the program still flagged the corresponding strip as a failed member. It was believed that the extremely low compression limit of the strip (i.e., close to zero) was responsible to this condition. Therefore, to avoid this incorrect behavior, the near-zero compression limit of the axial strip computed by the program [illustrated in figure 2-6(b)] was overwritten with an arbitrary value that was large enough compared to the previous critical buckling stress while simultaneously activating the *No Compression Strength* feature of SAP2000 to prevent the strip dissipating energy in compression. To expedite the process, the compression limit was set to be equal to the tension limit as shown in figure 2-6(c). This was done by manually copying the available tension limits from the previous generated hinge properties (i.e., no need to change the strip cross-section and its material properties). A

generic hysteretic curve of the strip having the modified axial hinge properties is shown in figure 2-6(d). In the figure, the point where the strip stops functioning as a bracing element is shown by the diamond dots. Case study analyses verified that this desired correct behavior was exhibited by each individual strips.

There is another approach available in SAP2000 to model tension-only bracing element via utilizing the *Hook Element*. This approach can also work, but is more convoluted compare to the one described above. For reference, Appendix D explains how this approach can be used for this purpose.

2.4 Summary

A three-story single-bay SPSW has been designed with two different philosophies. A common design approach encountered in practice, the Indirect Capacity Design Approach, was used to design the first shear walls (SPSW-ID). This approach does not guarantee that formation of in-span plastic hinges on horizontal boundary elements will be prevented. The second shear walls (SPSW-CD) was designed by the Capacity Design Approach which guarantees that plastic hinges can only occur at the ends of horizontal boundary elements. For the purpose of investigating their behavior (presented in the subsequent sections), strip models for monotonic pushover analysis and dual strip models for cyclic pushover analysis and time history analysis were developed to represent both SPSWs in the SAP2000 analyses. The *Axial-Hinge* and *Fiber-Hinge* were chosen to define the inelastic behavior of the infill plates and the boundary elements, respectively. The behavior of steels used was represented by an idealized elasto-perfectly plastic stress-strain material.

SECTION 3

NONLINEAR STATIC ANALYSIS

3.1 General

Using the numerical models developed in the preceding section, nonlinear static analysis is conducted in this section to investigate the possible significance of in-span plastic hinge developed on horizontal boundary elements (HBE). For this purpose, behavior of two shear walls (i.e., SPSW-ID and SPSW-CD) subjected to monotonic and incrementally cyclic pushover loadings is examined, which includes comparing global plastic strength, plastic hinge and strip yielding distributions, vertical and residual deformations on HBE, and HBE plastic rotation demands. In addition, a general equation to calculate the ultimate strength of both single and multistory SPSW with in-span plastic hinge (i.e., sway and beam combined mechanism) is developed using the kinematic method of plastic analysis. Several key behaviors observed during a cycle by cycle investigation on HBE deformation history under the cyclic pushover loading are identified.

3.2 Monotonic Pushover Analysis

A monotonic pushover analysis was conducted for both SPSW-ID and SPSW-CD until each structure reached a 4% lateral drift. Here, lateral drift is defined as the horizontal deformation at roof level divided by the total height of the structure of 360 in. A 4% drift corresponds to a 14.4 in roof lateral displacement. The inverted triangular vertical distribution presented in the FEMA 450 document was chosen to model the distribution of lateral loads along the height of the building; the vertical distribution coefficient for each floor follows the C_{vi} term expressed in (2-1). Note that in the particular SPSWs considered here, since the estimated fundamental period of the structure was less than 0.5 sec., the C_{vi} indeed gave an inverted triangular vertical distribution. In addition, it was assumed that lateral forces acting at every floor level were transferred equally to the left and right sides of the SPSWs.

Material non-linearities provided in a numerical model can lead to divergence problems. In the models at hand, those non-linearities mainly arise from the large number of plastic hinges used,

especially in the HBEs and VBEs with the *Fiber hinges*. To overcome possible divergence problems, a relatively small displacement increment was chosen for the analysis, by specifying a minimum of 100 steps to reach each incremental 1% drift. However, in most instances, the program automatically further reduced the increment as needed, up to 1000 steps to reach the same 1% incremental drift. In other words, the displacement increments varied from 0.0036 to 0.036 inches. In addition, the *Event-to-event* algorithm was turned off, which is appropriate for a model with a large number of plastic hinges (CSI 2007). Other nonlinear solution controls, such as type of iteration algorithms (the Newton-Raphson iteration was used), number of iterations at each step (40 iterations were used), and iteration convergence tolerance (i.e., 10^{-4}) were set to the default values recommended by the SAP2000.

Figure 3-1 shows the monotonic pushover results for both SPSW-ID and SPSW-CD. At 4% drift, the base shears are 311 and 477 kips for the respective structures. In addition, the theoretical values are also plotted in the figure (indicated by the dash lines). These values were obtained from the plastic analysis equations derived by Berman and Bruneau (2003) for uniform plastic sway mechanism. The governing equation for that plastic mechanism is:

$$\sum_{i=1}^{n_s} V_i H_i = 2 \sum_{i=0}^{n_s} M_{pbi} + \sum_{i=1}^{n_s} \frac{1}{2} F_{yp} L_p (t_{wi} - t_{wi+1}) \sin(2\alpha) H_i \quad (3-1)$$

where V_i is the applied lateral load at the i -th story; H_i is the height from the base to the i -th story; M_{pbi} is the plastic moment of HBE at the i -th story and the factor 2 reflects the two possible plastic hinge locations at HBE ends; and the other parameters have been defined previously.

To calculate the base shears, from (3-1), that correspond to the uniform plastic sway mechanism, it is necessary to assume a distribution of the lateral loads over the height of the structure; in this case, the relationship between V_1 , V_2 , and, V_3 . As mentioned previously, the lateral load distribution follows an inverted triangular shape. Hence, by applying (2-1), one can obtain the following relationships:

$$V_1 = 0.16V \quad V_2 = 0.32V \quad V_3 = 0.52V \quad (3-2)$$

and by substituting (3-2) into (3-1), one can calculate the theoretical base shears of 351 and 488 kips for SPSW-ID and SPSW-CD, respectively.

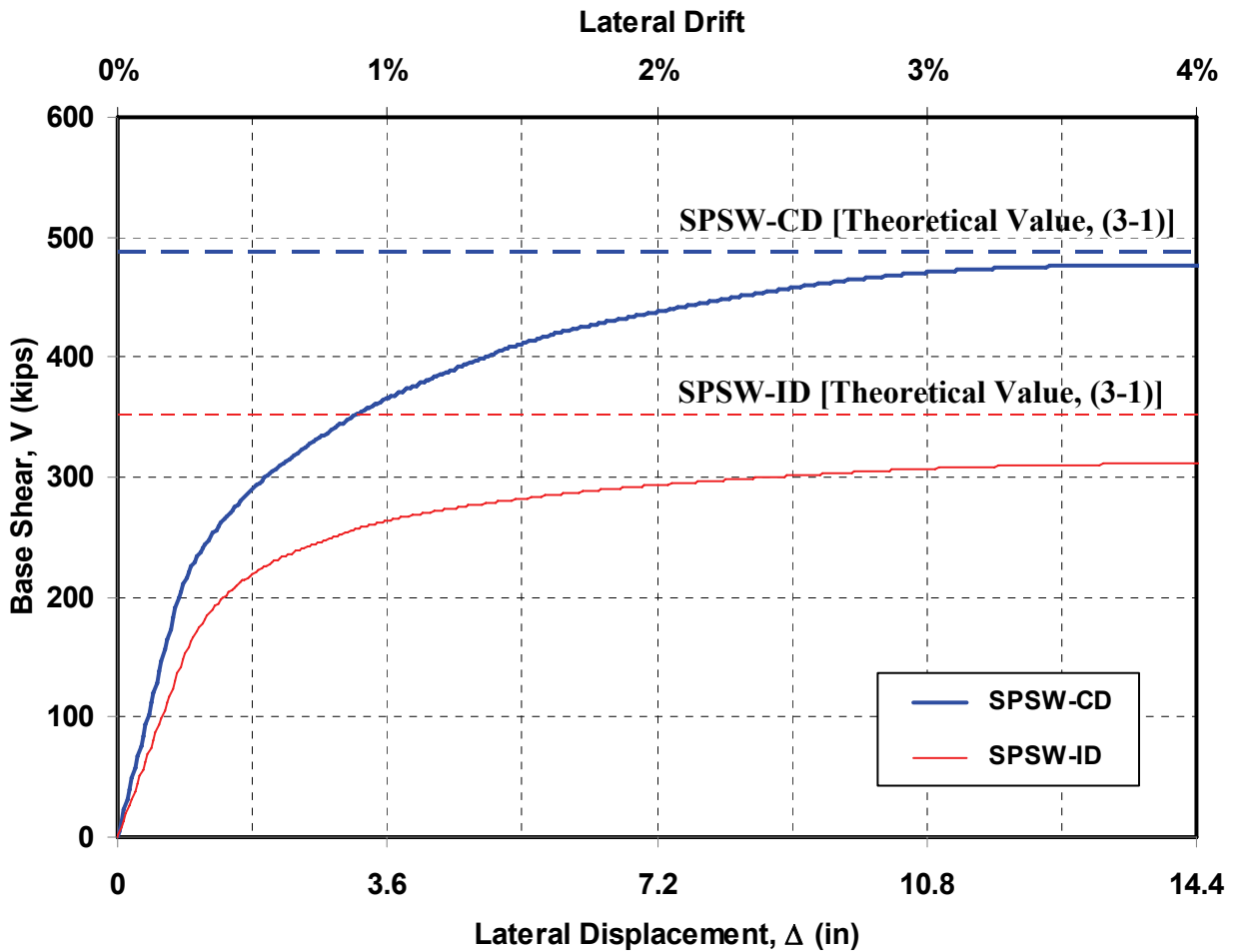


FIGURE 3-1 SAP2000 Monotonic Pushover Analysis versus Plastic Analysis Calculations

As compared in figure 3-1 for SPSW-CD, the base shear obtained from the monotonic pushover analysis using SAP2000 and the theoretical calculations using the plastic analysis approach are in a good agreement. The difference between the two is only 2.3% at 4% drift. Several factors explain this small discrepancy, namely: (1) some fibers, especially those that are closer to the plastic neutral axis, remain elastic even at 4% drift, while in the theoretical calculation, the cross section was assumed to exhibit a fully plastic condition; (2) reduction of HBE plastic moment capacity due to axial loads was not considered in the theoretical calculation, while that reduction is automatically considered in the calculation of the fiber hinge plastic moment capacity; (3) tension field angle in the SAP2000 model was 42°, similar to the one used in the preliminary design, while an updated angle of 44°, calculated using the AISC equation for the selected HBEs and VBEs sections, was used for the theoretical calculation; and (4) the area of the rounded

flange-to-web intersection in W-sections were neglected in calculation of the total area of the fiber hinges, which creates a slightly smaller HBE cross section area and plastic moment compared to that of used in the theoretical calculation. For theoretical calculation revised by considering individually each of the above factors, the theoretical base shears are reduced by 1.2%, 0.2%, 0.3%, and 0.4% for the above respective factors. Summing these percentages gives a total reduction for the combination of those individual factors of 2.1%, which is slightly less than the 2.3% discrepancy reported above. It is speculated that the remaining (and meaningless) difference of 0.2% is due to the interaction of those factors.

However for SPSW-ID, the theoretical base shear is significantly different from that obtained from the monotonic pushover analysis: a 13% disparity exists between the two results. Moreover, even if those factors listed above that account for the discrepancy of results in SPSW-CD are applied to this condition; further justification is needed to resolve the remaining 11% disparity. This discrepancy can be explained by observing the plastic mechanism obtained from the SAP2000 analyses compared to the assumed theoretical uniform plastic sway mechanism.

Figure 3-2 displays plastic hinge and strip yielding distributions at 4% lateral drift for SPSW-ID and SPSW-CD. Note that the current version of SAP2000 used in this analysis (i.e., SAP2000 v. 11.0.8) only provides direct graphical information for strip yielding (translated in the figure as the broken lines) but not for the plastic condition of *Fiber Hinges* used in the HBEs and VBEs. As a result, one needs to individually review the flexural moment magnitude and apply some judgment to assess whether “fully plastification” has occurred at a given cross section. Since it is numerically impossible to expect all the fibers of a cross-section to yield (unless curvature reaches infinity), flexural moment at a given cross section never perfectly equals to the theoretical plastic moment, but the earlier results show that 99% of the plastic moment can be approximately reached at 4% drift. Here, it is conservatively assumed that a fully plastic condition (shown in the figure as the solid circular markers) is reached if the flexural moment is equal to or higher than 97% of its theoretical plastic moment. Further explanation of this assumption is presented in Section 3.4.1.

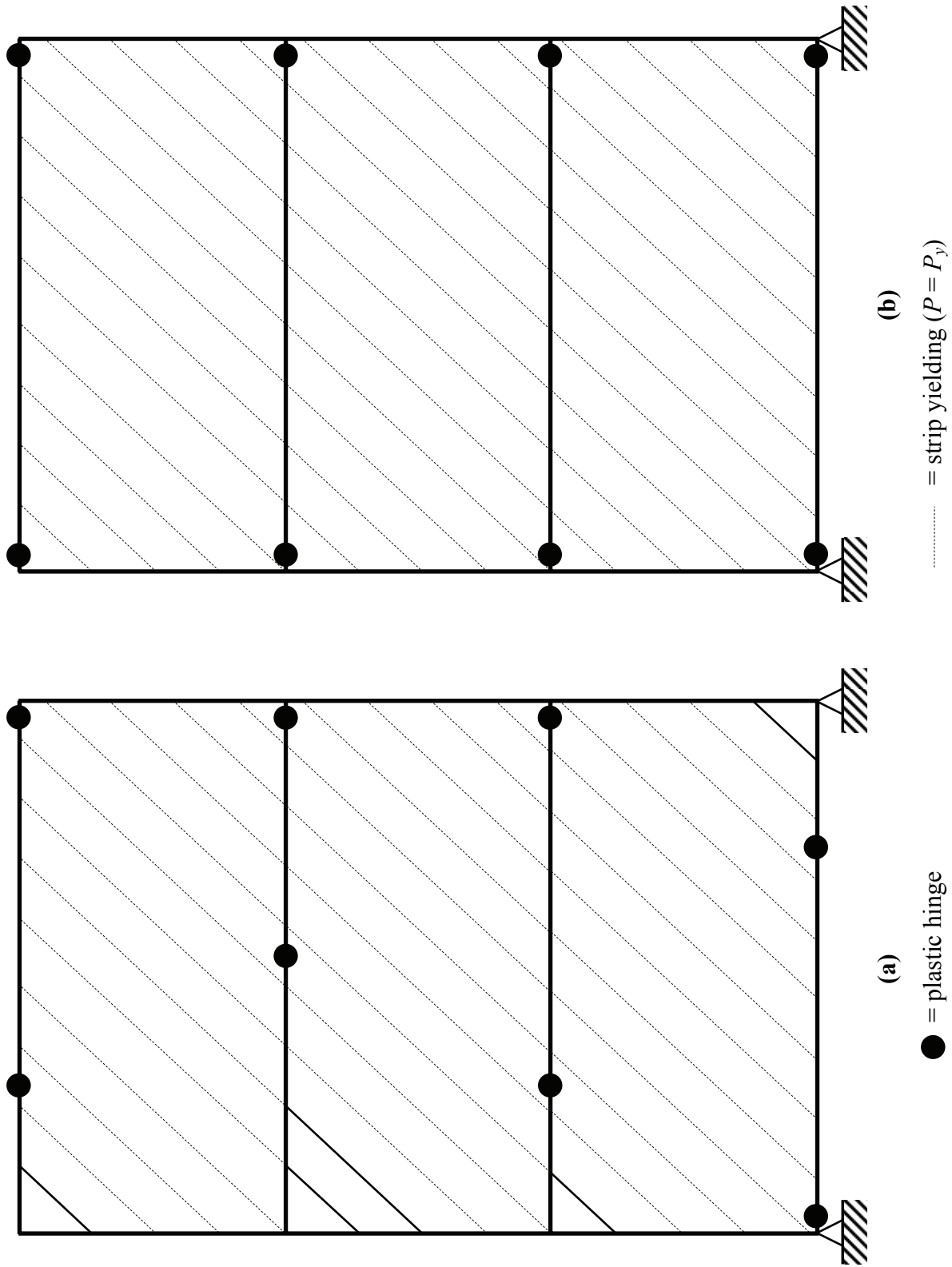


FIGURE 3-2 Plastic Hinge and Strip Yielding Distributions at 4% Lateral Drift (a) SPSW-ID; (b) SPSW-CD

As shown in part (a) of figure 3-2, five out of 36 strips in SPSW-ID remain elastic and four out of eight HBE ends did not develop plastic hinges. By contrast to the assumed uniform plastic mechanism described in the commentary to AISC Seismic Provisions (2010), four in-span plastic hinges have developed on the HBEs of SPSW-ID. Hence, SPSW-ID certainly does not follow the uniform plastic sway mechanism (also known as ‘panel mechanism’) but rather consists of a ‘sway’ and ‘beam’ combined mechanism. The significant vertical deformations along the HBEs spans of SPSW-ID shown in figure 3-3(a) confirm development of this mechanism. For example on the second and top floor HBEs, vertical deformations observed at their span are 4.3 and 2.4 inches at 4% drift, respectively. Note that results at 3% drift are also presented in the figure for further comparison to the cyclic pushover analysis, which was conducted up to that point. This behavior is consistent with the moment distributions along the HBEs of SPSW-ID shown in figure 2-4(a), for which the maximum moment locations (where plastic hinges will likely develop) are both at HBE ends and somewhere along the HBE spans. A schematic of this combined mechanism will be presented in a later section.

By comparison, all strips in SPSW-CD have yielded and plastic hinges occurred at each HBE end (i.e., total 8 plastic hinges). Though the *Fiber Hinge* elements were also present along the HBE span of SPSW-CD (at the same locations as for the SPSW-ID case), no in-span plastic hinge developed. Hence, this confirms that SPSW-CD follows the uniform plastic sway mechanism.

3.3 Plastic Analysis of SPSW having In-Span HBE Plastic Hinge

As reported in the previous section, plastic hinges developed along the span of the HBEs (rather than just at their ends) for the SPSW-ID design. It was also shown that the plastic mechanism of the SPSW-ID design did not match a uniform plastic sway mechanism but rather consisted of a ‘sway’ and ‘beam’ combined mechanism. Consequently, (3-1), developed for the case of uniform plastic sway mechanism where plastic hinges only occur at HBE ends, is not valid to calculate the ultimate base shear forces that will develop a SPSW-ID plastic mechanism. This explains why a 13% disparity of results for SPSW-ID between the SAP2000 result and the theoretical calculation using (3-1) was observed.

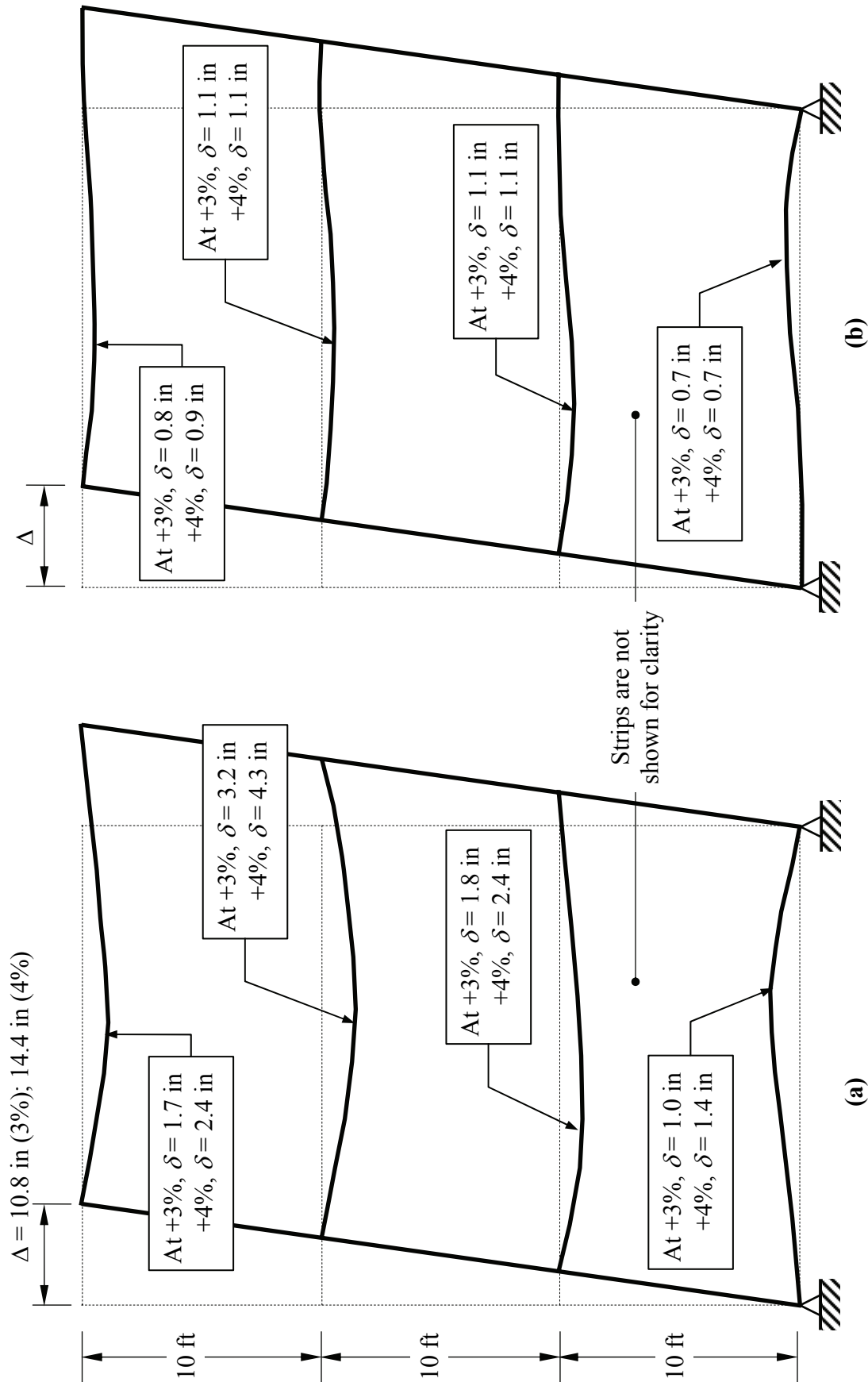


FIGURE 3-3 Schematic Deformed Shapes of Monotonic Pushover Analysis (a) SPSW-ID; (b) SPSW-CD

Therefore, building on the work of Berman and Bruneau (2003), the kinematic method of plastic analysis is used here to calculate the theoretical ultimate strength of a SPSW having a ‘sway’ and ‘beam’ combined plastic mechanism (i.e., accounting for possible plastic hinges along its HBE span). Prior to develop a general equation for multistory SPSW, it is convenient to start with single story SPSW. Here, consider a schematic of the combined plastic mechanism for the single story SPSW shown in figure 3-4.

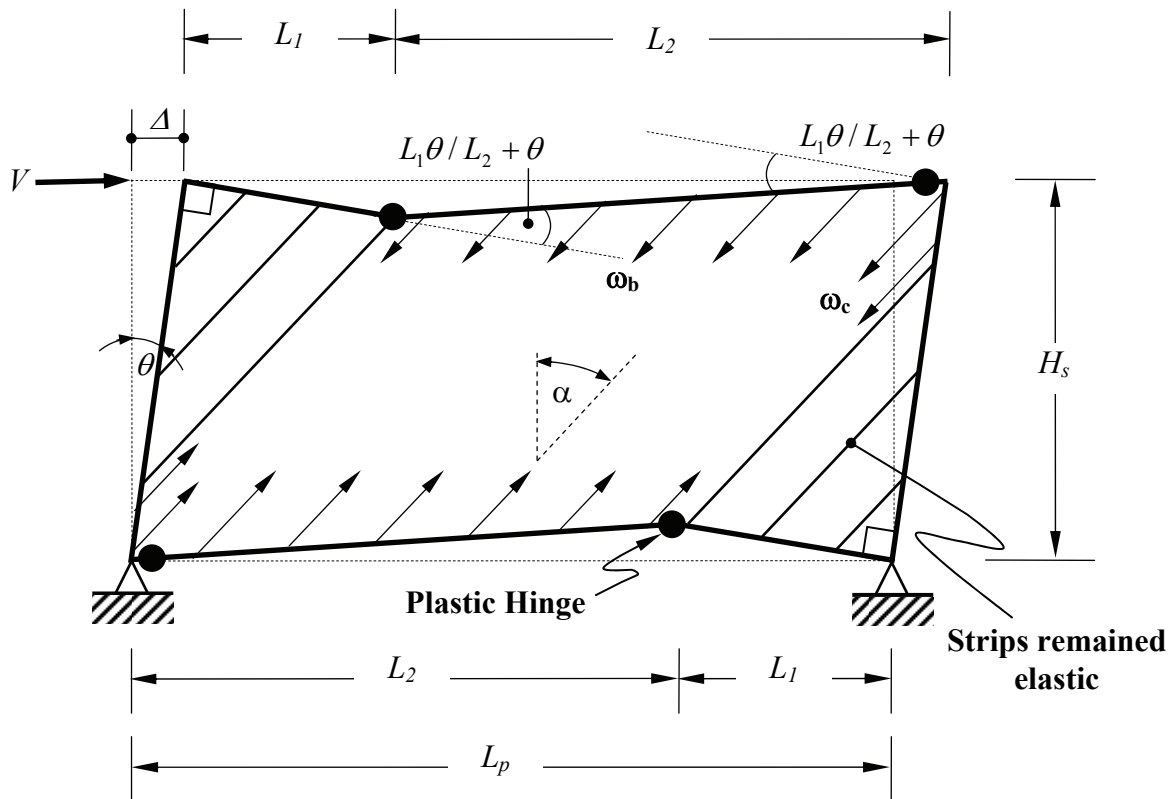


FIGURE 3-4 Sway and Beam Combined Plastic Mechanism for Single Story SPSW

When the shear force V displaces the top HBE by a magnitude Δ , the generated tension forces in the infill plates cause plastic hinges to develop both on the top and bottom HBEs at the same distance L_1 from the top-left and bottom-right joints, respectively. As a result, some of the infill plates (shown in the figure close to the top-left and bottom-right corners) remain elastic. The external work ($W_{external}$) produced by the shear force V is calculated as follows:

$$W_{external} = V \Delta = V H_s \theta \quad (3-3)$$

where Δ is the top HBE lateral displacement; H_s is the story height; and θ is the angle between the deformed structure and the vertical, which is also equal to the top HBE lateral displacement over the story height. On the other side of the equality, there are two components that contribute to the internal work, namely, work done by the plastic hinges on the HBEs and by the strips. The first component of internal work ($W_{internal_1}$) can be calculated as follows:

$$W_{internal_1} = (2M_{pb0} + 2M_{pb1}) \left(1 + \frac{L_1}{L_2}\right) \theta \quad (3-4)$$

where M_{pb0} and M_{pb1} are the plastic moment of the bottom and top HBE, respectively, with each HBE having two plastic hinges; and L_1 and L_2 are as shown in figure 3-4. As for the internal work done by the strips, only work by the yielding infill plates is included (the contribution from the elastic infill plates is neglected, as all other elastic work, in accordance to plastic theory). To calculate the strips contribution, it is easier to use the horizontal and vertical components of the strip yield forces. The distributed vertical and horizontal component of the strip yield forces on the VBEs are denoted as ω_{yc} and ω_{xc} , respectively; while on the HBEs, they are denoted as ω_{yb} and ω_{xb} for the same respective components. Their values can be determined as follows (Berman and Bruneau 2008):

$$\omega_{yc} = \frac{1}{2} F_{yp} t_w \sin(2\alpha) \quad \omega_{xc} = F_{yp} t_w \sin^2 \alpha \quad (3-5a)$$

$$\omega_{yb} = F_{yp} t_w \cos^2 \alpha \quad \omega_{xb} = \frac{1}{2} F_{yp} t_w \sin(2\alpha) \quad (3-5b)$$

Since the vertical deformation on the VBEs and the horizontal deformation on the bottom HBE are negligible, both ω_{yc} on the VBEs and ω_{xb} on the bottom HBE produce no internal work. Though the ω_{xc} does produce internal work, for simplicity, however, its contribution can be neglected. This is considered reasonable because the ω_{xc} on the left VBE produce negative internal work while the ω_{xc} on the right VBE produce positive internal work (Berman and Bruneau 2003) such that the net results between the two are considerably small. Therefore, only the ω_{xb} on the top HBE and ω_{yb} on both HBEs produce internal work; and all of them produce positive internal work. The internal work produced by these components is calculated as follows:

$$W_{internal_2} = \frac{1}{2} F_{yp} t_w \sin(2\alpha) L_2 H_s \theta + 2F_{yp} t_w \cos^2 \alpha L_2 \frac{L_1}{2} \theta \quad (3-6)$$

where all parameters are as defined previously. Equating the external and internal work [(3-3), (3-4), and (3-6)] gives the following general equation to calculate the ultimate strength of single story SPSW with combined mechanism:

$$V H_s = (2 M_{pb0} + 2 M_{pb1}) \left(1 + \frac{L_1}{L_2} \right) + \frac{1}{2} F_{yp} t_w \sin(2\alpha) L_2 H_s + 2 F_{yp} t_w \cos^2 \alpha L_2 \frac{L_1}{2} \quad (3-7)$$

Expanding from this knowledge for a single story SPSW, consider a schematic of the same combined plastic mechanism but for the multistory SPSW shown in figure 3-5. In general, this mechanism is somewhat similar to that of the single story SPSW in terms of the applied shear force at every story V_i displacing the corresponding floor by a magnitude Δ_i , the inadequacy of the HBE to resist the yielding forces causing in-span plastic hinges (in addition to plastic hinge at HBE end), and partially yielding infill plates.

Here, the total external work ($W_{external}$) is the summation of works produced by each shear force V_i as follows:

$$W_{external} = \sum_{i=1}^{n_s} V_i H_i \theta \quad (3-8)$$

where H_i is the height from the base to the i -th story; n_s is total number of stories; and the other parameters have been defined previously. Moreover, the total internal work produced by the plastic hinges ($W_{internal_1}$) on the HBEs is expressed by the following equation.

$$W_{internal_1} = 2 \sum_{i=0}^{n_s} M_{pbi} \left(1 + \frac{L_1}{L_2} \right) \theta \quad (3-9)$$

Note that since a strong-column weak-beam design approach is mandated in the design of SPSW, plastic hinges are assumed to develop in the HBEs instead of in the VBEs. This explains why only the plastic moment capacity of the HBE at every floor is captured by (3-9).

Furthermore, regarding the internal work produced by the strips, the strip yield forces acting on the anchor beams (i.e., the top and bottom HBEs) produce positive internal work while the forces acting on the intermediate HBEs produce both positive and negative work (i.e. the strip yield forces acting on the bottom of an HBE at a particular story produce positive internal work while

the strip forces acting on top of the same HBE produce negative internal work, as shown in Berman and Bruneau 2003). Thus, the total internal work produced by the yielding strips ($W_{internal_2}$) is expressed in (3-10).

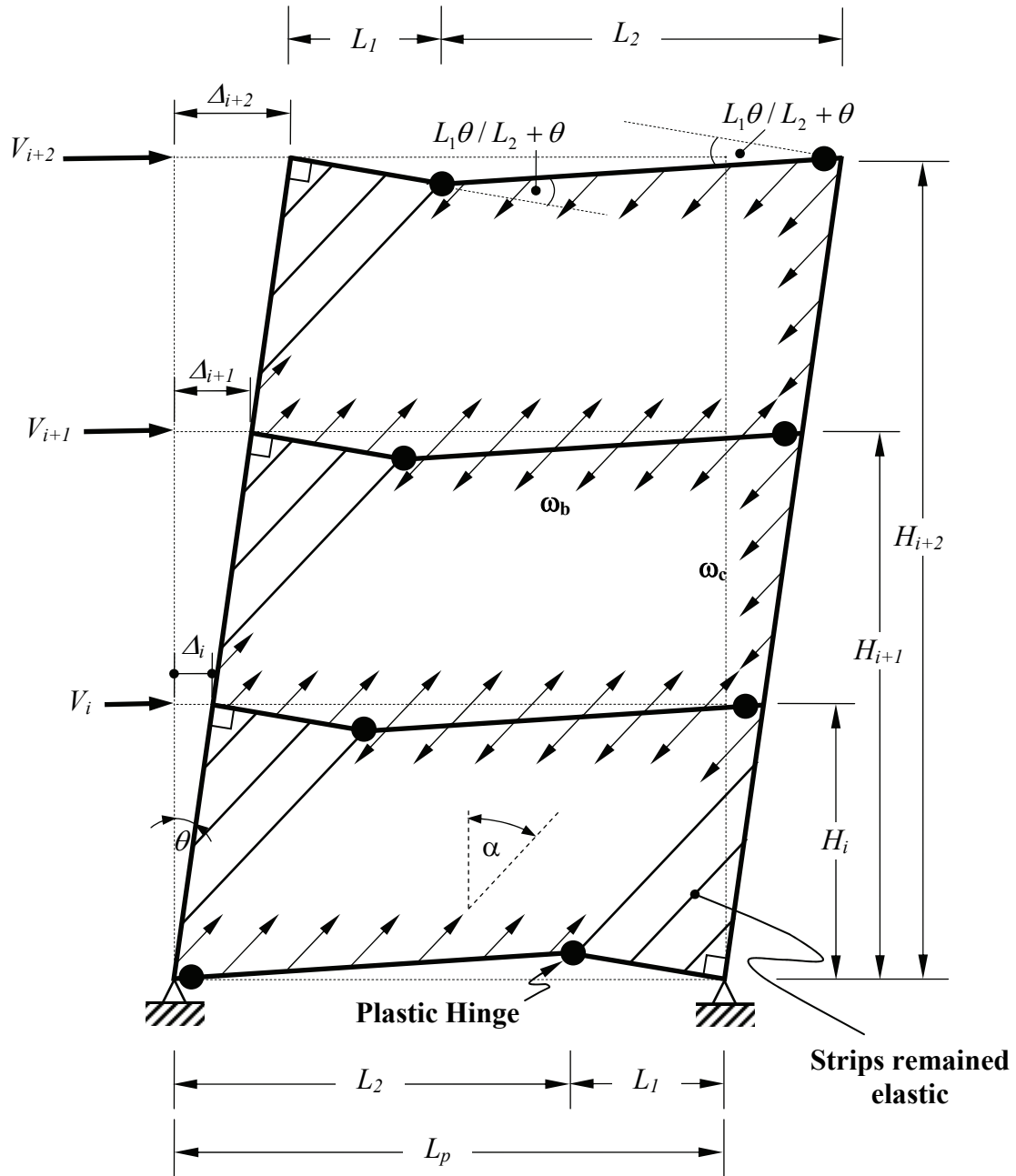


FIGURE 3-5 Sway and Beam Combined Plastic Mechanism for Multistory SPSW

$$\begin{aligned}
W_{internal_2} &= \underbrace{\sum_{i=1}^{n_s} \frac{1}{2} F_{yp} (t_{wi} L_2 - t_{wi+1} L_p) \sin(2\alpha) H_i \theta}_{\text{Horizontal component of the strip yield forces}} \\
&+ \underbrace{F_{yp} t_{w1} L_2 \cos^2 \alpha \frac{L_1}{2} \theta + \sum_{i=1}^{n_s} F_{yp} (t_{wi} L_2 - t_{wi+1} L_p) \cos^2 \alpha \frac{L_1}{2} \theta}_{\text{Vertical component of the strip yield forces}} \quad (3-10)
\end{aligned}$$

Again, equating the external and internal work [(3-8), (3-9), and (3-10)] gives the following general equation to calculate the ultimate strength of multistory SPSW with combined mechanism:

$$\begin{aligned}
\sum_{i=1}^{n_s} V_i H_i &= 2 \underbrace{\left(\frac{L_p}{L_p - L_1} \right) \sum_{i=0}^{n_s} M_{pbi}}_{\text{Plastic Hinge on the HBEs}} \\
&+ \underbrace{\sum_{i=1}^{n_s} \frac{1}{2} F_{yp} L_p (t_{wi} - t_{wi+1}) \sin(2\alpha) H_i - \sum_{i=1}^{n_s} \frac{1}{2} F_{yp} t_{wi} L_1 \sin(2\alpha) H_i}_{\text{Horizontal component of the strip yield forces}} \\
&+ \underbrace{F_{yp} t_{w1} L_2 \cos^2 \alpha \frac{L_1}{2} + \sum_{i=1}^{n_s} F_{yp} (t_{wi} L_2 - t_{wi+1} L_p) \cos^2 \alpha \frac{L_1}{2}}_{\text{Vertical component of the strip yield forces}} \quad (3-11)
\end{aligned}$$

Note that for comparison purposes, the above equation is arranged similarly to (3-1). This has been achieved by first substituting L_2 equals to $(L_p - L_1)$ into (3-9) and (3-10), followed by conducting some algebraic manipulations. Consider the internal work terms on the right part of (3-11): except for the third term, (i.e., internal work produced by the vertical component of the

strip yield forces), the first two terms are comparable to those in (3-1) but of a different magnitude. In the first term, the total internal work produced by plastic hinges on the HBEs is larger in the combined mechanism by a factor $L_p/(L_p - L_I)$ compared to that in the uniform mechanism. This is understandable because more plastic rotation is required to develop two plastic hinges (i.e., one in-span plastic hinge plus one plastic hinge at HBE end) in the combined mechanism compared to the uniform mechanism (i.e., two plastic hinges at HBE ends). However, because not all strips yield in the combined mechanism, the internal work produced by the horizontal component of the strip yield forces are smaller (i.e., due to the negative part in the second term) compared to that in the uniform mechanism.

Note that since there are more terms in the internal work of (3-11) than that of (3-1), one might be tempted to conclude that the combined mechanism has larger total internal work compared to that of the uniform mechanism. However, that is not the case because the reducing factor in the second term of (3-11) is much bigger than both the increasing factors in the first and the third term, meaning some of the infill plates that remained elastic predominantly reduce the internal capacity of the structure to resist the external load. This will become clearer further on when presenting the ultimate strength of SPSW-ID within the next paragraph.

At this point, the distance of the in-span plastic hinges L_I needs to be determined. One could obtain the exact location of that hinge by setting the first derivative of (3-11) to zero. However, this approach would be cumbersome. An easier approach is to take advantage of the SAP2000 results already obtained. As shown in figure 3-2, the location of in-span plastic hinges is at about quarter span except for the second floor HBE (labeled HBE2) where it is at about mid-span. Assuming that the location of in-span plastic hinge is somewhat similar at every floor (i.e., at about quarter span), the total internal work of SPSW-ID which developed the combined mechanism shown in figure 3-5 is 7178 kip-ft (i.e. 13.4% lower than that calculated using in the uniform sway mechanism). Using the relationship between the shear force in every floor as shown in (3-2), this corresponds to a theoretical base shear of 304 kips. This value is only 2.2% different from the one SAP2000 gave.

3.4 Cyclic Pushover Analysis

As presented in the previous section, SPSW-ID experienced a significant vertical deformation near the HBE mid-span. This deformation mainly arose from the pulling forces imposed by the yielding infill plates. After reached a certain lateral drift (i.e., 1.8% drift), as a result of the HBE inadequacy to resist that yielding forces, plastic hinge occurred along the HBE span (i.e., at the mid-span of HBE2). A significant vertical deformation in that HBE as shown in the deformed shape of SPSW-ID in figure 3-3 is a consequence of this phenomenon. In a seismic excitation environment, when a structure experiences cyclic loading, this plastic hinging along the HBE span could lead to progressively increasing deformations.

To investigate whether this phenomenon develops in the HBEs and whether it may affect structural performance, cyclic pushover analysis was conducted. The progressively increasing cyclic displacement history applied to the top floor of the structure for this purpose is shown in figure 3-6. Note that for this discussion, positive pushover displacement (producing positive base shear) is assumed to be acting from left to right of the structure. For comparisons, the same analysis was also performed on SPSW-CD. Results from the cyclic pushover analysis conducted on both SPSWs are compared below.

Figure 3-7 shows the resulting force-displacement hysteresis for a typical strip. Here, elastic deformations are excluded and only plastic deformations are plotted. Note that the resulting hysteresis is actually a combination of force-displacement outputs of two *Bracing Elements*, whose positions mirror each other in the SAP2000 model. The top-right part of the hysteresis was obtained from a member at the 3rd floor that yielded in the positive pushover displacement (called here the “right-leaning strip”) while the bottom-left part was obtained from its counterpart mirror member on the same floor that yielded in the negative pushover displacement (called here the “left-leaning strip”). In the first cycle of loading, for example, when positive pushover displacement applied to the structure, the first element experiences tension forces while the second element buckles immediately since it has no capacity in compression (i.e., no force nor displacement is developed). When the structure returns to its initial zero-displacement position and continue to the negative direction, the behavior is reversed; the second element experiences tension forces and the first element buckles. This interchanging role between the two elements

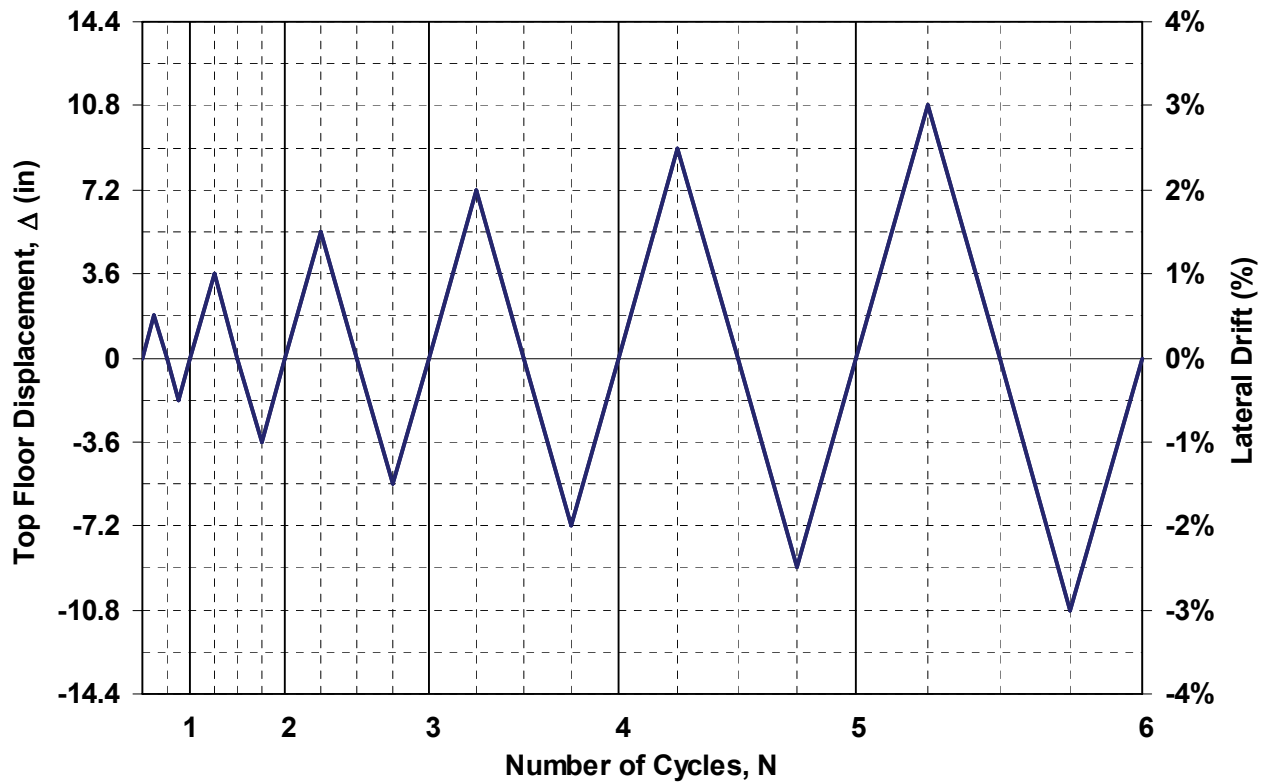


FIGURE 3-6 Displacement History for Cyclic Pushover Analysis

continues until the end of pushover displacement history. Hence, negative values in the figure should be understood as an indication of pushover direction rather than compression forces developed in the strips. In addition, these results verify the correctness of the strip hysteretic model applied in the SAP2000 model as defined in figure 2-6(d), which has strength only in tension but no strength in compression. Even though this hysteresis is unique to those particular strips (in this case, strips at the 3rd floor), the result is representative of any strip. This particular strip has cross section area and length of 0.71 in² and 164 in, respectively. For the light gauge steel ($F_y=30$ ksi) used in the strips, one can obtain the yield force (P_y) and strip yield displacement (δ_y) of 21.4 kips and 0.17 in, respectively.

Figure 3-8 shows the base shear versus lateral displacement hysteretic curves up to 3% drift for SPSW-ID and SPSW-CD, respectively. For comparisons, the previous monotonic pushover results are also plotted in both figures. The backbone of both cyclic pushover analyses follows the monotonic curves without perceptible differences until higher drift (i.e., $\geq 2\%$ drift). If the

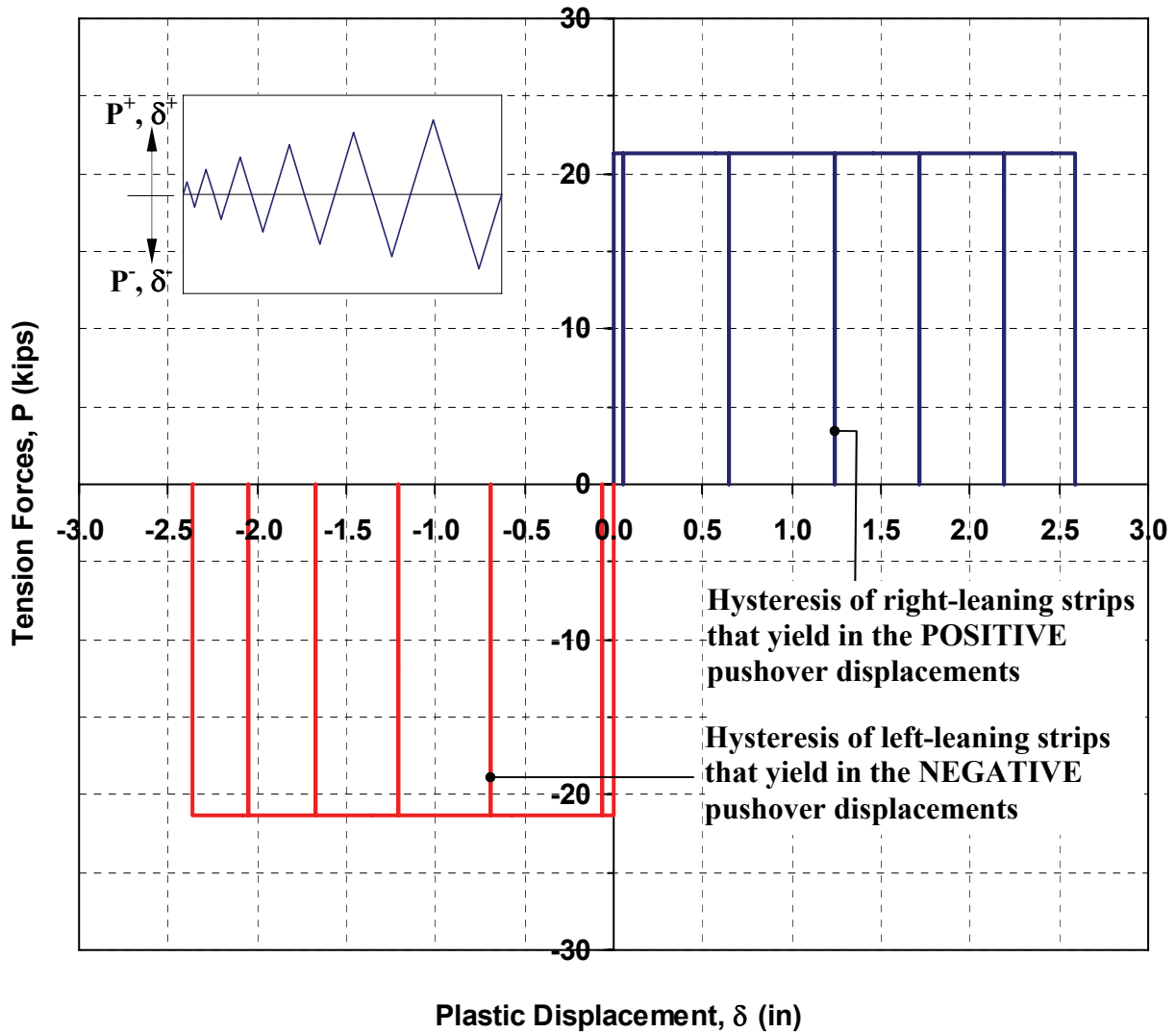


FIGURE 3-7 Typical Force-Displacement Hysteresis of Slender Strip

contribution to the total strength due to the boundary frame moment resisting action is calculated by analyzing it as a bare frame model without the infill plates, comparing the result with the total plastic strength of each SPSW, it is observed that the boundary frame plastic strength (in a sway mechanism) contributes about 30% and 48% of the plastic strength of SPSW-ID and SPSW-CD, respectively. This explains why SPSW-ID exhibits more pinching in its hysteretic behavior compared to SPSW-CD.

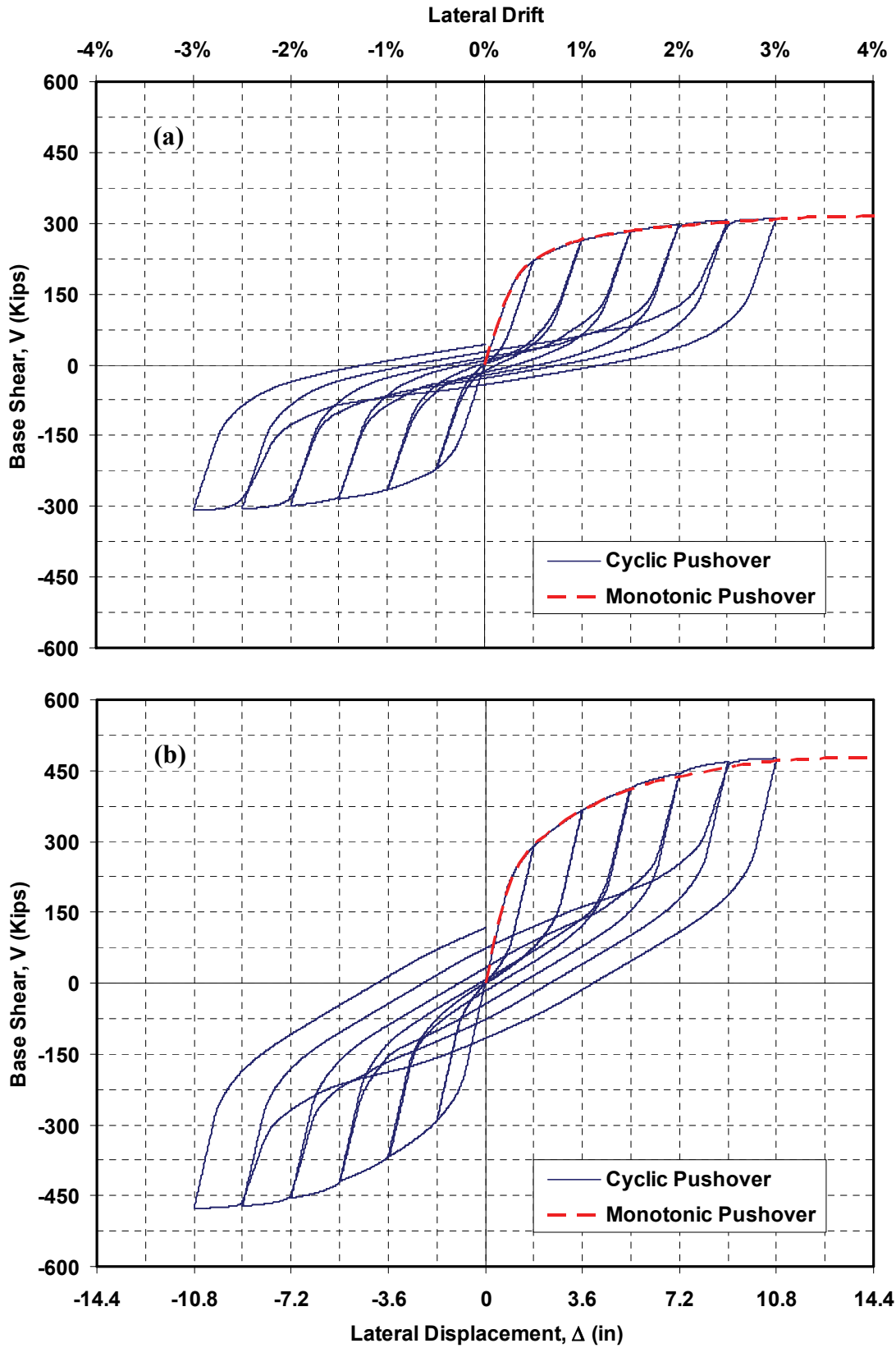


FIGURE 3-8 Cyclic Pushover Analysis Results (a) SPSW-ID; (b) SPSW-CD

3.4.1 Plastic Hinge and Strip Yielding Distributions

In the monotonic pushover analysis, the plastic hinge distribution was presented only at 4% lateral drift (figure 3-2). At this significantly high drift, the fully plastic criterion ($M \geq 0.97M_p$) was sufficient to illustrate the plastic mechanisms of both SPSWs. Here in the plastic hinge distribution of the cyclic pushover analysis, however, two early stages of plastification (in addition to the fully plastic condition that was shown in figure 3-2) have been defined to observe the progression of plastification at several drifts of interest. They are “yielding condition” and “partial plastification”. Knowing that for the W-sections typically used in North American steel construction, the ratio between yield moment and plastic moment (i.e., the shape factor) typically vary from 1.12 to 1.16 with an average of 1.14 (Bruneau *et al.* 1998), a given cross section only subjected to flexure can be deemed to have started to yield if its developed flexural moment is 88% of its theoretical plastic moment. Hence, in pure flexure, it would be reasonable to assume that the yielding condition is reached at a given plastic hinge location if the flexural moment is between 88% to 91% of its theoretical plastic moment; and partial plastification is reached if the flexural moments is between 91% and 97% of its theoretical plastic moment.

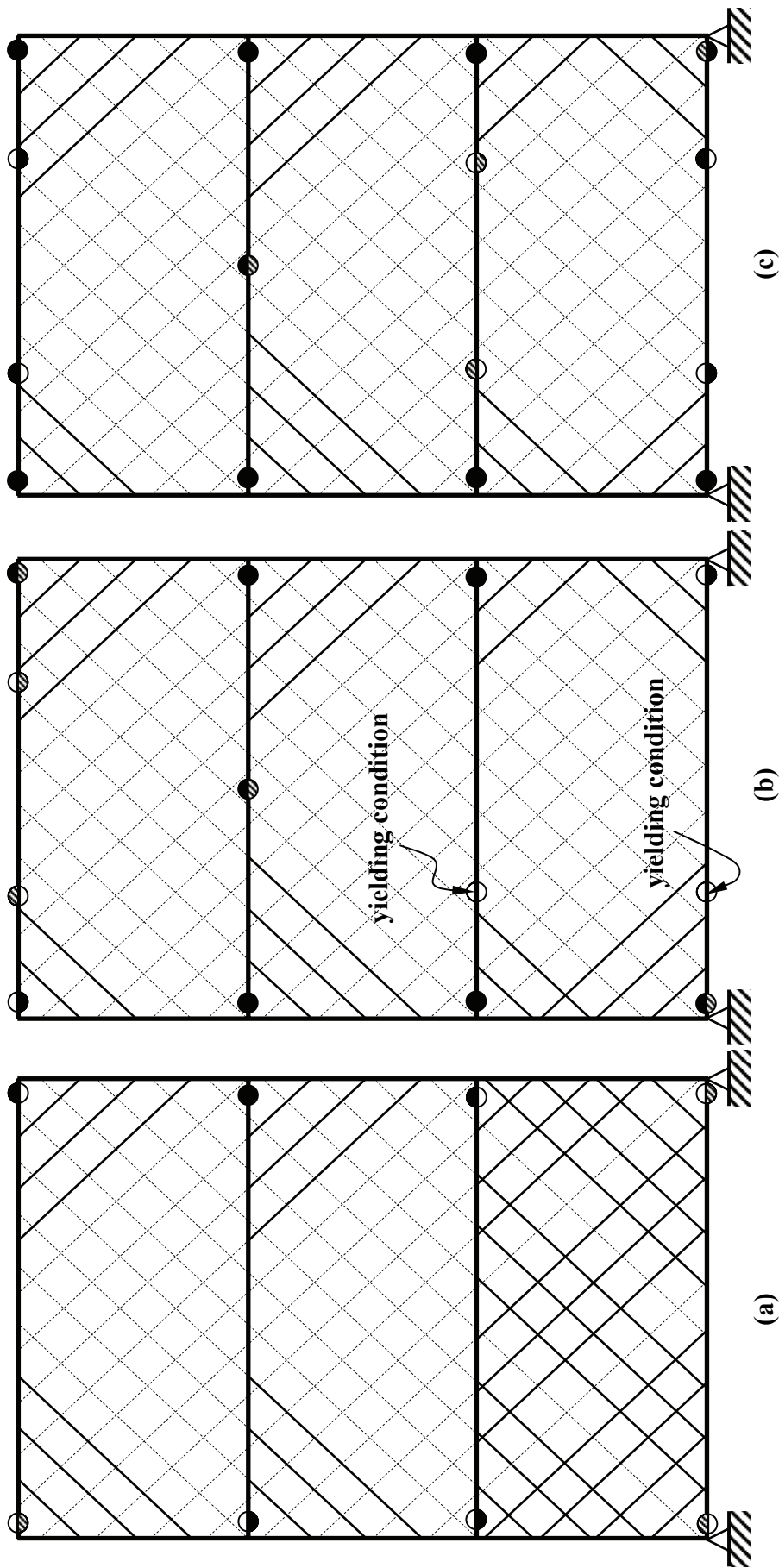
While those criteria are simple to apply, they do not actually consider the reduction of HBE plastic moment capacity due to its developed axial forces generated by the infill plate tension forces. Though the plastic moment capacity of a typical wide flange section starts to decrease when the developed axial force is higher than 15% of its axial yield strength (Bruneau *et al.* 1998), yielding of the cross section starts much earlier ($M_y = 0.74M_p$) at this same level of axial force. As a result, the corresponding range for those three stages of plastification should be modified. Accordingly, a comprehensive criterion to incorporate this earlier onset of yielding and reduced plastic moment capacity could be proposed (e.g., per the procedure presented in Qu and Bruneau 2008). However, because the reduced capacities vary between one HBE to another, depending on the level of axial force in one particular HBE relative to its axial yield strength (i.e., P/P_y), it would be difficult to define a fixed comprehensive criterion.

Hence, for the case when the magnitude of axial forces developed in one particular fiber hinge becomes significant (i.e., $P \geq 10\%P_y$), the fiber stress-strain information is expediently used to assess the plastic condition of the fiber hinges. This is possible because the fiber hinges automatically accounts for the interaction between the axial loads and moments. Therefore, in

this case, the “yielding condition” corresponds to the stage when the furthest fiber from the plastic neutral axis reaches the yield stress (extending that initial condition up to the “upper boundary” defined by the case when all fibers on one flange have yielded), the “fully plastic condition” corresponds to the instance when most of the fibers have yielded (i.e., only one or two fibers close to the plastic neutral axis remain elastic), and the “partial plastification condition” corresponds to the cases between the two conditions. On the other case, when the magnitude of axial force does not exceed what could be considered to be a moderate level, a limit defined here as $P \leq 10\%P_y$, the generic criteria outlined in the first paragraph of this section are used to assess the plastic condition of the fiber hinges. Hence, the circular markers in figures 3-2, 3-9, and 3-10, which indicate whether either partial plastification or full plastic moment have been reached on the HBE at selected locations, have been manually added to these figures based on those assumptions (i.e., level of flexural moment or fiber stress-strain information). The corresponding yielding conditions are also indicated in the figures by text.

Figure 3-9 shows the plastic hinge and strip yielding distributions on SPSW-ID. Plotted in parts (a), (b), and (c) are the condition at the end of the full cycle at 1% (2nd cycle), 2% (4th cycle), and 3% drift (6th cycle), respectively. To have a better understanding of which plastic hinges formed in each direction of pushover displacement, new markers have been introduced in the figure, which are slightly different from the one that was shown in figure 3-2 for monotonic pushover analysis. Here, symbolic hinges that are half-shaded or half-solid on the top part of the circular markers indicate that partial plastification or full plastic condition, respectively, have been reached on the HBE at the shown location when the structure undergoes positive drift excursion. When the structure undergoes an excursion in the reversed direction, those half-shaded or half-solid indications are shown on the bottom part of the circular markers to indicate the same respective conditions. Consequently, full-shaded or full-solid indicate that the respective conditions occurred in both directions (i.e., positive and negative directions).

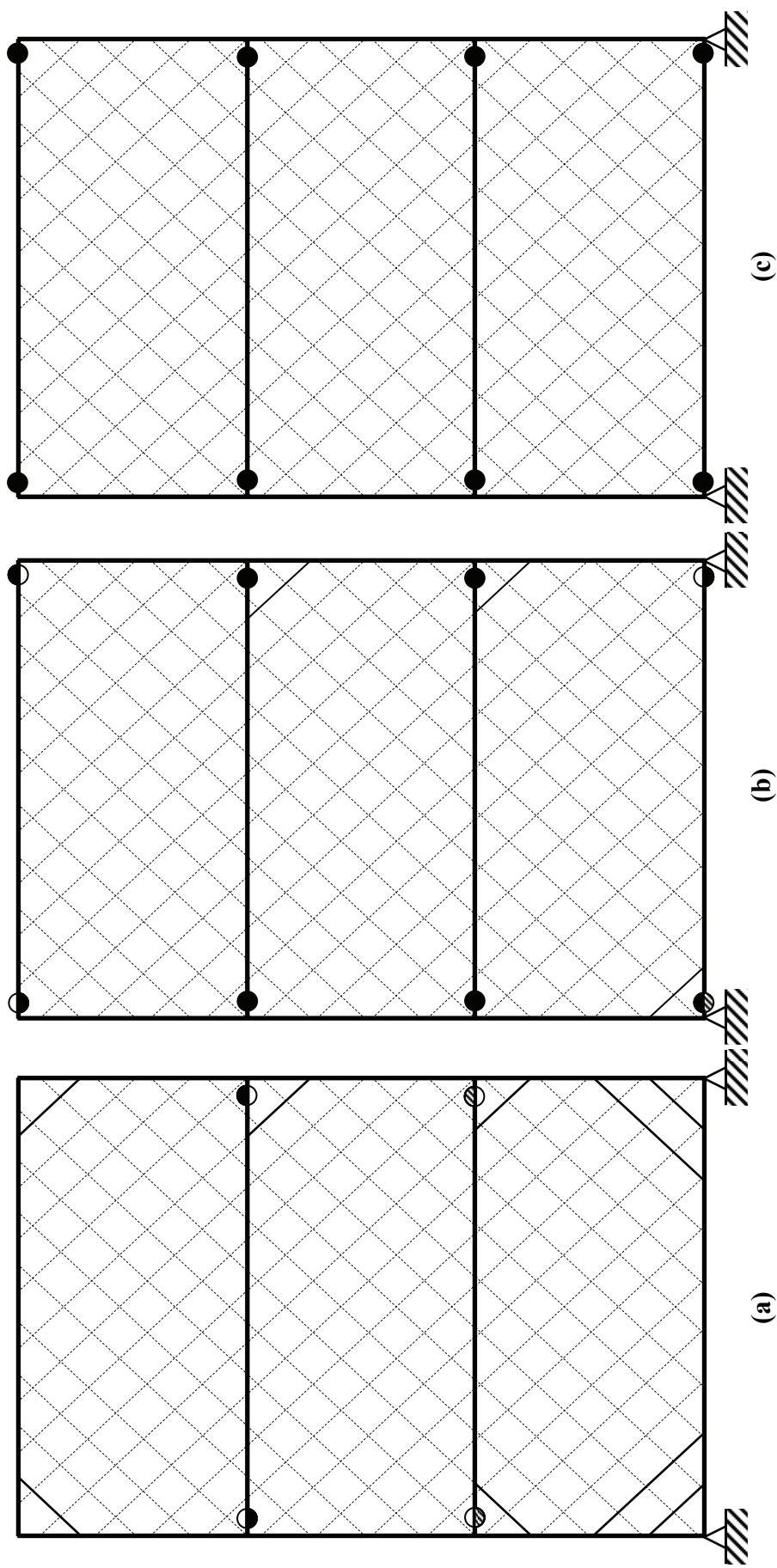
Using this notation, it is seen from figure 3-9 that the plastic hinge distribution at the end of the 1% drift cycle is somewhat symmetric in both directions. When the structure experienced +1% lateral drift, a total of four plastic hinges (1 partial plastification and 3 fully plastic) occurred at the HBE ends; and at the reversed excursion of -1% lateral drift, a total of five plastic hinges (2 partial plastifications and 3 fully plastic) occurred at the same HBE ends.



Legend:

- ⊘ | ● = partial plastification | fully plastic in **positive** drift. See Section 3.4.1 for the definitions.
- ⊘ | ○ = partial plastification | fully plastic in **negative** drift
- ⊘ | ● = partial plastification | fully plastic in both directions (**positive** and **negative** drifts)
- = yielding condition (yielding remains within HBE flanges)
- = strip yielding ($P = P_y$)

FIGURE 3-9 Plastic Hinge and Strip Yielding Distributions on SPSW-ID at the End of (a) 1% Drift; (b) 2% Drift; (c) 3% Drift



Legend:

- ⊙ | ● = partial plastification | fully plastic in **positive** drift. See Section 3.4.1 for the definitions.
- ⊗ | ⊙ = partial plastification | fully plastic in **negative** drift
- ⊗ | ● = partial plastification | fully plastic in both directions (**positive** and **negative** drifts)
- = strip yielding ($P = P_y$)

FIGURE 3-10 Plastic Hinge and Strip Yielding Distributions on SPSW-CD at the End of (a) 1% Drift; (b) 2% Drift; (c) 3% Drift

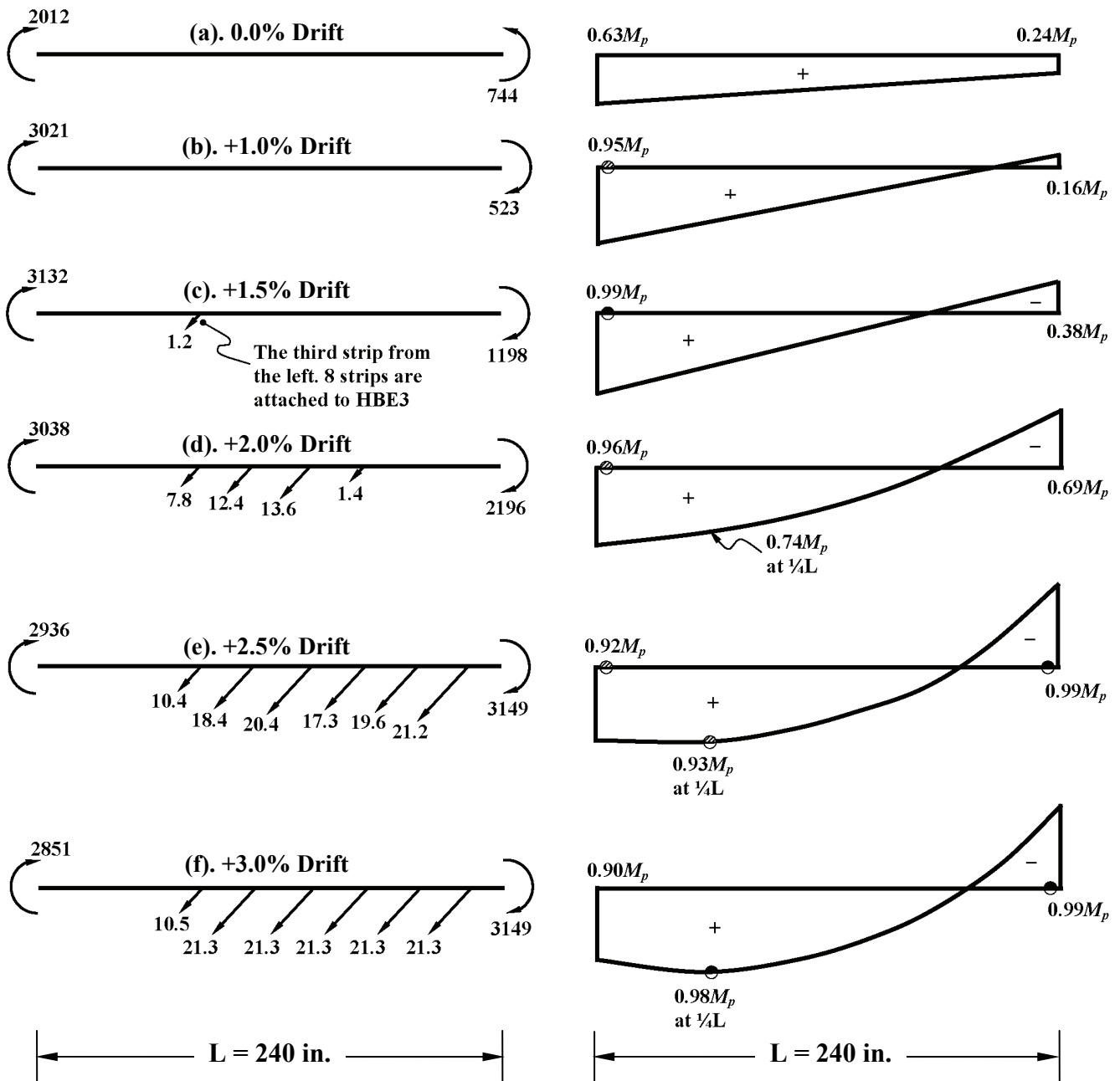
Furthermore, at the end of the 1% drift cycle, three strips on the second and the third floor remained elastic (in the figure shown as the solid lines close to the corner) and only two strips on the first floor had yielded (in the figure shown as the broken lines). One might notice in figure 3-9 that there are actually six strips shown to have remained elastic in the top floor as well as in the second floor and four strips shown to have yielded on the first floor. However, since the information is presented here in terms of pushover displacement results for each specific direction (for example, the case acting in the positive direction is defined as a displacement going from left to right of the structure), one should only count the strips oriented in the respective direction of interest (i.e., the right-leaning or left-leaning strips for the positive or negative direction, respectively).

As the pushover displacement increased, more strips yielded, predominantly on the first floor, while only one additional strip yielded on the top floor. As previously observed in the monotonic pushover analysis, even at higher lateral drifts (i.e., at the end of the 3% drift cycle) some strips remained elastic; more specifically, a total of 9 right-leaning strips and 10 left-leaning strips remained elastic. This phenomenon will be explained later in the next section through observation of the deformed shape of SPSW-ID plotted in figure 3-12. Moreover for the plastic hinge distribution, beyond the plastic hinges that occurred at the HBE ends, three locations of in-span plastic hinges were also observed on HBE2 and HBE3 at the end of 2% drift cycle. In addition, the yielding condition occurred along the span of HBE0 and HBE1. It is useful to illustrate how the fiber stress-strain information was used at this drift level, using the above definitions, to assess the plastic condition of the fiber hinges. Consider the hinge at the quarter point of HBE3 as an example. Flexural moment at this particular location at 2% drift was 2661 kip-in, less than the pure-flexure yield moment of W16x36 section used for HBE3 (i.e., $M_y = 2793$ kip-in). However, fiber stress-strain information confirmed that about 33% of the total area of cross section (all 16 fibers on the bottom flange + 3 fibers on the web) had reached the yield stress of 50 ksi. The significant developed axial force ($P = 12.5\% P_y$) primarily contributed to this behavior by reducing the yield moment by about 12.5% (i.e., M_y equals to 2443 kip-in at that axial force level).

At the end of the 3% drift cyclic, in-span plastic hinges on the HBEs occurred at 4 locations (1 partial plastification and 3 fully plastic) during the positive drift excursion and at 4 locations (2 for each partial plastification and fully plastic) during the negative drift excursion. Incidentally, one interesting behavior observed on the plastic hinge distribution of SPSW-ID after the structure experienced a higher drift (i.e., $\geq 2\%$ drift), was evidence of three plastic hinges having formed in some of the HBEs. For example, this was observed on HBE2 when the structure underwent its positive drift excursion during the 2% drift cycle and on each HBE in both excursion directions of the 3% drift cycle. This seems to contradict the results obtained for the theoretical sway and beam combined mechanism observed under monotonic push-over analysis for the corresponding multistory SPSW, as illustrated in figure 3-5, in which only two plastic hinges on the HBEs were required to form the plastic mechanism. Actually, there is no contradiction. However, before explaining this phenomenon through observation of the free-body diagram of the corresponding HBE (as will be done later in this section), results for the SPSW-CD case are first presented and compared to that of SPSW-ID.

Presented in figure 3-10 is the plastic hinge and strip yielding distributions on SPSW-CD. At the end of the 1% drift cycle, most of the strips had yielded; only four right-leaning strips and five left-leaning strips (i.e., close to corners) had remained elastic. By contrast with SPSW-ID for which 9 right-leaning strips and 10 left-leaning strips had remained elastic at the end of the 3% drift cycle, here for the SPSW-CD, all strips have completely yielded at that cycle. In addition, all plastic hinges have developed at the HBE ends of SPSW-CD and no in-span plastic hinge developed (contrary to the four in-span plastic hinges that developed in the SPSW-ID).

As mentioned previously, there is a discrepancy between the monotonic and the cyclic pushover analyses of SPSW-ID in terms of the number and location of in-span plastic hinges that ones observed to occur on several HBEs during development of the respective plastic mechanisms. To explain that phenomenon, a step-by-step investigation on the free-body diagram of the corresponding HBE (e.g., HBE3) in the SPSW-ID was conducted. Figure 3-11 shows the free-body diagram of HBE3 during the positive excursion of the 3% drift cycle. Part (a) of the figure informs the free-body diagram at the end of the 5th cycle (i.e., at 0% drift) after the structure was pushed to the right and to the left up to a maximum lateral drift of 2.5%. Here, residual moments



Units: moments (kip-in); forces (kips)

FIGURE 3-11 HBE3 Free-Body Diagram and Moment Diagram for SPSW-ID at Various Lateral Drifts during 3% Drift Cycle

at the left and the right ends of HBE3 were $0.63M_p$ and $0.24M_p$, respectively, and no tension forces remained in the strips. When the structure experienced +1% drift [part (b) in the figure], a partial plastification occurred at the left end of HBE3 while the moment at its right end changed curvature direction; and again no tension forces were present in the strips because the previous maximum elongation in the strips has not been reached back yet. At +1.5% drift, the left end

became a fully plastic condition ($M = 0.99M_p$), the right end moment was $-0.38M_p$, and a tension force of 1.2 kips started to develop in the third strip from the left. Interestingly, as more strips regained tension and resumed plastic energy dissipation anew at +2% drift, the left end moment reduced while moments at the quarter-span from the left as well as at the right end increased. In addition, the previously linear distribution of moment diagram became a quadratic shape due to the tension forces from the strips. By the end of the positive excursion at 3% drift, the plastic hinge that had occurred at the left end under increasing drifts was under elastic unloading and thus not plastic anymore. Plastic hinges were instead located at the quarter-span from the left and at the right end of HBE3, similarly to what was observed during the monotonic pushover analysis case. Hence, this distinctive transition mechanism between the sway and the combined mechanism in SPSW-ID explains the plastic hinge distribution observed on HBE0, HBE1, and HBE3 shown in figure 3-9. At the end of the cyclic pushover analysis, three plastic hinges indeed develop on those HBEs but they did not occur at the same time during the drift excursion. Note that a small drop of HBE end moment at a higher drift after the infill plates yielded actually also occurred in several HBEs of SPSW-CD. However, it was not followed by changing of the plastic hinge distribution (i.e., the system remained in its sway plastic mechanism) as opposed to the case of SPSW-ID. Section 3.4.4 also has additional explanations for this phenomenon.

3.4.2 HBE Vertical Deformation

A most significant phenomenon observed is the HBE vertical downward deformation of SPSW-ID, progressively increasing and of significant magnitude as the lateral drift increased. This can be observed especially on the top two HBEs as shown in figure 3-12(a). For example, the vertical deformation on the top HBE progressively increased from 0.8 to 2.3 in. when the structure was pushed from 1% to 3% drift; and when the structure returned to its original position after it went through a full 3% drift cycle, the residual vertical deformation of the top HBE remained significant, was at about 1.7 in. (later shown in figure 3-13). This significant HBE vertical deformation prevents the corner strips (i.e., the top left corner for positive pushover displacement) on the second and the third floor to completely stretch up to the yield displacement. Moreover, strips on the first floor behaved differently from the top two floors. Since the bottom HBE deformed upward and the HBE on the first floor deformed downward, both strips on the top left and bottom right corners remained elastic. This further explains why in figure 3-9 those

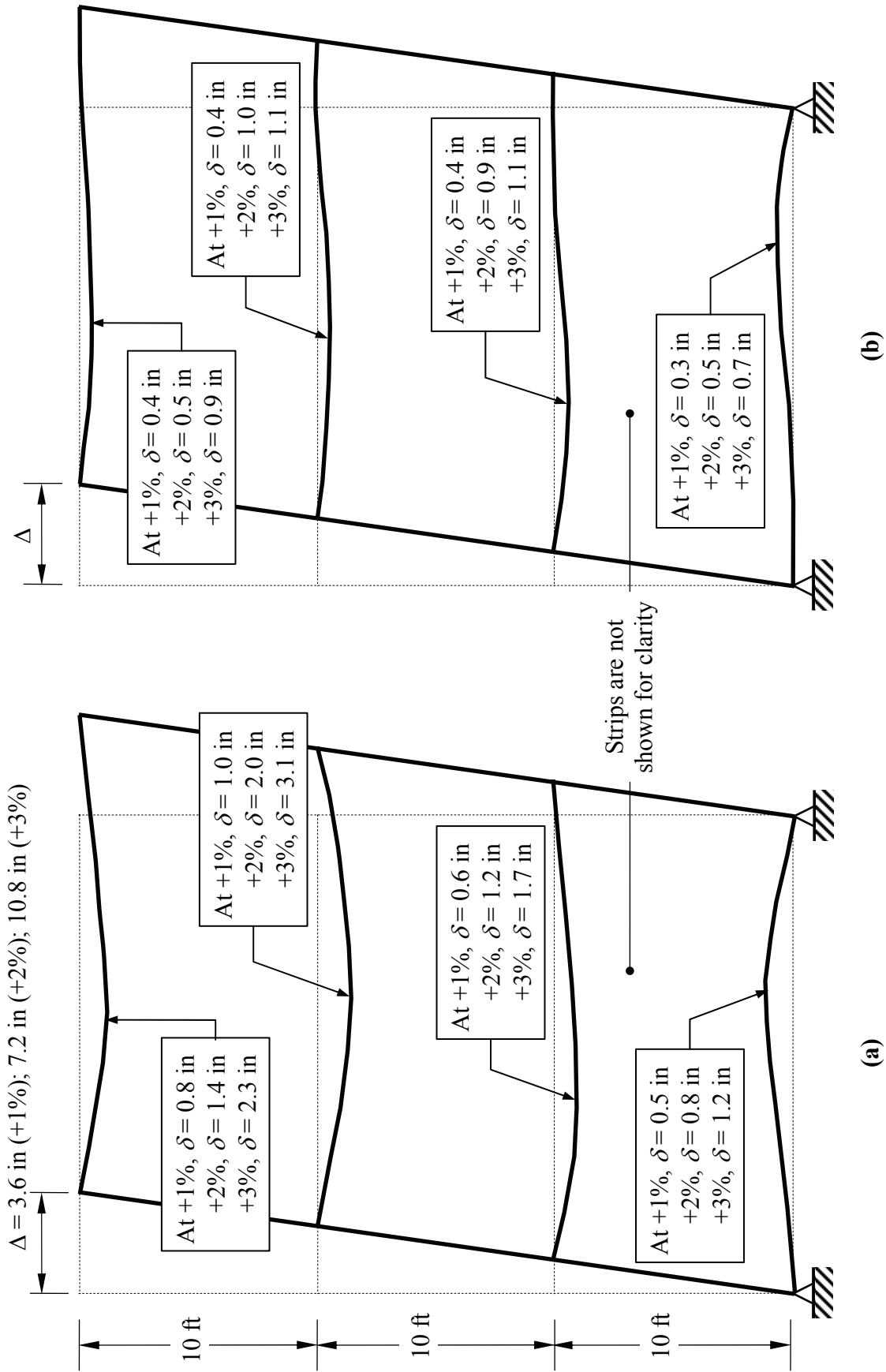


FIGURE 3-12 Schematic Deformed Shapes of Cyclic Pushover Analysis (a) SPSW-ID; (b) SPSW-CD

corner strips remained elastic and in-span hinges developed. Interestingly, more strips were found to be elastic during the cyclic pushover analysis than during the monotonic pushover analysis (i.e., 9 out of 36 right-leaning strips remained elastic in the cyclic analysis compared to only 5 in the monotonic pushover analysis). This can be explained by comparing the HBE deformed shapes obtained from monotonic and cyclic pushover analysis plotted in figures 3-3(a) and 3-12(a), respectively. For the same magnitude of drift (i.e., at +3% drift), the top floor HBE for example has larger vertical deformation in the cyclic pushover analysis than that in the monotonic pushover analysis. They are 2.3 and 1.7 in. for the respective analyses. The larger the HBE vertical deformation, the less the elongation in the corner strips and, as a result, the more strips remaining elastic. As a consequence of this behavior, the infill plates in SPSW-ID do not develop their full capacity to resist the specified lateral loads.

By comparison for SPSW-CD, relatively small vertical deformations actually occurred on the HBEs during cyclic pushover analysis. The largest HBE vertical deformation is 1.1 in. at +3% lateral drift. However, this is not large enough to create in-span plastic hinging and becomes only 0.5 in. (later shown in figure 3-13 for HBE3) when the structure returns to its original position after it went through a full 3% drift cycle.

While information in figures 3-9 to 3-12 is helpful to provide snap-shot views of the deformed shape and yield condition of SPSW at selected drifts, a complete history of the recorded vertical displacement of HBE as a function of structure lateral drift, such as the one shown in figure 3-13, is more instructive to explain the performance of the HBEs designed by the two different approaches. This figure compares vertical displacement history at the mid-span of the top HBE for both SPSWs.

Two key behaviors can be observed from the figure with respect to vertical displacement: (1) at the maximum drift of every cycle (called here the “backbone” displacement) and (2) when the structure returns to its original position at 0% drift (called here the “residual” displacement). The backbone-displacement slope of SPSW-ID is larger than that of SPSW-CD. This implies that the HBE vertical downward displacement for SPSW-ID increases faster than that for SPSW-CD. In other words, this accumulative plastic incremental deformation due to cyclic pushover

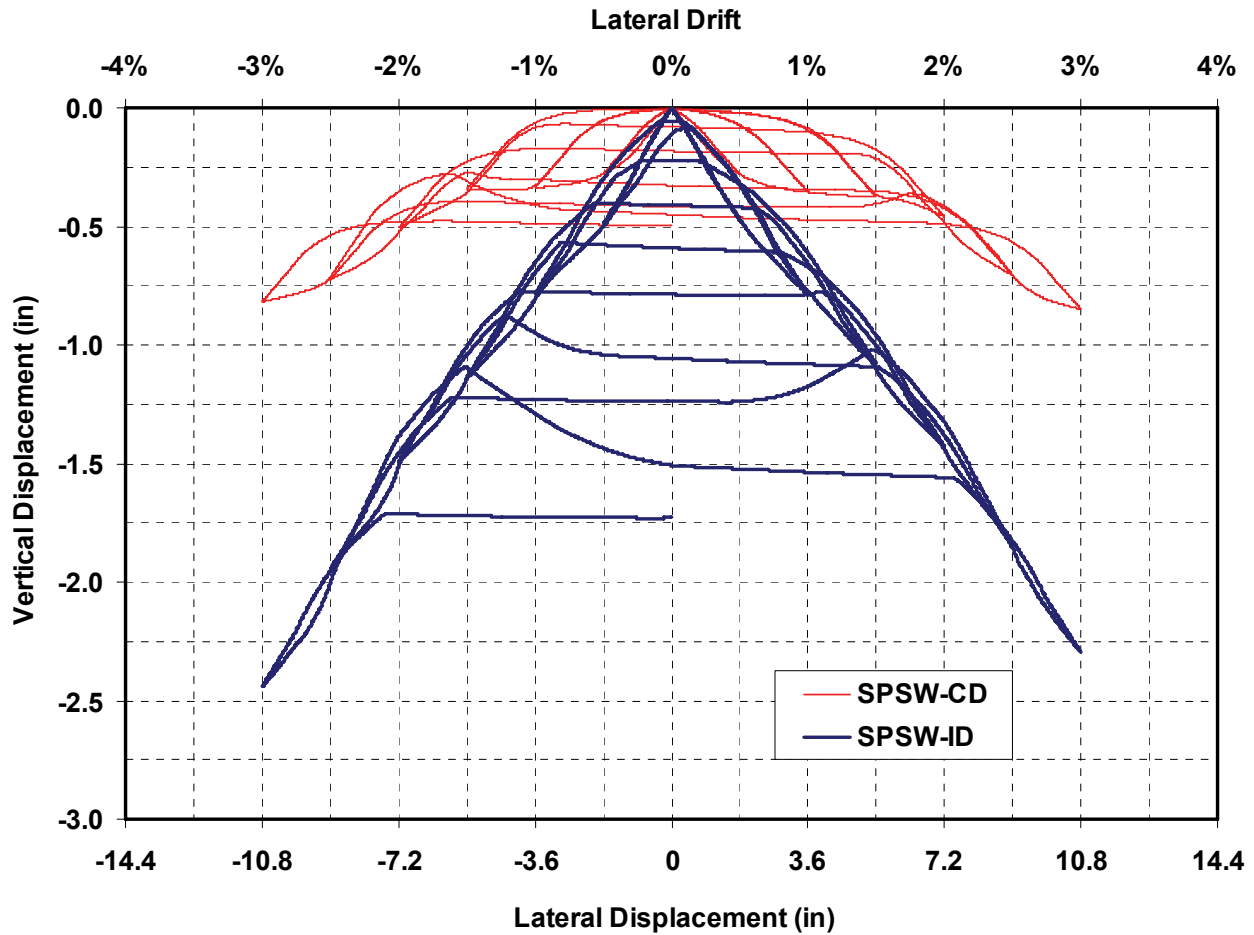


FIGURE 3-13 HBE3 Vertical Displacement versus Top Floor Lateral Displacement Obtained from Cyclic Pushover Analysis

displacement is more apparent on SPSW-ID. It also detrimentally affects the structural performance of SPSW-ID. For example at +3% drift, the HBE3 vertical displacement of SPSW-ID was 2.3 in.; about 2.6 times larger than that of SPSW-CD, which is 0.9 in. The same trend was also exhibited with the residual displacements. At the end of the 3% drift cycle, HBE3 residual displacement for the SPSW-ID was 3.5 times larger than that for the SPSW-CD. In addition, progression of the HBE residual displacement from one cycle to another cycle is quicker for the SPSW-ID than that for the SPSW-CD. For example, HBE3 residual displacements of SPSW-ID progressively increase from 0.06 in. (at the end of the 1% drift cycle) to 1.7 in. (at the end of the 3% drift cycle). By contrast, for SPSW-CD, they increase from 0.0 in. (no residual displacement) to 0.5 in. for the same respective cycles. Moreover, this phenomenon on SPSW-ID would be even worse if a smaller W-section had been used for the top HBE such

that its demand-to-capacity ratio was closer to 1.0; recall that a value of 0.88 (as shown in figure 2-2) was obtained for that top HBE in the SPSW-ID case, compared to the corresponding 0.99 value at the top HBE of SPSW-CD. If anything, this discrepancy reinforces the conclusions reached by this case study.

For a more through investigation of the behavior of the two SPSWs, vertical deformation of each HBE is plotted in figure 3-14 arranged vertically from the top HBE to the bottom HBE; plotted on the left side are curves for SPSW-ID, whereas on the right are curves for SPSW-CD. In general, each HBE has a behavior similar to the one presented in figure 3-13. Note that the maximum vertical deformation does not always occur at the HBE mid-span. As shown in figure 3-12, in some cases (e.g., HBE1 on SPSW-ID; HBE1 and HBE2 on SPSW-CD), the maximum location is close to the HBE quarter-span (i.e., about $\frac{1}{4}L$ measured from the left when the structure is pushed to the right). If the vertical deformation measured at this location is used to plot their hysteresis, the resulting curve is not symmetric because when the structure is pushed to the left, the maximum vertical deformation is not at this location anymore, but instead at the plastic hinging that develops at $\frac{1}{4}L$ measured from the right. Here, to have a better presentation of the hysteretic behavior of the in-span plastic hinges, the vertical deformation plotted in figure 3-14 is taken where the maximum deformation occurred in each HBE. Furthermore, since the location of maximum deformation of HBE3 for both SPSWs is always close to its mid-span, hysteresis curves of HBE3 plotted in figures 3-13 and 3-14 are somewhat identical.

The information presented in figures 3-9 to 3-14 demonstrates that plastification along HBE spans, in the case of SPSW-ID, can detrimentally impact behavior of the structure by inducing significant vertical and residual deformations on the HBEs, themselves leading to partial yielding of the infill plates and correspondingly lower global plastic strength. Globally, the results of cyclic pushover analysis showed that the SPSW-CD performed better than the SPSW-ID in terms of having plastic hinges only at HBE ends, completely yielded infill plates (i.e., in compliance with the behavior expected by the AISC Seismic Provisions 2005), and relatively smaller vertical displacements along the HBE spans. However, one might question why any residual vertical deformations were also observed in the SPSW-CD given that no in-span hinges occurred in that case. Explanation to this concern is presented in the following section.

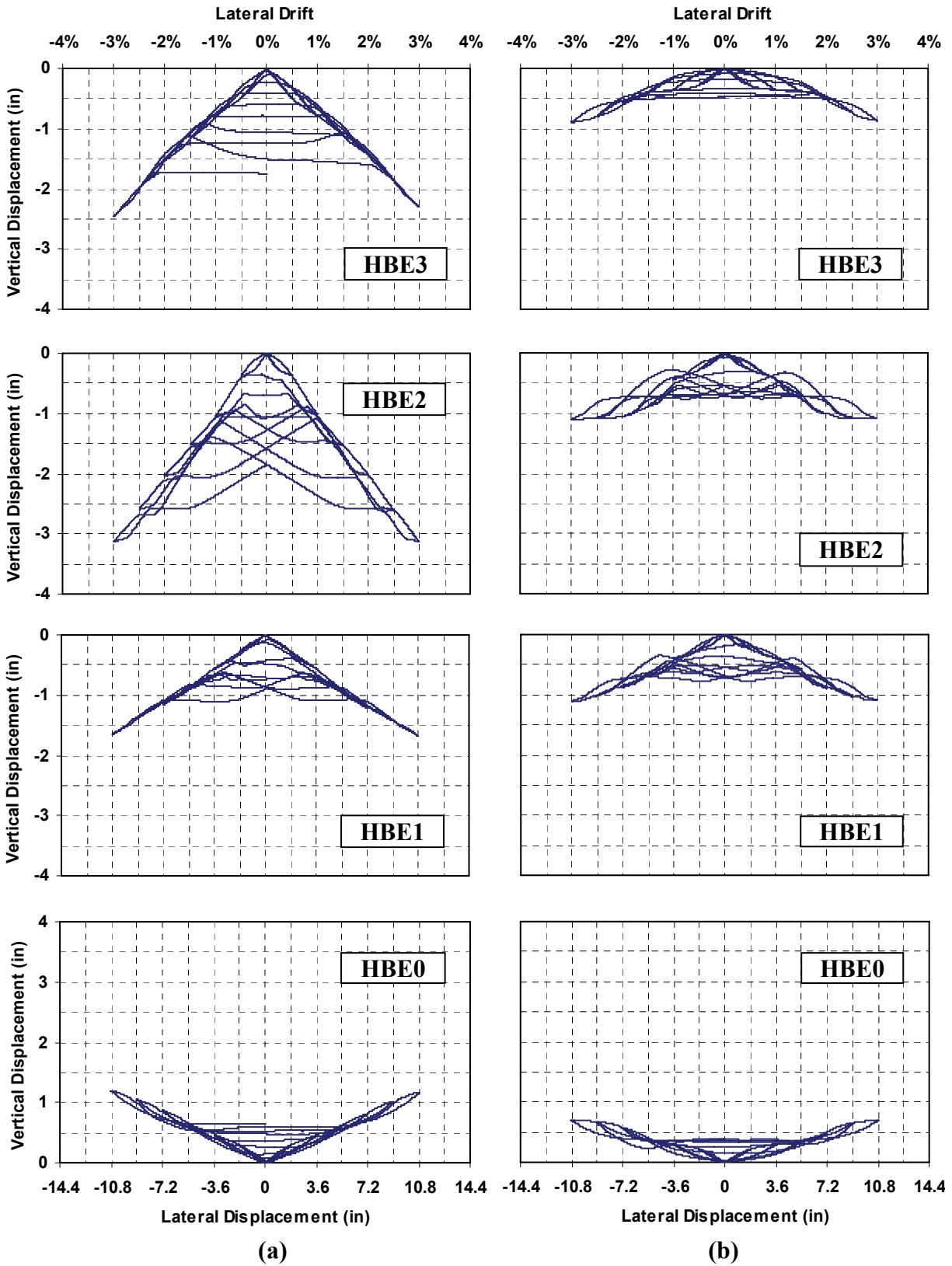


FIGURE 3-14 Structure Lateral Displacement versus HBE Vertical Displacement for (a) SPSW-ID; (b) SPSW-CD

3.4.3 Cycle by Cycle Investigation on HBE Deformation History of SPSW-CD

To investigate the above phenomenon in the SPSW-CD, a cycle by cycle investigation on the behavior of its HBE was conducted. Though similar observations could be made on any of the HBEs, behavior of only the top HBE was examined in this case. Free body diagrams and vertical deformation history of the top HBE at 0.5%, 1%, 2%, and 3% drift are plotted at the top part of Figs. 21(a), (b), (c), and (d), respectively. Note that those drifts correspond to the 1st, 2nd, 4th, and 6th cycles (consistently with the information in figure 3-12). Along with that information, force-displacement hysteretic history of the entire SPSW in terms of the structural base shear is presented in the bottom part of figure 3-15. In every cycle, observations were made at four key conditions, namely at the point of maximum positive drift (point A), when the structure passed the original position (point B), at the point of maximum negative drift (point C), and when the structure was pushed back to its original position upon completion of a full cycle (point D).

In the first cycle when the structure reached point A (i.e., corresponding to +0.5% drift), half of the strips connected to the top HBE had yielded, with the yielding forces P_y being equal to 21.3 kips. At that point, the HBE was elastic (i.e., no plastic hinge has occurred) and only 45% of its plastic moment capacity was used (i.e., $M_{max} = 3656$ kip-in out of $M_p = 8093$ kip-in) to resist the tension forces generated by the attached infill plates. The resulting vertical deformation of 0.28 in. was an elastic response of the HBE to those forces, which disappeared once the structure returned to point B at 0% drift. Note that though the HBE elastically deformed, the vertical-displacement-versus-lateral-drift curves (the top curve) did not trace-back on top of themselves, however taking different paths during the loading and unloading stages creating a loop in the curve. This is because the tension forces applied to the HBE did not increase proportionally at the same time on all strips, but rather gradually developed from the right toward the left strips as the structure was pushed to the right and unloaded in a reverse order when the structure was pushed to the opposite side. This also explains why moments were significantly different from one HBE end to the other. As shown by the HBE free body diagram at point A in figure 3-15(a), the left end moments are only about 10% of that of the right end. Furthermore, strip yielding in this cycle can also be observed in the history of base shear (the bottom curve). As the strips start to yield at about 0.2% drift, structural stiffness gradually softened until reaching point A, where the

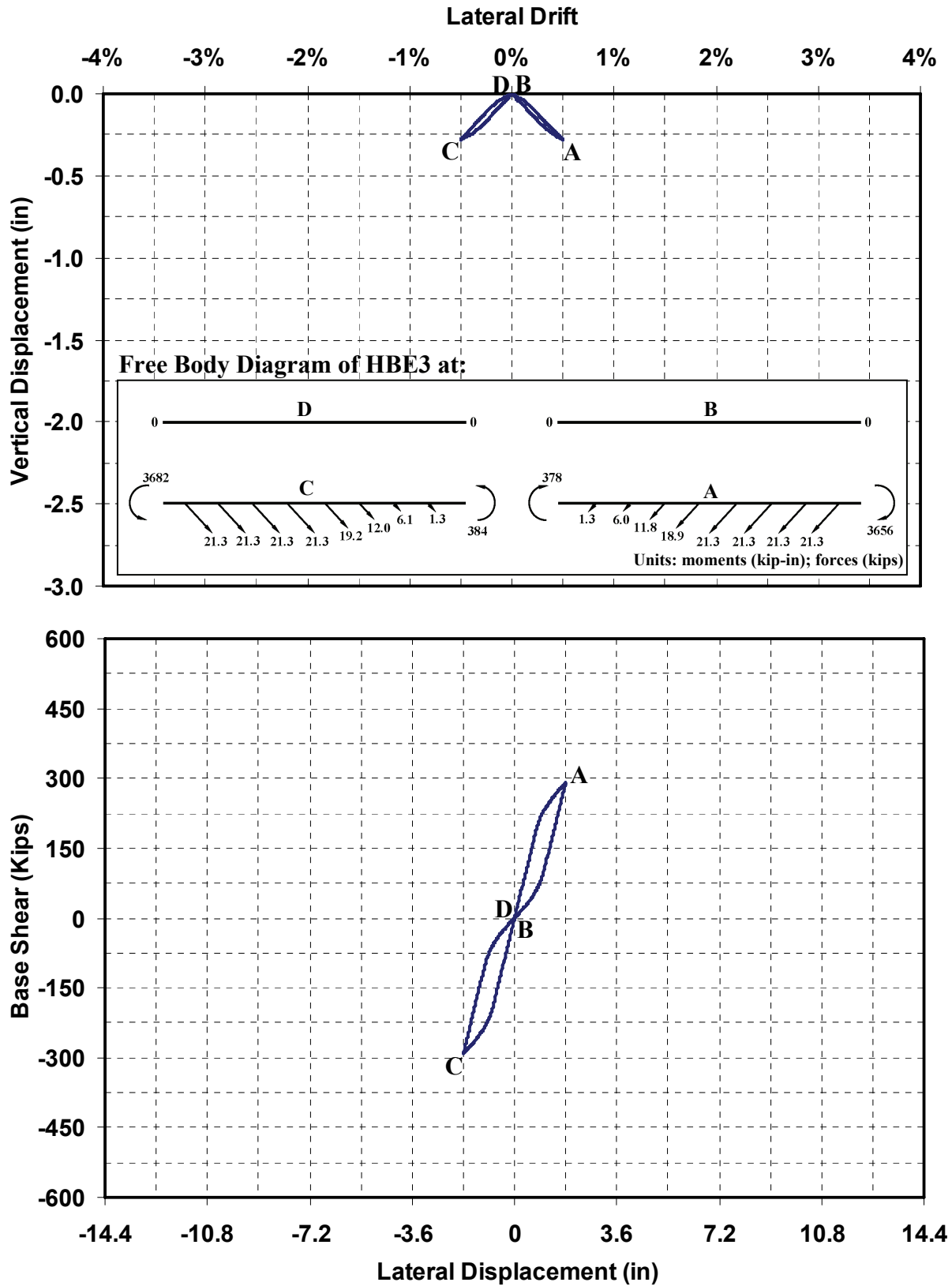


FIGURE 3-15 HBE3 Vertical Displacement and Structural Base Shear versus Top Floor Lateral Displacement for SPSW-CD at (a) 0.5% Drift Cycle (1st Cycle)

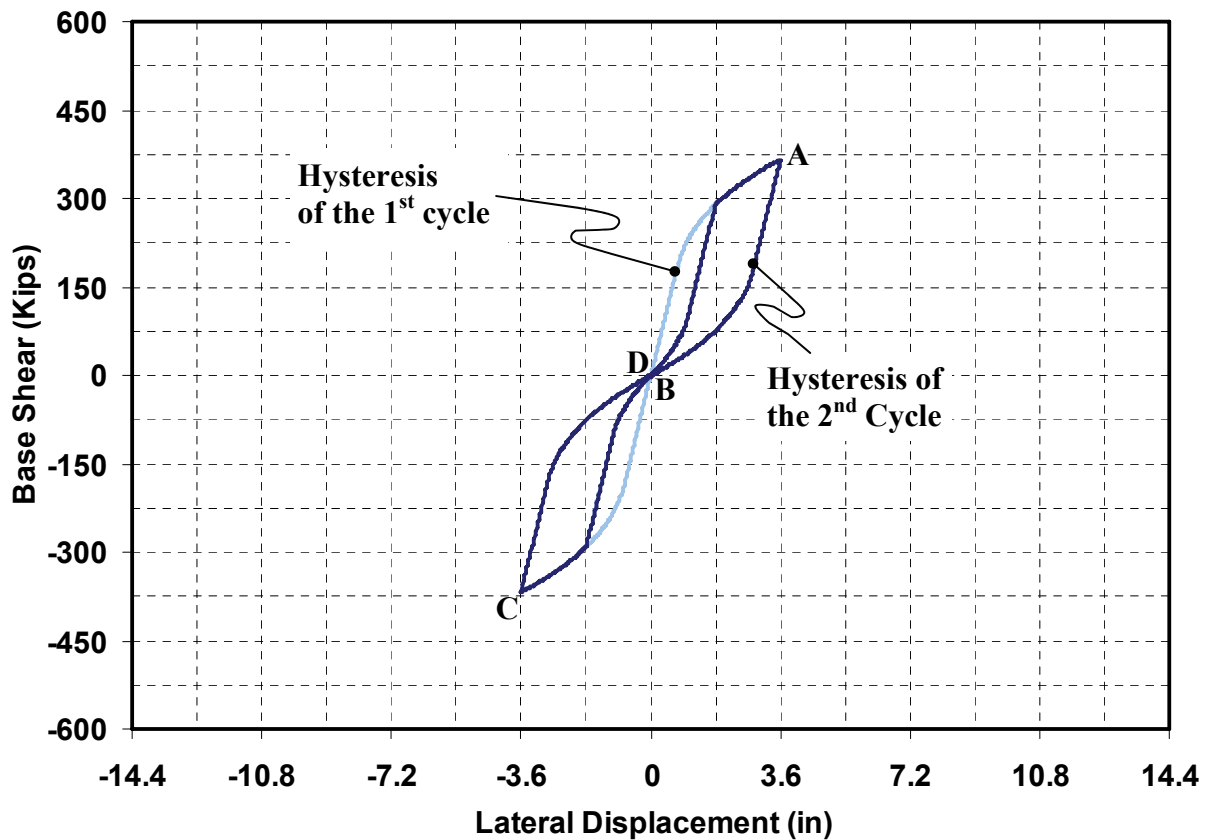
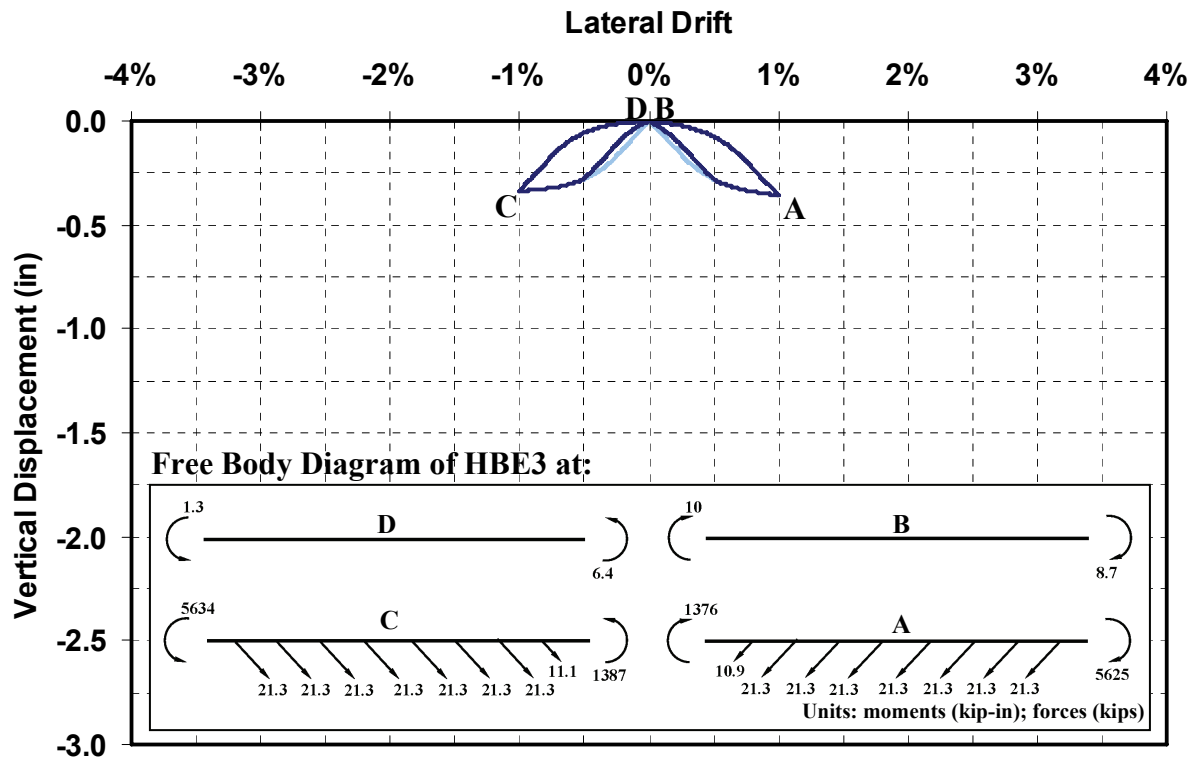


FIGURE 3-15 HBE3 Vertical Displacement and Structural Base Shear versus Top Floor Lateral Displacement for SPSW-CD at (b) 1% Drift Cycle (2nd Cycle) – Cont'd

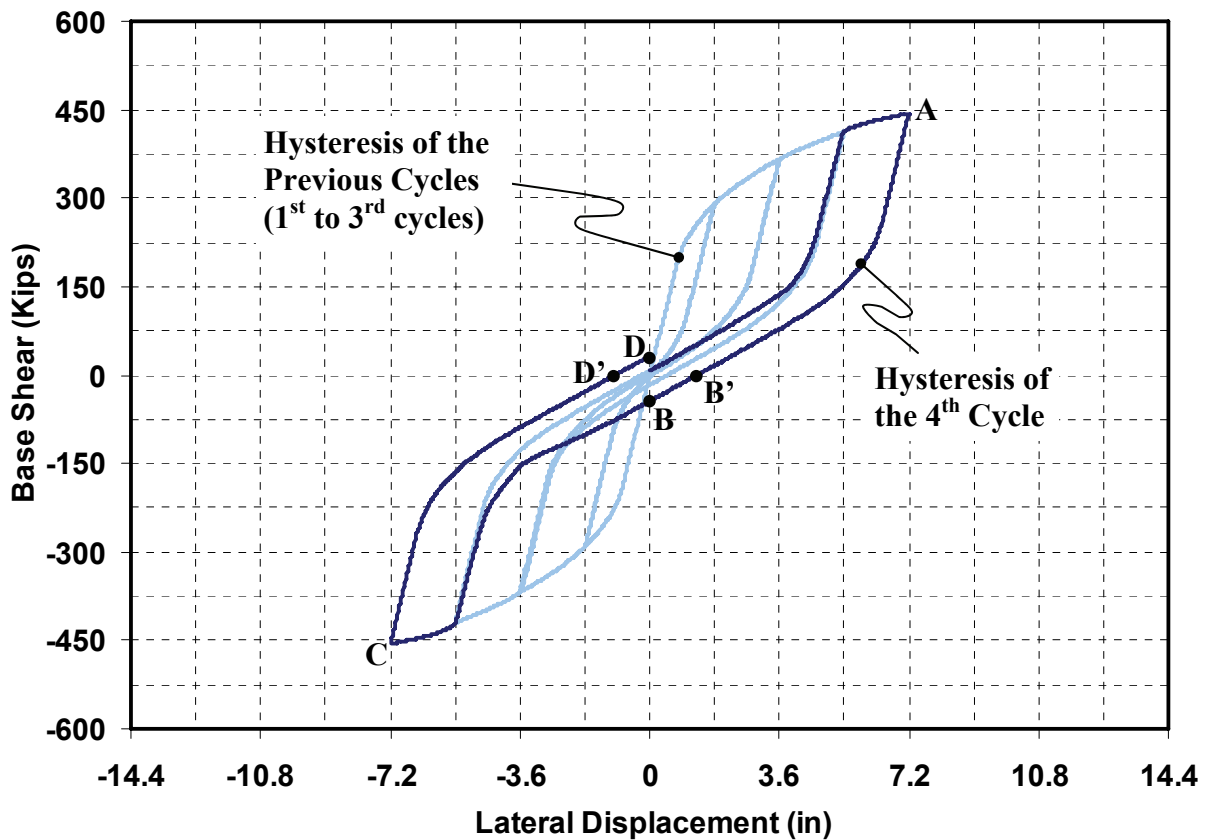
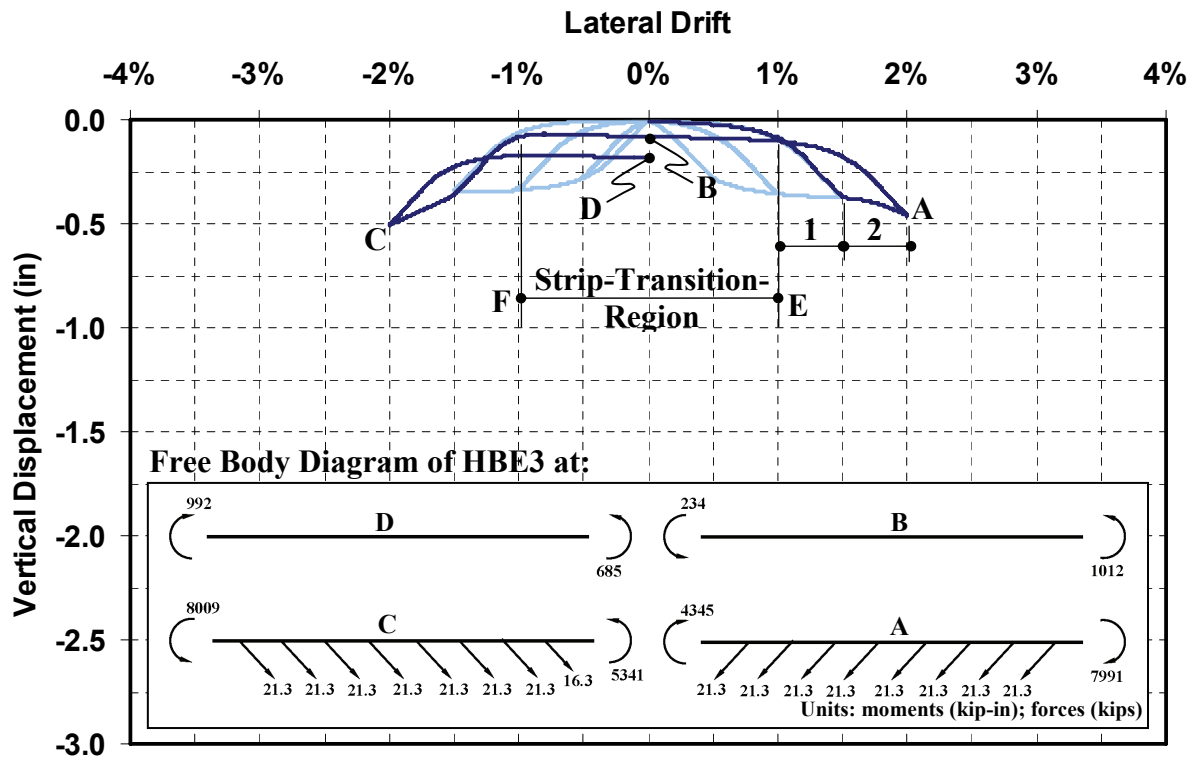


FIGURE 3-15 HBE3 Vertical Displacement and Structural Base Shear versus Top Floor Lateral Displacement for SPSW-CD at (c) 2% Drift Cycle (4th Cycle) – Cont'd

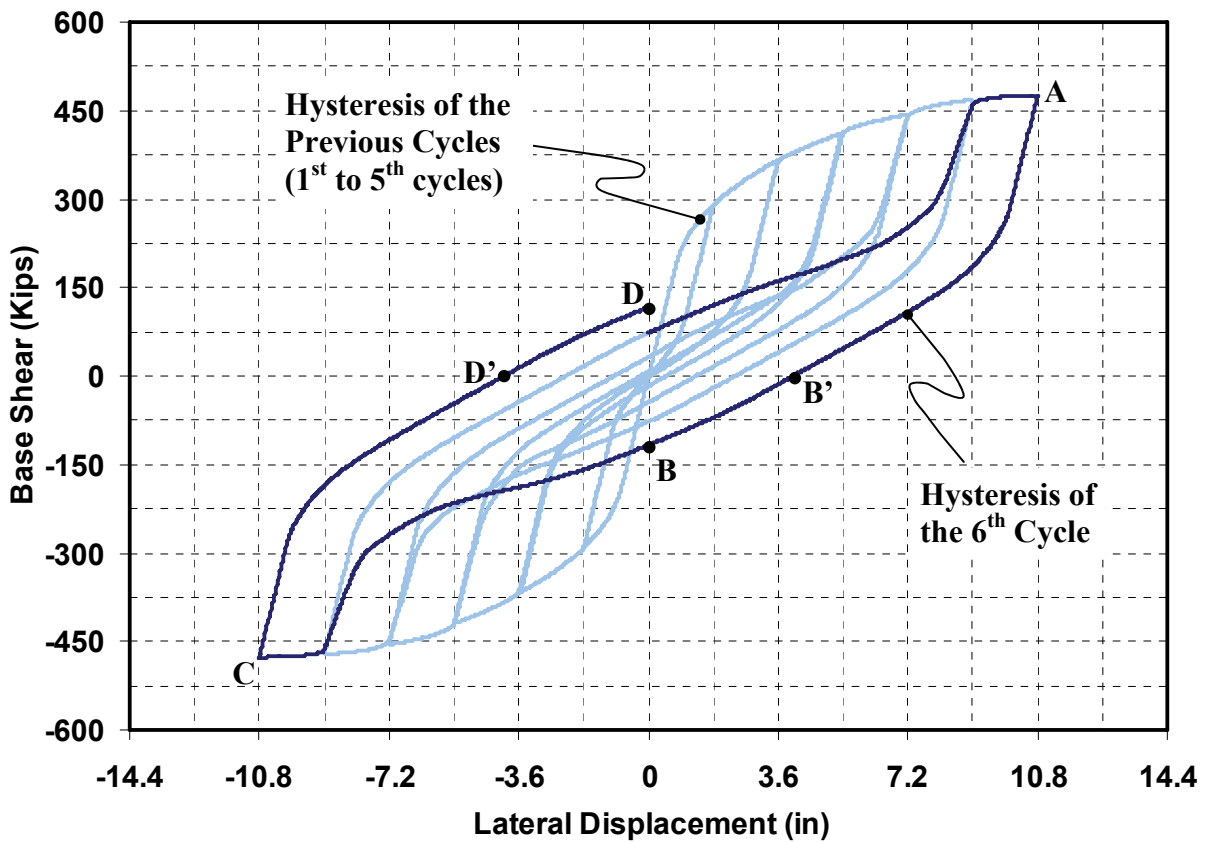
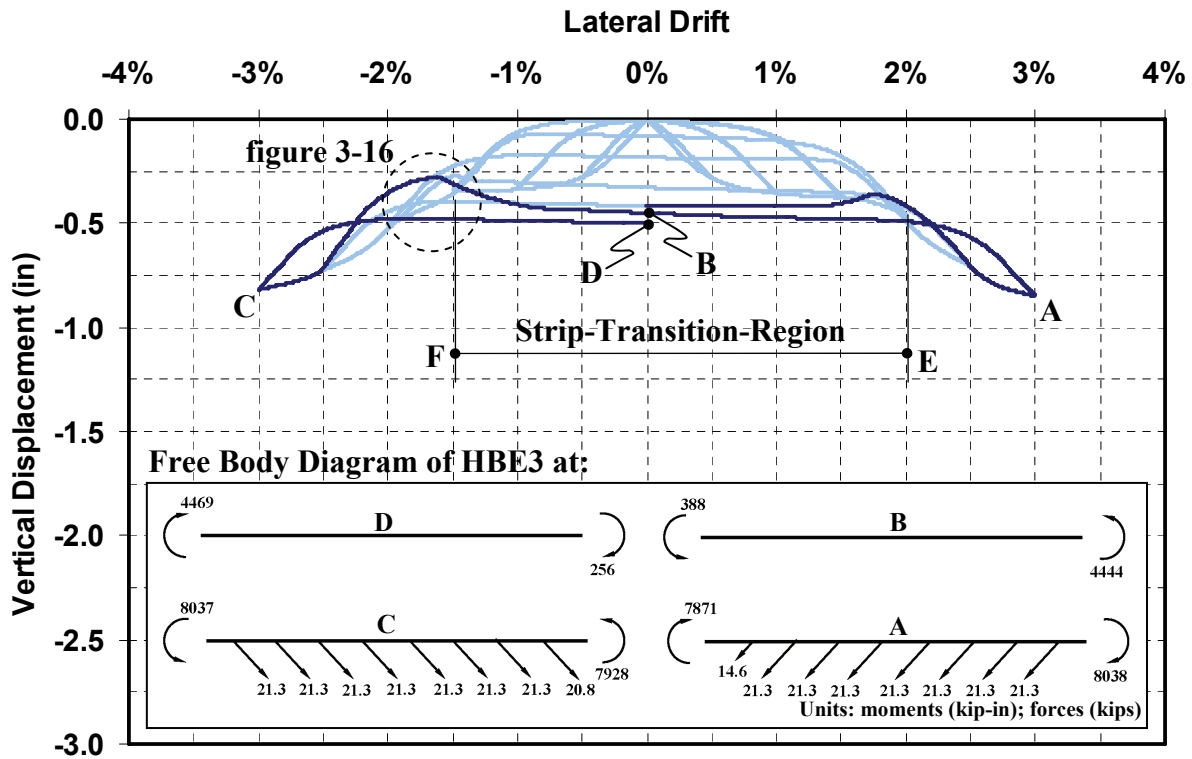


FIGURE 3-15 HBE3 Vertical Displacement and Structural Base Shear versus Top Floor Lateral Displacement for SPSW-CD at (d) 3% Drift Cycle (6th Cycle) – Cont'd

structure experienced a 290 kip base shear. A similar behavior was also exhibited when the structure was pushed to the opposite direction (i.e., to the left of the structure) up to point C, returning to point D. At the end of the cycle, point D overlapped point B in the original position. In other words, negligible residual vertical deformation remained in the HBE and base shear in the structure.

In the second cycle, during which the structure was pushed to the right and to the left up to a maximum lateral drift of 1%, the HBE behaved somewhat similarly to what was observed in the first cycle, except that more strips yielded. In fact, only one corner strip remained elastic; as shown in the HBE free body diagram at point A and C of figure 3-15(b), the axial force in the corner strip is 11 kips, which is less than the yielding forces P_y of 21.3 kips. As a result of the increasing tension forces from the infill plates, moments at the HBE ends also increased. The largest moment of 5634 kip-in occurred at the left end when the structure experienced -1% lateral drift (point C). Small moments, as high as 10 kip-in, remained at the HBE ends when structure returned to point B or D. Like in the previous cycle, negligible residual vertical deformation remained in the HBE and base shear in the structure.

Several newly observed behaviors emerged during the 2% drift cycle. First, all strips connected to the top HBE yielded, and each strip reached its yielding axial strength P_y of 21.3 kips, as shown in the HBE free body diagram at point A of figure 3-15(c). Hence, the maximum tension force from the infill plate has been reached and can not produce additional vertical deformation on the HBE. Note that this fully yielding condition of the infill plates has actually first occurred during the previous cycle (i.e., the 1.5% drift cycle). Although detailed results for the behavior of the HBE at 1.5% drift are not presented, the hysteretic trace at that drift is included along with that of all other cycles preceding the 2% cycle in figure 3-15(c); they are shown by the lighter color line in the figure. Here, the somewhat flat shape exhibited in the vertical displacement curve (i.e., on the 'loading' path starting from 1% to 1.5% drift, marked as region 1 in the figure) indicates the fully yielding condition of the infill plate, which does not induce additional vertical deformations on the HBE. Any increase in vertical deformations beyond that point (e.g., from 1.5% to 2.0% drift, marked as region 2 in the figure) were thus caused by the moments at the HBE ends that increased as the structure was pushed further to reach point A. Note that the same

behavior was also exhibited during the negative pushover displacement. Also note that although the axial forces in the corner strip (i.e., P equaled 16 kips when the structure reached point C) is less than the yield forces, this strip had actually yielded in the previous cycle (i.e., the 1.5% cycle).

Second, in addition to the previous behavior, complete plastification developed at the HBE right end during this cycle when the structure was at point A. Even though the developed end moment of 7991 kip-in was not perfectly equal to its theoretical plastic moment of 8093 kip-in (i.e., $M_{max} = 0.99M_p$), it is considered that a fully plastic condition has been reached based on the criteria described earlier in Section 3.4.1. Hence, a significant residual end moment of 1013 kip-in (or 12.5% M_p) remained at the HBE right end when the structure returned to its original position at point B. Consequently, even though no tension forces remained in the infill plates at that point, the vertical displacement at the mid-span did not return to zero but remained 0.1 in. downward as a residual deformation in the HBE. Furthermore, a somewhat similar behavior was also observed during the other half cycle when the structure was pushed to point C and returned to point D. In other words, complete plastification developed at the HBE left end at point C (i.e., M_{max} also equals to $0.99M_p$); and a significant residual moment of 992 kip-in (or 12.3% M_p) and a residual vertical displacement of 0.2 in. were observed at point D. Incidentally, also note that in terms of global behavior, if lateral forces were removed from the structure after the positive and negative pushover excursion cycles, lateral story displacements of 1.3 and 1.0 in., respectively, would have remained at the top floor as residual deformations. These residual story displacements are shown by point B' and D', respectively, in the base shear hysteresis curve of figure 3-15(c). In other words, lateral forces of 44 or 32 kips are needed to return the structure to its original position at point B or D, respectively.

Third, another interesting behavior observed during this cycle is the flat line on the vertical displacement curve in figure 3-15(c) marked from point E to F. The first point corresponds to a point at about +1% drift during the “unloading” path returned from point A, whereas the other point corresponds to a point at about -1% drift during the “loading” path to point C. This region (called here the “strip transition region”) is predominantly characterized as a state of behavior during which there are no axial forces in the strips – except for negligible axial forces observed in the corner strips at the beginning and the end of the region (i.e., the stage close to point E and F).

At point E, tension forces in the right-leaning strips have unloaded and become ineffective as the pushover displacement moved left (towards the negative drifts) while, at the same time, left-leaning strips have not yet recovered their elastic buckling deformations. Note that before the latter strips can resist loads again and provide plastic energy dissipation anew, the story frame must undergoes to its previous reached maximum drift, which in this case occurred at point F. At that point F, the left-leaning strips can anew resist the tension forces generated by the pushover displacement toward negative drifts. In this region, the vertical deformation in the HBE therefore was mainly affected by HBE end moments. Note that in this region the left and the right end moments have different curvatures (e.g., condition at point B). They produce contrary effects on the HBE vertical deformation: the left end moment reduces the deformation and the other one increases it as the structure gradually moves to left. Since the rate of moment changing at both ends is somewhat constant, consequently in this E-F region, the vertical deformation at the HBE mid-span is also somewhat constant.

In the last cycle considered here, at 3% drift, the strip-transition-region is even more apparent. As shown in figure 3-15(d), the region roughly exists between +1.5% and to -1.5% drift. The larger the pushover displacement applied to the structure, the longer the strip-transition-region will be. In terms of global behavior, the base shear history in this cycle is somewhat similar to that observed during the 2% drift cycle except that larger residual lateral displacements are observed at the top floor, on the order of 4 in. both at point B' and D'. However, one interesting trend first observed during the 3% drift cycle, is the 'bumps' exhibited in the vertical displacement curves, such the one circled by the dashed line in figure 3-15(d). This can be explained by tracking the free body diagram starting from point B, as done in figure 3-16. Here, the residual moments at the right and the left end are 55% and 4.7% of the HBE theoretical plastic moment, respectively. This significant difference plays an important role on the history of vertical displacements, as illustrated in figure 3-16. Up to the lateral drift of -1% from point B, the rate of moment changing at both ends is somewhat constant, which result in a flat curve similar to the one during the 2% drift cycle. However, as the pushover displacement continues and the magnitude of moment at the right end approaches the HBE plastic moment (i.e., condition at -1.5% drift), its contribution to increase the HBE vertical displacement gradually diminishes. By contrast, the left end which has sufficient capacity to absorb more moments becomes the primary factor in

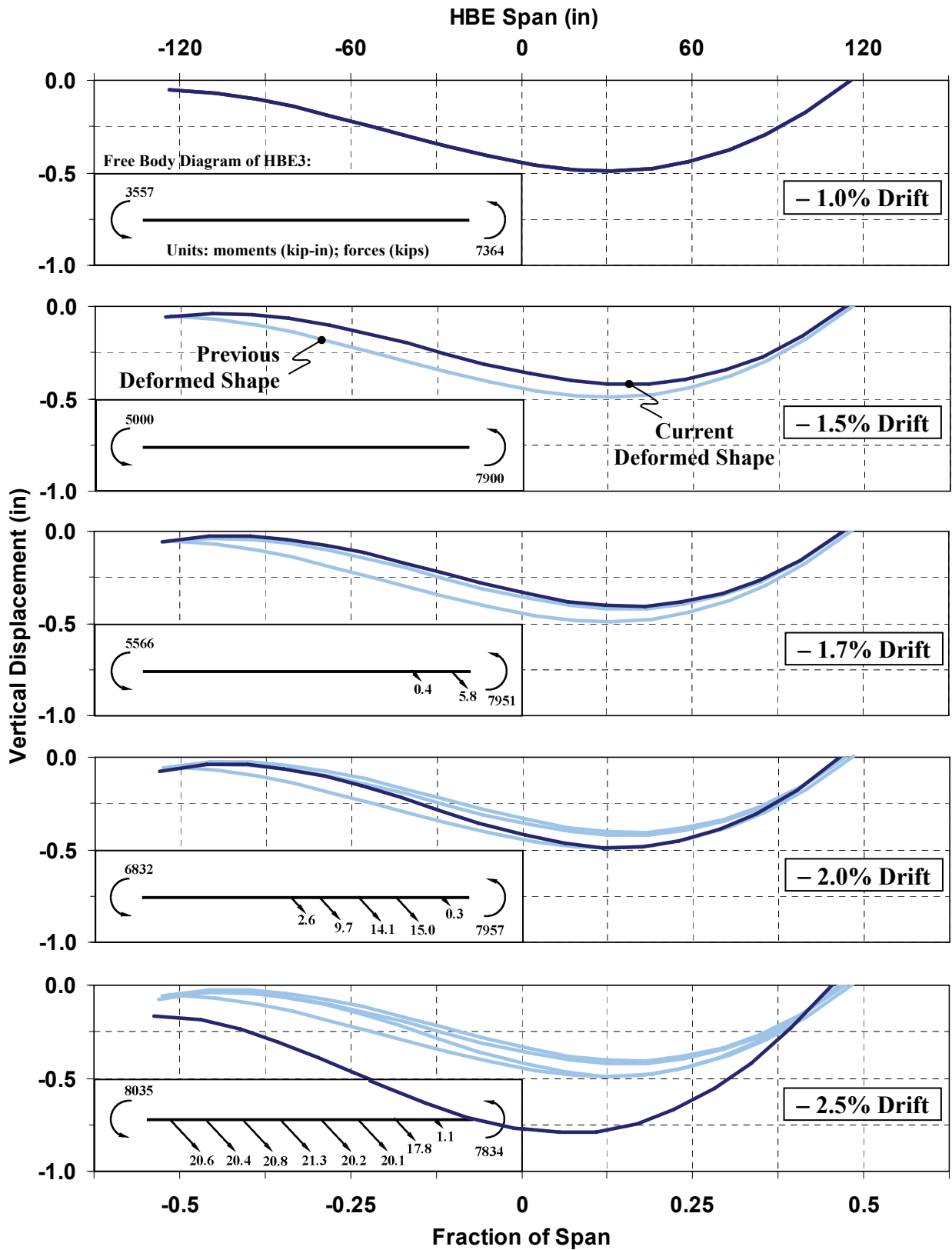


FIGURE 3-16 HBE3 Deformed Shapes at Various Lateral Drifts (“Bump” Behavior Observed in SPSW-CD)

reducing the HBE vertical displacement. This however does not remain for such a long duration because the left-leaning strips start to resist tension (i.e., condition at -1.7% drift) and the resulting tension forces bring the HBE down again (i.e., vertical displacement increases). Hence, this progressive transition between the right end moment, the left moment, and the tension force in the strips dictating behavior of the HBE explains the bump observed in the curve of the vertical displacement history.

Therefore, as demonstrated and explained above, the residual vertical deformations in the HBE of SPSW-CD are caused by the residual moments at the HBE ends after plastification has occurred at those locations. It was shown that prior to this plastification (i.e., at drifts less than 2% in this case), the HBE exhibited no residual deformations. Though such residual deformations appeared and increased beyond 2% drift, they stabilized once complete plastification occurred at both HBE ends. Note that if one would analyze a simply supported beam and apply end moments similar to the residual moments observed in the HBE (e.g., at 2% or 3% cycle), one would obtain vertical displacements identical to those obtained here. These results also confirm that tension forces from the infill plates do not produce detrimental effects along the HBE span of SPSW-CD. In other words, accumulation of plastic incremental deformation due to cyclic pushover displacement does not significantly develop for the SPSW-CD case.

3.4.4 Moment-Rotation Comparison

Another approach that can be used to examine the behavior of the two SPSWs is by comparing the moment-rotation hysteresis of their HBEs, as done in figure 3-17. The figure plots the normalized moment-rotation hysteresis of each HBE (arranged vertically from the top to the bottom HBE) obtained during the cyclic pushover displacements (figure 3-6). Plotted on the left side are curves for SPSW-ID, whereas on the right are curves for SPSW-CD. Here, normalized moment and rotation are plotted, respectively, relative to the corresponding HBE plastic moment capacity and to the required plastic rotation capacity of a special moment resisting frame, which equals to 0.03 radians (Bertero *et al.* 1994, SAC 1995). In other words, the normalized terms plotted are M/M_p and $\theta/\theta_{0.03}$, where M and M_p are the end moment and the corresponding HBE plastic moment capacity, respectively; θ and $\theta_{0.03}$ are the angle of rotation and the required plastic rotation capacity of a special moment resisting frame. In addition, diamond markers

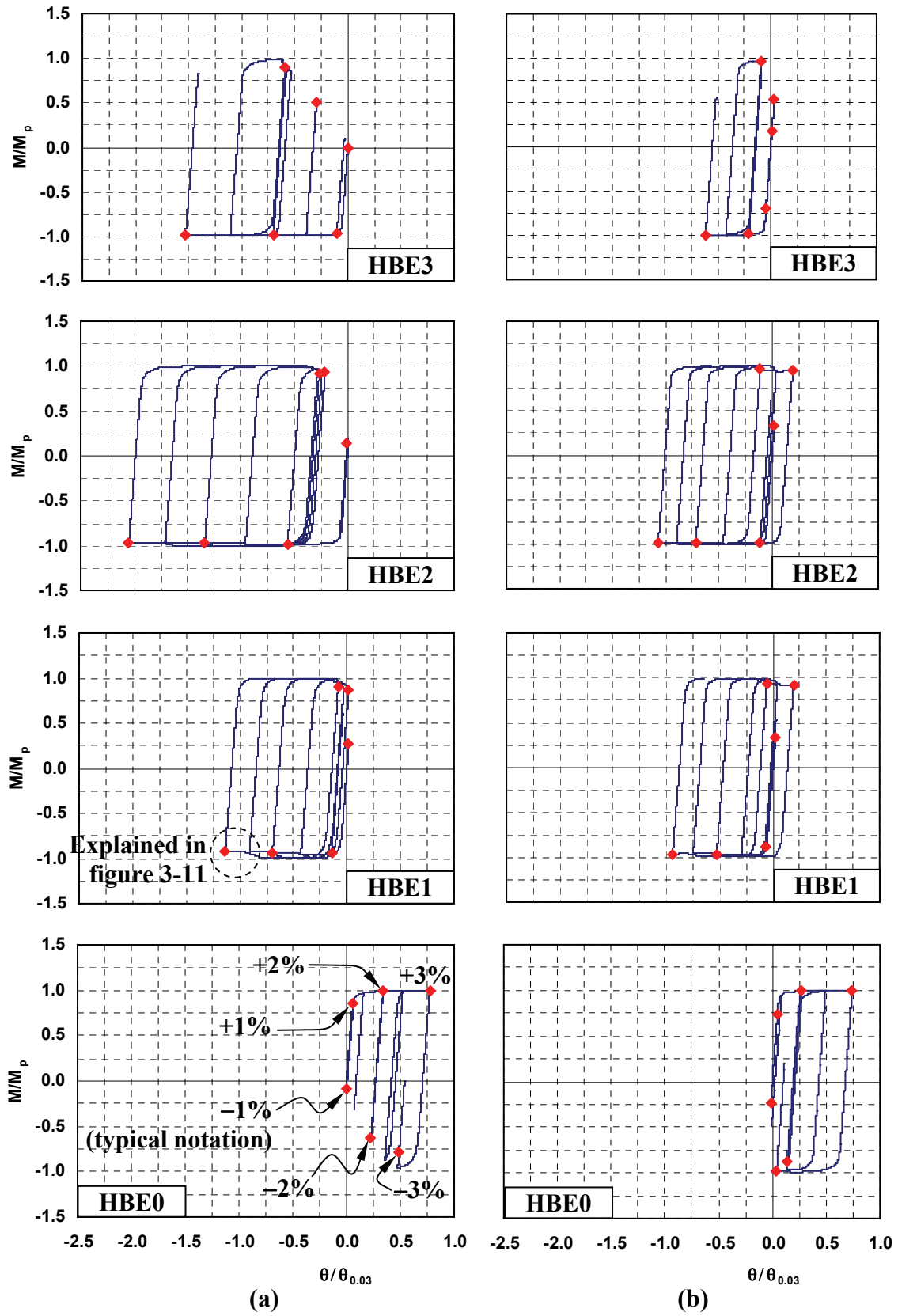


FIGURE 3-17 Normalized Moment Rotation Hysteresis at HBE Left End for (a) SPSW-ID; (b) SPSW-CD

included on each hysteretic curve correspond to the normalized values reached at lateral drifts of positive and negative 1%, 2%, and 3%, as indicated in the figure. Note that the hysteretic curves of both HBE ends are somewhat similar – except that they are the mirror image of each other – and thus only those of the HBE left end are presented.

Unlike the general hysteresis curve for special moment resisting frames, which is typically symmetric with respect to positive and negative rotations developed under a symmetric cyclic pushover displacement history, the hysteresis curves of both SPSWs considered here are not symmetric but looping with a bias toward one direction. It loops towards the positive side for the bottom HBE and to the negative side for the other HBEs, where positive and negative rotations here are respectively defined as corresponding to tension on the bottom and top side of the HBE. The tension forces from the infill plates contribute to this behavior by always pulling the HBE in the direction of the tension forces (i.e., pulling the bottom HBE upward and the other HBEs downward). For reference, Appendix E compares the hysteresis curves of both SPSWs and special moment resisting frames (i.e., their bare frames without the infill plates).

Moreover, one may notice in figure 3-17, at higher drifts, that after the plastic moment is reached, a small drop in the moment resisted is observed in several hysteresis curves before the maximum drift is reached (i.e., this is seen in the HBE0 and HBE1 hysteresis of SPSW-ID). Recall that no material degradation is considered in the analytical model (figure 2-6). Rather, this small drop of moment is an artifact of the transitional behavior previously explained in figure 3-11. To specifically relate the information in figure 3-11 with that in figure 3-17, one can observe that the diamond marker at +3% for HBE3 of SPSW-ID is located at 90% of the plastic moment ($M/M_p = 0.90$), as calculated and shown in figure 3-11.

Interestingly, except for the bottom HBE, all the moment-resisting ends of the HBEs of SPSW-ID developed a cross-section rotation (i.e., cross-section curvature multiplied by plastic hinge length) greater than 0.03 radians after the structure was pushed cyclically up to a maximum lateral drift of 3%. In one case (i.e., HBE2), the total (elastic and plastic) rotations even reached 0.062 radians. Such a significantly high cyclic rotation demand would be quite difficult to achieve using the type of moment resisting connections typically used in SPSW (recall that the

AISC 2005 Seismic Specifications only require that Ordinary-type connections be used in SPSW). In fact, it might also be difficult to achieve with special moment resisting frame (SMRF) beam-to-column connections approved by AISC 2005, which are experimentally verified to perform well up to ± 0.04 radians total rotations, or ± 0.03 radians plastic rotations. By comparison for SPSW-CD, all HBE total rotations obtained were less than or equal to 0.03 radians under the same cyclic pushover displacements up to 3% drift. This again implies that SPSW-CD has superior performance over SPSW-ID.

Given the objective of achieving proper connections in steel structures, moment-rotation relationships are frequently measured and reported at the locations of beam-to-column connections, as done in figure 3-17. Here, in light of the specific system behavior observed, it was also of interest to investigate the moment-rotation hysteresis at a typical location where in-span plastic hinge occurred. For this purpose, this was done for HBE2 of SPSW-ID, which is the HBE that developed the largest total rotations at its end [figure 3-17(a)] in the example considered; its normalized moment-rotation hysteresis at the mid-span (i.e., the location of in-span plastic hinge) is shown in figure 3-18.

Knowing that significant accumulation of plastic incremental deformations occurred in SPSW-ID, one might expect disproportionate rotations at the location of in-span plastic hinge. However, the result presented in figure 3-18 seems to contradict that expectation. Here, after the structure was pushed cyclically up to a maximum lateral drift of 3%, the total rotations at that hinge location only reached 0.024 radians (i.e., corresponding to the normalized rotation $\theta/\theta_{0.03}$ of 0.8). In reference to the plastic mechanism of SPSW-ID (figure 3-5), the total rotations were expected to be comparable in magnitude with that of the other plastic hinge at the right end of HBE2, which in this case was 0.062 radians (i.e., corresponding to a normalized rotation $\theta/\theta_{0.03}$ of 2.05). The flexibility of HBE2 primarily contributed to this phenomenon and difference between actual and expected rotations. As shown in the figure 3-12(a) for the deformed shape of SPSW-ID, due to elastic deformations, the slope at the mid-span of HBE2 (the location of in-span plastic hinge) was relatively small and no obvious “kink” was observed such as illustrated in figure 3-5. This explains why the cross-section rotation at the mid-span of HBE2 was less than that at the right end of HBE2.

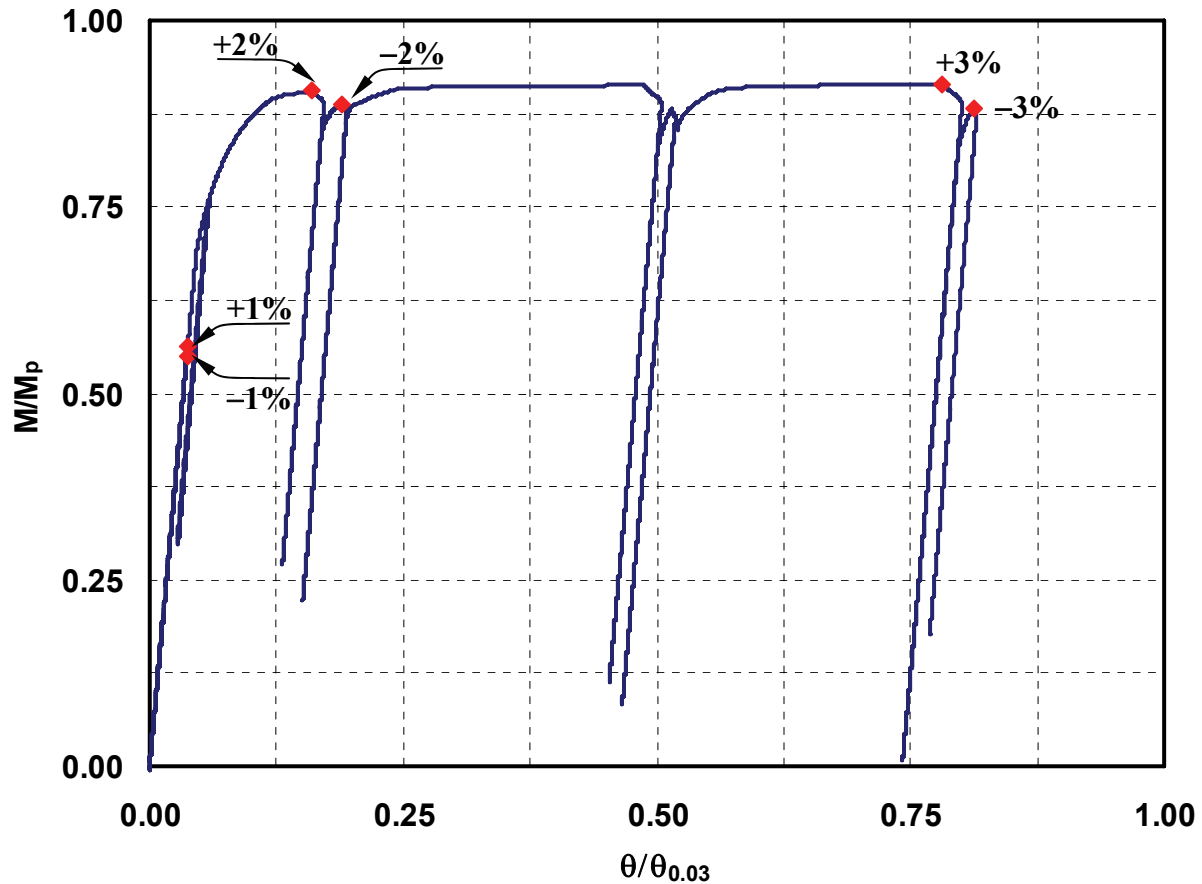


FIGURE 3-18 Normalized Moment Rotation Hysteresis at Mid-Span of HBE2 (SPSW-ID)

To verify this, a limited case study was conducted in which rigid members were assigned to all HBEs except at the location of fiber hinges, while the other analytical model properties remained the same as presented in Section 2.3. In the SAP2000, the rigid members were modeled by changing the HBE moment of inertias to be approximately 100 times their actual values. From this case study, it was verified that the total rotations at the mid-span indeed approached 0.06 radians.

An interesting behavior observed in the “hysteresis curve” of figure 3-18 is its “creeping” behavior, meaning that the rotation never comes back to zero, unlike what was observed in the end-span hinges (figure 3-17), but rather gradually increases regardless the direction of the cyclic pushover displacement. Here, the rotations were 0.002, 0.006, and 0.024 radians at the end of the 1%, 2%, and 3% cycles, respectively. Note that the normalized moment reached a maximum value of $0.92M_p$, shown by the flat line in the curve beyond the 2% drift cycle. This 8% reduction

of plastic moment capacity was due to the significant axial force developed at the mid-span of HBE2 ($P = 25\% P_y$ in this case). Note that a similar behavior was also observed at the locations of the other in-span plastic hinges in SPSW-ID, but with lesser total rotations.

In an overall perspective, although failures of HBE to VBE connections have been few in SPSW tested at the time of this writing, these results might also suggest that large drift may translate into large plastic rotations even for SPSW-CD. However, before mandating the use of SMRF connection for HBEs to VBEs, it is important to recognize that the plastic rotations demands observed here were not symmetric, by contrast with moment frame behavior. In other words, a SPSW-CD HBE rotation demand of $+0.0075$ to -0.03 radians is less critical than a SMRF beam rotation demand of ± 0.03 radians. The SPSW-ID HBE rotation demands of 0.0 to 0.06 radians, however, may approach that of the SMRF. More research may help develop a better understanding of this acceptable rotation demands in SPSW.

3.5 Summary

An analytical investigation on the seismic behavior of steel plate shear walls having boundary elements designed by two different philosophies was conducted. The investigation consisted of monotonic and cyclic pushover analyses. The monotonic pushover analysis has verified that one possible result of the Indirect Design Approach is that the SPSW-ID developed in-span plastic hinge on several of its horizontal boundary elements, while the SPSW-CD, designed with the Capacity Design Approach, only developed plastic hinges at the ends of its horizontal boundary elements. A sway and beam combined plastic mechanism occurred in SPSW-ID, whereas a sway plastic mechanism occurred in SPSW-CD. A general equation to calculate the ultimate strength of both single and multistory SPSW with the sway and beam combined mechanism was developed using the kinematic method of plastic analysis. In addition, several key behaviors observed during a cycle by cycle investigation on HBE deformation history under the cyclic loading were identified.

Using the monotonic and cyclic pushover analyses, significant consequences to having in-span plastic hinges were identified. It was demonstrated that plastification along HBE spans, such as in

the case of SPSW-ID, can detrimentally impact behavior of the structure by inducing significant accumulation of plastic incremental deformations on the HBEs, themselves leading to partial yielding of the infill plates and correspondingly lower global plastic strength compared to the values predicted by code equations (i.e., AISC 2010). By comparison, SPSW-CD developed plastic hinges only at HBE ends together with a completely yielded infill plates (i.e., in compliance with the behavior expected by the AISC Seismic Provisions 2005), and relatively smaller vertical displacements along the HBE spans. In addition, plastification along the HBE span of SPSW-ID caused total (elastic and plastic) rotations greater than 0.03 radians at the ends of the intermediate and top HBEs (in one case even reaching 0.062 radians) after the structure was pushed cyclically up to a maximum lateral drift of 3%. Under the same cyclic pushover displacements, all total rotations in the HBEs of SPSW-CD were less than or equal to 0.03 radians.

SECTION 4

NONLINEAR TIME HISTORY ANALYSIS

4.1 General

The cyclic pushover analysis in the preceding section has shown that plastification along the HBE spans of SPSW-ID has significant consequences on the behavior of the structure. Significant accumulation of plastic incremental deformations was observed on each of its HBE. As a result, it caused partial yielding of the infill plates and correspondingly lowered global plastic strength of the SPSW-ID. In addition, the analysis has validated that the SPSW-CD, which has plastic hinges only at HBE ends, performed better than the SPSW-ID in terms of completely yielding infill plates (i.e., reaching its global plastic strength) and relatively smaller vertical displacements along the HBE spans.

While several key seismic behaviors of steel plate shear walls having horizontal boundary elements designed to have different plastic mechanisms have been discovered through the incrementally cyclic pushover analysis, conducting time history analysis remains necessary to investigate whether those previous results would be replicated during earthquakes excitations and whether additional seismic behaviors for the aforementioned SPSW systems would emerge as a consequence of the random nature of earthquake records. This verification is also important given that unstiffened web plates can only yield in tension (i.e. requiring greater drifts to yield more).

This section describes the nonlinear time history analyses conducted on both SPSW-ID and SPSW-CD. Performance of both SPSWs is investigated when subjected to synthetic ground motions, with response spectra scaled to match the design basis earthquake target spectra. In addition, comparison of results between the previous cyclic pushover analysis and the time history analyses are presented. Finally, the nonlinear time history analyses are extended to investigate the performance of both SPSWs under the more severe considered ground motions.

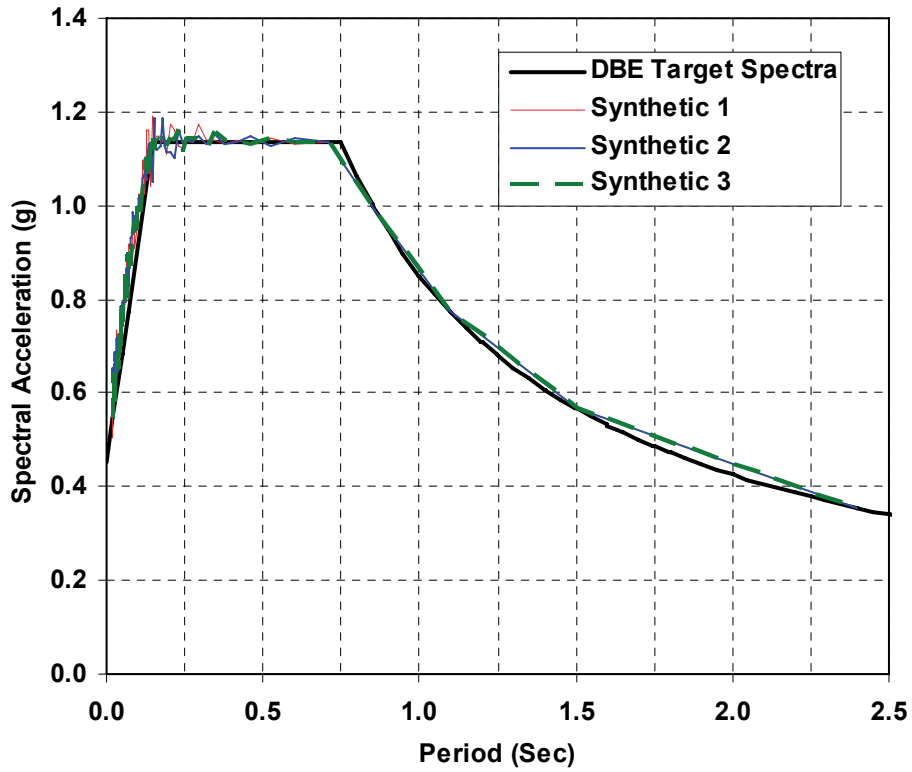
4.2 Synthetic Ground Motions

Three synthetic time histories of ground acceleration were used as ground motions for conducting nonlinear time history analyses. These synthetic ground motions were generated by the computer code TARSCTHS – Target Acceleration Spectra Compatible Time Histories (Papageorgiou *et al.*, 1999) after providing input data such as target response spectra, moment magnitude of seismic source (M_w), and site-to-source distance (R).

TARSCTHS-generated strong motions accurately match any user-specified spectra, which allows to investigate inelastic time-history behavior considering a small number of earthquake excitations that can simulate with high fidelity the demands anticipated for the specified target design spectra. Here, the target response spectra was the design response spectra shown in figure 2-1 and generated only up to the period of 2.5 seconds, which corresponded to the largest possible theoretical value of the fundamental period for the considered SPSWs (it was estimated for the condition after the infill plates of SPSW-ID have stretched during yielded and thus stopped contributing to the wall stiffness, and considering only the contribution of the boundary frames for lateral resistance). The moment magnitudes of the three synthetic ground motions denoted as SYNT1, SYNT2, and SYNT3 were 6.5, 7.0, and 7.5, respectively; and the site-to-source distances were 11, 18, and 25 km for the same respective synthetic ground motions. The spectral acceleration and synthetic ground motions were generated to last up to 25 seconds, with about 15 seconds of strong motions, as shown in figure 4-1. Part (a) of that figure presents the response spectra of these synthetic time histories, showing how closely they matched the design basis earthquake (DBE) target spectra over the periods of interest. The peak ground accelerations (PGA) of these synthetic ground motions are 0.51g, 0.63g, and 0.59g for the SYNT1, SYNT2, and SYNT3, respectively.

4.3 Analysis Results

The HBE maximum and residual vertical deformations of both SPSW-ID and SPSW-CD due to the synthetic ground motions SYNT1, SYNT2, and SYNT3 are compared in table 4-1. In general, each synthetic ground motion generates somewhat the same maximum deformation as well as residual deformation for a given HBE in a given SPSW, but values are smaller for SPSW-CD



(a) DBE Target Spectra and Synthetic Spectra

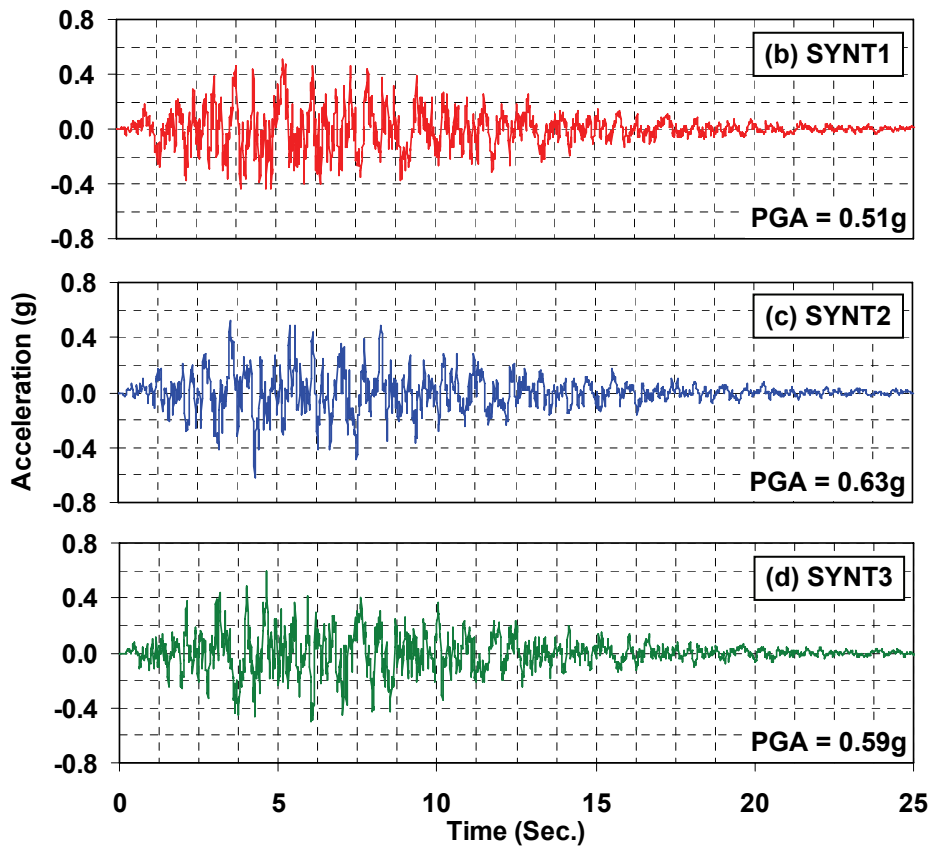


FIGURE 4-1 Spectral Acceleration and Synthetic Ground Motions

TABLE 4-1 HBE Maximum and Residual Vertical Deformations (DBE Case)

Location of HBE	Synthetic Ground Motion	SPSW-ID		SPSW-CD	
		δ_{\max} (in)	δ_{residual} (in)	δ_{\max} (in)	δ_{residual} (in)
HBE3	SYNT1	2.7	1.4	0.8	0.3
	SYNT2	3.2	2.0	0.9	0.2
	SYNT3	2.8	1.5	0.6	0.2
	Average	2.9	1.6	0.8	0.2
	Maximum	3.2	2.0	0.9	0.3
HBE2	SYNT1	3.0	1.4	1.1	0.3
	SYNT2	2.7	1.3	1.1	0.3
	SYNT3	2.6	1.1	1.0	0.3
	Average	2.8	1.3	1.1	0.3
	Maximum	3.0	1.4	1.1	0.3
HBE1	SYNT1	1.4	0.7	0.8	0.4
	SYNT2	1.5	0.6	0.9	0.4
	SYNT3	1.9	0.7	0.8	0.3
	Average	1.6	0.7	0.8	0.4
	Maximum	1.9	0.7	0.9	0.4
HBE0^a	SYNT1	0.8	0.2	0.5	0.2
	SYNT2	0.9	0.3	0.4	0.1
	SYNT3	1.0	0.4	0.5	0.1
	Average	0.9	0.3	0.5	0.1
	Maximum	1.0	0.4	0.5	0.2

Note: ^a Positive (upward) vertical deformation, while all other values are negative (downward) vertical deformations.

compared to SPSW-ID. For example, HBE3 maximum deformations for SPSW-ID are 2.7, 3.2, and 2.8 inches due to the synthetic ground motions SYT1, SYNT2, and SYNT3, respectively. For the SPSW-CD, those values are 0.8, 0.9 and 0.6 inches for the same respective synthetic ground motions. In this example, SYNT2 is the governing ground motion; in other cases however, SYNT1 (e.g., for HBE2) and SYNT3 (e.g., for HBE1) play that role. Hence, to represent the outcomes of the nonlinear time history analysis for the purpose of verifying the previous cyclic pushover analysis results, the governing ground motion per the ASCE 7-05 procedure is selected as being the one that creates the largest vertical deformation (HBE3). Here, it is SYNT2 and the results obtained from this ground motion on HBE3 (which experienced the largest deformations) are used predominantly in the following discussion.

Before presenting the comparison results of cyclic pushover and time history analyses, performance of SPSW-ID and SPSW-CD due to the ground excitation (i.e., SYNT2) is first compared, as plotted in figure 4-2. The figure shows the complete histories of HBE3 vertical deformation both for SPSW-ID and SPSW-CD. As previously observed in the case of cyclic pushover analysis, here in the nonlinear time history analysis, the accumulative plastic incremental deformation is still observed, with maximum and residual vertical deformations more apparent on SPSW-ID than on SPSW-CD. For example, when SPSW-CD reached a lateral drift of 1% for the first time (marked as point A in the figure), the largest HBE3 vertical displacement recorded was about 0.4 in., while at the same drift, the corresponding displacement for SPSW-ID (marked as point A' in the figure) had reached 0.9 in., namely 2.25 larger. Note that in the time history records, those two conditions did not occurred at the same time (i.e. 1% drift was reached at different times for different ground motions). As the ground excitation increased and caused a 2% lateral drift on both structures for the first time, the difference between the two became even greater (i.e., 4 times larger). Here, the largest HBE3 vertical displacements recorded were 0.7 and 2.8 in. for SPSW-CD and SPSW-ID (marked as points B and B' in the figure), respectively. This implies that the HBE3 vertical downward displacement for SPSW-ID increased faster than that for SPSW-CD as the lateral drift increased. Moreover, the same trend was exhibited for the maximum vertical displacement (0.9 in. vs. versus 3.2 in) as well as the residual vertical displacement at the end of the record (0.2 in. versus 2.0 in.), for the same respective SPSWs. Note that the maximum vertical displacements for SPSW-CD and SPSW-ID did not occur at the

same lateral drift. Figure 4-3 presents the complete histories of each HBE vertical displacement due to the synthetic ground excitation SYNT2. This information verifies that other HBEs for both SPSWs also have a behavior similar to that described for HBE3, except at a smaller magnitude.

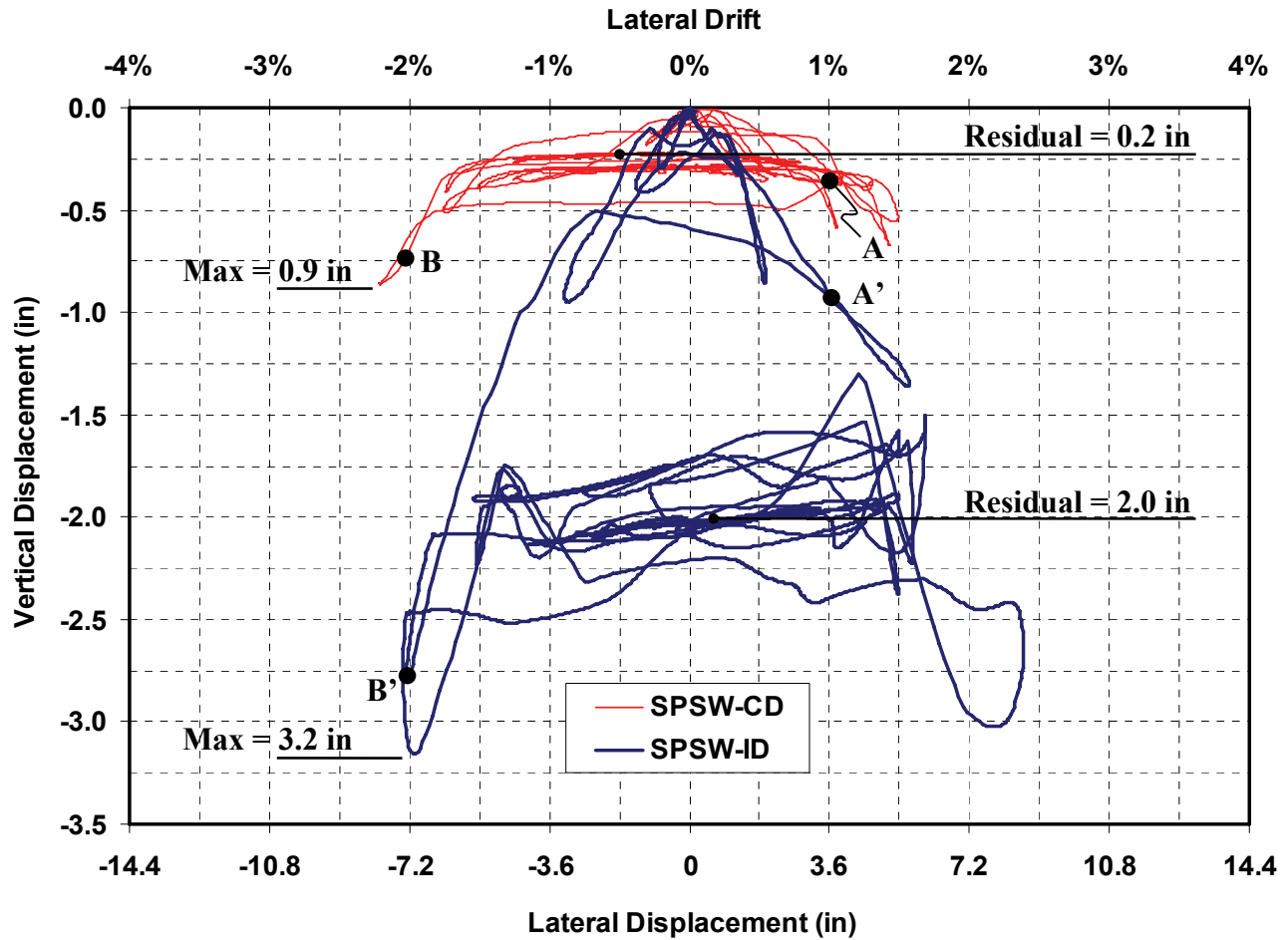


FIGURE 4-2 HBE3 Vertical Displacement versus Top Floor Lateral Displacement Obtained from Time History Analysis (SYNT2)

Figure 4-3 also compares the results obtained from the cyclic pushover analysis (shown by the lighter color line in the figure up to 2.5% drift). In general, vertical displacements of each HBE for both SPSWs obtained from both analyses have somewhat the same magnitude, except for HBE3 of SPSW-ID for which the nonlinear time history analysis gave a greater vertical displacement. This can be observed graphically at the top-left curve of figure 4-3 where the nonlinear time history curve is significantly offset from the cyclic pushover curve starting from about the 1% drift cycle. As numerically compared in table 4-2 for HBE3 of SPSW-ID, the maximum vertical deformation obtained from the nonlinear time history analysis is 1.8 times

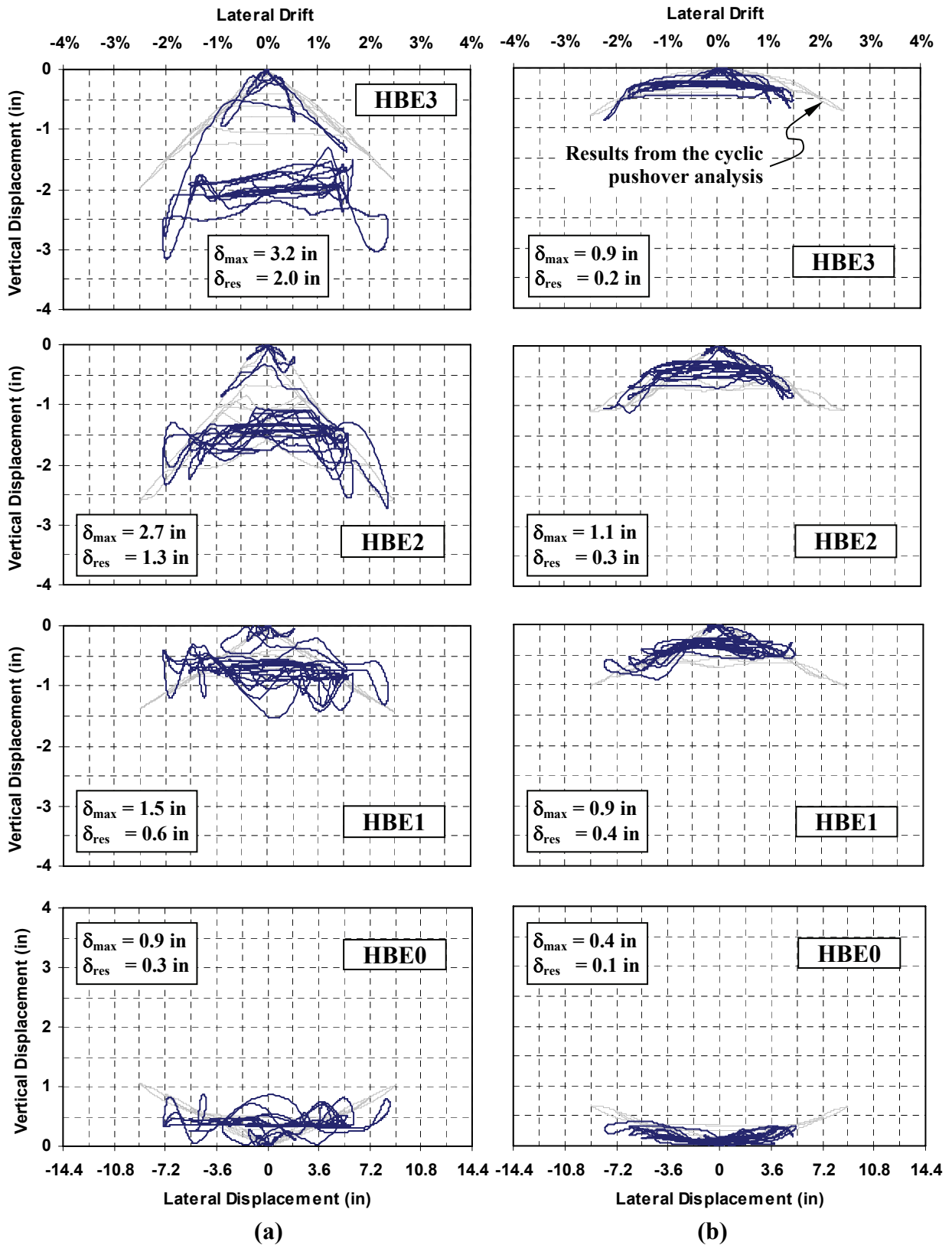


FIGURE 4-3 Nonlinear Time History Analysis Results (SYNT2): Structure Lateral Displacement versus HBE Vertical Displacement for (a) SPSW-ID; (b) SPSW-CD

TABLE 4-2 Comparison of HBE Maximum Vertical Deformation Obtained from Cyclic Pushover Analysis and Nonlinear Time History Analysis (SYNT2)

Location of HBE	SPSW-ID		SPSW-CD	
	$\delta_{\max\text{-CYC}}^1$ (in)	$\delta_{\max\text{-TH}}^2$ (in)	$\delta_{\max\text{-CYC}}^1$ (in)	$\delta_{\max\text{-TH}}^2$ (in)
HBE-3	1.8	3.2	0.7	0.9
HBE-2	2.5	2.7	1.1	1.1
HBE-1	1.4	1.5	0.9	0.9
HBE-0	1.0	0.9	0.6	0.4

Note: ¹⁾ HBE maximum vertical deformation at the corresponding absolute maximum drift (i.e., at 2.4% and 2.2% drift for SPSW-ID and SPSW-CD, respectively)

²⁾ Range of drifts (SYNT2): -2.1% to +2.4% (SPSW-ID) and -2.2% to +1.5% (SPSW-CD)

higher than that obtained from the cyclic pushover analysis, while for the other HBEs of both SPSWs, the magnitudes are relatively similar. Note that, to ensure a consistent comparison, information in table 4-2 for the cyclic pushover analysis is obtained at the maximum drift that occurred during the nonlinear time history analysis (i.e., at 2.4% and 2.2% drift for SPSW-ID and SPSW-CD, respectively). Note that a similar behavior presented here for the case of SYNT2 was also observed for the case of SYNT1 and SYNT3, although these redundant results are not presented here.

The nonlinear time history analyses were then extended to investigate the performance of both SPSWs under the more severe considered ground motions (typically defined by building codes as the Maximum Considered Earthquake or MCE). Again, the TARSC THS computer code was used to generate three synthetic time histories of ground motions, that had moment magnitudes and site-to-sources distances similar to those in the DBE case but whose response spectra matched the MCE target spectra (for which vertical ordinates are 1.5 times greater than the DBE target spectra plotted in figure 2-1). To distinguish from the DBE case, the resulting three synthetic ground motions are denoted as SYNT4, SYNT5, and SYNT6. Their PGAs were 0.81g, 0.79g, and 0.82g for the respective synthetic ground motions. The maximum vertical deformation for each HBE of both SPSWs is summarized in table 4-3. Here, the governing ground motion is SYNT5, which created the largest vertical deformation on HBE3.

TABLE 4-3 HBE Maximum and Residual Vertical Deformations (MCE Case)

Location of HBE	Synthetic Ground Motion	SPSW-ID		SPSW-CD	
		δ_{\max} (in)	δ_{residual} (in)	δ_{\max} (in)	δ_{residual} (in)
HBE3	SYNT4 ^a	4.8	3.3	0.9	0.1
	SYNT5	5.1	3.6	0.9	~0.1
	SYNT6	4.8	3.3	0.9	0.1
	Average	4.9	3.4	0.9	0.1
	Maximum	5.1	3.6	0.9	0.1
HBE2	SYNT4	3.7	2.0	1.4	0.1
	SYNT5	4.6	2.7	1.4	~0.1
	SYNT6	3.9	2.1	1.2	0.1
	Average	4.1	2.3	1.3	0.1
	Maximum	4.6	2.7	1.4	0.1
HBE1	SYNT4	2.1	0.6	1.1	0.3
	SYNT5	1.9	0.8	1.2	0.3
	SYNT6	2.1	0.8	1.1	0.2
	Average	2.0	0.7	1.1	0.3
	Maximum	2.1	0.8	1.2	0.3
HBE0^b	SYNT4	1.9	1.0	0.7	0.2
	SYNT5	1.5	0.8	0.7	0.2
	SYNT6	1.8	0.9	0.7	0.1
	Average	1.7	0.9	0.7	0.2
	Maximum	1.9	1.0	0.7	0.2

Note: ^{a)} To distinguish from the DBE case, the ID number is intentionally started from 4.

^{b)} Positive (upward) vertical deformation, while all other values are negative (downward) vertical deformations.

An interesting trend is observed when comparing the HBE vertical deformation results between the DBE and MCE cases as presented in table 4-4. As the severity of the synthetic ground motions increases for the MCE case (consequently generating higher lateral drifts on both SPSWs), HBE vertical deformations of SPSW-ID especially at the top two floors significantly increased compared to the corresponding magnitudes in the DBE case. For example, HBE3 maximum vertical deformation increased from 3.2 inches in the DBE case to 5.1 inches in the MCE case. By comparison for SPSW-CD, relatively minor changes occurred with respect to the magnitude of HBE vertical deformations. Hence, when formation of in-span plastic hinges on HBES is possible, such as in the case of SPSW-ID, the greater the severity of the ground excitations striking the structure, the more accumulation of plastic incremental deformation observed.

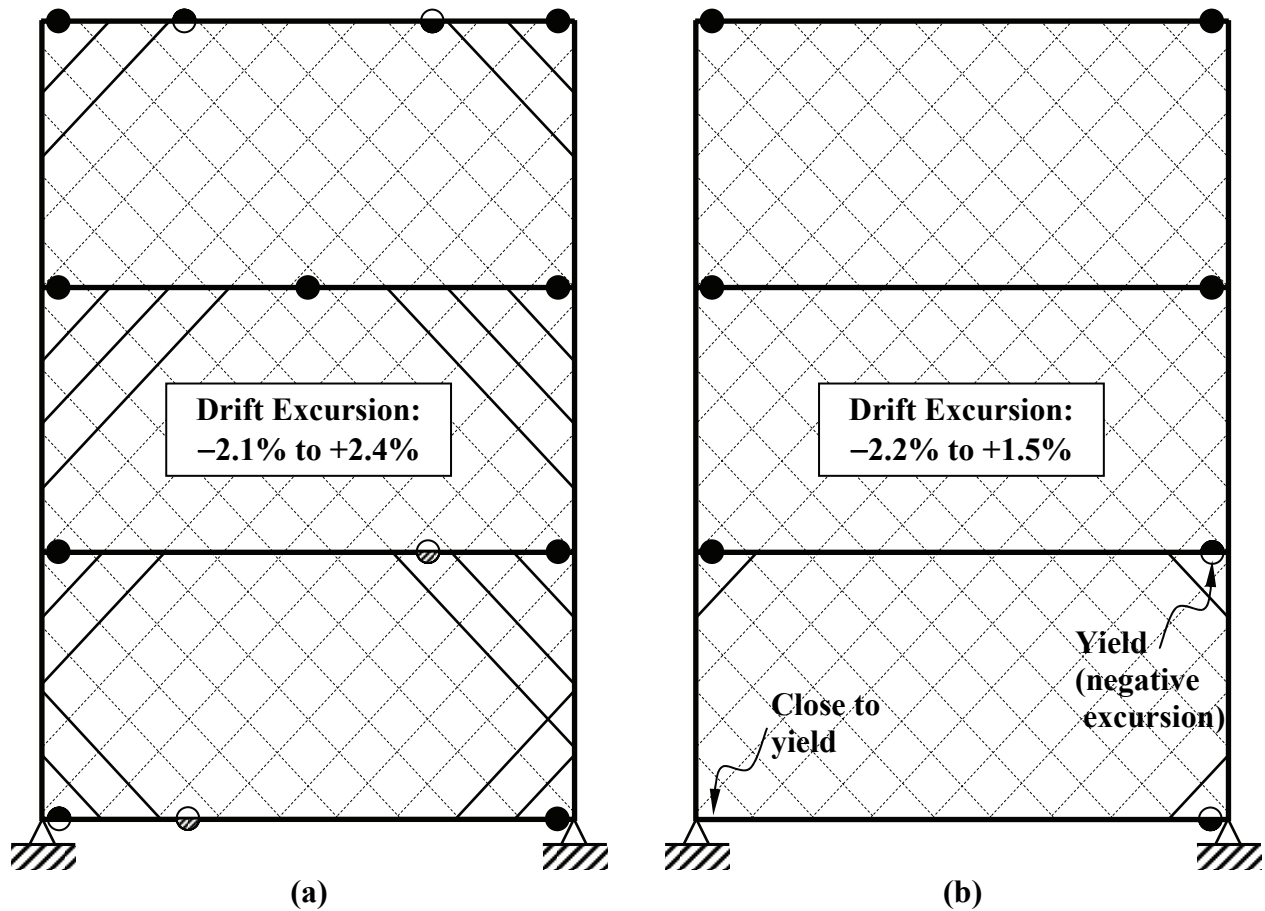
TABLE 4-4 Comparison of HBE Maximum Vertical Deformation Obtained from Nonlinear Time History Analysis of DBE and MCE Case

Location of HBE	SPSW-ID		SPSW-CD	
	$\delta_{\max\text{-DBE}}^1$ (in)	$\delta_{\max\text{-MCE}}^2$ (in)	$\delta_{\max\text{-DBE}}^1$ (in)	$\delta_{\max\text{-MCE}}^2$ (in)
HBE-3	3.2	5.1	0.9	0.9
HBE-2	2.7	4.6	1.1	1.4
HBE-1	1.5	1.9	0.9	1.2
HBE-0	0.9	1.5	0.4	0.7

Note: ¹⁾ Range of drifts (SYNT2): -2.1% to +2.4% (SPSW-ID) and -2.2% to +1.5% (SPSW-CD)

²⁾ Range of drifts (SYNT5): -2.7% to +4.0% (SPSW-ID) and -3.4% to +3.2% (SPSW-CD)

Lastly, plastic hinge and strip yielding distributions on SPSW-ID and SPSW-CD due to the synthetic ground motion SYNT2 are presented in figure 4-4. A similar condition with the one presented for the cyclic pushover analysis is observed. In-span plastic hinges and partially yielded infill plates characterize SPSW-ID, while plastic hinges only at the HBE ends and almost fully yielded infill plates characterize SPSW-CD.



Legend:

- ⊗ | ● = partial plastification | fully plastic in **positive** drift (defined in Section 3.4.1).
- ⊙ | ◐ = partial plastification | fully plastic in **negative** drift
- ⊘ | ● = partial plastification | fully plastic in both directions (**positive** and **negative** drifts)
- = strip yielding ($P = P_y$)

FIGURE 4-4 Plastic Hinge and Strip Yielding Distributions at the end of Nonlinear Time History Analysis (SYNT2) for (a) SPSW-ID; (b) SPSW-CD

4.4 Summary

Using computer generated synthetic ground motions, a series of nonlinear time history analyses has been conducted on both SPSW-ID and SPSW-CD. Good agreement between the cyclic pushover analysis and the nonlinear time history analysis was observed. As previously observed in the case of cyclic pushover analysis, here in the nonlinear time history analysis, significant accumulation of plastic incremental deformations were again observed, with maximum and

residual vertical deformations more apparent on SPSW-ID than on SPSW-CD. In-span plastic hinges and partially yielded infill plates characterized SPSW-ID, while plastic hinges only at the HBE ends and fully yielded infill plates characterized SPSW-CD. Moreover, the nonlinear time history analysis demonstrated that the more severe the ground excitations acting on SPSW-ID, the more accumulation of plastic incremental deformation developed in the structure, while this was not the case for SPSW-CD.

SECTION 5

SUMMARY, CONCLUSIONS, AND RECOMMENDATIONS

5.1 Summary

A case study investigating the seismic behavior of two steel plate shear walls, having boundary elements designed per two different philosophies, was conducted. A common design approach encountered in practice, the Indirect Capacity Design Approach, was used to design the first shear wall (SPSW-ID). This approach does not guarantee that formation of in-span plastic hinges on horizontal boundary elements will be prevented. The second shear wall (SPSW-CD) was designed by the Capacity Design Approach which guarantees that plastic hinges can only occur at the ends of horizontal boundary elements (HBEs). Note that the following conclusions on the behavior of the SPSW-ID are equally applicable to SPSWs designed by any method for which in-span hinges is not explicitly prevented.

The investigation consisted of monotonic and cyclic pushover analyses as well as time-history analyses. Strip models for monotonic pushover analysis and dual strip models for cyclic pushover analysis and time history analysis were used to represent both SPSWs in the SAP2000 analyses. The *Axial-Hinge* and *Fiber-Hinge* were chosen to define the inelastic behavior of the infill plates and the boundary elements, respectively. The behavior of steels used was represented by an idealized elasto-perfectly plastic stress-strain material.

The monotonic pushover analysis has verified that one possible result of the Indirect Design Approach is that the SPSW-ID developed in-span plastic hinge on several of its horizontal boundary elements, while the SPSW-CD only developed plastic hinges at the ends of its horizontal boundary elements. A sway and beam combined plastic mechanism occurred in SPSW-ID, whereas a sway plastic mechanism occurred in SPSW-CD. A general equation to calculate the ultimate strength of both single and multistory SPSW with the sway and beam combined mechanism was developed using the kinematic method of plastic analysis.

5.2 Conclusions

Using the monotonic and cyclic pushover analyses, significant consequences to having in-span plastic hinges were identified. It was demonstrated that plastification along HBE spans, such as in the case of SPSW-ID, can induce significant accumulation of plastic incremental deformations on the HBEs, themselves leading to partial yielding of the infill plates and correspondingly lower global plastic strength compared to the values predicted by code equations (i.e., AISC 2010). By comparison, SPSW-CD developed plastic hinges only at HBE ends together with a completely yielded infill plates (i.e., in compliance with the behavior expected by the AISC Seismic Provisions 2005), and relatively smaller vertical displacements along the HBE spans.

In addition, plastification along the HBE span of SPSW-ID caused total (elastic and plastic) rotations greater than 0.03 radians at the ends of the intermediate and top HBEs (in one case even reaching 0.062 radians) after the structure was pushed cyclically up to a maximum lateral drift of 3%. Under the same cyclic pushover displacements, all total rotations in the HBEs of SPSW-CD were less than or equal to 0.03 radians. Note that although these cyclic rotations were still significantly high in that latter case, they were not symmetric, by contrast with moment frame behavior. Hence, before amending the use of Ordinary-type connections typically used in SPSW (AISC 2005) or mandating the use of the special moment resisting frame (SMRF) connection for HBEs to VBEs, further research is needed to develop a better understanding of the consequence of these significantly high non-symmetric cyclic rotation demands in SPSW.

A good agreement between the cyclic pushover analysis and the nonlinear time history analysis was observed. Both analyses showed that in-span plastic hinges and partially yielded infill plates characterized SPSW-ID, while plastic hinges only at the HBE ends and fully yielded infill plates characterized SPSW-CD. Moreover, the nonlinear time history analysis demonstrated that increasing the severity the ground excitations (i.e., from DBE to MCE), accentuated the accumulation of plastic incremental deformations on the HBEs of SPSW-ID, while this was not the case for SPSW-CD.

5.3 Recommendations for Future Research

This report establishes the various potential consequences of in-span hinging, which is an essential starting point to inform future discussions on the topic, given the observed current trends in optimizing SPSW design. Future research is needed to assess how the magnitude of the above consequences varies as a function of various parameters, and investigate if bounds exist within which the above behaviors are not likely to occur. Such parametric studies could include various structure configurations (i.e., number of stories, different infill plate aspect ratios and plate thickness, relative stiffness between anchor beams and intermediate HBEs, etc.); various kinds of steel models (i.e., incorporate strain hardening, overstrength, material deterioration, etc.); different level of gravity loads; and various ground motion characteristics and variability. In addition, experimental verification would be desirable. The results and behavior presented here, obtained using simple plastic theory (as commonly done in similar studies), provide a first anchor point from which the effect of multiple other circumstances can be assessed.

Finally, an unanticipated valuable observation of this study was that the cyclic hysteretic moment-rotation curve of plastic hinges at the ends of HBEs are not symmetric, even in SPSWs that do not develop in-span hinging (i.e., SPSW-CD). These curves loop with a bias, without sign reversal of the rotations, resulting in maximum rotations of significant magnitude. Past research has typically not quantified plastic hinge rotations histories and, in light of the results reported here, this subject should deserve more attention in future research.

SECTION 6

REFERENCES

AISC. (2005a). "Specification for Structural Steel Buildings." ANSI/AISC 360-05, American Institute of Steel Construction, Inc., Chicago, Illinois.

AISC. (2005b). "Seismic Provisions for Structural Steel Buildings." ANSI/AISC 341-05, American Institute of Steel Construction, Inc., Chicago, Illinois.

AISC. (2007). "Modern Steel Construction." Cover Page Photo, January 2007.

AISC. (2008). "L.A. Live Hotel & Residences - An Innovative Steel-Plate Shear Wall Solution." <<http://www.aisc.org/content.aspx?id=16012>> (October 2008).

AISC. (2010). "Seismic Provisions for Structural Steel Buildings." ANSI/AISC 341-10, American Institute of Steel Construction, Inc., Chicago, Illinois.

Berman, J. W., and Bruneau, M. (2003). "Plastic Analysis and Design of Steel Plate Shear Walls." *Journal of Structural Engineering*, ASCE, Vol. 129, No. 11, pp. 1448-1456.

Berman, J. W. and Bruneau, M. (2005). "Experimental Investigation of Light-Gauge Steel Plate Shear Walls." *Journal of Structural Engineering*, ASCE, Vol. 131, No. 2, pp. 259-267.

Berman, J. W., and Bruneau, M. (2008). "Capacity Design of Vertical Boundary Elements in Steel Plate Shear Walls." *Engineering Journal*, AISC, First Quarter, pp. 57-71.

Bertero, V. V., Anderson, J. C., and Krawinkler, H. (1994) "Performance of Steel Building Structures during the Northridge Earthquake". *Report No. UCB/EERC-94/09*, Earthquake Engineering Research Center, University of California, Berkeley, California.

Bruneau, M., Whittaker, A. S., and Uang, C. M. (1998). "Ductile Design of Steel Structures." McGraw-Hill, New York, NY.

Caccese, V., Elgaaly, M., and Chen, R. (1993). "Experimental Study of Thin Steel Plate Shear Walls under Cyclic Load." *Journal of Structural Engineering*, ASCE, Vol. 119, No. 2, pp. 573-587

Computer and Structures, Inc. (CSI) (2007) “CSI Analysis Reference Manual for SAP2000.” Version 11.0.8, Computer and Structures, Inc., Berkeley, California.

Driver, R. G., Kulak, G. L., Kennedy, D. J. L., and Elwi, A. E. (1997). “Seismic Behavior of Steel Plate Shear Walls.” *Structural Engineering Report 215*, Department of Civil Engineering, University of Alberta, Edmonton, Alberta, Canada.

Elgaaly, M. (1998), “Thin Steel Plate Shear Walls Behavior and Analysis,” *Thin Walled Structures*, Elsevier, Vol. 32, Nos. 1–3, pp. 151–180.

FEMA. (2001). “NEHRP Recommended Provisions for Seismic Regulations for New Buildings and Other Structures, Part 2-Commentary.” *FEMA Report No. 369*, Building Seismic Safety Council for the Federal Emergency Management Agency, Washington, D.C.

FEMA. (2003). “NEHRP Recommended Provisions for Seismic Regulations for New Buildings and Other Structures.” *FEMA Report No. 450*, Building Seismic Safety Council for FEMA, Washington, D.C.

Keller, D. and Bruneau, M. (2008) “Development of a Steel Plate Shear Wall Bridge Pier System Conceived from a Multi-Hazard Perspective.” *Technical Report MCEER-08-0030*, Multidisciplinary Center for Earthquake Engineering Research, Buffalo, New York.

Liew, J. Y. R. and Shanmugam, N. E., (2003). “Theory and Analysis of Structures.” Chapter 47 in *Civil Engineering Handbook*, CRC Press, Florida.

Lopez-Garcia, D., and Bruneau, M. (2006). “Seismic Behavior of Intermediate Beams in Steel Plate Shear Walls.” *Proceeding, 8th U.S. National Conf. on Earthquake Engineering*, San Francisco, Paper No. 1089.

Papageorgiou, A., Halldorsson, B., and Dong, G. (1999). “Target acceleration spectra compatible time histories.” *TARSCTHS-User’s manual*, Engineering Seismology Laboratory, State Univ. of New York, Buffalo, N.Y.

Qu, B., Bruneau, M., Lin, C.H., and Tsai, K.C. (2008). “Testing of Full Scale Two-story Steel Plate Shear Walls with Reduced Beam Section Connections and Composite Floors.” *Journal of Structural Engineering*, ASCE, Vol. 134, No. 3, pp. 364-373

Qu, B., and Bruneau, M. (2008). “Seismic Behavior and Design of Boundary Frame Members of Steel Plate Shear Walls.” *Technical Report MCEER-08-0012*, Multidisciplinary Center for Earthquake Engineering Research, Buffalo, New York.

Qu, B., and Bruneau, M., (2009). "Design of Steel Plate Shear Walls Considering Boundary Frame Moment Resisting Action." *Journal of Structural Engineering*, ASCE, Vol.135, No.12, pp.1511-1521.

Sabelli, R., and Bruneau, M. (2007). "Steel Plate Shear Walls (AISC Design Guide)", American Institute of Steel Construction, Inc., Chicago, Illinois, 144 p.

SAC. (1995). "Interim Guidelines: Evaluation, Repair, Modification and Design of Welded Steel Moment Frame Structures." *Program to Reduce the Earthquake Hazards of Steel Moment Frame Structures*. Federal Emergency Management Agency. Report FEMA 267/SAC-95-02. SAC Joint Venture, Sacramento, California.

Thorburn, L. J., Kulak, G. L., and Montgomery, C. J. (1983). "Analysis of Steel Plate Shear Walls." *Structural Engineering Report No. 107*, Department of Civil Engineering, University of Alberta, Edmonton, Alberta, Canada.

Timler, P. A., and Kulak, G. L. (1983). "Experimental Study of Steel Plate Shear Walls." *Structural Engineering Report No. 114*, Department of Civil Engineering, University of Alberta, Edmonton, Alberta, Canada.

Tromposch, E.W., and Kulak, G.L. (1987). "Cyclic and Static Behavior of Thin Panel Steel Plate Shear Walls.", *Structural Engineering Report No. 145*, Department of Civil Engineering, University of Alberta, Edmonton, Alberta, Canada.

Vian, D., and Bruneau, M. (2005). "Steel plate shear walls for seismic design and retrofit of building structures." *Tech. Rep. MCEER-05-0010*, Multidisciplinary Center for Earthquake Engineering Research, State University of New York at Buffalo, Buffalo, New York.

APPENDIX A

DESIGN CALCULATION OF THREE-STORY STEEL PLATE SHEAR WALLS USING INDIRECT CAPACITY DESIGN APPROACH

Geometry and Loads

Number of stories

NF : 3 stories

Height of stories

h_1 :	3048	mm	120	in.
h_2 :	3048		120	
h_3 :	3048		120	

Bay width

b_w : 6096 mm 240 in.

Story weight

W_1 :	1564	kN	351.60	kips
W_2 :	1564		351.60	
W_3 :	1694		380.83	

Total Weight

W_s : 4822 kN 1084.03 kips

Earthquake loads

Location : Downtown San Fransisco, California

S_s : 1.7035 g F_a : 1.0

Type of Soil : D

S_1 : 0.8501 g F_v : 1.5

Design Base Earthquake (DBE), plotted in Fig. 1

S_{DS} :	1.136 g	S_{D1} :	0.850 g
T_s :	0.749 sec	T_0 :	0.150 sec

Approximate Natural Period

H :	9144 mm	30.0 ft
T_n :	0.256 sec	

Importance Factor

I : 1.0

Seismic coefficient

C_s : 0.162 (Assuming Viscous Damping

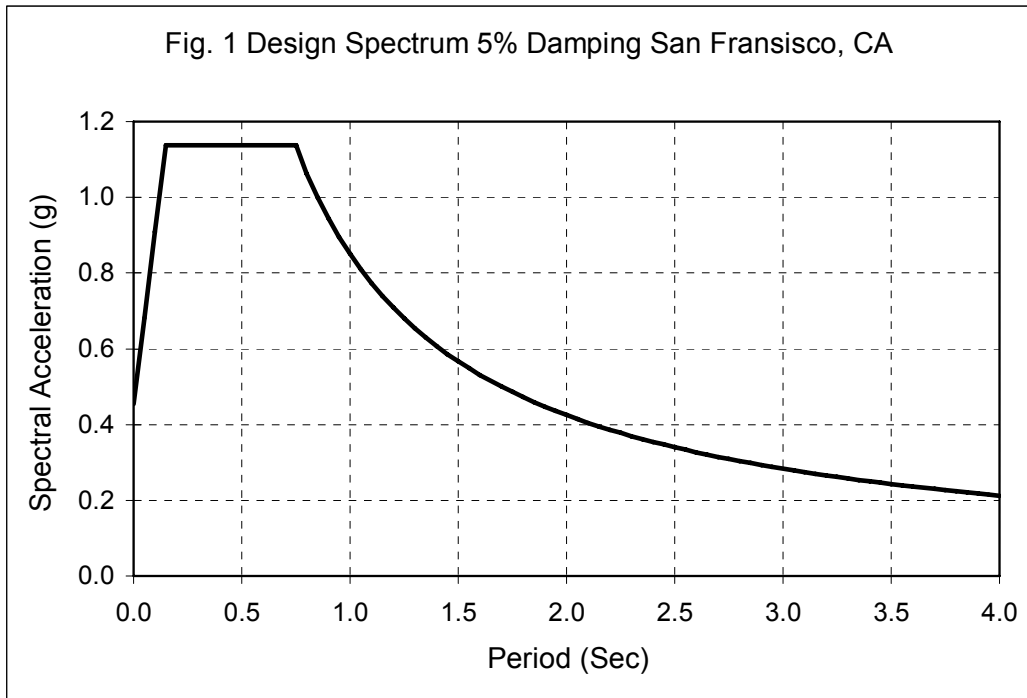
Response Modification Factor

$\xi = 5\%$ FEMA 356

R : 7.0

Total Base Shear

V_{base} : 782.312 kN 175.871 kips



Calculation of earthquake load on every floor

W_1 :	1564	kN
W_2 :	1564	
W_3 :	1694	
Floor Height from base		
h_{10} :	3048	mm
h_{20} :	6096	
h_{30} :	9144	
Story Shear		
V_1 :	175.87	kip
V_2 :	147.73	
V_3 :	91.44	

Therefore:

Earthquake load on every floor

F_1 :	28.14	kips
F_2 :	56.28	
F_3 :	91.44	

Applied Eq. load both on left and right side

F_{1-half} :	14.07	kips
F_{2-half} :	28.14	
F_{3-half} :	45.72	

Primary Design: Plate

Material Properties

E : 29000 ksi

A572 Gr. 50 Steel will be used for HBEs and VBEs

F_y : 50 ksi

R_y : 1.0

FEMA 350

Light Gauge Steel will be used for the web plates

F_{yp} : 30 ksi R_{yp} : 1.0

FEMA 350

For preliminary design assume a tension field angle for sizing the web plates

α_{assume} : 42.882 degree 0.748 radians

Resistance factor for SPSW strength

ϕ : 0.9

Assume the clear distance between panels to be the bay width minus depth of VBE

b_w : 20.00 ft 6.096 m

h_w : 10.00 ft 3.048 m

L_{cf1} : 18.03
 L_{cf2} : 18.50 ft
 L_{cf3} : 18.67

Plate thickness required

t_{req} : 0.072
 0.059 in
 0.036

Plate thickness provided is assume similar to

t_{prov} : 0.072
 0.059 in
 0.036

what was required

Primary Design: Boundary Elements

Vertical Boundary Elements (VBE)

Floor	1	2	3
Section	W24X62	W18X50	W16X40
Mp (kip-ft)	642.22	421.11	304.44
Vp (kip-ft)	305.56	192.22	146.67
A (in ²)	18.3	14.7	11.8
d (in)	23.7	18	16
b/2tf	5.97	6.57	6.93
h/tw	49.7	45.2	46.5
I _{xx} (in ⁴)	1560	800	518
Z _{xx} (in ³)	154	101	73
r _y (in)	1.37	1.65	1.57
r _x (in)	9.24	7.38	6.63
KL/r _x			
KL/r _y			

Column Minimum Inertia criteria

I_{min1} : 192.23163 OK

I_{min2} : 157.32553 OK

I_{min3} : 96.515191 OK

Horizontal Boundary Elements (HBE)

Floor	0	1	2	3
Section	W24X62	W12X19	W12X22	W16X36
Mp (kip-ft)	642.22	102.89	122.22	266.67
Vp (kip-ft)	305.56	86.00	95.89	141.11
A (in ²)	18.3	5.57	6.48	10.6
d (in)	23.7	12.2	12.3	15.9
b/2tf	5.97	5.72	4.74	6.38
h/tw	49.7	46.2	41.8	48.1
I _{xx} (in ⁴)	1560	130	156	448
Z _{xx} (in ³)	154	24.7	29.3	64
r _y (in)	1.37	0.822	0.848	1.52
r _x (in)	9.24	4.82	4.91	6.51
KL/r _x	1.41	2.70	2.65	2.00
KL/r _y	7.30	12.17	11.79	6.58

Strip Model Development

Calculation of α for selected Preliminary Shapes

α_1 :	0.758		43.418	
α_2 :	0.728	radians	41.688	degrees
α_3 :	0.760		43.540	
α_{ave} :	0.748	radians	42.882	degrees
$\alpha_{SAP2000}$:			47.118	degrees

Strip model set-up and strip dimensions

L_α :	257.520 in	
n :	12 pcs	Spasing for corner if needed
S :	19.809 in	9.905 in
S _x :	27.034 in	13.517 in
S _z :	29.110 in	14.555 in
As :	1.44	
	1.17	in ²
	0.72	

B-values for strip model

V_{e1} :	234.494		Then	B_1 :	1.33
V_{e2} :	196.971	kip		B_2 :	1.33
V_{e3} :	121.926			B_3 :	1.33

Strip Model Analysis Results (using SAP2000 v.11)

Interstory drift calculation

Δ_1 :	0.1174		δ_1 :	0.117	
Δ_2 :	0.2597	in	δ_2 :	0.142	in
Δ_3 :	0.4216		δ_3 :	0.162	

Displacement amplification factor

C_d : 6 SPSW

Story drift limit

δ_a :	0.02 H				
Δ_{a1} :	2.4000		δ_{a1} :	2.400	
Δ_{a2} :	4.8000	in	δ_{a2} :	2.400	in
Δ_{a3} :	7.2000		δ_{a3} :	2.400	
I :	1.0				

Amplified Interstory drift calculation

Δ_{1A} :	0.7046		δ_{1A} :	0.7046		Satisfied
Δ_{2A} :	1.5584	in	δ_{2A} :	0.8538	in	Satisfied
Δ_{3A} :	2.5296		δ_{3A} :	0.9712		Satisfied

Compactness Check on VBEs and HBEs

Vertical Boundary Elements (VBE)

Floor	1	2	3
Section	W24X62	W18X50	W16X40
A (in ²)	18.3	14.7	11.8
b/2tf	5.97	6.57	6.93
h/tw	49.7	45.20	46.5

Web Criterion for Compactness

P_u	-291.77	-164.45	-67.34
$\phi * P_y$	823.5	661.5	531
C_a	0.3543	0.2486	0.1268
λ_w	53.29	56.14	59.43
Status	OK	OK	OK

Flange Criterion for Compactness

λ_f	7.225	7.225	7.225
Status	OK	OK	OK

Horizontal Boundary Elements (HBE)

Floor	0	1	2	3
Section	W24X62	W12X19	W12X22	W16X36
A (in ²)	18.3	5.57	6.48	10.6
b/2tf	5.97	5.72	4.74	6.38
h/tw	49.7	46.2	41.8	48.1
Web Criterion for Compactness				
P _u	-86.20	32.26	38.35	-50.99
ϕ*P _y	823.5	250.65	291.6	477
C _a	0.1046764	0.1286894	0.1315123	0.1069015
λ _w	63.43	59.38	59.30	63.17
Status	OK	OK	OK	OK
Flange Criterion for Compactness				
λ _f	7.225	7.225	7.225	7.225
Status	OK	OK	OK	OK

Consider “acceptable”
for the bottom joint

Strong Column-Weak Beam Check

Location	P _u (kip)	Z(F _y -P _u /A) (kip-ft)	ΣZ(F _y -P _u /A) (kip-ft)	ΣM _p (kip-ft)	Ratio	Status
at base left	215.15	234.12	234.12	423.50	0.553	NOT OK
right	-291.77	180.39	180.39	423.50	0.426	NOT OK
at 1st left	129.47	294.21	480.79	67.93	7.078	OK
right	115.13	186.58	412.79	67.93	6.077	OK
	-186.17	254.44				
	-164.45	158.34				
at 2nd left	50.89	223.36	384.24	80.58	4.769	OK
right	41.95	160.88	352.17	80.58	4.371	OK
	-84.03	204.39				
	-67.34	147.78				
at top left	4.97	179.94	179.94	176.00	1.022	OK
right	-12.38	176.12	176.12	176.00	1.001	OK

APPENDIX B

DESIGN CALCULATION OF THREE-STORY STEEL PLATE SHEAR WALLS USING CAPACITY DESIGN APPROACH

Geometry and Loads

Number of stories

NF : 3 stories

Height of stories

h_1 :	3048	mm	120	in.
h_2 :	3048		120	
h_3 :	3048		120	

Bay width

b_w : 6096 mm 240 in.

Story weight

W_1 :	1564	kN	351.601	kips
W_2 :	1564		351.601	
W_3 :	1694		380.826	

Total Weight

W_s : 4822 kN 1084.0291 kips

Earthquake loads

Location : Downtown San Fransisco, California

S_s : 1.7035 g F_a : 1.0

Type of Soil : D

S_1 : 0.8501 g F_v : 1.5

Design Base Earthquake (DBE), plotted in Fig. 1

S_{DS} :	1.136 g	S_{D1} :	0.850 g
T_s :	0.749 sec	T_0 :	0.150 sec

Approximate Natural Period

H :	9144 mm	30.0 ft
T_n :	0.256 sec	

Importance Factor

I : 1.0

Seismic coefficient

C_s : 0.162 (Assuming Viscous Damping

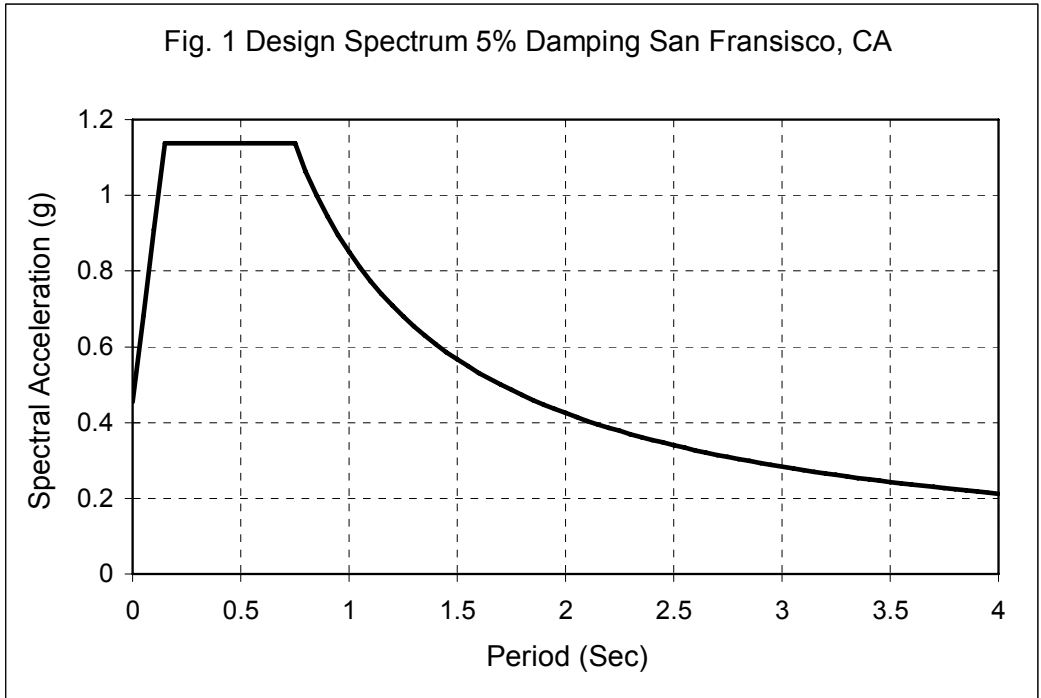
Response Modification Factor

$\xi = 5\%$ FEMA 356

R : 7.0

Total Base Shear

V_{base} : 782.312 kN 175.871 kips



Calculation of earthquake load on every floor

W_1 :	1564	kN
W_2 :	1564	
W_3 :	1694	
Floor Height from base		
h_{10} :	3048	mm
h_{20} :	6096	
h_{30} :	9144	
Story Shear		
V_1 :	175.871	kip
V_2 :	147.729	
V_3 :	91.444	

Therefore:

Earthquake load on every floor

F_1 :	28.142	kips
F_2 :	56.284	
F_3 :	91.444	

Applied Eq. load both on left and right side

F_{1-half} :	14.071	kips
F_{2-half} :	28.142	
F_{3-half} :	45.722	

Primary Design: Plate

Material Properties

E : 29000 ksi

A572 Gr. 50 Steel will be used for HBEs and VBEs

F_y : 50 ksi

R_y : 1.0

FEMA 350

Light Gauge Steel will be used for the web plates

F_{yp} : 30 ksi R_{yp} : 1.0 FEMA 350

For preliminary design assume a tension field angle for sizing the web plates

α_{assume} : 43.991 degree 0.76778 radians (has been updated)

Resistance factor for SPSW strength

ϕ : 0.9

Assume the clear distance between panels to be the bay width minus depth of VBE

b_w : 20.00 ft 6.096 m

h_w : 10.00 ft 3.048 m

L_{cf1} : 17.94
 L_{cf2} : 18.48 ft
 L_{cf3} : 18.60

Plate thickness required

t_{req} : 0.073
 0.059 in
 0.036

Plate thickness provided is assume similar to

t_{prov} : 0.072 what is required
 0.059 in
 0.036

Primary Design: Boundary Elements

Vertical Boundary Elements (VBE)

Floor	1	2	3
Section	W24X146	W18X76	W16X89
Mp (kip-ft)	1744.44	678.89	733.33
Vp (kip-ft)	481.11	232.22	264.44
A (in ²)	43	22.3	26.4
d (in)	24.7	18.2	16.8
b/2tf	5.92	6.53	5.92
h/tw	33.2	37.8	25.9
I _{xx} (in ⁴)	4580	1330	1310
Z _{xx} (in ³)	418	163	177
r _y (in)	3.01	2.61	2.48
r _x (in)	10.3	7.73	7.05
KL/r _x			
KL/r _y			

Column Minimum Inertia criteria

I_{min1} : 190.97856 OK

I_{min2} : 157.13478 OK

I_{min3} : 96.656526 OK

Horizontal Boundary Elements (HBE)

Floor	0	1	2	3
Section	W24X117	W12X45	W14X61	W18X76
Mp (kip-ft)	1366.67	267.78	425.56	678.89
Vp (kip-ft)	401.11	121.11	156.67	232.22
A (in ²)	34.4	13.1	17.9	22.3
d (in)	24.3	12.1	13.9	18.2
b/2tf	6.21	7	6.19	6.53
h/tw	39.2	29.6	30.4	37.8
I _{xx} (in ⁴)	3540	348	640	1330
Z _{xx} (in ³)	327	64.2	102	163
r _y (in)	2.94	1.95	2.45	2.61
r _x (in)	10.1	5.15	5.98	7.73
KL/r _x	1.29	2.52	2.17	1.68
KL/r _y	3.40	5.13	4.08	3.83

Strip Model Development

Calculation of α for selected Preliminary Shapes

α_1 :	0.766		43.894	
α_2 :	0.764	radians	43.772	degrees
α_3 :	0.773		44.306	
α_{ave} :	0.768	radians	43.991	degrees
$\alpha_{SAP2000}$:			46.009	degrees

Strip model set-up and strip dimensions

L_α :	256.014 in	
n :	12 pcs	Spacing for corner if needed
S :	19.693 in	9.847 in
S _x :	27.373 in	13.686 in
S _z :	28.355 in	14.177 in
As :	1.418	
	1.167	in ²
	0.718	

B-values for strip model

V_{e1} :	232.380		Then	B_1 :	1.32	
V_{e2} :	196.971	kip		B_2 :	1.33	
V_{e3} :	121.926			B_3 :	1.33	

Strip Model Analysis Results (using SAP2000 v.11)

Interstory drift calculation

Δ_1 :	0.2527		δ_1 :	0.253	
Δ_2 :	0.4918	in	δ_2 :	0.239	in
Δ_3 :	0.7115		δ_3 :	0.220	

Displacement amplification factor

C_d : 6 SPSW

Story drift limit

δ_a :	0.02 H				
Δ_{a1} :	2.4000		δ_{a1} :	2.400	
Δ_{a2} :	4.8000	in	δ_{a2} :	2.400	in
Δ_{a3} :	7.2000		δ_{a3} :	2.400	
I :	1.0				

Amplified Interstory drift calculation

Δ_{1A} :	1.5160		δ_{1A} :	1.5160		Satisfied
Δ_{2A} :	2.9510	in	δ_{2A} :	1.4350	in	Satisfied
Δ_{3A} :	4.2690		δ_{3A} :	1.3180		Satisfied

Compactness Check on VBEs and HBEs

Vertical Boundary Elements (VBE)

Floor	1	2	3
Section	W24X146	W18X76	W16X89
A (in ²)	43	22.3	26.4
b/2tf	5.92	6.53	5.92
h/tw	33.2	37.8	25.9
Web Criterion for Compactness			
P_u	-294.50	-168.41	-66.64
$\phi * P_y$	1935	1003.5	1188
C_a	0.1522	0.1678	0.0561
λ_w	58.74	58.32	69.09
Status	OK	OK	OK
Flange Criterion for Compactness			
λ_f	7.225	7.225	7.225
Status	OK	OK	OK

Horizontal Boundary Elements (HBE)

Floor	0	1	2	3
Section	W24X117	W12X45	W14X61	W18X76
A (in ²)	34.4	13.1	17.9	22.3
b/2tf	6.206	7	6.194	6.526
h/tw	39.2	29.6	30.4	37.8
Web Criterion for Compactness				
P _u	-86.34	24.36	39.56	-49.10
φ*P _y	1548	589.5	805.5	1003.5
C _a	0.0557765	0.0413215	0.0491111	0.0489248
λ _w	69.13	70.81	69.90	69.92
Status	OK	OK	OK	OK
Flange Criterion for Compactness				
λ _f	7.225	7.225	7.225	7.225
Status	OK	OK	OK	OK

Strong Column-Weak Beam Check

Location	P _u (kip)	Z(F _y -P _u /A) (kip-ft)	ΣZ(F _y -P _u /A) (kip-ft)	ΣM _p (kip-ft)	Ratio	Status
at base left	210.53	1571.12	1571.12	1498.75	1.048	OK
right	-294.50	1503.10	1503.10	1498.75	1.003	OK
at 1st left	128.72	1637.39	2248.24	294.25	7.641	OK
	112.16	610.85				
right	-193.60	1584.84	2161.43	294.25	7.346	OK
	-168.41	576.59				
at 2nd left	49.99	648.72	1365.13	467.50	2.920	OK
	37.73	716.42				
right	-89.28	624.78	1325.05	467.50	2.834	OK
	-66.64	700.27				
at top left	5.46	734.45	734.45	679.17	1.081	OK
right	-17.01	728.00	728.00	679.17	1.072	OK

Design of VBE (Berman and Bruneau 2008)

Table 1. Distributed Loads from Yielding Web Plates

Story	α		W_{xc} kip/in	W_{yc} kip/in	W_{xb} kip/in	W_{yb} kip/in
	degree	radians				
3	44.306	0.77328	0.53335	0.5464	0.5464	0.5598
2	43.772	0.76396	0.85053	0.8878	0.8878	0.9267
1	43.894	0.7661	1.03832	1.0792	1.0792	1.1217

Table 2. Linear VBE Parameters, Results and Corresponding HBE End Actions

HBE	Section	A_g in ²	M_p kip-in	k_b kip/in	P_s kips	P_s kips	P_{bl} kips
3	W18X76	22.3	8146.67	5389.2	-23.809	-32.001	-97.5741
2	W14X61	17.9	5106.67	4325.8	-91.406	-83.033	-123.996
1	W12X45	13.1	3213.33	3165.8	-120.72	-113.33	-136.299
0	W24X117	34.4	16400	8313.3	-55.43	-62.299	129.503

HBE	Section	P_{br} kips	M_{prl} kip-in	M_{prr} kip-in	V_{bl} kips	V_{br} kips	Ratio
3	1330	33.5716	8146.67	8146.7	0.7072	135.07	0.999
2	640	-42.071	5106.67	5106.7	-1.4656	86.577	0.998
1	348	-90.363	3002.71	3213.3	2.5011	49.299	0.950
0	3540	-129.5	16400	16400	2.0646	271.27	0.982

Table 3. Seismic Loading for Assumed Sway Mechanism

Story	h_i in	C_i	M_{frame} kip-in	M_{plate} kip-in	F kips
3	360	0.51995	16293.3	47212	253.21
2	240	0.32003	10213.3	19662	155.85
1	120	0.16002	6216.04	5512.4	77.925
0	0	0	32800	0	0
	$\Sigma =$	1	65522.7	72387	486.98

Table 4. VBE Sections

HBE	Section	A_g in ²	M_p		Ratio
			kip-in	kip-ft	
3	W16X89	26.4	8800	660	0.977
2	W18X76	22.3	8146.67	611	0.989
1	W24X146	43	20933.3	1570	0.958

APPENDIX C

FIBER HINGE STUDY

C.1 General

As previously mentioned in Section 2, the *Fiber P-M2-M3 Hinge* was chosen to define plastic hinges in the VBEs and HBEs. This type of hinge automatically accounts for the interaction between the axial loads and moments that can occur in the HBEs and VBEs. Using this hinge model, a cross section is modeled as having several fibers with a certain tributary area and placed at specified locations along the cross section. In addition, each fiber can have its own stress-strain relationship (CSI 2007). An earlier study conducted by Keller and Bruneau (2008) reported that the performance of the *Fiber Hinge* was satisfactory. This conclusion was based on an analytical investigation on a 120 in. cantilever column made of a circular tube, which the *Fiber Hinge* was assigned at the base of the column in SAP2000 model. The ultimate capacity of the column at various levels of axial loads matched its theoretical ultimate capacity derived using plastic analysis. This study investigates the plastic behavior of the *Fiber Hinge* on the same cantilever column but made of a W-section. In addition, the plastic behavior of the *P-M Hinge* (another plastic hinge model available in SAP2000 which is relatively simple to apply and also accounts for the interaction between the axial loads and moments) is examined in this study. The accuracy of numerical results by changing the number of fibers for the *Fiber Hinge* is studied and both hinge models are verified to see whether their plastic behavior match the theoretical plastic P-M interaction behavior of a W-section.

C.2 Case Study Set-up: Cantilever Column W14x48

Figure C-1 displays the cantilever column used in this study. The structure was made of W14x48 steel of 120 in. height. Axial force P was applied at the tip of the cantilever, which varies from zero axial force to 0.9 of the axial yield strength of the column (i.e., $P = 0.9P_y$). An increment of $0.1P_y$ was chosen to obtain a relatively large number of data points. The self-weight of the column was excluded (assuming that it is already included in the axial force P). For each level of axial loads, the column was pushed by the lateral load V until its ultimate plastic moment

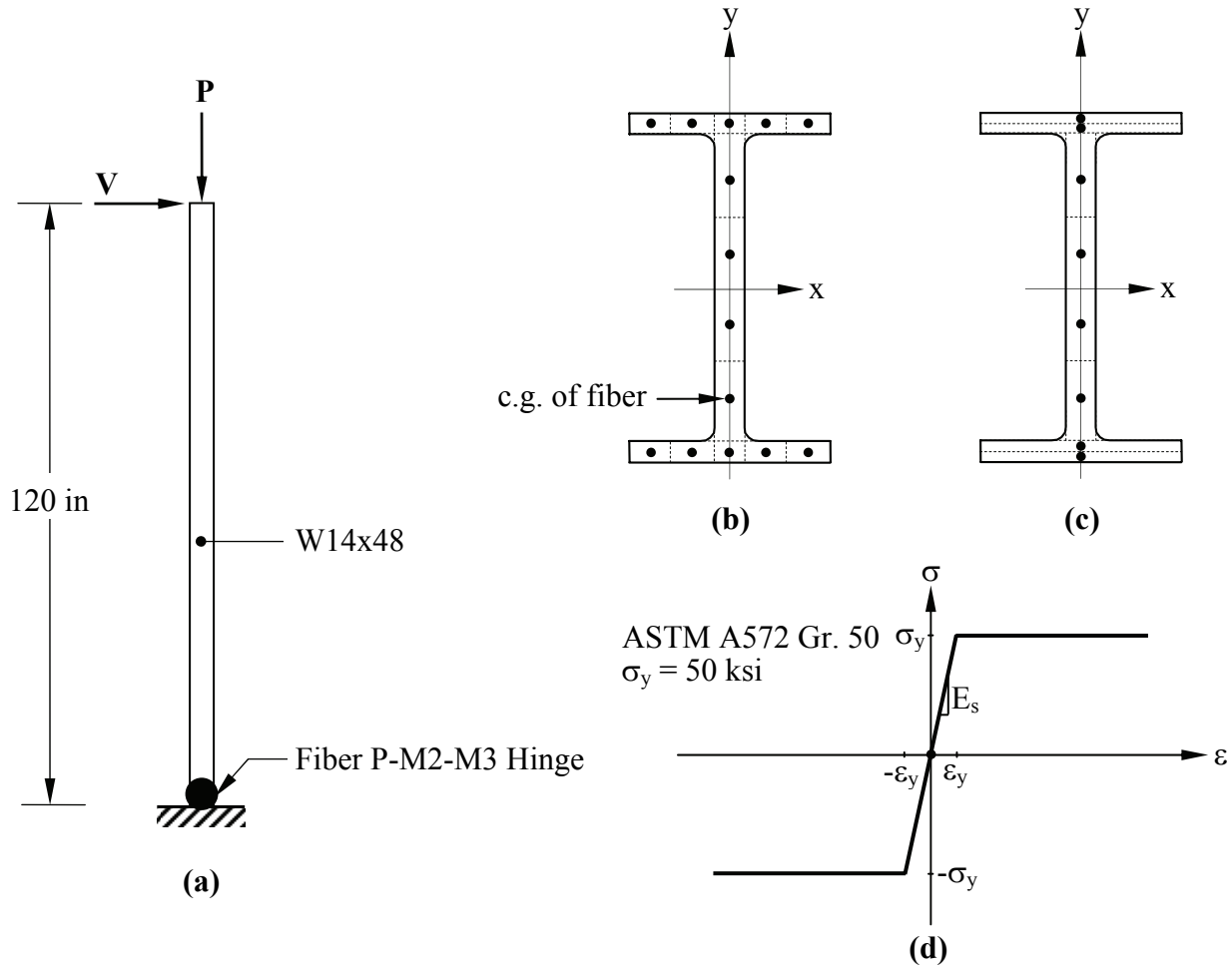


FIGURE C-1 Case Study Set-up for Fiber Hinge Study (a) Cantilever Column; (b) Horizontally and Vertically Sliced Fiber Configuration; (c) Vertically Sliced Fiber Configuration; (d) Stress-Strain Curve

capacity along the strong axis was reached. At the base of the column, the *Fiber-Hinge* was assigned in two different configurations. In the first configuration [figure C-1(b)], the W14x48 cross section was sliced both horizontally and vertically while in the other one [figure C-1(c)], it was only vertically sliced. In term of total number of fibers, four different sets of fibers were evaluated for the first configuration: 6, 12, 26, and 50 fibers; and five different sets for the second configuration: 4, 8, 16, 32, and 48 fibers. Each fiber was assigned the same stress-strain behavior of ASTM A572 Gr. 50 ($F_y = 50$ ksi) steel, which was idealized as elasto-perfectly plastic material for both tension and compression [figure C-1(d)]. Moreover for the *P-M hinge*, moment plastic-rotation curves corresponding to different values of axial force P were assigned on the W14x48 column.

For the theoretical calculation, closed-form equations of reduced plastic moment capacity due to axial force for wide flange sections area available from many sources. Here, the following equations were used (taken from Bruneau *et al.*, 1998):

$$\frac{M_{pr}}{M_p} = 1 - \left(\frac{P}{P_y} \right)^2 \frac{A_b^2}{4t_w Z_b} \quad \text{for } \frac{P}{P_{yb}} \leq \frac{A_w}{A_b} \quad (\text{C-1})$$

$$\frac{M_{pr}}{M_p} = A_b \left(1 - \frac{P}{P_y} \right) \left[d - \frac{A_b}{2b_f} \left(1 - \frac{P}{P_y} \right) \right] \frac{1}{2Z_b} \quad \text{for } \frac{P}{P_{yb}} \leq \frac{A_w}{A_b} \quad (\text{C-2})$$

where M_{pr} and M_p are the reduced and unreduced plastic moment, respectively; P is the axial load resisted by the column; P_{yb} is the axial yield strength of the column; A_b and A_w are the total cross-section area of the column and its web area, respectively; Z_b is the plastic section modulus of the column; t_w , d , and b_f are the web thickness, depth, and width of the cross section, respectively.

C.3 Analysis Results

Figure C-2 displays the results of this case study. Plotted on the part (a) is the result for the horizontally and vertically sliced fiber configuration, while on part (b) is that for the vertically sliced fiber configuration. No significant difference was observed between the two configurations. This can be understood because the applied lateral load V only produced moment in one direction (i.e., the strong axis bending). For both cases, plastic moment capacity of the column with the *Fiber P-M2-M3 Hinge* agreed well with the theoretical plastic moment capacity. Up to the level of $P = 0.7P_y$, the difference between the two was less than 8%, though at the very high axial load level (i.e., $P = 0.9P_y$) the difference approached 21%. Increasing the number of fibers improved the results significantly only at a low level of axial load.

On the other side, plastic moment capacity of the column with the *P-M Hinge* only matched the theoretical plastic moment at zero axial force (i.e., $M_p = 3920$ kip-in). As the axial forces increased in the column, the resulting plastic moment capacity obtained from SAP2000 significantly deviated from the theoretical plastic moment. For example, at the level of $P = 0.7P_y$, the reduced plastic moment capacity of the column was 79% lower than its theoretical value. In addition, at high level of axial loads, convergence issue during the analysis was observed.

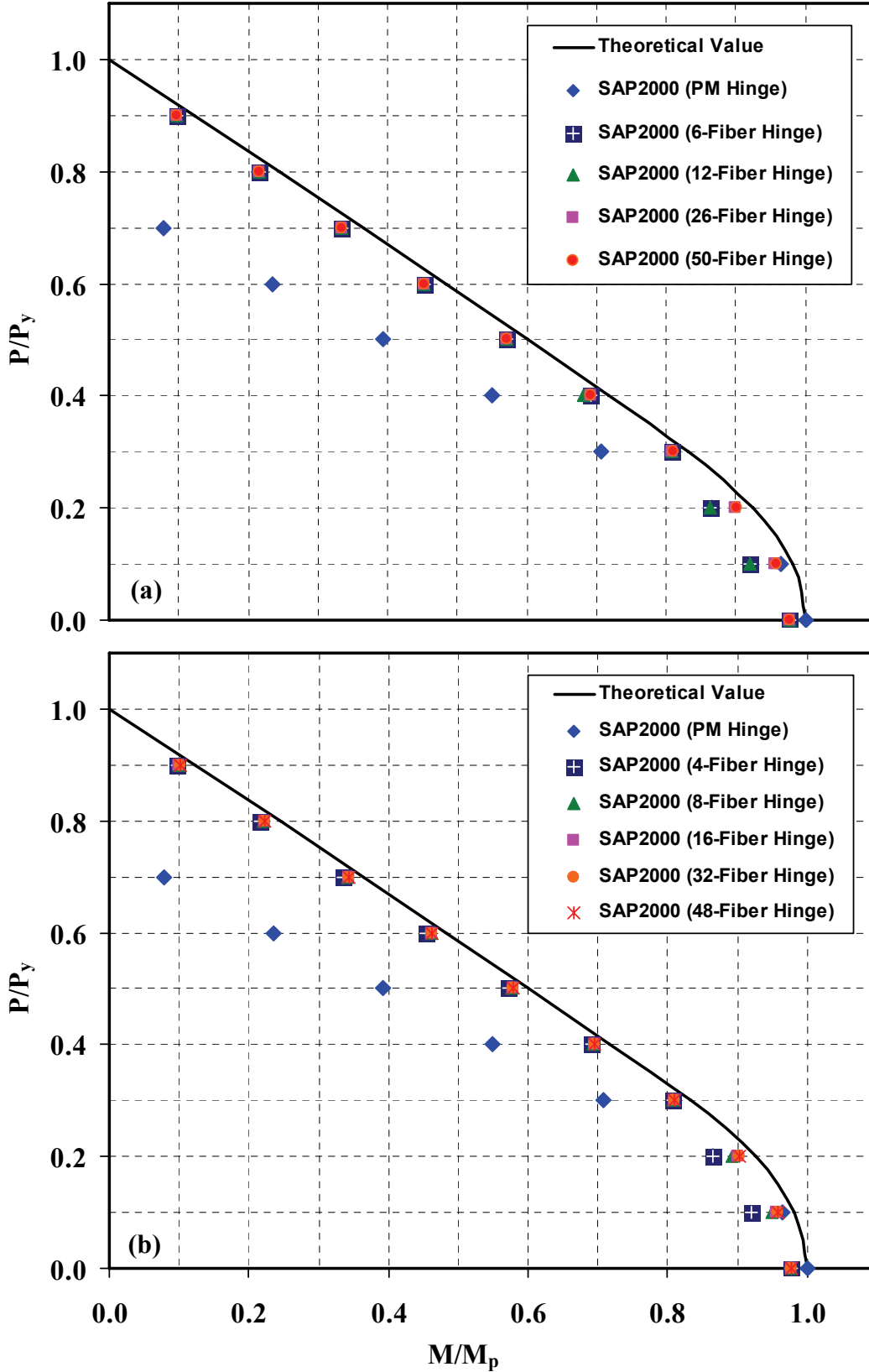


FIGURE C-2 Normalized Plastic P-M Interaction Diagram of W14x48
 (a) Horizontally & Vertically Sliced Fiber; (b) Vertically Sliced Fiber Configurations

APPENDIX D

HOOK ELEMENT STUDY

D.1 General

In Section 2, nonlinear behavior of the tension-only bracing element was modeled using the *Axial P-Hinge*. However, in order to capture correctly the actual behavior of the slender strips that can yield in tension but have no compression strength (i.e., buckle elastically in compression), the default behavior of this hinge was modified per the procedure described in Section 2. Another possible approach using SAP2000 is to model tension-only bracing behavior utilizing the *Hook Element*. This appendix describes how the *Hook Element* could be used for the SPSW strip model.

D.2 Application of Hook Element on Strip Model

Figure D-1 displays the definition of the *Hook Element* in SAP2000. It has spring constant k , which only works when the element experiences positive deformations (i.e., tension only). One could define zero or positive value as an initial hook opening (CSI 2007). For the strip model considered here, zero initial hook opening was assigned, which means that the *Hook Element*

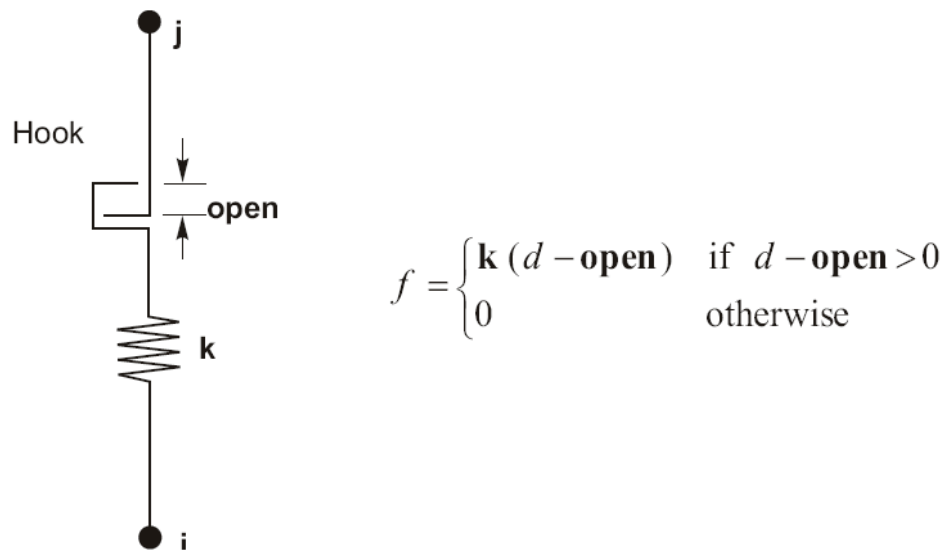


FIGURE D-1 Hook Property in SAP2000 (CSI 2007)

immediately engaged as soon as the strip was in tension. One *Hook Element* was assigned in series with a regular strip as illustrated in figure D-2. One advantage of this approach is that the default definition of the *Axial P-Hinge* can be used directly to model the nonlinear behavior of the strip. However, to use the *Hook Element* inline with the regular strip, one needs to cut the regular strip at an arbitrary offset length (L_1) and then insert a *Hook Element* (shown in the figure, from point A to B) for each strip. In addition, one needs to calculate the axial spring constant k and manually input the information as a *Hook Element* property. If force-deformation data of a particular strip is needed, one needs to extract the results from both the strip and its corresponding hook element and sum them up (e.g. using a spreadsheet program).

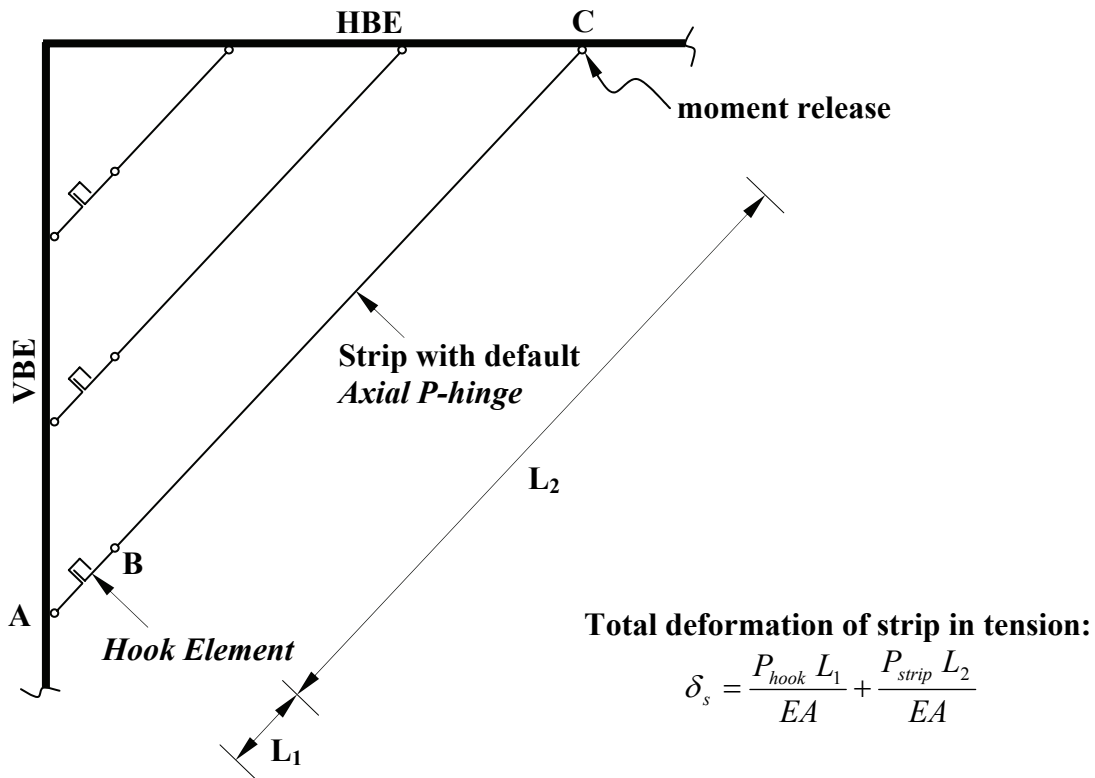


FIGURE D-2 Application of Hook Element on Strip Model

No significant different was observed between the previous results (i.e., outcomes from SPSW-ID with Modified *Axial P-Hinge*) and the current analysis result of SPSW-ID with *Hook Element*. Two examples of outcomes are compared in figure D-3; both base shear and vertical displacement curves of both models are on top of each other. However, a reliability issue might arise when observing the deformed shape of the structure. As shown in figure D-4, all strips that are in compression have relatively large deformations at the point where they are connected to the

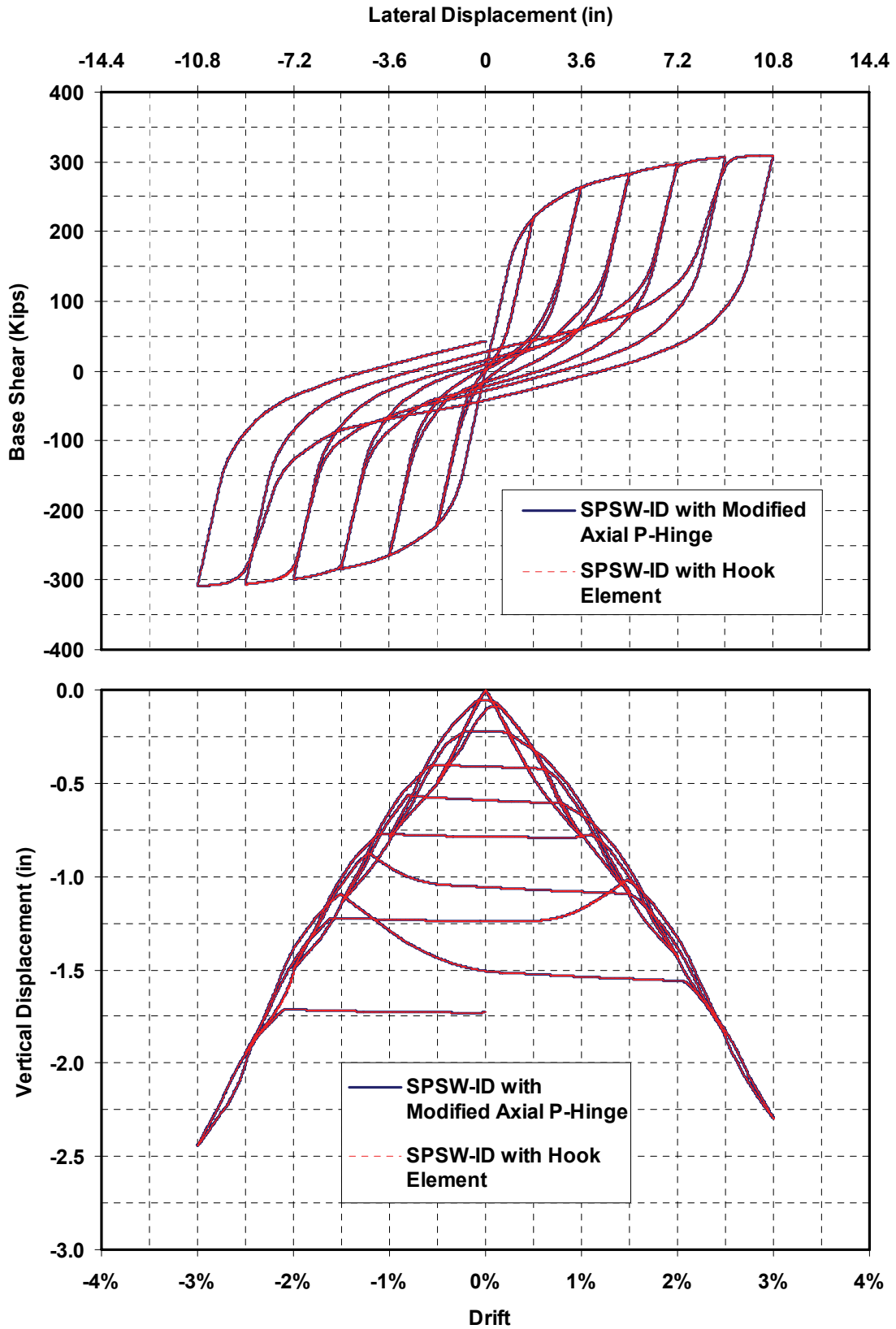


FIGURE D-3 Result Comparison between SPSW-ID with Modified Axial P-Hinge and SPSW-ID with Hook Element (a) Base Shear; (b) Vertical Deformation of HBE3

Hook Element (i.e., point B in the figure D-2). This is because the *Hook Element* does not work on those compression strips (i.e., $k = 0$), and during analysis, the program will treat these strips as if they were connected to the boundary frame only at one point (i.e. the end without the hook element). However, the program did not report warning or convergence issues during the analysis.

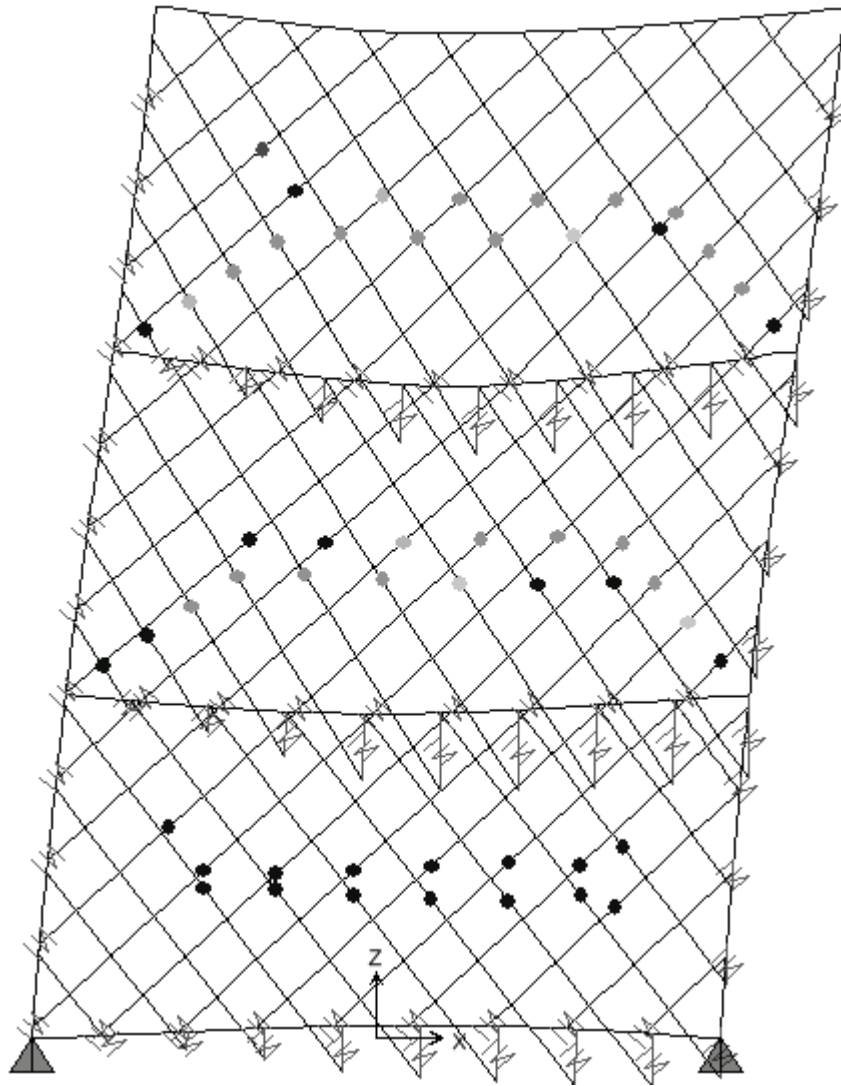


FIGURE D-4 Deformation of SPSW-ID with Hook Element at +3% Drift

APPENDIX E

COMPARISON OF NORMALIZED MOMENT ROTATION HYSTERESIS CURVE BETWEEN STEEL PLATE SHEAR WALLS AND SPECIAL MOMENT RESISTING FRAMES

Figures E-1 and E-2 compare hysteresis curves of both SPSWs (i.e., SPSW-ID and SPSW-CD, respectively) with special moment resisting frames (i.e., their bare frames without the infill plates). As explained in Section 3, unlike hysteresis curve for the special moment resisting frames, which is symmetric with respect to positive and negative rotations developed under a symmetric cyclic pushover displacement history (figure 3-6), the hysteresis curves of both SPSWs considered here are not symmetric but looping with a bias toward one direction. It loops towards the positive side for the bottom HBE and to the negative side for the other HBEs, where positive and negative rotations here are respectively defined as corresponding to tension on the bottom and top side of the HBE. The tension forces from the infill plates contribute to this behavior by always pulling the HBE in the direction of the tension forces (i.e., pulling the bottom HBE upward and the other HBEs downward).

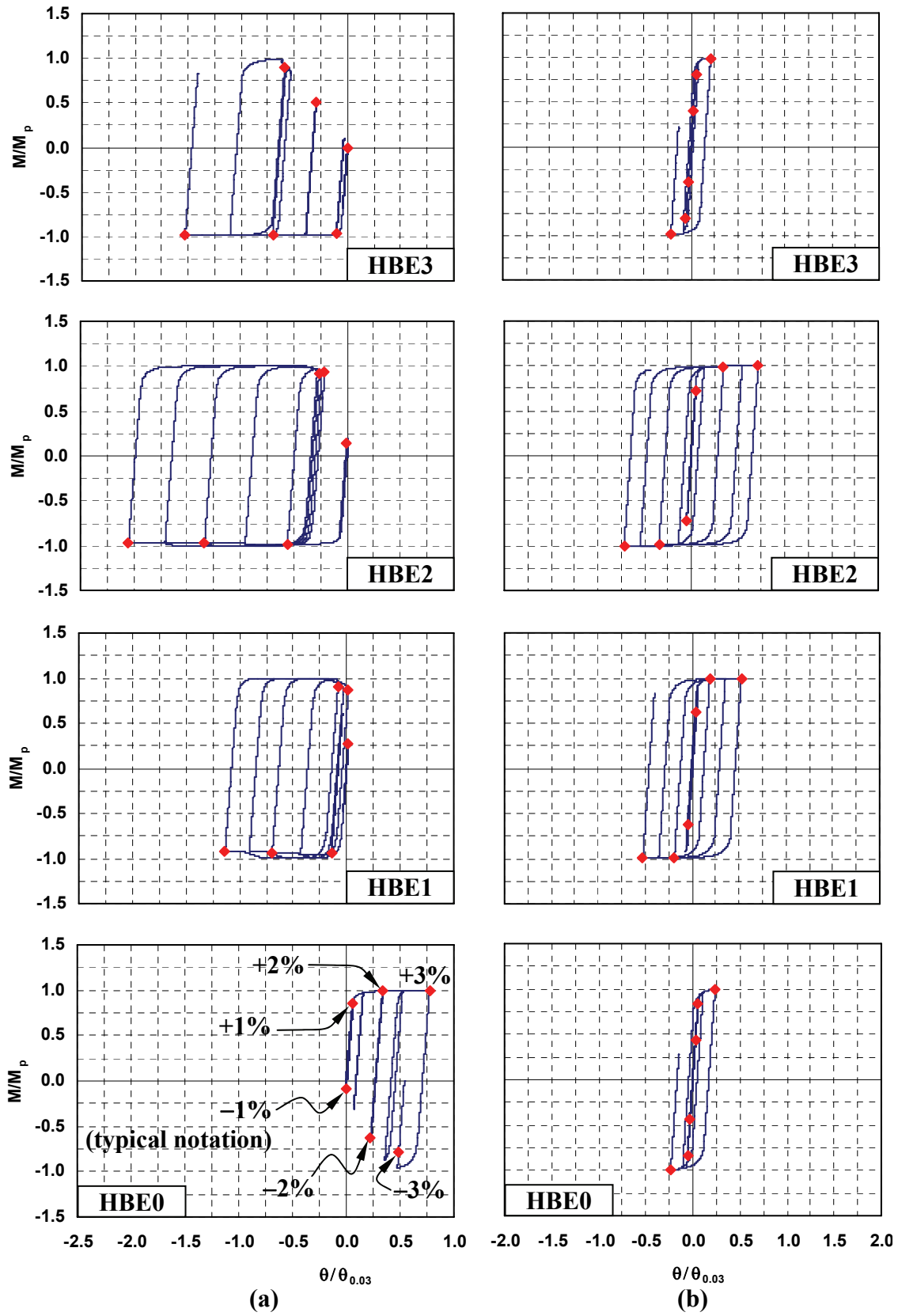


FIGURE E-1 Comparison of Normalized Moment Rotation Hysteresis between (a) SPSW-ID; and (b) Its Bare Frame (SMRF)

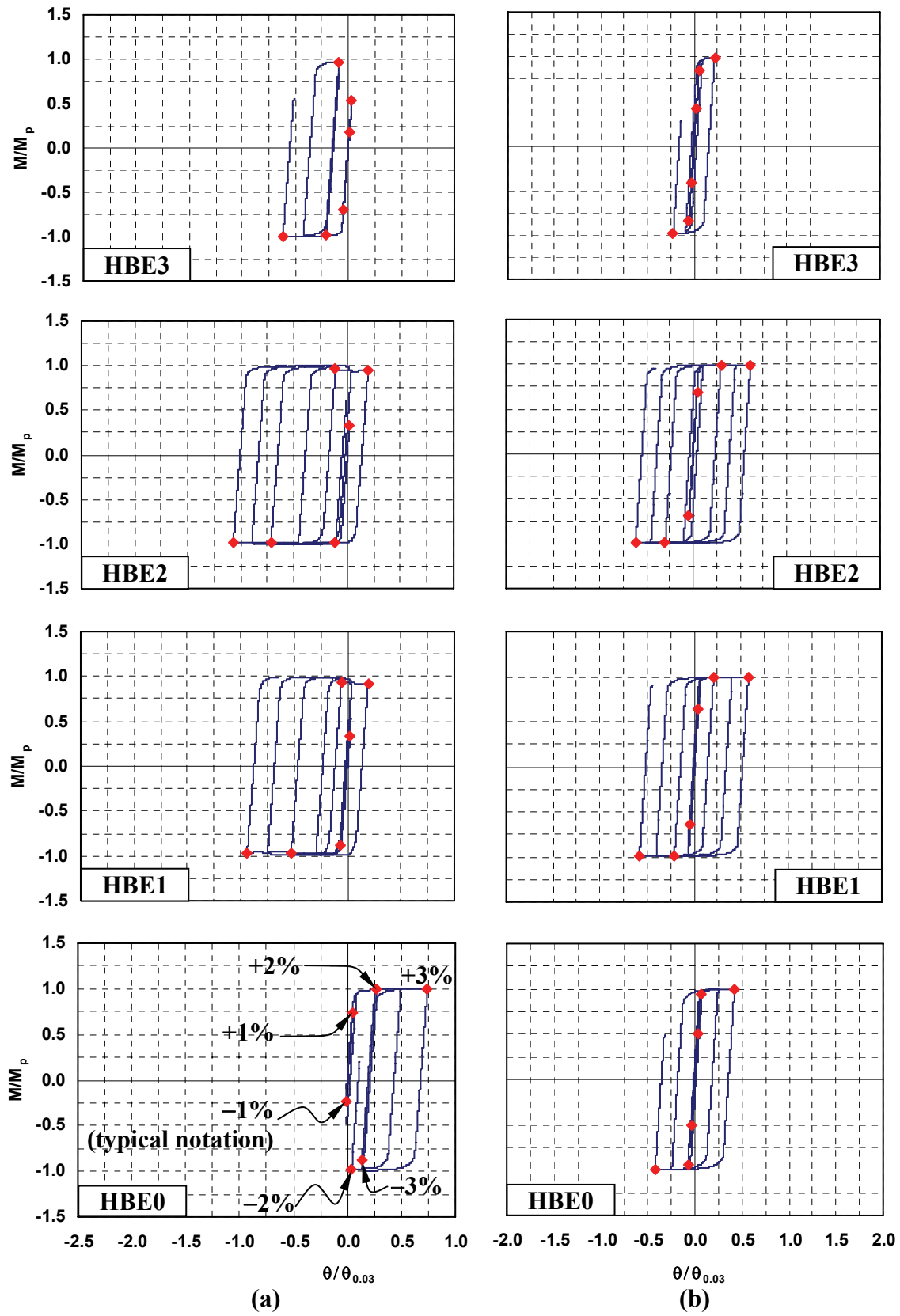


FIGURE E-2 Comparison of Normalized Moment Rotation Hysteresis between (a) SPSW-CD; and (b) Its Bare Frame (SMRF)

MCEER Technical Reports

MCEER publishes technical reports on a variety of subjects written by authors funded through MCEER. These reports are available from both MCEER Publications and the National Technical Information Service (NTIS). Requests for reports should be directed to MCEER Publications, MCEER, University at Buffalo, State University of New York, 133A Ketter Hall, Buffalo, New York 14260. Reports can also be requested through NTIS, P.O. Box 1425, Springfield, Virginia 22151. NTIS accession numbers are shown in parenthesis, if available.

- NCEER-87-0001 "First-Year Program in Research, Education and Technology Transfer," 3/5/87, (PB88-134275, A04, MF-A01).
- NCEER-87-0002 "Experimental Evaluation of Instantaneous Optimal Algorithms for Structural Control," by R.C. Lin, T.T. Soong and A.M. Reinhorn, 4/20/87, (PB88-134341, A04, MF-A01).
- NCEER-87-0003 "Experimentation Using the Earthquake Simulation Facilities at University at Buffalo," by A.M. Reinhorn and R.L. Ketter, to be published.
- NCEER-87-0004 "The System Characteristics and Performance of a Shaking Table," by J.S. Hwang, K.C. Chang and G.C. Lee, 6/1/87, (PB88-134259, A03, MF-A01). This report is available only through NTIS (see address given above).
- NCEER-87-0005 "A Finite Element Formulation for Nonlinear Viscoplastic Material Using a Q Model," by O. Gyebe and G. Dasgupta, 11/2/87, (PB88-213764, A08, MF-A01).
- NCEER-87-0006 "Symbolic Manipulation Program (SMP) - Algebraic Codes for Two and Three Dimensional Finite Element Formulations," by X. Lee and G. Dasgupta, 11/9/87, (PB88-218522, A05, MF-A01).
- NCEER-87-0007 "Instantaneous Optimal Control Laws for Tall Buildings Under Seismic Excitations," by J.N. Yang, A. Akbarpour and P. Ghaemmaghami, 6/10/87, (PB88-134333, A06, MF-A01). This report is only available through NTIS (see address given above).
- NCEER-87-0008 "IDARC: Inelastic Damage Analysis of Reinforced Concrete Frame - Shear-Wall Structures," by Y.J. Park, A.M. Reinhorn and S.K. Kunnath, 7/20/87, (PB88-134325, A09, MF-A01). This report is only available through NTIS (see address given above).
- NCEER-87-0009 "Liquefaction Potential for New York State: A Preliminary Report on Sites in Manhattan and Buffalo," by M. Budhu, V. Vijayakumar, R.F. Giese and L. Baumgras, 8/31/87, (PB88-163704, A03, MF-A01). This report is available only through NTIS (see address given above).
- NCEER-87-0010 "Vertical and Torsional Vibration of Foundations in Inhomogeneous Media," by A.S. Veletsos and K.W. Dotson, 6/1/87, (PB88-134291, A03, MF-A01). This report is only available through NTIS (see address given above).
- NCEER-87-0011 "Seismic Probabilistic Risk Assessment and Seismic Margins Studies for Nuclear Power Plants," by Howard H.M. Hwang, 6/15/87, (PB88-134267, A03, MF-A01). This report is only available through NTIS (see address given above).
- NCEER-87-0012 "Parametric Studies of Frequency Response of Secondary Systems Under Ground-Acceleration Excitations," by Y. Yong and Y.K. Lin, 6/10/87, (PB88-134309, A03, MF-A01). This report is only available through NTIS (see address given above).
- NCEER-87-0013 "Frequency Response of Secondary Systems Under Seismic Excitation," by J.A. HoLung, J. Cai and Y.K. Lin, 7/31/87, (PB88-134317, A05, MF-A01). This report is only available through NTIS (see address given above).
- NCEER-87-0014 "Modelling Earthquake Ground Motions in Seismically Active Regions Using Parametric Time Series Methods," by G.W. Ellis and A.S. Cakmak, 8/25/87, (PB88-134283, A08, MF-A01). This report is only available through NTIS (see address given above).
- NCEER-87-0015 "Detection and Assessment of Seismic Structural Damage," by E. DiPasquale and A.S. Cakmak, 8/25/87, (PB88-163712, A05, MF-A01). This report is only available through NTIS (see address given above).

- NCEER-87-0016 "Pipeline Experiment at Parkfield, California," by J. Isenberg and E. Richardson, 9/15/87, (PB88-163720, A03, MF-A01). This report is available only through NTIS (see address given above).
- NCEER-87-0017 "Digital Simulation of Seismic Ground Motion," by M. Shinozuka, G. Deodatis and T. Harada, 8/31/87, (PB88-155197, A04, MF-A01). This report is available only through NTIS (see address given above).
- NCEER-87-0018 "Practical Considerations for Structural Control: System Uncertainty, System Time Delay and Truncation of Small Control Forces," J.N. Yang and A. Akbarpour, 8/10/87, (PB88-163738, A08, MF-A01). This report is only available through NTIS (see address given above).
- NCEER-87-0019 "Modal Analysis of Nonclassically Damped Structural Systems Using Canonical Transformation," by J.N. Yang, S. Sarkani and F.X. Long, 9/27/87, (PB88-187851, A04, MF-A01).
- NCEER-87-0020 "A Nonstationary Solution in Random Vibration Theory," by J.R. Red-Horse and P.D. Spanos, 11/3/87, (PB88-163746, A03, MF-A01).
- NCEER-87-0021 "Horizontal Impedances for Radially Inhomogeneous Viscoelastic Soil Layers," by A.S. Veletsos and K.W. Dotson, 10/15/87, (PB88-150859, A04, MF-A01).
- NCEER-87-0022 "Seismic Damage Assessment of Reinforced Concrete Members," by Y.S. Chung, C. Meyer and M. Shinozuka, 10/9/87, (PB88-150867, A05, MF-A01). This report is available only through NTIS (see address given above).
- NCEER-87-0023 "Active Structural Control in Civil Engineering," by T.T. Soong, 11/11/87, (PB88-187778, A03, MF-A01).
- NCEER-87-0024 "Vertical and Torsional Impedances for Radially Inhomogeneous Viscoelastic Soil Layers," by K.W. Dotson and A.S. Veletsos, 12/87, (PB88-187786, A03, MF-A01).
- NCEER-87-0025 "Proceedings from the Symposium on Seismic Hazards, Ground Motions, Soil-Liquefaction and Engineering Practice in Eastern North America," October 20-22, 1987, edited by K.H. Jacob, 12/87, (PB88-188115, A23, MF-A01). This report is available only through NTIS (see address given above).
- NCEER-87-0026 "Report on the Whittier-Narrows, California, Earthquake of October 1, 1987," by J. Pantelic and A. Reinhorn, 11/87, (PB88-187752, A03, MF-A01). This report is available only through NTIS (see address given above).
- NCEER-87-0027 "Design of a Modular Program for Transient Nonlinear Analysis of Large 3-D Building Structures," by S. Srivastav and J.F. Abel, 12/30/87, (PB88-187950, A05, MF-A01). This report is only available through NTIS (see address given above).
- NCEER-87-0028 "Second-Year Program in Research, Education and Technology Transfer," 3/8/88, (PB88-219480, A04, MF-A01).
- NCEER-88-0001 "Workshop on Seismic Computer Analysis and Design of Buildings With Interactive Graphics," by W. McGuire, J.F. Abel and C.H. Conley, 1/18/88, (PB88-187760, A03, MF-A01). This report is only available through NTIS (see address given above).
- NCEER-88-0002 "Optimal Control of Nonlinear Flexible Structures," by J.N. Yang, F.X. Long and D. Wong, 1/22/88, (PB88-213772, A06, MF-A01).
- NCEER-88-0003 "Substructuring Techniques in the Time Domain for Primary-Secondary Structural Systems," by G.D. Manolis and G. Juhn, 2/10/88, (PB88-213780, A04, MF-A01).
- NCEER-88-0004 "Iterative Seismic Analysis of Primary-Secondary Systems," by A. Singhal, L.D. Lutes and P.D. Spanos, 2/23/88, (PB88-213798, A04, MF-A01).
- NCEER-88-0005 "Stochastic Finite Element Expansion for Random Media," by P.D. Spanos and R. Ghanem, 3/14/88, (PB88-213806, A03, MF-A01).

- NCEER-88-0006 "Combining Structural Optimization and Structural Control," by F.Y. Cheng and C.P. Pantelides, 1/10/88, (PB88-213814, A05, MF-A01).
- NCEER-88-0007 "Seismic Performance Assessment of Code-Designed Structures," by H.H-M. Hwang, J-W. Jaw and H-J. Shau, 3/20/88, (PB88-219423, A04, MF-A01). This report is only available through NTIS (see address given above).
- NCEER-88-0008 "Reliability Analysis of Code-Designed Structures Under Natural Hazards," by H.H-M. Hwang, H. Ushiba and M. Shinozuka, 2/29/88, (PB88-229471, A07, MF-A01). This report is only available through NTIS (see address given above).
- NCEER-88-0009 "Seismic Fragility Analysis of Shear Wall Structures," by J-W Jaw and H.H-M. Hwang, 4/30/88, (PB89-102867, A04, MF-A01).
- NCEER-88-0010 "Base Isolation of a Multi-Story Building Under a Harmonic Ground Motion - A Comparison of Performances of Various Systems," by F-G Fan, G. Ahmadi and I.G. Tadjbakhsh, 5/18/88, (PB89-122238, A06, MF-A01). This report is only available through NTIS (see address given above).
- NCEER-88-0011 "Seismic Floor Response Spectra for a Combined System by Green's Functions," by F.M. Lavelle, L.A. Bergman and P.D. Spanos, 5/1/88, (PB89-102875, A03, MF-A01).
- NCEER-88-0012 "A New Solution Technique for Randomly Excited Hysteretic Structures," by G.Q. Cai and Y.K. Lin, 5/16/88, (PB89-102883, A03, MF-A01).
- NCEER-88-0013 "A Study of Radiation Damping and Soil-Structure Interaction Effects in the Centrifuge," by K. Weissman, supervised by J.H. Prevost, 5/24/88, (PB89-144703, A06, MF-A01).
- NCEER-88-0014 "Parameter Identification and Implementation of a Kinematic Plasticity Model for Frictional Soils," by J.H. Prevost and D.V. Griffiths, to be published.
- NCEER-88-0015 "Two- and Three- Dimensional Dynamic Finite Element Analyses of the Long Valley Dam," by D.V. Griffiths and J.H. Prevost, 6/17/88, (PB89-144711, A04, MF-A01).
- NCEER-88-0016 "Damage Assessment of Reinforced Concrete Structures in Eastern United States," by A.M. Reinhorn, M.J. Seidel, S.K. Kunnath and Y.J. Park, 6/15/88, (PB89-122220, A04, MF-A01). This report is only available through NTIS (see address given above).
- NCEER-88-0017 "Dynamic Compliance of Vertically Loaded Strip Foundations in Multilayered Viscoelastic Soils," by S. Ahmad and A.S.M. Israil, 6/17/88, (PB89-102891, A04, MF-A01).
- NCEER-88-0018 "An Experimental Study of Seismic Structural Response With Added Viscoelastic Dampers," by R.C. Lin, Z. Liang, T.T. Soong and R.H. Zhang, 6/30/88, (PB89-122212, A05, MF-A01). This report is available only through NTIS (see address given above).
- NCEER-88-0019 "Experimental Investigation of Primary - Secondary System Interaction," by G.D. Manolis, G. Juhn and A.M. Reinhorn, 5/27/88, (PB89-122204, A04, MF-A01).
- NCEER-88-0020 "A Response Spectrum Approach For Analysis of Nonclassically Damped Structures," by J.N. Yang, S. Sarkani and F.X. Long, 4/22/88, (PB89-102909, A04, MF-A01).
- NCEER-88-0021 "Seismic Interaction of Structures and Soils: Stochastic Approach," by A.S. Veletsos and A.M. Prasad, 7/21/88, (PB89-122196, A04, MF-A01). This report is only available through NTIS (see address given above).
- NCEER-88-0022 "Identification of the Serviceability Limit State and Detection of Seismic Structural Damage," by E. DiPasquale and A.S. Cakmak, 6/15/88, (PB89-122188, A05, MF-A01). This report is available only through NTIS (see address given above).
- NCEER-88-0023 "Multi-Hazard Risk Analysis: Case of a Simple Offshore Structure," by B.K. Bhartia and E.H. Vanmarcke, 7/21/88, (PB89-145213, A05, MF-A01).

- NCEER-88-0024 "Automated Seismic Design of Reinforced Concrete Buildings," by Y.S. Chung, C. Meyer and M. Shinozuka, 7/5/88, (PB89-122170, A06, MF-A01). This report is available only through NTIS (see address given above).
- NCEER-88-0025 "Experimental Study of Active Control of MDOF Structures Under Seismic Excitations," by L.L. Chung, R.C. Lin, T.T. Soong and A.M. Reinhorn, 7/10/88, (PB89-122600, A04, MF-A01).
- NCEER-88-0026 "Earthquake Simulation Tests of a Low-Rise Metal Structure," by J.S. Hwang, K.C. Chang, G.C. Lee and R.L. Ketter, 8/1/88, (PB89-102917, A04, MF-A01).
- NCEER-88-0027 "Systems Study of Urban Response and Reconstruction Due to Catastrophic Earthquakes," by F. Kozin and H.K. Zhou, 9/22/88, (PB90-162348, A04, MF-A01).
- NCEER-88-0028 "Seismic Fragility Analysis of Plane Frame Structures," by H.H-M. Hwang and Y.K. Low, 7/31/88, (PB89-131445, A06, MF-A01).
- NCEER-88-0029 "Response Analysis of Stochastic Structures," by A. Kardara, C. Bucher and M. Shinozuka, 9/22/88, (PB89-174429, A04, MF-A01).
- NCEER-88-0030 "Nonnormal Accelerations Due to Yielding in a Primary Structure," by D.C.K. Chen and L.D. Lutes, 9/19/88, (PB89-131437, A04, MF-A01).
- NCEER-88-0031 "Design Approaches for Soil-Structure Interaction," by A.S. Veletsos, A.M. Prasad and Y. Tang, 12/30/88, (PB89-174437, A03, MF-A01). This report is available only through NTIS (see address given above).
- NCEER-88-0032 "A Re-evaluation of Design Spectra for Seismic Damage Control," by C.J. Turkstra and A.G. Tallin, 11/7/88, (PB89-145221, A05, MF-A01).
- NCEER-88-0033 "The Behavior and Design of Noncontact Lap Splices Subjected to Repeated Inelastic Tensile Loading," by V.E. Sagan, P. Gergely and R.N. White, 12/8/88, (PB89-163737, A08, MF-A01).
- NCEER-88-0034 "Seismic Response of Pile Foundations," by S.M. Mamoon, P.K. Banerjee and S. Ahmad, 11/1/88, (PB89-145239, A04, MF-A01).
- NCEER-88-0035 "Modeling of R/C Building Structures With Flexible Floor Diaphragms (IDARC2)," by A.M. Reinhorn, S.K. Kunnath and N. Panahshahi, 9/7/88, (PB89-207153, A07, MF-A01).
- NCEER-88-0036 "Solution of the Dam-Reservoir Interaction Problem Using a Combination of FEM, BEM with Particular Integrals, Modal Analysis, and Substructuring," by C-S. Tsai, G.C. Lee and R.L. Ketter, 12/31/88, (PB89-207146, A04, MF-A01).
- NCEER-88-0037 "Optimal Placement of Actuators for Structural Control," by F.Y. Cheng and C.P. Pantelides, 8/15/88, (PB89-162846, A05, MF-A01).
- NCEER-88-0038 "Teflon Bearings in Aseismic Base Isolation: Experimental Studies and Mathematical Modeling," by A. Mokha, M.C. Constantinou and A.M. Reinhorn, 12/5/88, (PB89-218457, A10, MF-A01). This report is available only through NTIS (see address given above).
- NCEER-88-0039 "Seismic Behavior of Flat Slab High-Rise Buildings in the New York City Area," by P. Weidlinger and M. Ettouney, 10/15/88, (PB90-145681, A04, MF-A01).
- NCEER-88-0040 "Evaluation of the Earthquake Resistance of Existing Buildings in New York City," by P. Weidlinger and M. Ettouney, 10/15/88, to be published.
- NCEER-88-0041 "Small-Scale Modeling Techniques for Reinforced Concrete Structures Subjected to Seismic Loads," by W. Kim, A. El-Attar and R.N. White, 11/22/88, (PB89-189625, A05, MF-A01).
- NCEER-88-0042 "Modeling Strong Ground Motion from Multiple Event Earthquakes," by G.W. Ellis and A.S. Cakmak, 10/15/88, (PB89-174445, A03, MF-A01).

- NCEER-88-0043 "Nonstationary Models of Seismic Ground Acceleration," by M. Grigoriu, S.E. Ruiz and E. Rosenblueth, 7/15/88, (PB89-189617, A04, MF-A01).
- NCEER-88-0044 "SARCF User's Guide: Seismic Analysis of Reinforced Concrete Frames," by Y.S. Chung, C. Meyer and M. Shinozuka, 11/9/88, (PB89-174452, A08, MF-A01).
- NCEER-88-0045 "First Expert Panel Meeting on Disaster Research and Planning," edited by J. Pantelic and J. Stoyke, 9/15/88, (PB89-174460, A05, MF-A01).
- NCEER-88-0046 "Preliminary Studies of the Effect of Degrading Infill Walls on the Nonlinear Seismic Response of Steel Frames," by C.Z. Chrysostomou, P. Gergely and J.F. Abel, 12/19/88, (PB89-208383, A05, MF-A01).
- NCEER-88-0047 "Reinforced Concrete Frame Component Testing Facility - Design, Construction, Instrumentation and Operation," by S.P. Pessiki, C. Conley, T. Bond, P. Gergely and R.N. White, 12/16/88, (PB89-174478, A04, MF-A01).
- NCEER-89-0001 "Effects of Protective Cushion and Soil Compliancy on the Response of Equipment Within a Seismically Excited Building," by J.A. HoLung, 2/16/89, (PB89-207179, A04, MF-A01).
- NCEER-89-0002 "Statistical Evaluation of Response Modification Factors for Reinforced Concrete Structures," by H.H-M. Hwang and J-W. Jaw, 2/17/89, (PB89-207187, A05, MF-A01).
- NCEER-89-0003 "Hysteretic Columns Under Random Excitation," by G-Q. Cai and Y.K. Lin, 1/9/89, (PB89-196513, A03, MF-A01).
- NCEER-89-0004 "Experimental Study of 'Elephant Foot Bulge' Instability of Thin-Walled Metal Tanks," by Z-H. Jia and R.L. Ketter, 2/22/89, (PB89-207195, A03, MF-A01).
- NCEER-89-0005 "Experiment on Performance of Buried Pipelines Across San Andreas Fault," by J. Isenberg, E. Richardson and T.D. O'Rourke, 3/10/89, (PB89-218440, A04, MF-A01). This report is available only through NTIS (see address given above).
- NCEER-89-0006 "A Knowledge-Based Approach to Structural Design of Earthquake-Resistant Buildings," by M. Subramani, P. Gergely, C.H. Conley, J.F. Abel and A.H. Zaghaw, 1/15/89, (PB89-218465, A06, MF-A01).
- NCEER-89-0007 "Liquefaction Hazards and Their Effects on Buried Pipelines," by T.D. O'Rourke and P.A. Lane, 2/1/89, (PB89-218481, A09, MF-A01).
- NCEER-89-0008 "Fundamentals of System Identification in Structural Dynamics," by H. Imai, C-B. Yun, O. Maruyama and M. Shinozuka, 1/26/89, (PB89-207211, A04, MF-A01).
- NCEER-89-0009 "Effects of the 1985 Michoacan Earthquake on Water Systems and Other Buried Lifelines in Mexico," by A.G. Ayala and M.J. O'Rourke, 3/8/89, (PB89-207229, A06, MF-A01).
- NCEER-89-R010 "NCEER Bibliography of Earthquake Education Materials," by K.E.K. Ross, Second Revision, 9/1/89, (PB90-125352, A05, MF-A01). This report is replaced by NCEER-92-0018.
- NCEER-89-0011 "Inelastic Three-Dimensional Response Analysis of Reinforced Concrete Building Structures (IDARC-3D), Part I - Modeling," by S.K. Kunnath and A.M. Reinhorn, 4/17/89, (PB90-114612, A07, MF-A01). This report is available only through NTIS (see address given above).
- NCEER-89-0012 "Recommended Modifications to ATC-14," by C.D. Poland and J.O. Malley, 4/12/89, (PB90-108648, A15, MF-A01).
- NCEER-89-0013 "Repair and Strengthening of Beam-to-Column Connections Subjected to Earthquake Loading," by M. Corazao and A.J. Durrani, 2/28/89, (PB90-109885, A06, MF-A01).
- NCEER-89-0014 "Program EXKAL2 for Identification of Structural Dynamic Systems," by O. Maruyama, C-B. Yun, M. Hoshiya and M. Shinozuka, 5/19/89, (PB90-109877, A09, MF-A01).

- NCEER-89-0015 "Response of Frames With Bolted Semi-Rigid Connections, Part I - Experimental Study and Analytical Predictions," by P.J. DiCorso, A.M. Reinhorn, J.R. Dickerson, J.B. Radzinski and W.L. Harper, 6/1/89, to be published.
- NCEER-89-0016 "ARMA Monte Carlo Simulation in Probabilistic Structural Analysis," by P.D. Spanos and M.P. Mignolet, 7/10/89, (PB90-109893, A03, MF-A01).
- NCEER-89-P017 "Preliminary Proceedings from the Conference on Disaster Preparedness - The Place of Earthquake Education in Our Schools," Edited by K.E.K. Ross, 6/23/89, (PB90-108606, A03, MF-A01).
- NCEER-89-0017 "Proceedings from the Conference on Disaster Preparedness - The Place of Earthquake Education in Our Schools," Edited by K.E.K. Ross, 12/31/89, (PB90-207895, A012, MF-A02). This report is available only through NTIS (see address given above).
- NCEER-89-0018 "Multidimensional Models of Hysteretic Material Behavior for Vibration Analysis of Shape Memory Energy Absorbing Devices, by E.J. Graesser and F.A. Cozzarelli, 6/7/89, (PB90-164146, A04, MF-A01).
- NCEER-89-0019 "Nonlinear Dynamic Analysis of Three-Dimensional Base Isolated Structures (3D-BASIS)," by S. Nagarajaiah, A.M. Reinhorn and M.C. Constantinou, 8/3/89, (PB90-161936, A06, MF-A01). This report has been replaced by NCEER-93-0011.
- NCEER-89-0020 "Structural Control Considering Time-Rate of Control Forces and Control Rate Constraints," by F.Y. Cheng and C.P. Pantelides, 8/3/89, (PB90-120445, A04, MF-A01).
- NCEER-89-0021 "Subsurface Conditions of Memphis and Shelby County," by K.W. Ng, T-S. Chang and H-H.M. Hwang, 7/26/89, (PB90-120437, A03, MF-A01).
- NCEER-89-0022 "Seismic Wave Propagation Effects on Straight Jointed Buried Pipelines," by K. Elhadi and M.J. O'Rourke, 8/24/89, (PB90-162322, A10, MF-A02).
- NCEER-89-0023 "Workshop on Serviceability Analysis of Water Delivery Systems," edited by M. Grigoriu, 3/6/89, (PB90-127424, A03, MF-A01).
- NCEER-89-0024 "Shaking Table Study of a 1/5 Scale Steel Frame Composed of Tapered Members," by K.C. Chang, J.S. Hwang and G.C. Lee, 9/18/89, (PB90-160169, A04, MF-A01).
- NCEER-89-0025 "DYNA1D: A Computer Program for Nonlinear Seismic Site Response Analysis - Technical Documentation," by Jean H. Prevost, 9/14/89, (PB90-161944, A07, MF-A01). This report is available only through NTIS (see address given above).
- NCEER-89-0026 "1:4 Scale Model Studies of Active Tendon Systems and Active Mass Dampers for Aseismic Protection," by A.M. Reinhorn, T.T. Soong, R.C. Lin, Y.P. Yang, Y. Fukao, H. Abe and M. Nakai, 9/15/89, (PB90-173246, A10, MF-A02). This report is available only through NTIS (see address given above).
- NCEER-89-0027 "Scattering of Waves by Inclusions in a Nonhomogeneous Elastic Half Space Solved by Boundary Element Methods," by P.K. Hadley, A. Askar and A.S. Cakmak, 6/15/89, (PB90-145699, A07, MF-A01).
- NCEER-89-0028 "Statistical Evaluation of Deflection Amplification Factors for Reinforced Concrete Structures," by H.H.M. Hwang, J-W. Jaw and A.L. Ch'ng, 8/31/89, (PB90-164633, A05, MF-A01).
- NCEER-89-0029 "Bedrock Accelerations in Memphis Area Due to Large New Madrid Earthquakes," by H.H.M. Hwang, C.H.S. Chen and G. Yu, 11/7/89, (PB90-162330, A04, MF-A01).
- NCEER-89-0030 "Seismic Behavior and Response Sensitivity of Secondary Structural Systems," by Y.Q. Chen and T.T. Soong, 10/23/89, (PB90-164658, A08, MF-A01).
- NCEER-89-0031 "Random Vibration and Reliability Analysis of Primary-Secondary Structural Systems," by Y. Ibrahim, M. Grigoriu and T.T. Soong, 11/10/89, (PB90-161951, A04, MF-A01).

- NCEER-89-0032 "Proceedings from the Second U.S. - Japan Workshop on Liquefaction, Large Ground Deformation and Their Effects on Lifelines, September 26-29, 1989," Edited by T.D. O'Rourke and M. Hamada, 12/1/89, (PB90-209388, A22, MF-A03).
- NCEER-89-0033 "Deterministic Model for Seismic Damage Evaluation of Reinforced Concrete Structures," by J.M. Bracci, A.M. Reinhorn, J.B. Mander and S.K. Kunnath, 9/27/89, (PB91-108803, A06, MF-A01).
- NCEER-89-0034 "On the Relation Between Local and Global Damage Indices," by E. DiPasquale and A.S. Cakmak, 8/15/89, (PB90-173865, A05, MF-A01).
- NCEER-89-0035 "Cyclic Undrained Behavior of Nonplastic and Low Plasticity Silts," by A.J. Walker and H.E. Stewart, 7/26/89, (PB90-183518, A10, MF-A01).
- NCEER-89-0036 "Liquefaction Potential of Surficial Deposits in the City of Buffalo, New York," by M. Budhu, R. Giese and L. Baumgrass, 1/17/89, (PB90-208455, A04, MF-A01).
- NCEER-89-0037 "A Deterministic Assessment of Effects of Ground Motion Incoherence," by A.S. Veletsos and Y. Tang, 7/15/89, (PB90-164294, A03, MF-A01).
- NCEER-89-0038 "Workshop on Ground Motion Parameters for Seismic Hazard Mapping," July 17-18, 1989, edited by R.V. Whitman, 12/1/89, (PB90-173923, A04, MF-A01).
- NCEER-89-0039 "Seismic Effects on Elevated Transit Lines of the New York City Transit Authority," by C.J. Costantino, C.A. Miller and E. Heymsfield, 12/26/89, (PB90-207887, A06, MF-A01).
- NCEER-89-0040 "Centrifugal Modeling of Dynamic Soil-Structure Interaction," by K. Weissman, Supervised by J.H. Prevost, 5/10/89, (PB90-207879, A07, MF-A01).
- NCEER-89-0041 "Linearized Identification of Buildings With Cores for Seismic Vulnerability Assessment," by I-K. Ho and A.E. Aktan, 11/1/89, (PB90-251943, A07, MF-A01).
- NCEER-90-0001 "Geotechnical and Lifeline Aspects of the October 17, 1989 Loma Prieta Earthquake in San Francisco," by T.D. O'Rourke, H.E. Stewart, F.T. Blackburn and T.S. Dickerman, 1/90, (PB90-208596, A05, MF-A01).
- NCEER-90-0002 "Nonnormal Secondary Response Due to Yielding in a Primary Structure," by D.C.K. Chen and L.D. Lutes, 2/28/90, (PB90-251976, A07, MF-A01).
- NCEER-90-0003 "Earthquake Education Materials for Grades K-12," by K.E.K. Ross, 4/16/90, (PB91-251984, A05, MF-A05). This report has been replaced by NCEER-92-0018.
- NCEER-90-0004 "Catalog of Strong Motion Stations in Eastern North America," by R.W. Busby, 4/3/90, (PB90-251984, A05, MF-A01).
- NCEER-90-0005 "NCEER Strong-Motion Data Base: A User Manual for the GeoBase Release (Version 1.0 for the Sun3)," by P. Friberg and K. Jacob, 3/31/90 (PB90-258062, A04, MF-A01).
- NCEER-90-0006 "Seismic Hazard Along a Crude Oil Pipeline in the Event of an 1811-1812 Type New Madrid Earthquake," by H.H.M. Hwang and C-H.S. Chen, 4/16/90, (PB90-258054, A04, MF-A01).
- NCEER-90-0007 "Site-Specific Response Spectra for Memphis Sheahan Pumping Station," by H.H.M. Hwang and C.S. Lee, 5/15/90, (PB91-108811, A05, MF-A01).
- NCEER-90-0008 "Pilot Study on Seismic Vulnerability of Crude Oil Transmission Systems," by T. Ariman, R. Dobry, M. Grigoriu, F. Kozin, M. O'Rourke, T. O'Rourke and M. Shinozuka, 5/25/90, (PB91-108837, A06, MF-A01).
- NCEER-90-0009 "A Program to Generate Site Dependent Time Histories: EQGEN," by G.W. Ellis, M. Srinivasan and A.S. Cakmak, 1/30/90, (PB91-108829, A04, MF-A01).
- NCEER-90-0010 "Active Isolation for Seismic Protection of Operating Rooms," by M.E. Talbott, Supervised by M. Shinozuka, 6/8/9, (PB91-110205, A05, MF-A01).

- NCEER-90-0011 "Program LINEARID for Identification of Linear Structural Dynamic Systems," by C-B. Yun and M. Shinozuka, 6/25/90, (PB91-110312, A08, MF-A01).
- NCEER-90-0012 "Two-Dimensional Two-Phase Elasto-Plastic Seismic Response of Earth Dams," by A.N. Yiagos, Supervised by J.H. Prevost, 6/20/90, (PB91-110197, A13, MF-A02).
- NCEER-90-0013 "Secondary Systems in Base-Isolated Structures: Experimental Investigation, Stochastic Response and Stochastic Sensitivity," by G.D. Manolis, G. Juhn, M.C. Constantinou and A.M. Reinhorn, 7/1/90, (PB91-110320, A08, MF-A01).
- NCEER-90-0014 "Seismic Behavior of Lightly-Reinforced Concrete Column and Beam-Column Joint Details," by S.P. Pessiki, C.H. Conley, P. Gergely and R.N. White, 8/22/90, (PB91-108795, A11, MF-A02).
- NCEER-90-0015 "Two Hybrid Control Systems for Building Structures Under Strong Earthquakes," by J.N. Yang and A. Daniellians, 6/29/90, (PB91-125393, A04, MF-A01).
- NCEER-90-0016 "Instantaneous Optimal Control with Acceleration and Velocity Feedback," by J.N. Yang and Z. Li, 6/29/90, (PB91-125401, A03, MF-A01).
- NCEER-90-0017 "Reconnaissance Report on the Northern Iran Earthquake of June 21, 1990," by M. Mehrain, 10/4/90, (PB91-125377, A03, MF-A01).
- NCEER-90-0018 "Evaluation of Liquefaction Potential in Memphis and Shelby County," by T.S. Chang, P.S. Tang, C.S. Lee and H. Hwang, 8/10/90, (PB91-125427, A09, MF-A01).
- NCEER-90-0019 "Experimental and Analytical Study of a Combined Sliding Disc Bearing and Helical Steel Spring Isolation System," by M.C. Constantinou, A.S. Mokha and A.M. Reinhorn, 10/4/90, (PB91-125385, A06, MF-A01). This report is available only through NTIS (see address given above).
- NCEER-90-0020 "Experimental Study and Analytical Prediction of Earthquake Response of a Sliding Isolation System with a Spherical Surface," by A.S. Mokha, M.C. Constantinou and A.M. Reinhorn, 10/11/90, (PB91-125419, A05, MF-A01).
- NCEER-90-0021 "Dynamic Interaction Factors for Floating Pile Groups," by G. Gazetas, K. Fan, A. Kaynia and E. Kausel, 9/10/90, (PB91-170381, A05, MF-A01).
- NCEER-90-0022 "Evaluation of Seismic Damage Indices for Reinforced Concrete Structures," by S. Rodriguez-Gomez and A.S. Cakmak, 9/30/90, PB91-171322, A06, MF-A01).
- NCEER-90-0023 "Study of Site Response at a Selected Memphis Site," by H. Desai, S. Ahmad, E.S. Gazetas and M.R. Oh, 10/11/90, (PB91-196857, A03, MF-A01).
- NCEER-90-0024 "A User's Guide to Strongmo: Version 1.0 of NCEER's Strong-Motion Data Access Tool for PCs and Terminals," by P.A. Friberg and C.A.T. Susch, 11/15/90, (PB91-171272, A03, MF-A01).
- NCEER-90-0025 "A Three-Dimensional Analytical Study of Spatial Variability of Seismic Ground Motions," by L-L. Hong and A.H.-S. Ang, 10/30/90, (PB91-170399, A09, MF-A01).
- NCEER-90-0026 "MUMOID User's Guide - A Program for the Identification of Modal Parameters," by S. Rodriguez-Gomez and E. DiPasquale, 9/30/90, (PB91-171298, A04, MF-A01).
- NCEER-90-0027 "SARCF-II User's Guide - Seismic Analysis of Reinforced Concrete Frames," by S. Rodriguez-Gomez, Y.S. Chung and C. Meyer, 9/30/90, (PB91-171280, A05, MF-A01).
- NCEER-90-0028 "Viscous Dampers: Testing, Modeling and Application in Vibration and Seismic Isolation," by N. Makris and M.C. Constantinou, 12/20/90 (PB91-190561, A06, MF-A01).
- NCEER-90-0029 "Soil Effects on Earthquake Ground Motions in the Memphis Area," by H. Hwang, C.S. Lee, K.W. Ng and T.S. Chang, 8/2/90, (PB91-190751, A05, MF-A01).

- NCEER-91-0001 "Proceedings from the Third Japan-U.S. Workshop on Earthquake Resistant Design of Lifeline Facilities and Countermeasures for Soil Liquefaction, December 17-19, 1990," edited by T.D. O'Rourke and M. Hamada, 2/1/91, (PB91-179259, A99, MF-A04).
- NCEER-91-0002 "Physical Space Solutions of Non-Proportionally Damped Systems," by M. Tong, Z. Liang and G.C. Lee, 1/15/91, (PB91-179242, A04, MF-A01).
- NCEER-91-0003 "Seismic Response of Single Piles and Pile Groups," by K. Fan and G. Gazetas, 1/10/91, (PB92-174994, A04, MF-A01).
- NCEER-91-0004 "Damping of Structures: Part 1 - Theory of Complex Damping," by Z. Liang and G. Lee, 10/10/91, (PB92-197235, A12, MF-A03).
- NCEER-91-0005 "3D-BASIS - Nonlinear Dynamic Analysis of Three Dimensional Base Isolated Structures: Part II," by S. Nagarajaiah, A.M. Reinhorn and M.C. Constantinou, 2/28/91, (PB91-190553, A07, MF-A01). This report has been replaced by NCEER-93-0011.
- NCEER-91-0006 "A Multidimensional Hysteretic Model for Plasticity Deforming Metals in Energy Absorbing Devices," by E.J. Graesser and F.A. Cozzarelli, 4/9/91, (PB92-108364, A04, MF-A01).
- NCEER-91-0007 "A Framework for Customizable Knowledge-Based Expert Systems with an Application to a KBES for Evaluating the Seismic Resistance of Existing Buildings," by E.G. Ibarra-Anaya and S.J. Fenves, 4/9/91, (PB91-210930, A08, MF-A01).
- NCEER-91-0008 "Nonlinear Analysis of Steel Frames with Semi-Rigid Connections Using the Capacity Spectrum Method," by G.G. Deierlein, S-H. Hsieh, Y-J. Shen and J.F. Abel, 7/2/91, (PB92-113828, A05, MF-A01).
- NCEER-91-0009 "Earthquake Education Materials for Grades K-12," by K.E.K. Ross, 4/30/91, (PB91-212142, A06, MF-A01). This report has been replaced by NCEER-92-0018.
- NCEER-91-0010 "Phase Wave Velocities and Displacement Phase Differences in a Harmonically Oscillating Pile," by N. Makris and G. Gazetas, 7/8/91, (PB92-108356, A04, MF-A01).
- NCEER-91-0011 "Dynamic Characteristics of a Full-Size Five-Story Steel Structure and a 2/5 Scale Model," by K.C. Chang, G.C. Yao, G.C. Lee, D.S. Hao and Y.C. Yeh," 7/2/91, (PB93-116648, A06, MF-A02).
- NCEER-91-0012 "Seismic Response of a 2/5 Scale Steel Structure with Added Viscoelastic Dampers," by K.C. Chang, T.T. Soong, S-T. Oh and M.L. Lai, 5/17/91, (PB92-110816, A05, MF-A01).
- NCEER-91-0013 "Earthquake Response of Retaining Walls; Full-Scale Testing and Computational Modeling," by S. Alampalli and A-W.M. Elgamal, 6/20/91, to be published.
- NCEER-91-0014 "3D-BASIS-M: Nonlinear Dynamic Analysis of Multiple Building Base Isolated Structures," by P.C. Tsopelas, S. Nagarajaiah, M.C. Constantinou and A.M. Reinhorn, 5/28/91, (PB92-113885, A09, MF-A02).
- NCEER-91-0015 "Evaluation of SEAOC Design Requirements for Sliding Isolated Structures," by D. Theodossiou and M.C. Constantinou, 6/10/91, (PB92-114602, A11, MF-A03).
- NCEER-91-0016 "Closed-Loop Modal Testing of a 27-Story Reinforced Concrete Flat Plate-Core Building," by H.R. Somaprasad, T. Toksoy, H. Yoshiyuki and A.E. Aktan, 7/15/91, (PB92-129980, A07, MF-A02).
- NCEER-91-0017 "Shake Table Test of a 1/6 Scale Two-Story Lightly Reinforced Concrete Building," by A.G. El-Attar, R.N. White and P. Gergely, 2/28/91, (PB92-222447, A06, MF-A02).
- NCEER-91-0018 "Shake Table Test of a 1/8 Scale Three-Story Lightly Reinforced Concrete Building," by A.G. El-Attar, R.N. White and P. Gergely, 2/28/91, (PB93-116630, A08, MF-A02).
- NCEER-91-0019 "Transfer Functions for Rigid Rectangular Foundations," by A.S. Veletsos, A.M. Prasad and W.H. Wu, 7/31/91, to be published.

- NCEER-91-0020 "Hybrid Control of Seismic-Excited Nonlinear and Inelastic Structural Systems," by J.N. Yang, Z. Li and A. Daniellians, 8/1/91, (PB92-143171, A06, MF-A02).
- NCEER-91-0021 "The NCEER-91 Earthquake Catalog: Improved Intensity-Based Magnitudes and Recurrence Relations for U.S. Earthquakes East of New Madrid," by L. Seeber and J.G. Armbruster, 8/28/91, (PB92-176742, A06, MF-A02).
- NCEER-91-0022 "Proceedings from the Implementation of Earthquake Planning and Education in Schools: The Need for Change - The Roles of the Changemakers," by K.E.K. Ross and F. Winslow, 7/23/91, (PB92-129998, A12, MF-A03).
- NCEER-91-0023 "A Study of Reliability-Based Criteria for Seismic Design of Reinforced Concrete Frame Buildings," by H.H.M. Hwang and H-M. Hsu, 8/10/91, (PB92-140235, A09, MF-A02).
- NCEER-91-0024 "Experimental Verification of a Number of Structural System Identification Algorithms," by R.G. Ghanem, H. Gavin and M. Shinozuka, 9/18/91, (PB92-176577, A18, MF-A04).
- NCEER-91-0025 "Probabilistic Evaluation of Liquefaction Potential," by H.H.M. Hwang and C.S. Lee," 11/25/91, (PB92-143429, A05, MF-A01).
- NCEER-91-0026 "Instantaneous Optimal Control for Linear, Nonlinear and Hysteretic Structures - Stable Controllers," by J.N. Yang and Z. Li, 11/15/91, (PB92-163807, A04, MF-A01).
- NCEER-91-0027 "Experimental and Theoretical Study of a Sliding Isolation System for Bridges," by M.C. Constantinou, A. Kartoum, A.M. Reinhorn and P. Bradford, 11/15/91, (PB92-176973, A10, MF-A03).
- NCEER-92-0001 "Case Studies of Liquefaction and Lifeline Performance During Past Earthquakes, Volume 1: Japanese Case Studies," Edited by M. Hamada and T. O'Rourke, 2/17/92, (PB92-197243, A18, MF-A04).
- NCEER-92-0002 "Case Studies of Liquefaction and Lifeline Performance During Past Earthquakes, Volume 2: United States Case Studies," Edited by T. O'Rourke and M. Hamada, 2/17/92, (PB92-197250, A20, MF-A04).
- NCEER-92-0003 "Issues in Earthquake Education," Edited by K. Ross, 2/3/92, (PB92-222389, A07, MF-A02).
- NCEER-92-0004 "Proceedings from the First U.S. - Japan Workshop on Earthquake Protective Systems for Bridges," Edited by I.G. Buckle, 2/4/92, (PB94-142239, A99, MF-A06).
- NCEER-92-0005 "Seismic Ground Motion from a Haskell-Type Source in a Multiple-Layered Half-Space," A.P. Theoharis, G. Deodatis and M. Shinozuka, 1/2/92, to be published.
- NCEER-92-0006 "Proceedings from the Site Effects Workshop," Edited by R. Whitman, 2/29/92, (PB92-197201, A04, MF-A01).
- NCEER-92-0007 "Engineering Evaluation of Permanent Ground Deformations Due to Seismically-Induced Liquefaction," by M.H. Baziar, R. Dobry and A-W.M. Elgamal, 3/24/92, (PB92-222421, A13, MF-A03).
- NCEER-92-0008 "A Procedure for the Seismic Evaluation of Buildings in the Central and Eastern United States," by C.D. Poland and J.O. Malley, 4/2/92, (PB92-222439, A20, MF-A04).
- NCEER-92-0009 "Experimental and Analytical Study of a Hybrid Isolation System Using Friction Controllable Sliding Bearings," by M.Q. Feng, S. Fujii and M. Shinozuka, 5/15/92, (PB93-150282, A06, MF-A02).
- NCEER-92-0010 "Seismic Resistance of Slab-Column Connections in Existing Non-Ductile Flat-Plate Buildings," by A.J. Durrani and Y. Du, 5/18/92, (PB93-116812, A06, MF-A02).
- NCEER-92-0011 "The Hysteretic and Dynamic Behavior of Brick Masonry Walls Upgraded by Ferrocement Coatings Under Cyclic Loading and Strong Simulated Ground Motion," by H. Lee and S.P. Prawl, 5/11/92, to be published.
- NCEER-92-0012 "Study of Wire Rope Systems for Seismic Protection of Equipment in Buildings," by G.F. Demetriades, M.C. Constantinou and A.M. Reinhorn, 5/20/92, (PB93-116655, A08, MF-A02).

- NCEER-92-0013 "Shape Memory Structural Dampers: Material Properties, Design and Seismic Testing," by P.R. Witting and F.A. Cozzarelli, 5/26/92, (PB93-116663, A05, MF-A01).
- NCEER-92-0014 "Longitudinal Permanent Ground Deformation Effects on Buried Continuous Pipelines," by M.J. O'Rourke, and C. Nordberg, 6/15/92, (PB93-116671, A08, MF-A02).
- NCEER-92-0015 "A Simulation Method for Stationary Gaussian Random Functions Based on the Sampling Theorem," by M. Grigoriu and S. Balopoulou, 6/11/92, (PB93-127496, A05, MF-A01).
- NCEER-92-0016 "Gravity-Load-Designed Reinforced Concrete Buildings: Seismic Evaluation of Existing Construction and Detailing Strategies for Improved Seismic Resistance," by G.W. Hoffmann, S.K. Kunnath, A.M. Reinhorn and J.B. Mander, 7/15/92, (PB94-142007, A08, MF-A02).
- NCEER-92-0017 "Observations on Water System and Pipeline Performance in the Limón Area of Costa Rica Due to the April 22, 1991 Earthquake," by M. O'Rourke and D. Ballantyne, 6/30/92, (PB93-126811, A06, MF-A02).
- NCEER-92-0018 "Fourth Edition of Earthquake Education Materials for Grades K-12," Edited by K.E.K. Ross, 8/10/92, (PB93-114023, A07, MF-A02).
- NCEER-92-0019 "Proceedings from the Fourth Japan-U.S. Workshop on Earthquake Resistant Design of Lifeline Facilities and Countermeasures for Soil Liquefaction," Edited by M. Hamada and T.D. O'Rourke, 8/12/92, (PB93-163939, A99, MF-E11).
- NCEER-92-0020 "Active Bracing System: A Full Scale Implementation of Active Control," by A.M. Reinhorn, T.T. Soong, R.C. Lin, M.A. Riley, Y.P. Wang, S. Aizawa and M. Higashino, 8/14/92, (PB93-127512, A06, MF-A02).
- NCEER-92-0021 "Empirical Analysis of Horizontal Ground Displacement Generated by Liquefaction-Induced Lateral Spreads," by S.F. Bartlett and T.L. Youd, 8/17/92, (PB93-188241, A06, MF-A02).
- NCEER-92-0022 "IDARC Version 3.0: Inelastic Damage Analysis of Reinforced Concrete Structures," by S.K. Kunnath, A.M. Reinhorn and R.F. Lobo, 8/31/92, (PB93-227502, A07, MF-A02).
- NCEER-92-0023 "A Semi-Empirical Analysis of Strong-Motion Peaks in Terms of Seismic Source, Propagation Path and Local Site Conditions, by M. Kamiyama, M.J. O'Rourke and R. Flores-Berrones, 9/9/92, (PB93-150266, A08, MF-A02).
- NCEER-92-0024 "Seismic Behavior of Reinforced Concrete Frame Structures with Nonductile Details, Part I: Summary of Experimental Findings of Full Scale Beam-Column Joint Tests," by A. Beres, R.N. White and P. Gergely, 9/30/92, (PB93-227783, A05, MF-A01).
- NCEER-92-0025 "Experimental Results of Repaired and Retrofitted Beam-Column Joint Tests in Lightly Reinforced Concrete Frame Buildings," by A. Beres, S. El-Borgi, R.N. White and P. Gergely, 10/29/92, (PB93-227791, A05, MF-A01).
- NCEER-92-0026 "A Generalization of Optimal Control Theory: Linear and Nonlinear Structures," by J.N. Yang, Z. Li and S. Vongchavalitkul, 11/2/92, (PB93-188621, A05, MF-A01).
- NCEER-92-0027 "Seismic Resistance of Reinforced Concrete Frame Structures Designed Only for Gravity Loads: Part I - Design and Properties of a One-Third Scale Model Structure," by J.M. Bracci, A.M. Reinhorn and J.B. Mander, 12/1/92, (PB94-104502, A08, MF-A02).
- NCEER-92-0028 "Seismic Resistance of Reinforced Concrete Frame Structures Designed Only for Gravity Loads: Part II - Experimental Performance of Subassemblages," by L.E. Aycaardi, J.B. Mander and A.M. Reinhorn, 12/1/92, (PB94-104510, A08, MF-A02).
- NCEER-92-0029 "Seismic Resistance of Reinforced Concrete Frame Structures Designed Only for Gravity Loads: Part III - Experimental Performance and Analytical Study of a Structural Model," by J.M. Bracci, A.M. Reinhorn and J.B. Mander, 12/1/92, (PB93-227528, A09, MF-A01).

- NCEER-92-0030 "Evaluation of Seismic Retrofit of Reinforced Concrete Frame Structures: Part I - Experimental Performance of Retrofitted Subassemblages," by D. Choudhuri, J.B. Mander and A.M. Reinhorn, 12/8/92, (PB93-198307, A07, MF-A02).
- NCEER-92-0031 "Evaluation of Seismic Retrofit of Reinforced Concrete Frame Structures: Part II - Experimental Performance and Analytical Study of a Retrofitted Structural Model," by J.M. Bracci, A.M. Reinhorn and J.B. Mander, 12/8/92, (PB93-198315, A09, MF-A03).
- NCEER-92-0032 "Experimental and Analytical Investigation of Seismic Response of Structures with Supplemental Fluid Viscous Dampers," by M.C. Constantinou and M.D. Symans, 12/21/92, (PB93-191435, A10, MF-A03). This report is available only through NTIS (see address given above).
- NCEER-92-0033 "Reconnaissance Report on the Cairo, Egypt Earthquake of October 12, 1992," by M. Khater, 12/23/92, (PB93-188621, A03, MF-A01).
- NCEER-92-0034 "Low-Level Dynamic Characteristics of Four Tall Flat-Plate Buildings in New York City," by H. Gavin, S. Yuan, J. Grossman, E. Pekelis and K. Jacob, 12/28/92, (PB93-188217, A07, MF-A02).
- NCEER-93-0001 "An Experimental Study on the Seismic Performance of Brick-Infilled Steel Frames With and Without Retrofit," by J.B. Mander, B. Nair, K. Wojtkowski and J. Ma, 1/29/93, (PB93-227510, A07, MF-A02).
- NCEER-93-0002 "Social Accounting for Disaster Preparedness and Recovery Planning," by S. Cole, E. Pantoja and V. Razak, 2/22/93, (PB94-142114, A12, MF-A03).
- NCEER-93-0003 "Assessment of 1991 NEHRP Provisions for Nonstructural Components and Recommended Revisions," by T.T. Soong, G. Chen, Z. Wu, R-H. Zhang and M. Grigoriu, 3/1/93, (PB93-188639, A06, MF-A02).
- NCEER-93-0004 "Evaluation of Static and Response Spectrum Analysis Procedures of SEAOC/UBC for Seismic Isolated Structures," by C.W. Winters and M.C. Constantinou, 3/23/93, (PB93-198299, A10, MF-A03).
- NCEER-93-0005 "Earthquakes in the Northeast - Are We Ignoring the Hazard? A Workshop on Earthquake Science and Safety for Educators," edited by K.E.K. Ross, 4/2/93, (PB94-103066, A09, MF-A02).
- NCEER-93-0006 "Inelastic Response of Reinforced Concrete Structures with Viscoelastic Braces," by R.F. Lobo, J.M. Bracci, K.L. Shen, A.M. Reinhorn and T.T. Soong, 4/5/93, (PB93-227486, A05, MF-A02).
- NCEER-93-0007 "Seismic Testing of Installation Methods for Computers and Data Processing Equipment," by K. Kosar, T.T. Soong, K.L. Shen, J.A. HoLung and Y.K. Lin, 4/12/93, (PB93-198299, A07, MF-A02).
- NCEER-93-0008 "Retrofit of Reinforced Concrete Frames Using Added Dampers," by A. Reinhorn, M. Constantinou and C. Li, to be published.
- NCEER-93-0009 "Seismic Behavior and Design Guidelines for Steel Frame Structures with Added Viscoelastic Dampers," by K.C. Chang, M.L. Lai, T.T. Soong, D.S. Hao and Y.C. Yeh, 5/1/93, (PB94-141959, A07, MF-A02).
- NCEER-93-0010 "Seismic Performance of Shear-Critical Reinforced Concrete Bridge Piers," by J.B. Mander, S.M. Waheed, M.T.A. Chaudhary and S.S. Chen, 5/12/93, (PB93-227494, A08, MF-A02).
- NCEER-93-0011 "3D-BASIS-TABS: Computer Program for Nonlinear Dynamic Analysis of Three Dimensional Base Isolated Structures," by S. Nagarajaiah, C. Li, A.M. Reinhorn and M.C. Constantinou, 8/2/93, (PB94-141819, A09, MF-A02).
- NCEER-93-0012 "Effects of Hydrocarbon Spills from an Oil Pipeline Break on Ground Water," by O.J. Helweg and H.H.M. Hwang, 8/3/93, (PB94-141942, A06, MF-A02).
- NCEER-93-0013 "Simplified Procedures for Seismic Design of Nonstructural Components and Assessment of Current Code Provisions," by M.P. Singh, L.E. Suarez, E.E. Matheu and G.O. Maldonado, 8/4/93, (PB94-141827, A09, MF-A02).
- NCEER-93-0014 "An Energy Approach to Seismic Analysis and Design of Secondary Systems," by G. Chen and T.T. Soong, 8/6/93, (PB94-142767, A11, MF-A03).

- NCEER-93-0015 "Proceedings from School Sites: Becoming Prepared for Earthquakes - Commemorating the Third Anniversary of the Loma Prieta Earthquake," Edited by F.E. Winslow and K.E.K. Ross, 8/16/93, (PB94-154275, A16, MF-A02).
- NCEER-93-0016 "Reconnaissance Report of Damage to Historic Monuments in Cairo, Egypt Following the October 12, 1992 Dahshur Earthquake," by D. Sykora, D. Look, G. Croci, E. Karaesmen and E. Karaesmen, 8/19/93, (PB94-142221, A08, MF-A02).
- NCEER-93-0017 "The Island of Guam Earthquake of August 8, 1993," by S.W. Swan and S.K. Harris, 9/30/93, (PB94-141843, A04, MF-A01).
- NCEER-93-0018 "Engineering Aspects of the October 12, 1992 Egyptian Earthquake," by A.W. Elgamal, M. Amer, K. Adalier and A. Abul-Fadl, 10/7/93, (PB94-141983, A05, MF-A01).
- NCEER-93-0019 "Development of an Earthquake Motion Simulator and its Application in Dynamic Centrifuge Testing," by I. Krstelj, Supervised by J.H. Prevost, 10/23/93, (PB94-181773, A-10, MF-A03).
- NCEER-93-0020 "NCEER-Taisei Corporation Research Program on Sliding Seismic Isolation Systems for Bridges: Experimental and Analytical Study of a Friction Pendulum System (FPS)," by M.C. Constantinou, P. Tsopelas, Y-S. Kim and S. Okamoto, 11/1/93, (PB94-142775, A08, MF-A02).
- NCEER-93-0021 "Finite Element Modeling of Elastomeric Seismic Isolation Bearings," by L.J. Billings, Supervised by R. Shepherd, 11/8/93, to be published.
- NCEER-93-0022 "Seismic Vulnerability of Equipment in Critical Facilities: Life-Safety and Operational Consequences," by K. Porter, G.S. Johnson, M.M. Zadeh, C. Scawthorn and S. Eder, 11/24/93, (PB94-181765, A16, MF-A03).
- NCEER-93-0023 "Hokkaido Nansei-oki, Japan Earthquake of July 12, 1993, by P.I. Yanev and C.R. Scawthorn, 12/23/93, (PB94-181500, A07, MF-A01).
- NCEER-94-0001 "An Evaluation of Seismic Serviceability of Water Supply Networks with Application to the San Francisco Auxiliary Water Supply System," by I. Markov, Supervised by M. Grigoriu and T. O'Rourke, 1/21/94, (PB94-204013, A07, MF-A02).
- NCEER-94-0002 "NCEER-Taisei Corporation Research Program on Sliding Seismic Isolation Systems for Bridges: Experimental and Analytical Study of Systems Consisting of Sliding Bearings, Rubber Restoring Force Devices and Fluid Dampers," Volumes I and II, by P. Tsopelas, S. Okamoto, M.C. Constantinou, D. Ozaki and S. Fujii, 2/4/94, (PB94-181740, A09, MF-A02 and PB94-181757, A12, MF-A03).
- NCEER-94-0003 "A Markov Model for Local and Global Damage Indices in Seismic Analysis," by S. Rahman and M. Grigoriu, 2/18/94, (PB94-206000, A12, MF-A03).
- NCEER-94-0004 "Proceedings from the NCEER Workshop on Seismic Response of Masonry Infills," edited by D.P. Abrams, 3/1/94, (PB94-180783, A07, MF-A02).
- NCEER-94-0005 "The Northridge, California Earthquake of January 17, 1994: General Reconnaissance Report," edited by J.D. Goltz, 3/11/94, (PB94-193943, A10, MF-A03).
- NCEER-94-0006 "Seismic Energy Based Fatigue Damage Analysis of Bridge Columns: Part I - Evaluation of Seismic Capacity," by G.A. Chang and J.B. Mander, 3/14/94, (PB94-219185, A11, MF-A03).
- NCEER-94-0007 "Seismic Isolation of Multi-Story Frame Structures Using Spherical Sliding Isolation Systems," by T.M. Al-Hussaini, V.A. Zayas and M.C. Constantinou, 3/17/94, (PB94-193745, A09, MF-A02).
- NCEER-94-0008 "The Northridge, California Earthquake of January 17, 1994: Performance of Highway Bridges," edited by I.G. Buckle, 3/24/94, (PB94-193851, A06, MF-A02).
- NCEER-94-0009 "Proceedings of the Third U.S.-Japan Workshop on Earthquake Protective Systems for Bridges," edited by I.G. Buckle and I. Friedland, 3/31/94, (PB94-195815, A99, MF-A06).

- NCEER-94-0010 "3D-BASIS-ME: Computer Program for Nonlinear Dynamic Analysis of Seismically Isolated Single and Multiple Structures and Liquid Storage Tanks," by P.C. Tsopelas, M.C. Constantinou and A.M. Reinhorn, 4/12/94, (PB94-204922, A09, MF-A02).
- NCEER-94-0011 "The Northridge, California Earthquake of January 17, 1994: Performance of Gas Transmission Pipelines," by T.D. O'Rourke and M.C. Palmer, 5/16/94, (PB94-204989, A05, MF-A01).
- NCEER-94-0012 "Feasibility Study of Replacement Procedures and Earthquake Performance Related to Gas Transmission Pipelines," by T.D. O'Rourke and M.C. Palmer, 5/25/94, (PB94-206638, A09, MF-A02).
- NCEER-94-0013 "Seismic Energy Based Fatigue Damage Analysis of Bridge Columns: Part II - Evaluation of Seismic Demand," by G.A. Chang and J.B. Mander, 6/1/94, (PB95-18106, A08, MF-A02).
- NCEER-94-0014 "NCEER-Taisei Corporation Research Program on Sliding Seismic Isolation Systems for Bridges: Experimental and Analytical Study of a System Consisting of Sliding Bearings and Fluid Restoring Force/Damping Devices," by P. Tsopelas and M.C. Constantinou, 6/13/94, (PB94-219144, A10, MF-A03).
- NCEER-94-0015 "Generation of Hazard-Consistent Fragility Curves for Seismic Loss Estimation Studies," by H. Hwang and J-R. Huo, 6/14/94, (PB95-181996, A09, MF-A02).
- NCEER-94-0016 "Seismic Study of Building Frames with Added Energy-Absorbing Devices," by W.S. Pong, C.S. Tsai and G.C. Lee, 6/20/94, (PB94-219136, A10, A03).
- NCEER-94-0017 "Sliding Mode Control for Seismic-Excited Linear and Nonlinear Civil Engineering Structures," by J. Yang, J. Wu, A. Agrawal and Z. Li, 6/21/94, (PB95-138483, A06, MF-A02).
- NCEER-94-0018 "3D-BASIS-TABS Version 2.0: Computer Program for Nonlinear Dynamic Analysis of Three Dimensional Base Isolated Structures," by A.M. Reinhorn, S. Nagarajaiah, M.C. Constantinou, P. Tsopelas and R. Li, 6/22/94, (PB95-182176, A08, MF-A02).
- NCEER-94-0019 "Proceedings of the International Workshop on Civil Infrastructure Systems: Application of Intelligent Systems and Advanced Materials on Bridge Systems," Edited by G.C. Lee and K.C. Chang, 7/18/94, (PB95-252474, A20, MF-A04).
- NCEER-94-0020 "Study of Seismic Isolation Systems for Computer Floors," by V. Lambrou and M.C. Constantinou, 7/19/94, (PB95-138533, A10, MF-A03).
- NCEER-94-0021 "Proceedings of the U.S.-Italian Workshop on Guidelines for Seismic Evaluation and Rehabilitation of Unreinforced Masonry Buildings," Edited by D.P. Abrams and G.M. Calvi, 7/20/94, (PB95-138749, A13, MF-A03).
- NCEER-94-0022 "NCEER-Taisei Corporation Research Program on Sliding Seismic Isolation Systems for Bridges: Experimental and Analytical Study of a System Consisting of Lubricated PTFE Sliding Bearings and Mild Steel Dampers," by P. Tsopelas and M.C. Constantinou, 7/22/94, (PB95-182184, A08, MF-A02).
- NCEER-94-0023 "Development of Reliability-Based Design Criteria for Buildings Under Seismic Load," by Y.K. Wen, H. Hwang and M. Shinozuka, 8/1/94, (PB95-211934, A08, MF-A02).
- NCEER-94-0024 "Experimental Verification of Acceleration Feedback Control Strategies for an Active Tendon System," by S.J. Dyke, B.F. Spencer, Jr., P. Quast, M.K. Sain, D.C. Kaspari, Jr. and T.T. Soong, 8/29/94, (PB95-212320, A05, MF-A01).
- NCEER-94-0025 "Seismic Retrofitting Manual for Highway Bridges," Edited by I.G. Buckle and I.F. Friedland, published by the Federal Highway Administration (PB95-212676, A15, MF-A03).
- NCEER-94-0026 "Proceedings from the Fifth U.S.-Japan Workshop on Earthquake Resistant Design of Lifeline Facilities and Countermeasures Against Soil Liquefaction," Edited by T.D. O'Rourke and M. Hamada, 11/7/94, (PB95-220802, A99, MF-E08).

- NCEER-95-0001 “Experimental and Analytical Investigation of Seismic Retrofit of Structures with Supplemental Damping: Part 1 - Fluid Viscous Damping Devices,” by A.M. Reinhorn, C. Li and M.C. Constantinou, 1/3/95, (PB95-266599, A09, MF-A02).
- NCEER-95-0002 “Experimental and Analytical Study of Low-Cycle Fatigue Behavior of Semi-Rigid Top-And-Seat Angle Connections,” by G. Pekcan, J.B. Mander and S.S. Chen, 1/5/95, (PB95-220042, A07, MF-A02).
- NCEER-95-0003 “NCEER-ATC Joint Study on Fragility of Buildings,” by T. Anagnos, C. Rojahn and A.S. Kiremidjian, 1/20/95, (PB95-220026, A06, MF-A02).
- NCEER-95-0004 “Nonlinear Control Algorithms for Peak Response Reduction,” by Z. Wu, T.T. Soong, V. Gattulli and R.C. Lin, 2/16/95, (PB95-220349, A05, MF-A01).
- NCEER-95-0005 “Pipeline Replacement Feasibility Study: A Methodology for Minimizing Seismic and Corrosion Risks to Underground Natural Gas Pipelines,” by R.T. Eguchi, H.A. Seligson and D.G. Honegger, 3/2/95, (PB95-252326, A06, MF-A02).
- NCEER-95-0006 “Evaluation of Seismic Performance of an 11-Story Frame Building During the 1994 Northridge Earthquake,” by F. Naeim, R. DiSulio, K. Benuska, A. Reinhorn and C. Li, to be published.
- NCEER-95-0007 “Prioritization of Bridges for Seismic Retrofitting,” by N. Basöz and A.S. Kiremidjian, 4/24/95, (PB95-252300, A08, MF-A02).
- NCEER-95-0008 “Method for Developing Motion Damage Relationships for Reinforced Concrete Frames,” by A. Singhal and A.S. Kiremidjian, 5/11/95, (PB95-266607, A06, MF-A02).
- NCEER-95-0009 “Experimental and Analytical Investigation of Seismic Retrofit of Structures with Supplemental Damping: Part II - Friction Devices,” by C. Li and A.M. Reinhorn, 7/6/95, (PB96-128087, A11, MF-A03).
- NCEER-95-0010 “Experimental Performance and Analytical Study of a Non-Ductile Reinforced Concrete Frame Structure Retrofitted with Elastomeric Spring Dampers,” by G. Pekcan, J.B. Mander and S.S. Chen, 7/14/95, (PB96-137161, A08, MF-A02).
- NCEER-95-0011 “Development and Experimental Study of Semi-Active Fluid Damping Devices for Seismic Protection of Structures,” by M.D. Symans and M.C. Constantinou, 8/3/95, (PB96-136940, A23, MF-A04).
- NCEER-95-0012 “Real-Time Structural Parameter Modification (RSPM): Development of Innervated Structures,” by Z. Liang, M. Tong and G.C. Lee, 4/11/95, (PB96-137153, A06, MF-A01).
- NCEER-95-0013 “Experimental and Analytical Investigation of Seismic Retrofit of Structures with Supplemental Damping: Part III - Viscous Damping Walls,” by A.M. Reinhorn and C. Li, 10/1/95, (PB96-176409, A11, MF-A03).
- NCEER-95-0014 “Seismic Fragility Analysis of Equipment and Structures in a Memphis Electric Substation,” by J-R. Huo and H.H.M. Hwang, 8/10/95, (PB96-128087, A09, MF-A02).
- NCEER-95-0015 “The Hanshin-Awaji Earthquake of January 17, 1995: Performance of Lifelines,” Edited by M. Shinozuka, 11/3/95, (PB96-176383, A15, MF-A03).
- NCEER-95-0016 “Highway Culvert Performance During Earthquakes,” by T.L. Youd and C.J. Beckman, available as NCEER-96-0015.
- NCEER-95-0017 “The Hanshin-Awaji Earthquake of January 17, 1995: Performance of Highway Bridges,” Edited by I.G. Buckle, 12/1/95, to be published.
- NCEER-95-0018 “Modeling of Masonry Infill Panels for Structural Analysis,” by A.M. Reinhorn, A. Madan, R.E. Valles, Y. Reichmann and J.B. Mander, 12/8/95, (PB97-110886, MF-A01, A06).
- NCEER-95-0019 “Optimal Polynomial Control for Linear and Nonlinear Structures,” by A.K. Agrawal and J.N. Yang, 12/11/95, (PB96-168737, A07, MF-A02).

- NCEER-95-0020 "Retrofit of Non-Ductile Reinforced Concrete Frames Using Friction Dampers," by R.S. Rao, P. Gergely and R.N. White, 12/22/95, (PB97-133508, A10, MF-A02).
- NCEER-95-0021 "Parametric Results for Seismic Response of Pile-Supported Bridge Bents," by G. Mylonakis, A. Nikolaou and G. Gazetas, 12/22/95, (PB97-100242, A12, MF-A03).
- NCEER-95-0022 "Kinematic Bending Moments in Seismically Stressed Piles," by A. Nikolaou, G. Mylonakis and G. Gazetas, 12/23/95, (PB97-113914, MF-A03, A13).
- NCEER-96-0001 "Dynamic Response of Unreinforced Masonry Buildings with Flexible Diaphragms," by A.C. Costley and D.P. Abrams, 10/10/96, (PB97-133573, MF-A03, A15).
- NCEER-96-0002 "State of the Art Review: Foundations and Retaining Structures," by I. Po Lam, to be published.
- NCEER-96-0003 "Ductility of Rectangular Reinforced Concrete Bridge Columns with Moderate Confinement," by N. Wehbe, M. Saiidi, D. Sanders and B. Douglas, 11/7/96, (PB97-133557, A06, MF-A02).
- NCEER-96-0004 "Proceedings of the Long-Span Bridge Seismic Research Workshop," edited by I.G. Buckle and I.M. Friedland, to be published.
- NCEER-96-0005 "Establish Representative Pier Types for Comprehensive Study: Eastern United States," by J. Kulicki and Z. Prucz, 5/28/96, (PB98-119217, A07, MF-A02).
- NCEER-96-0006 "Establish Representative Pier Types for Comprehensive Study: Western United States," by R. Imbsen, R.A. Schamber and T.A. Osterkamp, 5/28/96, (PB98-118607, A07, MF-A02).
- NCEER-96-0007 "Nonlinear Control Techniques for Dynamical Systems with Uncertain Parameters," by R.G. Ghanem and M.I. Bujakov, 5/27/96, (PB97-100259, A17, MF-A03).
- NCEER-96-0008 "Seismic Evaluation of a 30-Year Old Non-Ductile Highway Bridge Pier and Its Retrofit," by J.B. Mander, B. Mahmoodzadegan, S. Bhadra and S.S. Chen, 5/31/96, (PB97-110902, MF-A03, A10).
- NCEER-96-0009 "Seismic Performance of a Model Reinforced Concrete Bridge Pier Before and After Retrofit," by J.B. Mander, J.H. Kim and C.A. Ligozio, 5/31/96, (PB97-110910, MF-A02, A10).
- NCEER-96-0010 "IDARC2D Version 4.0: A Computer Program for the Inelastic Damage Analysis of Buildings," by R.E. Valles, A.M. Reinhorn, S.K. Kunnath, C. Li and A. Madan, 6/3/96, (PB97-100234, A17, MF-A03).
- NCEER-96-0011 "Estimation of the Economic Impact of Multiple Lifeline Disruption: Memphis Light, Gas and Water Division Case Study," by S.E. Chang, H.A. Seligson and R.T. Eguchi, 8/16/96, (PB97-133490, A11, MF-A03).
- NCEER-96-0012 "Proceedings from the Sixth Japan-U.S. Workshop on Earthquake Resistant Design of Lifeline Facilities and Countermeasures Against Soil Liquefaction, Edited by M. Hamada and T. O'Rourke, 9/11/96, (PB97-133581, A99, MF-A06).
- NCEER-96-0013 "Chemical Hazards, Mitigation and Preparedness in Areas of High Seismic Risk: A Methodology for Estimating the Risk of Post-Earthquake Hazardous Materials Release," by H.A. Seligson, R.T. Eguchi, K.J. Tierney and K. Richmond, 11/7/96, (PB97-133565, MF-A02, A08).
- NCEER-96-0014 "Response of Steel Bridge Bearings to Reversed Cyclic Loading," by J.B. Mander, D-K. Kim, S.S. Chen and G.J. Premus, 11/13/96, (PB97-140735, A12, MF-A03).
- NCEER-96-0015 "Highway Culvert Performance During Past Earthquakes," by T.L. Youd and C.J. Beckman, 11/25/96, (PB97-133532, A06, MF-A01).
- NCEER-97-0001 "Evaluation, Prevention and Mitigation of Pounding Effects in Building Structures," by R.E. Valles and A.M. Reinhorn, 2/20/97, (PB97-159552, A14, MF-A03).
- NCEER-97-0002 "Seismic Design Criteria for Bridges and Other Highway Structures," by C. Rojahn, R. Mayes, D.G. Anderson, J. Clark, J.H. Hom, R.V. Nutt and M.J. O'Rourke, 4/30/97, (PB97-194658, A06, MF-A03).

- NCEER-97-0003 "Proceedings of the U.S.-Italian Workshop on Seismic Evaluation and Retrofit," Edited by D.P. Abrams and G.M. Calvi, 3/19/97, (PB97-194666, A13, MF-A03).
- NCEER-97-0004 "Investigation of Seismic Response of Buildings with Linear and Nonlinear Fluid Viscous Dampers," by A.A. Seleemah and M.C. Constantinou, 5/21/97, (PB98-109002, A15, MF-A03).
- NCEER-97-0005 "Proceedings of the Workshop on Earthquake Engineering Frontiers in Transportation Facilities," edited by G.C. Lee and I.M. Friedland, 8/29/97, (PB98-128911, A25, MR-A04).
- NCEER-97-0006 "Cumulative Seismic Damage of Reinforced Concrete Bridge Piers," by S.K. Kunnath, A. El-Bahy, A. Taylor and W. Stone, 9/2/97, (PB98-108814, A11, MF-A03).
- NCEER-97-0007 "Structural Details to Accommodate Seismic Movements of Highway Bridges and Retaining Walls," by R.A. Imbsen, R.A. Schamber, E. Thorkildsen, A. Kartoum, B.T. Martin, T.N. Rosser and J.M. Kulicki, 9/3/97, (PB98-108996, A09, MF-A02).
- NCEER-97-0008 "A Method for Earthquake Motion-Damage Relationships with Application to Reinforced Concrete Frames," by A. Singhal and A.S. Kiremidjian, 9/10/97, (PB98-108988, A13, MF-A03).
- NCEER-97-0009 "Seismic Analysis and Design of Bridge Abutments Considering Sliding and Rotation," by K. Fishman and R. Richards, Jr., 9/15/97, (PB98-108897, A06, MF-A02).
- NCEER-97-0010 "Proceedings of the FHWA/NCEER Workshop on the National Representation of Seismic Ground Motion for New and Existing Highway Facilities," edited by I.M. Friedland, M.S. Power and R.L. Mayes, 9/22/97, (PB98-128903, A21, MF-A04).
- NCEER-97-0011 "Seismic Analysis for Design or Retrofit of Gravity Bridge Abutments," by K.L. Fishman, R. Richards, Jr. and R.C. Divito, 10/2/97, (PB98-128937, A08, MF-A02).
- NCEER-97-0012 "Evaluation of Simplified Methods of Analysis for Yielding Structures," by P. Tsopelas, M.C. Constantinou, C.A. Kircher and A.S. Whittaker, 10/31/97, (PB98-128929, A10, MF-A03).
- NCEER-97-0013 "Seismic Design of Bridge Columns Based on Control and Repairability of Damage," by C-T. Cheng and J.B. Mander, 12/8/97, (PB98-144249, A11, MF-A03).
- NCEER-97-0014 "Seismic Resistance of Bridge Piers Based on Damage Avoidance Design," by J.B. Mander and C-T. Cheng, 12/10/97, (PB98-144223, A09, MF-A02).
- NCEER-97-0015 "Seismic Response of Nominally Symmetric Systems with Strength Uncertainty," by S. Balopoulou and M. Grigoriu, 12/23/97, (PB98-153422, A11, MF-A03).
- NCEER-97-0016 "Evaluation of Seismic Retrofit Methods for Reinforced Concrete Bridge Columns," by T.J. Wipf, F.W. Klaiber and F.M. Russo, 12/28/97, (PB98-144215, A12, MF-A03).
- NCEER-97-0017 "Seismic Fragility of Existing Conventional Reinforced Concrete Highway Bridges," by C.L. Mullen and A.S. Cakmak, 12/30/97, (PB98-153406, A08, MF-A02).
- NCEER-97-0018 "Loss Assessment of Memphis Buildings," edited by D.P. Abrams and M. Shinozuka, 12/31/97, (PB98-144231, A13, MF-A03).
- NCEER-97-0019 "Seismic Evaluation of Frames with Infill Walls Using Quasi-static Experiments," by K.M. Mosalam, R.N. White and P. Gergely, 12/31/97, (PB98-153455, A07, MF-A02).
- NCEER-97-0020 "Seismic Evaluation of Frames with Infill Walls Using Pseudo-dynamic Experiments," by K.M. Mosalam, R.N. White and P. Gergely, 12/31/97, (PB98-153430, A07, MF-A02).
- NCEER-97-0021 "Computational Strategies for Frames with Infill Walls: Discrete and Smeared Crack Analyses and Seismic Fragility," by K.M. Mosalam, R.N. White and P. Gergely, 12/31/97, (PB98-153414, A10, MF-A02).

- NCEER-97-0022 "Proceedings of the NCEER Workshop on Evaluation of Liquefaction Resistance of Soils," edited by T.L. Youd and I.M. Idriss, 12/31/97, (PB98-155617, A15, MF-A03).
- MCEER-98-0001 "Extraction of Nonlinear Hysteretic Properties of Seismically Isolated Bridges from Quick-Release Field Tests," by Q. Chen, B.M. Douglas, E.M. Maragakis and I.G. Buckle, 5/26/98, (PB99-118838, A06, MF-A01).
- MCEER-98-0002 "Methodologies for Evaluating the Importance of Highway Bridges," by A. Thomas, S. Eshenaur and J. Kulicki, 5/29/98, (PB99-118846, A10, MF-A02).
- MCEER-98-0003 "Capacity Design of Bridge Piers and the Analysis of Overstrength," by J.B. Mander, A. Dutta and P. Goel, 6/1/98, (PB99-118853, A09, MF-A02).
- MCEER-98-0004 "Evaluation of Bridge Damage Data from the Loma Prieta and Northridge, California Earthquakes," by N. Basoz and A. Kiremidjian, 6/2/98, (PB99-118861, A15, MF-A03).
- MCEER-98-0005 "Screening Guide for Rapid Assessment of Liquefaction Hazard at Highway Bridge Sites," by T. L. Youd, 6/16/98, (PB99-118879, A06, not available on microfiche).
- MCEER-98-0006 "Structural Steel and Steel/Concrete Interface Details for Bridges," by P. Ritchie, N. Kauh and J. Kulicki, 7/13/98, (PB99-118945, A06, MF-A01).
- MCEER-98-0007 "Capacity Design and Fatigue Analysis of Confined Concrete Columns," by A. Dutta and J.B. Mander, 7/14/98, (PB99-118960, A14, MF-A03).
- MCEER-98-0008 "Proceedings of the Workshop on Performance Criteria for Telecommunication Services Under Earthquake Conditions," edited by A.J. Schiff, 7/15/98, (PB99-118952, A08, MF-A02).
- MCEER-98-0009 "Fatigue Analysis of Unconfined Concrete Columns," by J.B. Mander, A. Dutta and J.H. Kim, 9/12/98, (PB99-123655, A10, MF-A02).
- MCEER-98-0010 "Centrifuge Modeling of Cyclic Lateral Response of Pile-Cap Systems and Seat-Type Abutments in Dry Sands," by A.D. Gadre and R. Dobry, 10/2/98, (PB99-123606, A13, MF-A03).
- MCEER-98-0011 "IDARC-BRIDGE: A Computational Platform for Seismic Damage Assessment of Bridge Structures," by A.M. Reinhorn, V. Simeonov, G. Mylonakis and Y. Reichman, 10/2/98, (PB99-162919, A15, MF-A03).
- MCEER-98-0012 "Experimental Investigation of the Dynamic Response of Two Bridges Before and After Retrofitting with Elastomeric Bearings," by D.A. Wendichansky, S.S. Chen and J.B. Mander, 10/2/98, (PB99-162927, A15, MF-A03).
- MCEER-98-0013 "Design Procedures for Hinge Restrainers and Hinge Sear Width for Multiple-Frame Bridges," by R. Des Roches and G.L. Fenves, 11/3/98, (PB99-140477, A13, MF-A03).
- MCEER-98-0014 "Response Modification Factors for Seismically Isolated Bridges," by M.C. Constantinou and J.K. Quarshie, 11/3/98, (PB99-140485, A14, MF-A03).
- MCEER-98-0015 "Proceedings of the U.S.-Italy Workshop on Seismic Protective Systems for Bridges," edited by I.M. Friedland and M.C. Constantinou, 11/3/98, (PB2000-101711, A22, MF-A04).
- MCEER-98-0016 "Appropriate Seismic Reliability for Critical Equipment Systems: Recommendations Based on Regional Analysis of Financial and Life Loss," by K. Porter, C. Scawthorn, C. Taylor and N. Blais, 11/10/98, (PB99-157265, A08, MF-A02).
- MCEER-98-0017 "Proceedings of the U.S. Japan Joint Seminar on Civil Infrastructure Systems Research," edited by M. Shinozuka and A. Rose, 11/12/98, (PB99-156713, A16, MF-A03).
- MCEER-98-0018 "Modeling of Pile Footings and Drilled Shafts for Seismic Design," by I. PoLam, M. Kapuskar and D. Chaudhuri, 12/21/98, (PB99-157257, A09, MF-A02).

- MCEER-99-0001 "Seismic Evaluation of a Masonry Infilled Reinforced Concrete Frame by Pseudodynamic Testing," by S.G. Buonopane and R.N. White, 2/16/99, (PB99-162851, A09, MF-A02).
- MCEER-99-0002 "Response History Analysis of Structures with Seismic Isolation and Energy Dissipation Systems: Verification Examples for Program SAP2000," by J. Scheller and M.C. Constantinou, 2/22/99, (PB99-162869, A08, MF-A02).
- MCEER-99-0003 "Experimental Study on the Seismic Design and Retrofit of Bridge Columns Including Axial Load Effects," by A. Dutta, T. Kokorina and J.B. Mander, 2/22/99, (PB99-162877, A09, MF-A02).
- MCEER-99-0004 "Experimental Study of Bridge Elastomeric and Other Isolation and Energy Dissipation Systems with Emphasis on Uplift Prevention and High Velocity Near-source Seismic Excitation," by A. Kasalanati and M. C. Constantinou, 2/26/99, (PB99-162885, A12, MF-A03).
- MCEER-99-0005 "Truss Modeling of Reinforced Concrete Shear-flexure Behavior," by J.H. Kim and J.B. Mander, 3/8/99, (PB99-163693, A12, MF-A03).
- MCEER-99-0006 "Experimental Investigation and Computational Modeling of Seismic Response of a 1:4 Scale Model Steel Structure with a Load Balancing Supplemental Damping System," by G. Pekcan, J.B. Mander and S.S. Chen, 4/2/99, (PB99-162893, A11, MF-A03).
- MCEER-99-0007 "Effect of Vertical Ground Motions on the Structural Response of Highway Bridges," by M.R. Button, C.J. Cronin and R.L. Mayes, 4/10/99, (PB2000-101411, A10, MF-A03).
- MCEER-99-0008 "Seismic Reliability Assessment of Critical Facilities: A Handbook, Supporting Documentation, and Model Code Provisions," by G.S. Johnson, R.E. Sheppard, M.D. Quilici, S.J. Eder and C.R. Scawthorn, 4/12/99, (PB2000-101701, A18, MF-A04).
- MCEER-99-0009 "Impact Assessment of Selected MCEER Highway Project Research on the Seismic Design of Highway Structures," by C. Rojahn, R. Mayes, D.G. Anderson, J.H. Clark, D'Appolonia Engineering, S. Gloyd and R.V. Nutt, 4/14/99, (PB99-162901, A10, MF-A02).
- MCEER-99-0010 "Site Factors and Site Categories in Seismic Codes," by R. Dobry, R. Ramos and M.S. Power, 7/19/99, (PB2000-101705, A08, MF-A02).
- MCEER-99-0011 "Restrainer Design Procedures for Multi-Span Simply-Supported Bridges," by M.J. Randall, M. Saiidi, E. Maragakis and T. Isakovic, 7/20/99, (PB2000-101702, A10, MF-A02).
- MCEER-99-0012 "Property Modification Factors for Seismic Isolation Bearings," by M.C. Constantinou, P. Tsopelas, A. Kasalanati and E. Wolff, 7/20/99, (PB2000-103387, A11, MF-A03).
- MCEER-99-0013 "Critical Seismic Issues for Existing Steel Bridges," by P. Ritchie, N. Kauh and J. Kulicki, 7/20/99, (PB2000-101697, A09, MF-A02).
- MCEER-99-0014 "Nonstructural Damage Database," by A. Kao, T.T. Soong and A. Vender, 7/24/99, (PB2000-101407, A06, MF-A01).
- MCEER-99-0015 "Guide to Remedial Measures for Liquefaction Mitigation at Existing Highway Bridge Sites," by H.G. Cooke and J. K. Mitchell, 7/26/99, (PB2000-101703, A11, MF-A03).
- MCEER-99-0016 "Proceedings of the MCEER Workshop on Ground Motion Methodologies for the Eastern United States," edited by N. Abrahamson and A. Becker, 8/11/99, (PB2000-103385, A07, MF-A02).
- MCEER-99-0017 "Quindío, Colombia Earthquake of January 25, 1999: Reconnaissance Report," by A.P. Asfura and P.J. Flores, 10/4/99, (PB2000-106893, A06, MF-A01).
- MCEER-99-0018 "Hysteretic Models for Cyclic Behavior of Deteriorating Inelastic Structures," by M.V. Sivaselvan and A.M. Reinhorn, 11/5/99, (PB2000-103386, A08, MF-A02).

- MCEER-99-0019 "Proceedings of the 7th U.S.- Japan Workshop on Earthquake Resistant Design of Lifeline Facilities and Countermeasures Against Soil Liquefaction," edited by T.D. O'Rourke, J.P. Bardet and M. Hamada, 11/19/99, (PB2000-103354, A99, MF-A06).
- MCEER-99-0020 "Development of Measurement Capability for Micro-Vibration Evaluations with Application to Chip Fabrication Facilities," by G.C. Lee, Z. Liang, J.W. Song, J.D. Shen and W.C. Liu, 12/1/99, (PB2000-105993, A08, MF-A02).
- MCEER-99-0021 "Design and Retrofit Methodology for Building Structures with Supplemental Energy Dissipating Systems," by G. Pekcan, J.B. Mander and S.S. Chen, 12/31/99, (PB2000-105994, A11, MF-A03).
- MCEER-00-0001 "The Marmara, Turkey Earthquake of August 17, 1999: Reconnaissance Report," edited by C. Scawthorn; with major contributions by M. Bruneau, R. Eguchi, T. Holzer, G. Johnson, J. Mander, J. Mitchell, W. Mitchell, A. Papageorgiou, C. Scaethorn, and G. Webb, 3/23/00, (PB2000-106200, A11, MF-A03).
- MCEER-00-0002 "Proceedings of the MCEER Workshop for Seismic Hazard Mitigation of Health Care Facilities," edited by G.C. Lee, M. Ettouney, M. Grigoriu, J. Hauer and J. Nigg, 3/29/00, (PB2000-106892, A08, MF-A02).
- MCEER-00-0003 "The Chi-Chi, Taiwan Earthquake of September 21, 1999: Reconnaissance Report," edited by G.C. Lee and C.H. Loh, with major contributions by G.C. Lee, M. Bruneau, I.G. Buckle, S.E. Chang, P.J. Flores, T.D. O'Rourke, M. Shinozuka, T.T. Soong, C-H. Loh, K-C. Chang, Z-J. Chen, J-S. Hwang, M-L. Lin, G-Y. Liu, K-C. Tsai, G.C. Yao and C-L. Yen, 4/30/00, (PB2001-100980, A10, MF-A02).
- MCEER-00-0004 "Seismic Retrofit of End-Sway Frames of Steel Deck-Truss Bridges with a Supplemental Tendon System: Experimental and Analytical Investigation," by G. Pekcan, J.B. Mander and S.S. Chen, 7/1/00, (PB2001-100982, A10, MF-A02).
- MCEER-00-0005 "Sliding Fragility of Unrestrained Equipment in Critical Facilities," by W.H. Chong and T.T. Soong, 7/5/00, (PB2001-100983, A08, MF-A02).
- MCEER-00-0006 "Seismic Response of Reinforced Concrete Bridge Pier Walls in the Weak Direction," by N. Abo-Shadi, M. Saiidi and D. Sanders, 7/17/00, (PB2001-100981, A17, MF-A03).
- MCEER-00-0007 "Low-Cycle Fatigue Behavior of Longitudinal Reinforcement in Reinforced Concrete Bridge Columns," by J. Brown and S.K. Kunnath, 7/23/00, (PB2001-104392, A08, MF-A02).
- MCEER-00-0008 "Soil Structure Interaction of Bridges for Seismic Analysis," I. PoLam and H. Law, 9/25/00, (PB2001-105397, A08, MF-A02).
- MCEER-00-0009 "Proceedings of the First MCEER Workshop on Mitigation of Earthquake Disaster by Advanced Technologies (MEDAT-1), edited by M. Shinozuka, D.J. Inman and T.D. O'Rourke, 11/10/00, (PB2001-105399, A14, MF-A03).
- MCEER-00-0010 "Development and Evaluation of Simplified Procedures for Analysis and Design of Buildings with Passive Energy Dissipation Systems, Revision 01," by O.M. Ramirez, M.C. Constantinou, C.A. Kircher, A.S. Whittaker, M.W. Johnson, J.D. Gomez and C. Chrysostomou, 11/16/01, (PB2001-105523, A23, MF-A04).
- MCEER-00-0011 "Dynamic Soil-Foundation-Structure Interaction Analyses of Large Caissons," by C-Y. Chang, C-M. Mok, Z-L. Wang, R. Settgast, F. Waggoner, M.A. Ketchum, H.M. Gonnermann and C-C. Chin, 12/30/00, (PB2001-104373, A07, MF-A02).
- MCEER-00-0012 "Experimental Evaluation of Seismic Performance of Bridge Restrainers," by A.G. Vlassis, E.M. Maragakis and M. Saiid Saiidi, 12/30/00, (PB2001-104354, A09, MF-A02).
- MCEER-00-0013 "Effect of Spatial Variation of Ground Motion on Highway Structures," by M. Shinozuka, V. Saxena and G. Deodatis, 12/31/00, (PB2001-108755, A13, MF-A03).
- MCEER-00-0014 "A Risk-Based Methodology for Assessing the Seismic Performance of Highway Systems," by S.D. Werner, C.E. Taylor, J.E. Moore, II, J.S. Walton and S. Cho, 12/31/00, (PB2001-108756, A14, MF-A03).

- MCEER-01-0001 “Experimental Investigation of P-Delta Effects to Collapse During Earthquakes,” by D. Vian and M. Bruneau, 6/25/01, (PB2002-100534, A17, MF-A03).
- MCEER-01-0002 “Proceedings of the Second MCEER Workshop on Mitigation of Earthquake Disaster by Advanced Technologies (MEDAT-2),” edited by M. Bruneau and D.J. Inman, 7/23/01, (PB2002-100434, A16, MF-A03).
- MCEER-01-0003 “Sensitivity Analysis of Dynamic Systems Subjected to Seismic Loads,” by C. Roth and M. Grigoriu, 9/18/01, (PB2003-100884, A12, MF-A03).
- MCEER-01-0004 “Overcoming Obstacles to Implementing Earthquake Hazard Mitigation Policies: Stage 1 Report,” by D.J. Alesch and W.J. Petak, 12/17/01, (PB2002-107949, A07, MF-A02).
- MCEER-01-0005 “Updating Real-Time Earthquake Loss Estimates: Methods, Problems and Insights,” by C.E. Taylor, S.E. Chang and R.T. Eguchi, 12/17/01, (PB2002-107948, A05, MF-A01).
- MCEER-01-0006 “Experimental Investigation and Retrofit of Steel Pile Foundations and Pile Bents Under Cyclic Lateral Loadings,” by A. Shama, J. Mander, B. Blabac and S. Chen, 12/31/01, (PB2002-107950, A13, MF-A03).
- MCEER-02-0001 “Assessment of Performance of Bolu Viaduct in the 1999 Duzce Earthquake in Turkey” by P.C. Roussis, M.C. Constantinou, M. Erdik, E. Durukal and M. Dicleli, 5/8/02, (PB2003-100883, A08, MF-A02).
- MCEER-02-0002 “Seismic Behavior of Rail Counterweight Systems of Elevators in Buildings,” by M.P. Singh, Rildova and L.E. Suarez, 5/27/02. (PB2003-100882, A11, MF-A03).
- MCEER-02-0003 “Development of Analysis and Design Procedures for Spread Footings,” by G. Mylonakis, G. Gazetas, S. Nikolaou and A. Chauncey, 10/02/02, (PB2004-101636, A13, MF-A03, CD-A13).
- MCEER-02-0004 “Bare-Earth Algorithms for Use with SAR and LIDAR Digital Elevation Models,” by C.K. Huyck, R.T. Eguchi and B. Houshmand, 10/16/02, (PB2004-101637, A07, CD-A07).
- MCEER-02-0005 “Review of Energy Dissipation of Compression Members in Concentrically Braced Frames,” by K.Lee and M. Bruneau, 10/18/02, (PB2004-101638, A10, CD-A10).
- MCEER-03-0001 “Experimental Investigation of Light-Gauge Steel Plate Shear Walls for the Seismic Retrofit of Buildings” by J. Berman and M. Bruneau, 5/2/03, (PB2004-101622, A10, MF-A03, CD-A10).
- MCEER-03-0002 “Statistical Analysis of Fragility Curves,” by M. Shinozuka, M.Q. Feng, H. Kim, T. Uzawa and T. Ueda, 6/16/03, (PB2004-101849, A09, CD-A09).
- MCEER-03-0003 “Proceedings of the Eighth U.S.-Japan Workshop on Earthquake Resistant Design of Lifeline Facilities and Countermeasures Against Liquefaction,” edited by M. Hamada, J.P. Bardet and T.D. O’Rourke, 6/30/03, (PB2004-104386, A99, CD-A99).
- MCEER-03-0004 “Proceedings of the PRC-US Workshop on Seismic Analysis and Design of Special Bridges,” edited by L.C. Fan and G.C. Lee, 7/15/03, (PB2004-104387, A14, CD-A14).
- MCEER-03-0005 “Urban Disaster Recovery: A Framework and Simulation Model,” by S.B. Miles and S.E. Chang, 7/25/03, (PB2004-104388, A07, CD-A07).
- MCEER-03-0006 “Behavior of Underground Piping Joints Due to Static and Dynamic Loading,” by R.D. Meis, M. Maragakis and R. Siddharthan, 11/17/03, (PB2005-102194, A13, MF-A03, CD-A00).
- MCEER-04-0001 “Experimental Study of Seismic Isolation Systems with Emphasis on Secondary System Response and Verification of Accuracy of Dynamic Response History Analysis Methods,” by E. Wolff and M. Constantinou, 1/16/04 (PB2005-102195, A99, MF-E08, CD-A00).
- MCEER-04-0002 “Tension, Compression and Cyclic Testing of Engineered Cementitious Composite Materials,” by K. Kesner and S.L. Billington, 3/1/04, (PB2005-102196, A08, CD-A08).

- MCEER-04-0003 “Cyclic Testing of Braces Laterally Restrained by Steel Studs to Enhance Performance During Earthquakes,” by O.C. Celik, J.W. Berman and M. Bruneau, 3/16/04, (PB2005-102197, A13, MF-A03, CD-A00).
- MCEER-04-0004 “Methodologies for Post Earthquake Building Damage Detection Using SAR and Optical Remote Sensing: Application to the August 17, 1999 Marmara, Turkey Earthquake,” by C.K. Huyck, B.J. Adams, S. Cho, R.T. Eguchi, B. Mansouri and B. Houshmand, 6/15/04, (PB2005-104888, A10, CD-A00).
- MCEER-04-0005 “Nonlinear Structural Analysis Towards Collapse Simulation: A Dynamical Systems Approach,” by M.V. Sivaselvan and A.M. Reinhorn, 6/16/04, (PB2005-104889, A11, MF-A03, CD-A00).
- MCEER-04-0006 “Proceedings of the Second PRC-US Workshop on Seismic Analysis and Design of Special Bridges,” edited by G.C. Lee and L.C. Fan, 6/25/04, (PB2005-104890, A16, CD-A00).
- MCEER-04-0007 “Seismic Vulnerability Evaluation of Axially Loaded Steel Built-up Laced Members,” by K. Lee and M. Bruneau, 6/30/04, (PB2005-104891, A16, CD-A00).
- MCEER-04-0008 “Evaluation of Accuracy of Simplified Methods of Analysis and Design of Buildings with Damping Systems for Near-Fault and for Soft-Soil Seismic Motions,” by E.A. Pavlou and M.C. Constantinou, 8/16/04, (PB2005-104892, A08, MF-A02, CD-A00).
- MCEER-04-0009 “Assessment of Geotechnical Issues in Acute Care Facilities in California,” by M. Lew, T.D. O’Rourke, R. Dobry and M. Koch, 9/15/04, (PB2005-104893, A08, CD-A00).
- MCEER-04-0010 “Scissor-Jack-Damper Energy Dissipation System,” by A.N. Sigaher-Boyle and M.C. Constantinou, 12/1/04 (PB2005-108221).
- MCEER-04-0011 “Seismic Retrofit of Bridge Steel Truss Piers Using a Controlled Rocking Approach,” by M. Pollino and M. Bruneau, 12/20/04 (PB2006-105795).
- MCEER-05-0001 “Experimental and Analytical Studies of Structures Seismically Isolated with an Uplift-Restraint Isolation System,” by P.C. Roussis and M.C. Constantinou, 1/10/05 (PB2005-108222).
- MCEER-05-0002 “A Versatile Experimentation Model for Study of Structures Near Collapse Applied to Seismic Evaluation of Irregular Structures,” by D. Kusumastuti, A.M. Reinhorn and A. Rutenberg, 3/31/05 (PB2006-101523).
- MCEER-05-0003 “Proceedings of the Third PRC-US Workshop on Seismic Analysis and Design of Special Bridges,” edited by L.C. Fan and G.C. Lee, 4/20/05, (PB2006-105796).
- MCEER-05-0004 “Approaches for the Seismic Retrofit of Braced Steel Bridge Piers and Proof-of-Concept Testing of an Eccentrically Braced Frame with Tubular Link,” by J.W. Berman and M. Bruneau, 4/21/05 (PB2006-101524).
- MCEER-05-0005 “Simulation of Strong Ground Motions for Seismic Fragility Evaluation of Nonstructural Components in Hospitals,” by A. Wanitkorkul and A. Filiatrault, 5/26/05 (PB2006-500027).
- MCEER-05-0006 “Seismic Safety in California Hospitals: Assessing an Attempt to Accelerate the Replacement or Seismic Retrofit of Older Hospital Facilities,” by D.J. Alesch, L.A. Arendt and W.J. Petak, 6/6/05 (PB2006-105794).
- MCEER-05-0007 “Development of Seismic Strengthening and Retrofit Strategies for Critical Facilities Using Engineered Cementitious Composite Materials,” by K. Kesner and S.L. Billington, 8/29/05 (PB2006-111701).
- MCEER-05-0008 “Experimental and Analytical Studies of Base Isolation Systems for Seismic Protection of Power Transformers,” by N. Murota, M.Q. Feng and G-Y. Liu, 9/30/05 (PB2006-111702).
- MCEER-05-0009 “3D-BASIS-ME-MB: Computer Program for Nonlinear Dynamic Analysis of Seismically Isolated Structures,” by P.C. Tsopelas, P.C. Roussis, M.C. Constantinou, R. Buchanan and A.M. Reinhorn, 10/3/05 (PB2006-111703).
- MCEER-05-0010 “Steel Plate Shear Walls for Seismic Design and Retrofit of Building Structures,” by D. Vian and M. Bruneau, 12/15/05 (PB2006-111704).


- MCEER-05-0011 "The Performance-Based Design Paradigm," by M.J. Astrella and A. Whittaker, 12/15/05 (PB2006-111705).
- MCEER-06-0001 "Seismic Fragility of Suspended Ceiling Systems," H. Badillo-Almaraz, A.S. Whittaker, A.M. Reinhorn and G.P. Cimellaro, 2/4/06 (PB2006-111706).
- MCEER-06-0002 "Multi-Dimensional Fragility of Structures," by G.P. Cimellaro, A.M. Reinhorn and M. Bruneau, 3/1/06 (PB2007-106974, A09, MF-A02, CD A00).
- MCEER-06-0003 "Built-Up Shear Links as Energy Dissipators for Seismic Protection of Bridges," by P. Dusicka, A.M. Itani and I.G. Buckle, 3/15/06 (PB2006-111708).
- MCEER-06-0004 "Analytical Investigation of the Structural Fuse Concept," by R.E. Vargas and M. Bruneau, 3/16/06 (PB2006-111709).
- MCEER-06-0005 "Experimental Investigation of the Structural Fuse Concept," by R.E. Vargas and M. Bruneau, 3/17/06 (PB2006-111710).
- MCEER-06-0006 "Further Development of Tubular Eccentrically Braced Frame Links for the Seismic Retrofit of Braced Steel Truss Bridge Piers," by J.W. Berman and M. Bruneau, 3/27/06 (PB2007-105147).
- MCEER-06-0007 "REDARS Validation Report," by S. Cho, C.K. Huyck, S. Ghosh and R.T. Eguchi, 8/8/06 (PB2007-106983).
- MCEER-06-0008 "Review of Current NDE Technologies for Post-Earthquake Assessment of Retrofitted Bridge Columns," by J.W. Song, Z. Liang and G.C. Lee, 8/21/06 (PB2007-106984).
- MCEER-06-0009 "Liquefaction Remediation in Silty Soils Using Dynamic Compaction and Stone Columns," by S. Thevanayagam, G.R. Martin, R. Nashed, T. Shenthan, T. Kanagalingam and N. Ecemis, 8/28/06 (PB2007-106985).
- MCEER-06-0010 "Conceptual Design and Experimental Investigation of Polymer Matrix Composite Infill Panels for Seismic Retrofitting," by W. Jung, M. Chiewanichakorn and A.J. Aref, 9/21/06 (PB2007-106986).
- MCEER-06-0011 "A Study of the Coupled Horizontal-Vertical Behavior of Elastomeric and Lead-Rubber Seismic Isolation Bearings," by G.P. Warn and A.S. Whittaker, 9/22/06 (PB2007-108679).
- MCEER-06-0012 "Proceedings of the Fourth PRC-US Workshop on Seismic Analysis and Design of Special Bridges: Advancing Bridge Technologies in Research, Design, Construction and Preservation," Edited by L.C. Fan, G.C. Lee and L. Ziang, 10/12/06 (PB2007-109042).
- MCEER-06-0013 "Cyclic Response and Low Cycle Fatigue Characteristics of Plate Steels," by P. Dusicka, A.M. Itani and I.G. Buckle, 11/1/06 06 (PB2007-106987).
- MCEER-06-0014 "Proceedings of the Second US-Taiwan Bridge Engineering Workshop," edited by W.P. Yen, J. Shen, J-Y. Chen and M. Wang, 11/15/06 (PB2008-500041).
- MCEER-06-0015 "User Manual and Technical Documentation for the REDARSTM Import Wizard," by S. Cho, S. Ghosh, C.K. Huyck and S.D. Werner, 11/30/06 (PB2007-114766).
- MCEER-06-0016 "Hazard Mitigation Strategy and Monitoring Technologies for Urban and Infrastructure Public Buildings: Proceedings of the China-US Workshops," edited by X.Y. Zhou, A.L. Zhang, G.C. Lee and M. Tong, 12/12/06 (PB2008-500018).
- MCEER-07-0001 "Static and Kinetic Coefficients of Friction for Rigid Blocks," by C. Kafali, S. Fathali, M. Grigoriu and A.S. Whittaker, 3/20/07 (PB2007-114767).
- MCEER-07-0002 "Hazard Mitigation Investment Decision Making: Organizational Response to Legislative Mandate," by L.A. Arendt, D.J. Alesch and W.J. Petak, 4/9/07 (PB2007-114768).
- MCEER-07-0003 "Seismic Behavior of Bidirectional-Resistant Ductile End Diaphragms with Unbonded Braces in Straight or Skewed Steel Bridges," by O. Celik and M. Bruneau, 4/11/07 (PB2008-105141).

- MCEER-07-0004 “Modeling Pile Behavior in Large Pile Groups Under Lateral Loading,” by A.M. Dodds and G.R. Martin, 4/16/07(PB2008-105142).
- MCEER-07-0005 “Experimental Investigation of Blast Performance of Seismically Resistant Concrete-Filled Steel Tube Bridge Piers,” by S. Fujikura, M. Bruneau and D. Lopez-Garcia, 4/20/07 (PB2008-105143).
- MCEER-07-0006 “Seismic Analysis of Conventional and Isolated Liquefied Natural Gas Tanks Using Mechanical Analogs,” by I.P. Christovasilis and A.S. Whittaker, 5/1/07.
- MCEER-07-0007 “Experimental Seismic Performance Evaluation of Isolation/Restraint Systems for Mechanical Equipment – Part 1: Heavy Equipment Study,” by S. Fathali and A. Filiatrault, 6/6/07 (PB2008-105144).
- MCEER-07-0008 “Seismic Vulnerability of Timber Bridges and Timber Substructures,” by A.A. Sharma, J.B. Mander, I.M. Friedland and D.R. Allicock, 6/7/07 (PB2008-105145).
- MCEER-07-0009 “Experimental and Analytical Study of the XY-Friction Pendulum (XY-FP) Bearing for Bridge Applications,” by C.C. Marin-Artieda, A.S. Whittaker and M.C. Constantinou, 6/7/07 (PB2008-105191).
- MCEER-07-0010 “Proceedings of the PRC-US Earthquake Engineering Forum for Young Researchers,” Edited by G.C. Lee and X.Z. Qi, 6/8/07 (PB2008-500058).
- MCEER-07-0011 “Design Recommendations for Perforated Steel Plate Shear Walls,” by R. Purba and M. Bruneau, 6/18/07, (PB2008-105192).
- MCEER-07-0012 “Performance of Seismic Isolation Hardware Under Service and Seismic Loading,” by M.C. Constantinou, A.S. Whittaker, Y. Kalpakidis, D.M. Fenz and G.P. Warn, 8/27/07, (PB2008-105193).
- MCEER-07-0013 “Experimental Evaluation of the Seismic Performance of Hospital Piping Subassemblies,” by E.R. Goodwin, E. Maragakis and A.M. Itani, 9/4/07, (PB2008-105194).
- MCEER-07-0014 “A Simulation Model of Urban Disaster Recovery and Resilience: Implementation for the 1994 Northridge Earthquake,” by S. Miles and S.E. Chang, 9/7/07, (PB2008-106426).
- MCEER-07-0015 “Statistical and Mechanistic Fragility Analysis of Concrete Bridges,” by M. Shinozuka, S. Banerjee and S-H. Kim, 9/10/07, (PB2008-106427).
- MCEER-07-0016 “Three-Dimensional Modeling of Inelastic Buckling in Frame Structures,” by M. Schachter and AM. Reinhorn, 9/13/07, (PB2008-108125).
- MCEER-07-0017 “Modeling of Seismic Wave Scattering on Pile Groups and Caissons,” by I. Po Lam, H. Law and C.T. Yang, 9/17/07 (PB2008-108150).
- MCEER-07-0018 “Bridge Foundations: Modeling Large Pile Groups and Caissons for Seismic Design,” by I. Po Lam, H. Law and G.R. Martin (Coordinating Author), 12/1/07 (PB2008-111190).
- MCEER-07-0019 “Principles and Performance of Roller Seismic Isolation Bearings for Highway Bridges,” by G.C. Lee, Y.C. Ou, Z. Liang, T.C. Niu and J. Song, 12/10/07 (PB2009-110466).
- MCEER-07-0020 “Centrifuge Modeling of Permeability and Pinning Reinforcement Effects on Pile Response to Lateral Spreading,” by L.L Gonzalez-Lagos, T. Abdoun and R. Dobry, 12/10/07 (PB2008-111191).
- MCEER-07-0021 “Damage to the Highway System from the Pisco, Perú Earthquake of August 15, 2007,” by J.S. O’Connor, L. Mesa and M. Nykamp, 12/10/07, (PB2008-108126).
- MCEER-07-0022 “Experimental Seismic Performance Evaluation of Isolation/Restraint Systems for Mechanical Equipment – Part 2: Light Equipment Study,” by S. Fathali and A. Filiatrault, 12/13/07 (PB2008-111192).
- MCEER-07-0023 “Fragility Considerations in Highway Bridge Design,” by M. Shinozuka, S. Banerjee and S.H. Kim, 12/14/07 (PB2008-111193).

- MCEER-07-0024 “Performance Estimates for Seismically Isolated Bridges,” by G.P. Warn and A.S. Whittaker, 12/30/07 (PB2008-112230).
- MCEER-08-0001 “Seismic Performance of Steel Girder Bridge Superstructures with Conventional Cross Frames,” by L.P. Carden, A.M. Itani and I.G. Buckle, 1/7/08, (PB2008-112231).
- MCEER-08-0002 “Seismic Performance of Steel Girder Bridge Superstructures with Ductile End Cross Frames with Seismic Isolators,” by L.P. Carden, A.M. Itani and I.G. Buckle, 1/7/08 (PB2008-112232).
- MCEER-08-0003 “Analytical and Experimental Investigation of a Controlled Rocking Approach for Seismic Protection of Bridge Steel Truss Piers,” by M. Pollino and M. Bruneau, 1/21/08 (PB2008-112233).
- MCEER-08-0004 “Linking Lifeline Infrastructure Performance and Community Disaster Resilience: Models and Multi-Stakeholder Processes,” by S.E. Chang, C. Pasion, K. Tatebe and R. Ahmad, 3/3/08 (PB2008-112234).
- MCEER-08-0005 “Modal Analysis of Generally Damped Linear Structures Subjected to Seismic Excitations,” by J. Song, Y-L. Chu, Z. Liang and G.C. Lee, 3/4/08 (PB2009-102311).
- MCEER-08-0006 “System Performance Under Multi-Hazard Environments,” by C. Kafali and M. Grigoriu, 3/4/08 (PB2008-112235).
- MCEER-08-0007 “Mechanical Behavior of Multi-Spherical Sliding Bearings,” by D.M. Fenz and M.C. Constantinou, 3/6/08 (PB2008-112236).
- MCEER-08-0008 “Post-Earthquake Restoration of the Los Angeles Water Supply System,” by T.H.P. Tabucchi and R.A. Davidson, 3/7/08 (PB2008-112237).
- MCEER-08-0009 “Fragility Analysis of Water Supply Systems,” by A. Jacobson and M. Grigoriu, 3/10/08 (PB2009-105545).
- MCEER-08-0010 “Experimental Investigation of Full-Scale Two-Story Steel Plate Shear Walls with Reduced Beam Section Connections,” by B. Qu, M. Bruneau, C-H. Lin and K-C. Tsai, 3/17/08 (PB2009-106368).
- MCEER-08-0011 “Seismic Evaluation and Rehabilitation of Critical Components of Electrical Power Systems,” S. Ersoy, B. Feizi, A. Ashrafi and M. Ala Saadeghvaziri, 3/17/08 (PB2009-105546).
- MCEER-08-0012 “Seismic Behavior and Design of Boundary Frame Members of Steel Plate Shear Walls,” by B. Qu and M. Bruneau, 4/26/08 . (PB2009-106744).
- MCEER-08-0013 “Development and Appraisal of a Numerical Cyclic Loading Protocol for Quantifying Building System Performance,” by A. Filiatrault, A. Wanitkorkul and M. Constantinou, 4/27/08 (PB2009-107906).
- MCEER-08-0014 “Structural and Nonstructural Earthquake Design: The Challenge of Integrating Specialty Areas in Designing Complex, Critical Facilities,” by W.J. Petak and D.J. Alesch, 4/30/08 (PB2009-107907).
- MCEER-08-0015 “Seismic Performance Evaluation of Water Systems,” by Y. Wang and T.D. O’Rourke, 5/5/08 (PB2009-107908).
- MCEER-08-0016 “Seismic Response Modeling of Water Supply Systems,” by P. Shi and T.D. O’Rourke, 5/5/08 (PB2009-107910).
- MCEER-08-0017 “Numerical and Experimental Studies of Self-Centering Post-Tensioned Steel Frames,” by D. Wang and A. Filiatrault, 5/12/08 (PB2009-110479).
- MCEER-08-0018 “Development, Implementation and Verification of Dynamic Analysis Models for Multi-Spherical Sliding Bearings,” by D.M. Fenz and M.C. Constantinou, 8/15/08 (PB2009-107911).
- MCEER-08-0019 “Performance Assessment of Conventional and Base Isolated Nuclear Power Plants for Earthquake Blast Loadings,” by Y.N. Huang, A.S. Whittaker and N. Luco, 10/28/08 (PB2009-107912).


- MCEER-08-0020 “Remote Sensing for Resilient Multi-Hazard Disaster Response – Volume I: Introduction to Damage Assessment Methodologies,” by B.J. Adams and R.T. Eguchi, 11/17/08 (PB2010-102695).
- MCEER-08-0021 “Remote Sensing for Resilient Multi-Hazard Disaster Response – Volume II: Counting the Number of Collapsed Buildings Using an Object-Oriented Analysis: Case Study of the 2003 Bam Earthquake,” by L. Gusella, C.K. Huyck and B.J. Adams, 11/17/08 (PB2010-100925).
- MCEER-08-0022 “Remote Sensing for Resilient Multi-Hazard Disaster Response – Volume III: Multi-Sensor Image Fusion Techniques for Robust Neighborhood-Scale Urban Damage Assessment,” by B.J. Adams and A. McMillan, 11/17/08 (PB2010-100926).
- MCEER-08-0023 “Remote Sensing for Resilient Multi-Hazard Disaster Response – Volume IV: A Study of Multi-Temporal and Multi-Resolution SAR Imagery for Post-Katrina Flood Monitoring in New Orleans,” by A. McMillan, J.G. Morley, B.J. Adams and S. Chesworth, 11/17/08 (PB2010-100927).
- MCEER-08-0024 “Remote Sensing for Resilient Multi-Hazard Disaster Response – Volume V: Integration of Remote Sensing Imagery and VIEWS™ Field Data for Post-Hurricane Charley Building Damage Assessment,” by J.A. Womble, K. Mehta and B.J. Adams, 11/17/08 (PB2009-115532).
- MCEER-08-0025 “Building Inventory Compilation for Disaster Management: Application of Remote Sensing and Statistical Modeling,” by P. Sarabandi, A.S. Kiremidjian, R.T. Eguchi and B. J. Adams, 11/20/08 (PB2009-110484).
- MCEER-08-0026 “New Experimental Capabilities and Loading Protocols for Seismic Qualification and Fragility Assessment of Nonstructural Systems,” by R. Retamales, G. Mosqueda, A. Filiatrault and A. Reinhorn, 11/24/08 (PB2009-110485).
- MCEER-08-0027 “Effects of Heating and Load History on the Behavior of Lead-Rubber Bearings,” by I.V. Kalpakidis and M.C. Constantinou, 12/1/08 (PB2009-115533).
- MCEER-08-0028 “Experimental and Analytical Investigation of Blast Performance of Seismically Resistant Bridge Piers,” by S.Fujikura and M. Bruneau, 12/8/08 (PB2009-115534).
- MCEER-08-0029 “Evolutionary Methodology for Aseismic Decision Support,” by Y. Hu and G. Dargush, 12/15/08.
- MCEER-08-0030 “Development of a Steel Plate Shear Wall Bridge Pier System Conceived from a Multi-Hazard Perspective,” by D. Keller and M. Bruneau, 12/19/08 (PB2010-102696).
- MCEER-09-0001 “Modal Analysis of Arbitrarily Damped Three-Dimensional Linear Structures Subjected to Seismic Excitations,” by Y.L. Chu, J. Song and G.C. Lee, 1/31/09 (PB2010-100922).
- MCEER-09-0002 “Air-Blast Effects on Structural Shapes,” by G. Ballantyne, A.S. Whittaker, A.J. Aref and G.F. Dargush, 2/2/09 (PB2010-102697).
- MCEER-09-0003 “Water Supply Performance During Earthquakes and Extreme Events,” by A.L. Bonneau and T.D. O’Rourke, 2/16/09 (PB2010-100923).
- MCEER-09-0004 “Generalized Linear (Mixed) Models of Post-Earthquake Ignitions,” by R.A. Davidson, 7/20/09 (PB2010-102698).
- MCEER-09-0005 “Seismic Testing of a Full-Scale Two-Story Light-Frame Wood Building: NEESWood Benchmark Test,” by I.P. Christovasilis, A. Filiatrault and A. Wanitkorkul, 7/22/09.
- MCEER-09-0006 “IDARC2D Version 7.0: A Program for the Inelastic Damage Analysis of Structures,” by A.M. Reinhorn, H. Roh, M. Sivaselvan, S.K. Kunnath, R.E. Valles, A. Madan, C. Li, R. Lobo and Y.J. Park, 7/28/09 (PB2010-103199).
- MCEER-09-0007 “Enhancements to Hospital Resiliency: Improving Emergency Planning for and Response to Hurricanes,” by D.B. Hess and L.A. Arendt, 7/30/09 (PB2010-100924).

- MCEER-09-0008 “Assessment of Base-Isolated Nuclear Structures for Design and Beyond-Design Basis Earthquake Shaking,” by Y.N. Huang, A.S. Whittaker, R.P. Kennedy and R.L. Mayes, 8/20/09 (PB2010-102699).
- MCEER-09-0009 “Quantification of Disaster Resilience of Health Care Facilities,” by G.P. Cimellaro, C. Fumo, A.M. Reinhorn and M. Bruneau, 9/14/09.
- MCEER-09-0010 “Performance-Based Assessment and Design of Squat Reinforced Concrete Shear Walls,” by C.K. Gulec and A.S. Whittaker, 9/15/09 (PB2010-102700).
- MCEER-09-0011 “Proceedings of the Fourth US-Taiwan Bridge Engineering Workshop,” edited by W.P. Yen, J.J. Shen, T.M. Lee and R.B. Zheng, 10/27/09 (PB2010-500009).
- MCEER-09-0012 “Proceedings of the Special International Workshop on Seismic Connection Details for Segmental Bridge Construction,” edited by W. Phillip Yen and George C. Lee, 12/21/09.
- MCEER-10-0001 “Direct Displacement Procedure for Performance-Based Seismic Design of Multistory Woodframe Structures,” by W. Pang and D. Rosowsky, 4/26/10.
- MCEER-10-0002 “Simplified Direct Displacement Design of Six-Story NEESWood Capstone Building and Pre-Test Seismic Performance Assessment,” by W. Pang, D. Rosowsky, J. van de Lindt and S. Pei, 5/28/10.
- MCEER-10-0003 “Integration of Seismic Protection Systems in Performance-Based Seismic Design of Woodframed Structures,” by J.K. Shinde and M.D. Symans, 6/18/10.
- MCEER-10-0004 “Modeling and Seismic Evaluation of Nonstructural Components: Testing Frame for Experimental Evaluation of Suspended Ceiling Systems,” by A.M. Reinhorn, K.P. Ryu and G. Maddaloni, 6/30/10.
- MCEER-10-0005 “Analytical Development and Experimental Validation of a Structural-Fuse Bridge Pier Concept,” by S. El-Bahey and M. Bruneau, 10/1/10.
- MCEER-10-0006 “A Framework for Defining and Measuring Resilience at the Community Scale: The PEOPLES Resilience Framework,” by C.S. Renschler, A.E. Frazier, L.A. Arendt, G.P. Cimellaro, A.M. Reinhorn and M. Bruneau, 10/8/10.
- MCEER-10-0007 “Impact of Horizontal Boundary Elements Design on Seismic Behavior of Steel Plate Shear Walls,” by R. Purba and M. Bruneau, 11/14/10.



EARTHQUAKE ENGINEERING TO EXTREME EVENTS

University at Buffalo, The State University of New York
Red Jacket Quadrangle ▪ Buffalo, New York 14261
Phone: (716) 645-3391 ▪ Fax: (716) 645-3399
E-mail: mceer@buffalo.edu ▪ WWW Site <http://mceer.buffalo.edu>



University at Buffalo *The State University of New York*

ISSN 1520-295X